A STUDY OF STRESS AND ANISOTROPY IN IDEALIZED GRANULAR ASSEMBLIES

by

Richard John Bathurst, B.Sc., M.Sc. (Queen's)

A thesis submitted to the
School of Graduate Studies and Research
in partial fulfilment of the requirement for the
degree of
Doctor of Philosophy

Department of Civil Engineering
Queen's University
at Kingston, Ontario, Canada
October, 1985

ISBN 0-315-30448-0

ABSTRACT

The present study is directed at investigation of relationships between stress and parameters characterizing properties of microstructure and load transmission in idealized granular systems. Fundamental relationships for three-dimensional idealized granular systems are developed using a theoretical approach similar to that reported by Rothenburg (1980) and Rothenburg and Selvadurai (1981b). Verification of fundamental relationships is prohibitively expensive using numerical simulation. However, fundamental expressions have a limited two-dimensional analogue and information necessary for verification can be obtained more readily from numerical simulation of these systems. The objective of the study is not to formulate constitutive relationships for idealized granular systems but, rather, to verify fundamental relationships between stress and microfeatures which must be respected in any physically realistic continuum model.

The primary method used to investigate theories presented in the study is computer-based numerical simulation of two-dimensional assemblies of discs. The simulation employs a numerical technique which has been reported by Cundall and Strack (1979). Additional verification of fundamental assumptions in theoretical developments is provided through interpretation of a limited amount of data from experiments with planar granular assemblies such as those reported by Oda and Konishi (1974a).

Truncated Fourier series expressions of the form originally proposed by Rothenburg (1980) describing the distribution of contact normal orientations and distributions of *average* contact force components are shown to be reasonable approximations to measured data from physical tests and the results of numerical experiments in the current study. Substitution of distribution functions into mathematically manageable expressions for stress quantities in the limit of infinite, spatially homogeneous two-dimensional granular assemblies results in predicted stress quantities which are within 10% of directly measured values.

The results of numerical simulations support the hypothesis that system shear capacity is due to the sum of invariant quantities which measure anisotropy in the orientation distribution of contact normals, interparticle normal forces and interparticle tangential (shear) forces. Examination of contributing system anisotropies shows that the direct contribution of interparticle tangential forces is very small. Under monotonic shearing deformations, microstructure evolves such that load-carrying chains of contacts are oriented in the direction of maximum loading and are characterized by interparticle forces with little or no tangential contact force component.

Careful examination of numerical assemblies at an ultimate state (failure) leads to the concept of *steady state* of micromechanical behaviour for granular media. Steady state is characterized by limiting values of invariant quantities describing microstructure and contact force components under continuing shearing deformations. At steady state, the ratio of normal contact force to contact normal anisotropy was observed to approach unity for numerical assemblies with a variety of disc properties. This limiting condition leads to a simple expression for the invariant stress ratio of these systems as a function of microstructural anisotropy at steady state.

Macroscopically-observed changes in sample stiffness and shear capacity can be traced to changes in parameters describing system anisotropy when discs with variable disc properties are investigated. Numerical assemblies with particle stiffnesses and interparticle friction angle considered typical of actual granular media approach a steady state coordination number predicted for static determinancy in these systems.

Mathematical developments show that fundamental relationships which equate stress quantities to microstructure and assembly interparticle forces can be expressed in equivalent tensorial form. Tensorial expressions are expected to retain their form for three-dimensional granular media comprising spherical or near-spherical particles. Because of this correspondence, implications to three-dimensional assemblies are drawn from the results of numerical experiments and original (theoretically developed) fundamental expressions for three-dimensional systems are modified.

ACKNOWLEDGEMENTS

The author would like to express his appreciation to a number of individuals who have been helpful in the successful completion of this study.

Appreciation is extended to co-supervisors Dr. R.J. Mitchell (Queen's University at Kingston) and Dr. L. Rothenburg (University of Waterloo). The author is particularly indebted to Dr. Rothenburg who introduced the author to the general problem and was generous with his time to see the project through to completion.

Appreciation is extended to personnel at the Royal Military College of Canada and Honeywell Ltd. who assisted the author by making available the computer resources required to undertake the numerical simulation portions of the investigation. These persons include Dr. R. Benesch (Director ADP, RMC) and Messrs. R. Philip, P. Barrett, G. Thomas, B. Baskett, and D. Williams of Honeywell Ltd..

Additional support was received from members of the Civil Engineering Department at RMC: Messrs. J. DiPietrantonio and L. Harvey assisted the author by drafting a number of the figures. Special appreciation is expressed to Dr. D.W. Kirk and Dr. P.M. Jarrett for their encouragement and support during the period of study.

TABLE OF CONTENTS

LIST OF FIGURES

LIST OF TABLES

CHAPTER 1

INTRODUCTION

1.1 Introduction

An understanding of the micromechanical response of granular media under static loading is fundamental to our understanding of the macroscopic behaviour of these systems. Of particular importance are relationships between the distribution of externally applied forces, which act at the boundaries of a granular assembly, and the fabric (or microstructure) and distribution of interparticle forces which evolve in response to boundary disturbances.

The problem that this study addresses and the micromechanical approach which is adopted to investigate the problem can be introduced by reference to some interesting laboratory experiments which have been carried out in recent years by a number of researchers.

For example, De Josselin De Jong and Verruijt (1969) investigated assemblies of photo-elastic discs as two-dimensional analogues to granular media. In these experiments photo-elastic discs, having a range of diameters, were stacked between glass plates and loaded through vertical and horizontal platens. Contact forces at various stages in assembly loading were calculated from the pattern of isochromatics viewed in polarized light. Figure 1.1a shows an assembly of discs at one stage during static loading. The dark lines in the figure represent the action of contact forces. The thickness of the lines are proportional to the intensity of the interparticle forces.

The figure shows that the assembly of discs has evolved a certain particle arrangement (or microstructure) and a certain distribution of interparticle forces in order to maintain the sample in static equilibrium with the platen forces acting at the system boundaries. The relationship of microstructure and contact forces to the boundary loads is visually apparent in the figure. Chains of relatively high contact forces can be identified which appear to be biased in the direction of the maximum applied load. If the centres of all mutually loaded discs were connected, then, a network of lines (called branch lengths) would result which would reflect a similar bias in the microstructure of the sample. To emphasize this bias, Figures 1.1b and 1.1c plot groups of branch lengths representing interparticle contacts having vertical or horizontal orientations. Comparison of the figures shows that there are a greater number of contacts in the vertical direction. The relative number of contacts in these two groups illustrates a fundamental characteristic of microstructural anisotropy in this assembly.

Similar anisotropic microstructure can be anticipated for three-dimensional assemblies comprising rounded sand particles. For example, Oda (1972c) has plotted the distribution of contact orientations for sand samples at stages during drained triaxial compression. Figure 1.2c shows the distribution

of contacts projected on an equal area stereonet for sand samples at an initial compacted state and at a state close to the peak shear strength for the material. The plots show that the distribution of contacts has readjusted under deviatoric loading to maximize contact density at orientations close to the direction of maximum principal stress.

The geometrical anisotropy identified in the systems above is responsible for anisotropy in all observed macroscopic properties for these granular assemblies. However, the processes leading to the creation of anisotropic structure are complex. In very general and brief terms, these processes are related to the stability of particulate systems under destabilizing deviatoric loads. A granular material will carry load by distributing external forces between interparticle contacts. Whether or not the load can be sustained depends on the stability of microstructure under the system of contact forces imposed upon it. If stability cannot be maintained, granular materials can adjust their system of contacts and will regulate contact forces internally to satisfy conditions of internal stability. The process of adjusting contacts to maintain stability results in development of anisotropic microstructure which partially offsets the destabilizing action of deviatoric loads and reduces the level of contact forces.

Two fundamental questions can be posed at this stage: First, how do we quantify microstructure and the distribution of contact forces? Secondly, once quantified, how are these parameters related to the shearing resistance of the sample?

Our ability to answer these questions is hampered by the lack of complete information on the spatial arrangement of constituent particles and load transmission through these media. Granular assemblies typically comprise a great number of particles and a corresponding large number of degrees of freedom. As a result, microfeatures of these systems, including patterns of contact forces and individual particle movements, are prohibitively complex. Nevertheless, at the macroscale, the entire system exhibits well defined deformations under uniform external loads. It is this type of behaviour which is idealized in the notion of stress-strain relations. Within the framework of continuum theories the existence of stress-strain relationships is a well confirmed postulate which, however, cannot be taken for granted when macroscale description is attempted based on behaviour at the particulate level.

From a physical point of view the tendency to a regular response under uniform external conditions is a statistical trend related to an almost independent behaviour of different large parts of a large system when significantly separated particles do not affect each other directly. Any large system essentially behaves as a collection of nearly independent parts which contribute to the overall response in an uncorrelated manner so that the overall behaviour appears regular as a result of statistical

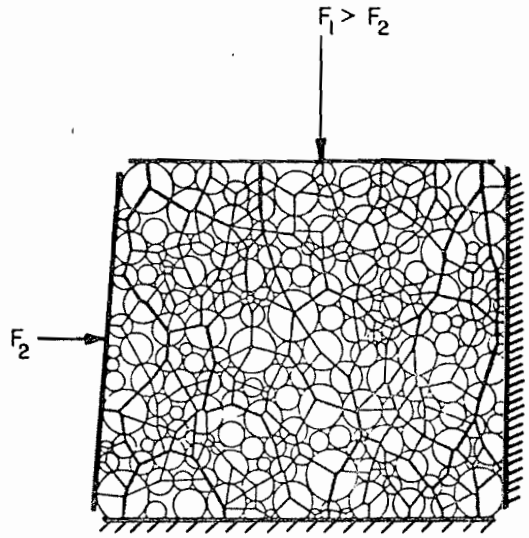

a) Distribution of Contact Forces

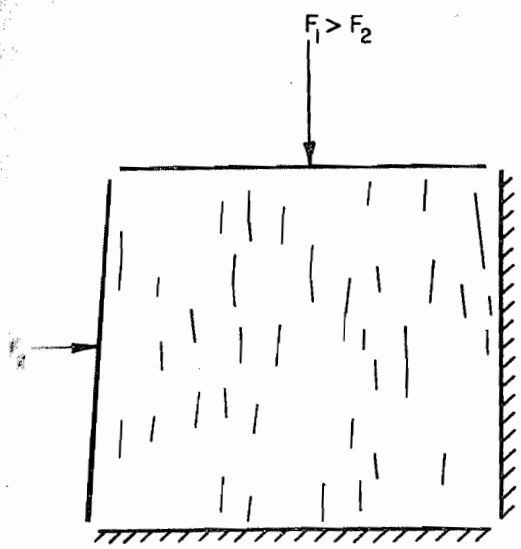

b) Vertical Contacts

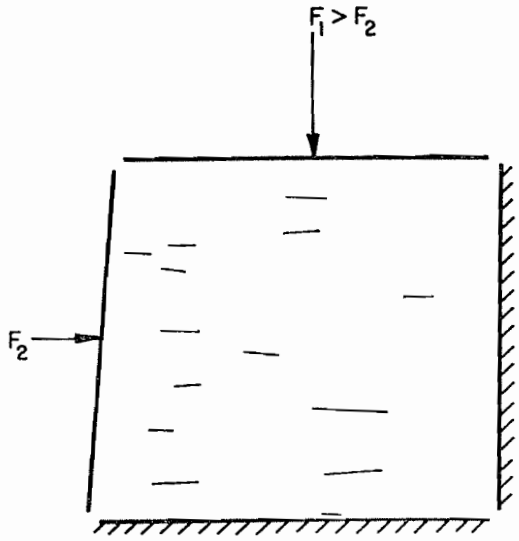

c) Horizontal Contacts

Figure 1.1 Two-Dimensional Assembly of Photo-Elastic Discs
(after De Josselin De Jong and Verruijt, 1969)

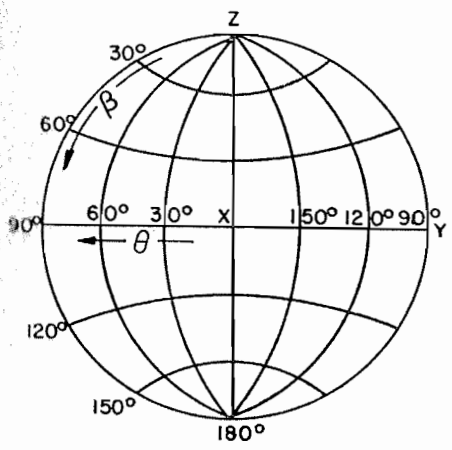

a) Equal Area Stereonet

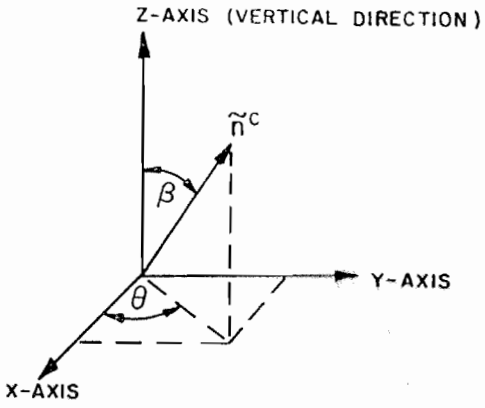

b) Contact Orientation

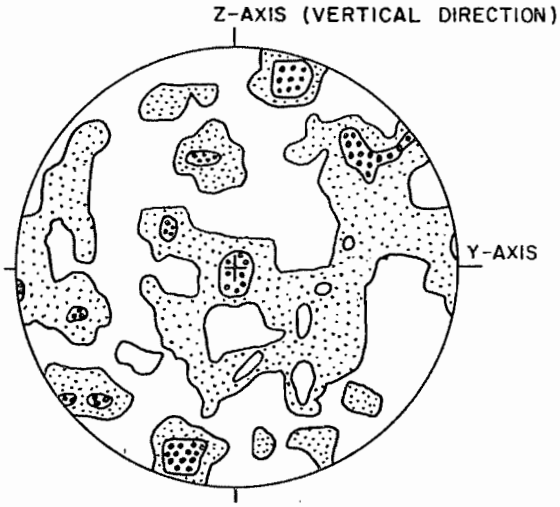

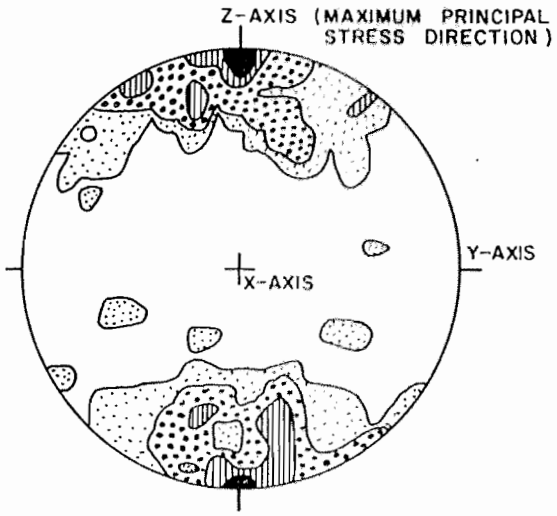

c) Contact Density Distributions for Initial Specimen and at Peak Stress Ratio
(Density Levels 4%, 3%, 2%, 1% per 1% area)

Figure 1.2 Contact Density Distributions from the Results of Triaxial Compression Tests on Sand Samples *(after Oda, 1972c)*

averaging. From this point of view, macro-descriptors, like stress and strain, must be averages of microscopic characteristics of a system. For some simple substances like gases, fluids and some solids the link between macro and micro-descriptors is established in classical statistical physics (Landau and Lifshitz, 1959). Recently Rothenburg (1980) applied to granular materials some methods routinely employed in statistical physics and developed a relationship between stress tensor, averages of contact forces and averages describing microstructure of granular materials.

1.2 General Objectives and Approach

The objective of this study is to investigate relationships between stress and parameters characterizing anisotropic properties of microstructure and load transmission in idealized granular systems. The theoretical basis of this investigation is an approach similar to that reported by Rothenburg (1980) and Rothenburg and Selvadurai (1981b). The current study is primarily directed at the verification of these theoretical developments for assemblies in static equilibrium. However, verification of expressions for three-dimensional systems requires complete information on contact forces and position of all particles. This information can only be obtained from the results of numerical simulations which, for three-dimensional systems, is prohibitively expensive. Fortunately, fundamental expressions have a limited two-dimensional analogue (e.g. assemblies of discs) and information necessary for verification can be obtained more readily from numerical simulation of these systems and interpretation of a limited amount of data from experiments similar to those reported by De Josselin De Jong and Verruijt (1969). The primary method used to investigate theories presented in this study is computer-based numerical simulation of two-dimensional assemblies of discs. The simulation employs a numerical technique which involves the solution of equations of motion for all assembly particles. This technique has been reported by Cundall and Strack (1979a).

The ultimate collective aim of engineering research into the mechanical behaviour of granular systems is to formulate constitutive relationships for these materials. The current study is not aimed at this objective but rather concentrates on verifying fundamental relationships between stress and microfeatures which must be respected in any physically realistic continuum model. Recently, the task of deriving a micromechanically-based constitutive model has been successfully accomplished (Rothenburg, 1985). The work reported here is a parallel investigation which serves to verify fundamental relationships upon which this recent model is founded. In addition, this study establishes many qualitative features of microscopic processes in granular materials which help to understand important macroscopic phenomena (such as the development of critical state and mechanisms of strain-hardening/strain-softening) and their relationship to physical properties of particles.

1.3 Organization

The current study has been organized in the following way:

Chapter 1 introduces the topic of investigation, objectives and presents an outline of the adopted approach. Some terminology is introduced that is common to micromechanical description of particulate media. A literature review is undertaken which includes laboratory investigations and theoretical developments which are important to the current study.

Chapter 2 presents a phenomenological description of granular materials based on introduction of the stress tensor as a volume-average of discrete quantities characterizing contact forces and geometrical features of microstructure. Fundamental descriptors used in this approach are illustrated based on the results of limited experimental data reported in the literature. Expressions for the stress tensor are formulated for three-dimensional systems comprising particles of arbitrary shape and size distribution.

Chapter 3 presents assemblies of material discs as a limited two-dimensional analogue to a three-dimensional system of particles. Fundamental expressions developed for three-dimensional systems are further simplified to quantitatively relate the average assembly stress tensor to fabric anisotropy and to the distribution of average interparticle force components within the assembly. The developed expressions are assessed from the results of laboratory tests on two-dimensional assemblies of discs reported in the literature.

Chapter 4 reviews a numerical simulation approach which involves solution of equations of motion for individual particles. The numerical simulation provides complete information on disc assemblies which can be used to verify developed theoretical relationships. The technique is implemented through a computer program DISC which is also described in this chapter.

Chapter 5 reports the results of a series of tests using program DISC which were undertaken to provide an independent verification of the relationships proposed in Chapter 3 and to gain insight into the micromechanical behaviour of idealized granular systems. Fundamental aspects of micromechanical behaviour are synthesized based on the results of the two-dimensional numerical tests. Implications to three-dimensional systems are identified.

Chapter 6 summarizes the major conclusions drawn from the current investigation and presents recommendations for further research.

1.4 Terminology for the Description of Microstructure

Micromechanical studies of granular materials require introduction of some unique physical concepts and have necessarily evolved a terminology specific to the discipline. It is useful at this stage to introduce basic concepts and terminology related to the characterization of microstructure. In soil mechanics literature the term *fabric* has been used extensively as a generic term to describe the geometry of particle packing (microstructure).

Granular materials are assemblies of discrete cohesionless particles having arbitrary shape and (typically) a range of particle sizes. A reasonable assumption is that the particles are essentially rigid but interact through compliant point contacts.

An individual particle at static equilibrium may be in contact with several neighbours as shown on Figure 1.3. The number of contacts per particle is called the *coordination number* of the particle. Clearly each *physical contact* contributes two *contacts* to the assembly. The *average coordination number*, γ of the assembly is:

$$\gamma = \frac{M_V}{N} \tag{1.1}$$

Here M_V represents the total number of contacts within the assembly volume and N, the total number of particles. For brevity in the following text, γ is often referred to as the assembly *coordination number*.

Results of numerous investigations have shown that coordination number is intimately related to familiar descriptions of particle packing such as assembly density ρ, or void ratio e (e.g. Smith, Foote and Budang, 1929; Oda, 1977). In general, an assembly of particles with a high coordination number is more stable and less mobile than the same assembly with a lower coordination number.

Coordination number introduced above is an incomplete description of particle packing as it carries no information on relative particle orientations. This aspect of microstructure is often described by particle *contact normals* where a contact normal $\tilde{n}^c$ is the exterior directed normal to the tangent plane at the point of contact between particles as shown on Figure 1.3.

Additional information on relative particle orientations can be obtained from the distribution of lines joining the mass centres of contacting particles. These lines are often referred to as *branch lengths* (e.g. Satake, 1978). An alternative description, which implicitly includes the influence of particle shape, identifies a *contact vector* pair at each physical contact. A contact vector $\tilde{l}^c$ is defined as a vector directed from the mass centre of a particle to a point of contact with a neighbour (Rothenburg, 1980). Both definitions are shown on Figure 1.4. The latter description is used in this work but both give the same fundamental information on particle arrangement. For spherical particles, contact

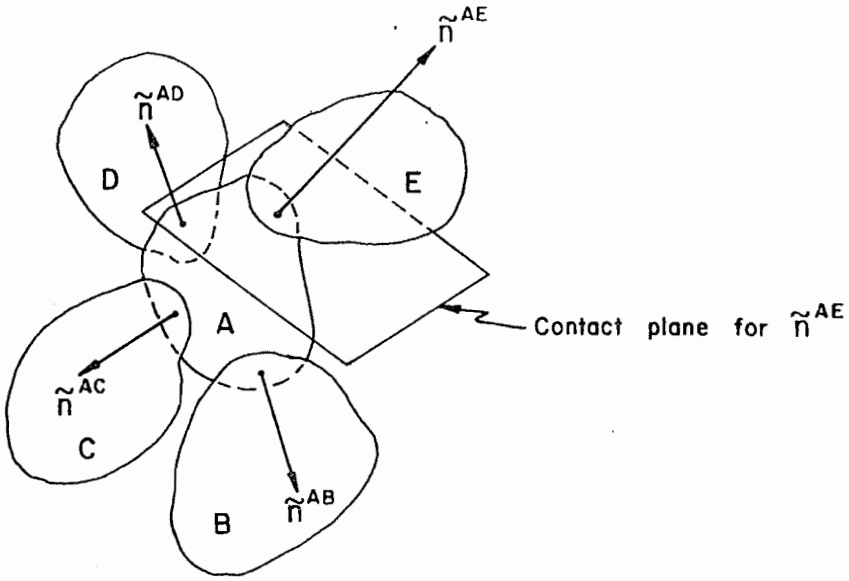

Figure 1.3 Contact Normals for Particle A

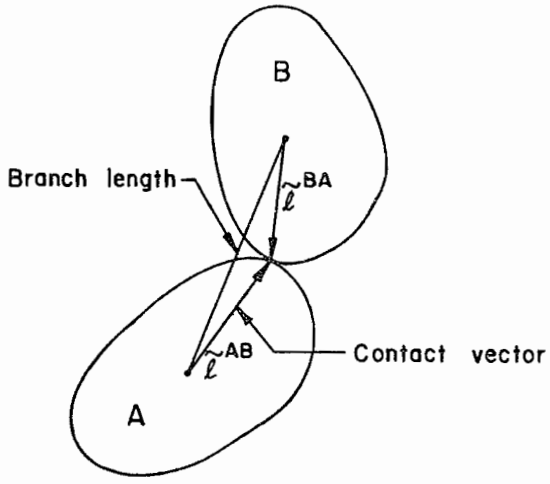

Figure 1.4 Branch Length and Contact Vectors

vectors and contact normals are coincident.

The study of discrete particulate systems with a very large number of particles requires the knowledge of the relative proportion of contacts falling within different orientation intervals. As illustrated on Figures 1.1b and 1.1c, an assembly may have a greater number contacts in the vertical direction as compared to the horizontal direction. Complete description requires knowledge of the proportion of contacts falling over the entire range of possible orientations. In addition, the statistical description of granular systems comprising a very large number of particles is greatly facilitated if contact normals and contact vectors (or chains of contact vectors) are distributed homogeneously through the loaded assembly. Under these conditions contact orientations can be described by continuous distributions which relate contact vectors and contact vector lengths to orientation. If these distributions exhibit preferred directions then, these directions are commonly referred to as *directions of anisotropy*.

1.5 Notation

Indicial notation has been used throughout this study. In general, mathematical expressions are referenced to a fixed Cartesian coordinate system having base unit vectors e_i, $i = 1, 2, 3$ (or $i = 1, 2$ in two-dimensions). Terms are defined where they first appear and important quantities are summarized in the list of nomenclature which appears as a preface to this study. As much as possible, soil mechanics terminology has been adopted since it is the micromechanical behaviour of granular materials which has inspired the current investigation.

1.6 Literature Review

1.6.1 General

Modern directions of research on micromechanics of granular materials date back to the mid-fifties when Schneebeli (1956) introduced a model of granular materials as an assembly of metal rods. Two and three-dimensional physical models were subsequently improved by using optically sensitive materials (Dantu, 1957). Visualization of load transmission in these systems intuitively identified the important elements of microstructure which are responsible for macroscopic behaviour of granular materials. These elements of microstructure have been identified in the previous section (e.g. coordination number, contact orientations). More recently, micromechanics research using assemblies of photo-elastic discs as two-dimensional analogues to granular systems has been directed at quantifying observed patterns of load transmission and empirical introduction of plausible descriptors of fabric (e.g. De Josselin De Jong and Verruijt 1969; Oda and Konishi, 1974a, 1974b). While this research has

provided important insight into microscopic processes in granular materials, only in the last few years has a proper physical framework emerged which provides a mathematically manageable link between macroscopic behaviour and microscopic observation (Rothenburg, 1980).

The subsequent review traces major steps in the evolution of micromechanical ideas and methods. Finally, developments that are the starting point of this investigation are presented.

1.0.2 Selected Previous Investigations

Dantu (1957)

Dantu (1957) investigated in a qualitative manner load transmission in two-dimensional assemblies of cohesionless photo-sensitive cylinders (discs) and three-dimensional assemblies consisting of glass beads. These experiments were among the first to demonstrate that load transmission occurred through highly-oriented chains of particles. Dantu recognized that density was an incomplete description of fabric and that any statistical description of microstructure must include the geometrical arrangement of particles.

Biarez and Wiendieck (1963)

Biarez and Wiendieck (1963) examined the distribution of contacts for two-dimensional assemblies of irregular-shaped particles. The assemblies were compressed horizontally and then vertically and photographed at intervals to extract contact distributions. The results at several stages of loading are shown on Figure 1.5a and have been replotted from the original data. The plots represent frequency distributions for contact normals with orientations between 0 and 90 degrees to the vertical counted over 10 degree intervals. The test data shows that the distribution of contact normals was symmetrical about horizontal and vertical axes and that the direction of contact anisotropy was sensibly coincident with the direction of applied loading. Biarez and Wiendieck noted that if the frequency distribution data was plotted in the form of a rosette, the distribution of contact orientations formed an elliptical shape. A *coefficient of anisotropy A* was defined based on this geometry according to:

$$A = \frac{\alpha_1 - \alpha_2}{\alpha_1 + \alpha_2} \tag{1.2}$$

where α_1 and α_2 are the scaled vertical and horizontal semi-axis lengths of the ellipse. The intensity of contact anisotropy in the sample was seen to depend on the magnitude and history of loading as shown on Figure 1.5b. In addition, Biarez and Wiendieck observed that initial contact anisotropy, defined by coefficient A, and initial void ratio e were both sensitive to details of sample preparation.

Importantly, both parameters appeared interrelated since the value of A for initial samples was seen to increase in a linear fashion with increasing void ratio.

Hill (1963)

Hill (1963) examined the properties of homogeneous two-phase solid elastic mixtures. In this study he proposed that similar representative volumes of the assembly would exhibit fluctuations in the second-order stress tensor σ about some *average stress tensor* value $\overline{\sigma}$. For large homogeneous sub-assemblies these fluctuations could be considered insignificant and the average stress tensor $\overline{\sigma}$ taken as an adequate description of the state of stress throughout the total volume. Further, the average stress tensor could be related to boundary force components (tractions) according to:

$$\overline{\sigma}_{ij} = \frac{1}{V}\int_V \sigma_{ij}\, dV = \frac{1}{2V}\int_S (x_i^\beta T_j^\beta + x_j^\beta T_i^\beta)\, dS \qquad i,j = 1,2,3 \tag{1.3}$$

Here T_i^β represents boundary tractions acting at a point with coordinates x_i^β on the boundary surface S.

The concept of an average stress tensor for homogeneous discrete granular systems has been adopted by subsequent researchers including Drescher and De Josselin De Jong (1972), Strack and Cundall (1978), Rothenburg (1980) and Mehrabadi et al. (1982) among others.

Horne (1965)

Horne (1965) proposed that anisotropy in the distribution of particle contacts for irregular assemblies of uniform spheres may be described by some distribution function $E(\theta, \beta)$.

If a spherical coordinate system is adopted, such as that shown on Figure 1.2b, then, the fraction of total contact normals falling within the solid angle β to $\beta + \Delta\beta$, θ to $\theta + \Delta\theta$ is:

$$\frac{M_g(\theta,\beta)}{M_V} = \int_\theta^{\theta+\Delta\theta}\int_\beta^{\beta+\Delta\beta} E(\theta,\beta)\sin\beta\, d\beta\, d\theta \tag{1.4}$$

Here $M_g(\theta,\beta)$ represents the number of contacts in the interval and M_V the total number of contacts in the assembly. Integration of (1.4) over the complete solid angle $0 \le \theta \le 2\pi$ and $0 \le \beta \le \pi$ gives:

$$\int_0^{2\pi}\int_0^{\pi} E(\theta,\beta)\sin\beta\, d\beta\, d\theta = 1 \tag{1.5}$$

For an isotropic assembly (i.e. an assembly with no preferred contact orientation) $E(\theta,\beta) = 1/4\pi$. Implicit within the above formulations is the assumption that the number of particles is large enough that the arrangement of contact normals is approximated by a continuous distribution function. Functions similar to (1.4) have been used by subsequent researchers to describe aspects of microstructure for assemblies comprising non-spherical particles and a range of particle sizes (e.g. Oda 1972a,b,c, 1977, Oda and Konishi, 1978, and Rothenburg, 1980, among others).

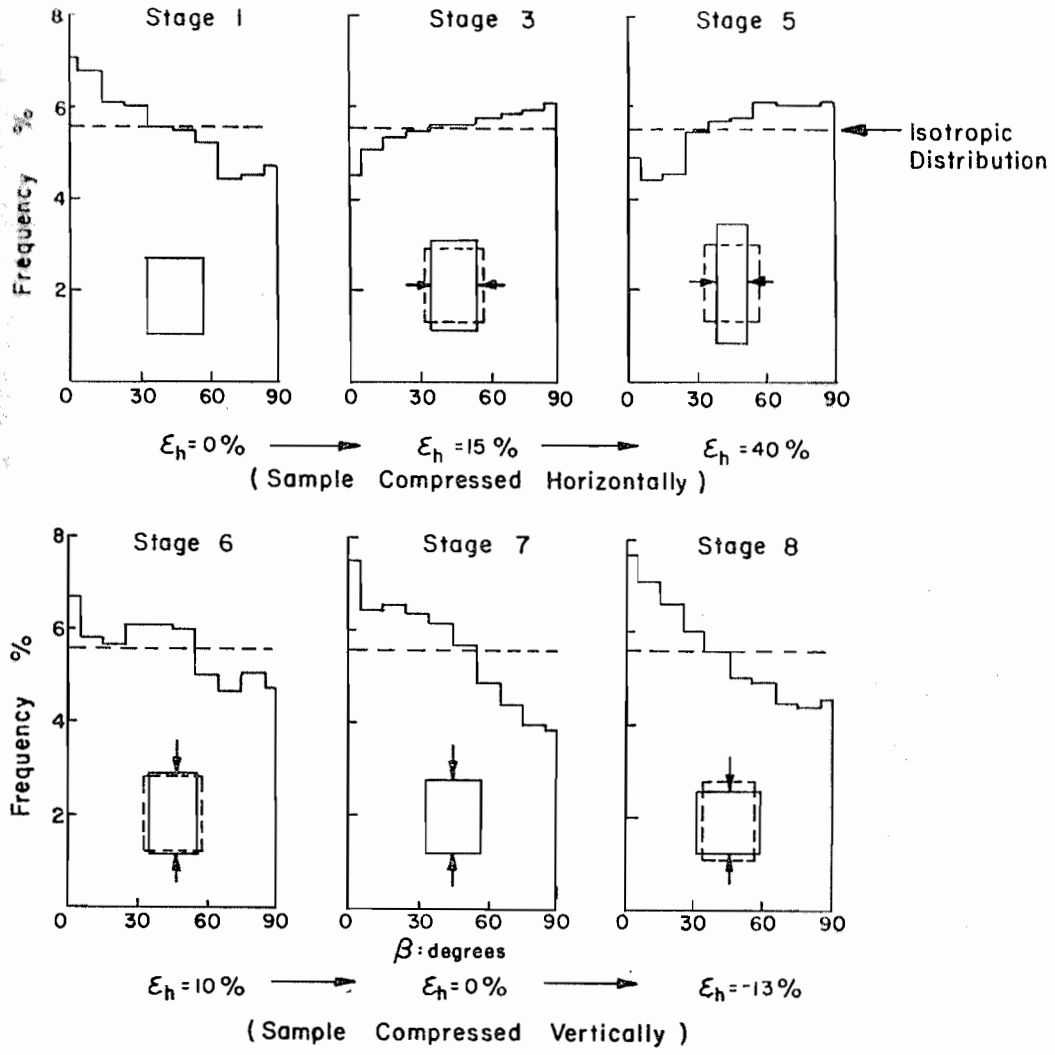

a) Contact Normal Distributions during Biaxial Compression

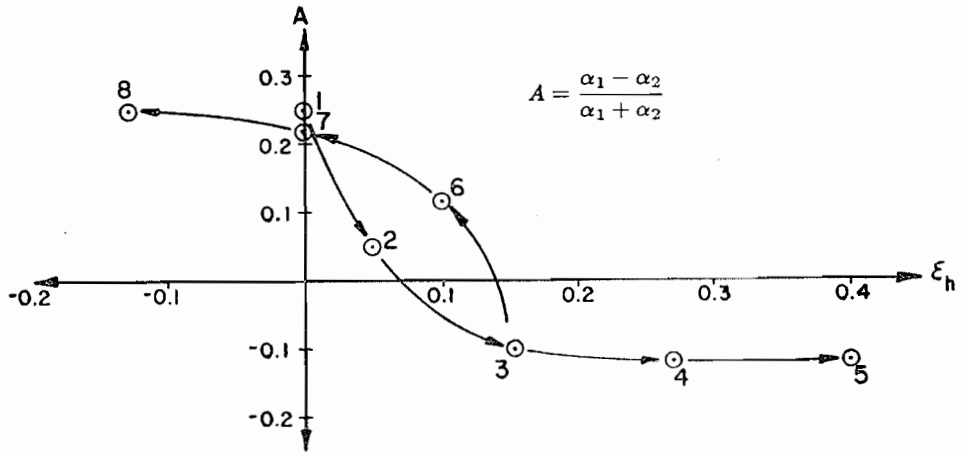

b) Coefficient of Anisotropy A versus Horizontal Strain ε_h

Figure 1.5 Contact Normal Anisotropy from Two-Dimensional Biaxial Tests *(data after Biarez and Wiendieck, 1963)*

Weber (1966)

Weber (1966) proposed that a macroscopic stress tensor σ^β could be equated to assembly contact forces and the geometrical arrangement of contacting particles. The equivalent expression rewritten in the indicial notation adopted in the current study is as follows:

$$\sigma_{ij}^\beta = \frac{1}{V} \sum_{c \epsilon V} f_i^c l_j^c \qquad i,j = 1,2,3 \tag{1.6}$$

Here $c \epsilon V$ denotes all contacts in the assembly volume. Terms f_i^c and l_j^c refer to scalar components of contact forces and the contact vector associated with each assembly contact.

De Josselin De Jong and Verruijt (1969), Drescher and De Josselin De Jong (1972)

Inspired by earlier research reported by Dantu (1957), De Josselin De Jong and Verruijt (1969) investigated assemblies of photo-elastic discs as two-dimensional models of idealized granular media. Important aspects of these tests have been described in the introduction to the current work.

Drescher and De Jong (1972) used a similar technique to examine the behaviour of two-dimensional assemblies under conditions of flow (i.e. large assembly deformations under conditions of constant volume and stress). These researchers calculated the second-order average stress tensor $\bar{\sigma}$ for circular sub-assemblies located in regions sufficiently removed from the rigid sample boundaries that the distribution of contact forces was essentially homogeneous. The average stress tensor was calculated using the following approximation:

$$\bar{\sigma}_{ij} = \frac{1}{V} \sum_{c \epsilon \beta} x_i^\beta f_j^\beta \qquad i,j = 1,2 \tag{1.7}$$

where f_j^β represents equivalent sub-assembly boundary force components and x_i^β the coordinates of the intersection points of these forces on the boundary. Calculations showed that moment equilibrium was satisfied in these tests according to $\sum x_i^\beta f_j^\beta = \sum x_j^\beta f_i^\beta$ for $i \neq j$. Consequently, the average stress tensor description (1.7) satisfied the condition of symmetry (i.e. $\bar{\sigma}_{ij} = \bar{\sigma}_{ji}$, $i \neq j$).

Skinner (1969)

Skinner (1969) reported the results of a series of physical tests designed to examine the influence of interparticle friction angle on the macroscopically observed shearing resistance of assemblies of spherical particles during simple shear. Skinner noted that the directly measured maximum value of interparticle friction angle ϕ_μ for dry assemblies could be increased dramatically by flooding the samples with water. Figures 1.6a and 1.6b show the results of shear tests comprising 1mm diameter glass ballotini with high and low interparticle friction angles. The ratio of friction angles was at least

five in these tests yet no significant difference in measured peak macroscopic shearing angle ϕ_{max} or ϕ_{cv} at the ultimate condition was observed between samples. The results of several tests are given on Figure 1.6c which shows that the value of ϕ_{cv} is relatively insensitive to the magnitude of ϕ_{μ}. Skinner suggested that interparticle rolling mechanisms may predominate for high friction materials thereby reducing the direct contribution of interparticle friction angle to the shearing resistance of these materials.

Oda (1972a,1972b,1972c)

Oda (1972a,b,c) used the concept of a *probability density distribution* function $E(\theta, \beta)$, similar to Horne (1965), to describe the distribution of contact normals extracted from cylindrical samples of compacted sand. The same references report the results of drained triaxial compression tests performed on samples of sand comprising rounded to subrounded particles. The samples were impregnated with a water-resin mixture at stages in the tests and orientation data interpreted from vertically and horizontally cut thin-sections. Examples of his contact orientation analyses have been presented in the form of contact density plots projected on equal area stereonets (Figure 1.2c).

From measured contact orientation data, Oda extracted the value of the axially-symmetric distribution function $E(\beta)$ at stages during triaxial testing. The change in $E(\beta)$ provided a quantitative measure of the evolution of contact anisotropy during triaxial loading. For example, Figure 1.7 shows that the distribution of contact normals became progressively anisotropic with increasing vertical principal stress. Furthermore, principal directions of contact anisotropy and stress appeared coincident. In addition, Oda noted that the change in $E(\beta)$ was most dramatic prior to the peak principal stress ratio, after which, $E(\beta)$ did not change markedly.

Smith et al. (1929), Oda (1977), Field (1963), Athanasiou-Grivas and Harr (1980)

Smith et al. (1929) proposed that the average coordination number for assemblies of mono-sized spheres was strongly correlated to the assembly void ratio e (or density ρ). More recently, Field (1963), Oda (1977) and others have shown that for assemblies comprising a limited range of particle sizes a similar strong correlation exists. For example, data presented on Figure 1.8 from Oda shows that the relationship between void ratio and average coordination number is essentially independent of size distribution. On this figure, the two-mixed assembly comprised spheres of two different radii and the multi-mixed assembly comprised spheres with four different radii.

Field (1963), Athanasiou-Grivas and Harr (1980) and others have proposed simple mathematical relationships between average coordination number and assemble void ratio (or porosity n) for a

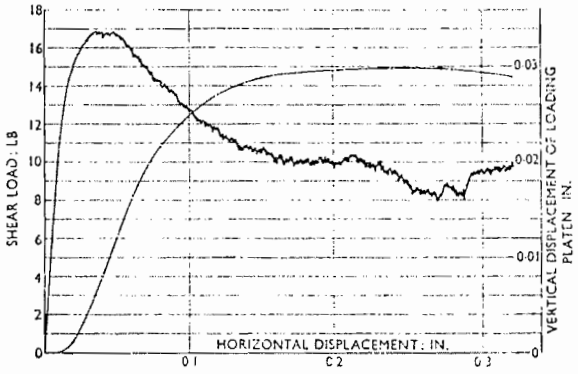

a) Test with Dry Ballotini ($\phi_\mu = 4°$)

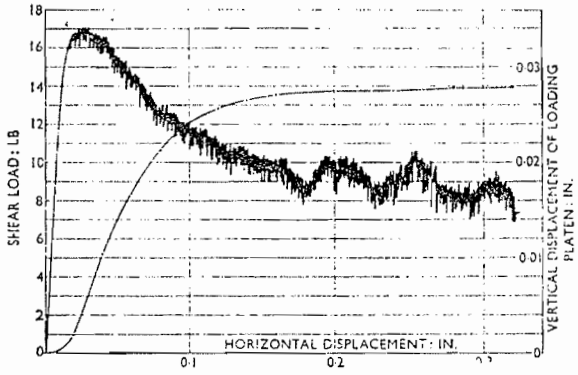

b) Test with Flooded Ballotini ($\phi_\mu = 32°$)

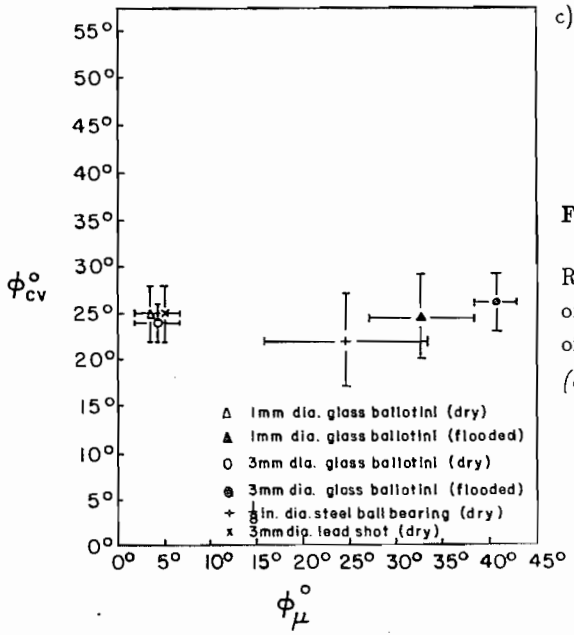

c) Measured Macroscopic Friction Angle at Critical Void Ratio ϕ_{cv} versus Directly Measured Mobilized Interparticle Friction Angle ϕ_μ

Figure 1.6

Results of Shear Box Tests
on Random Assemblies
of 1mm Diameter Glass Ballotini
(after Skinner, 1969)

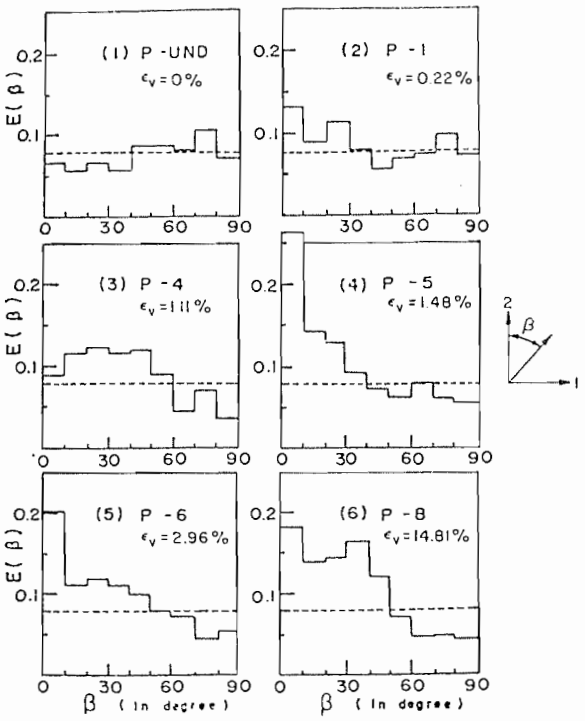

Figure 1.7 Progressive Change in Contact Normal Distribution Function $E(\beta)$ during Triaxial Compression Test on Sand
(Oda, 1972b)

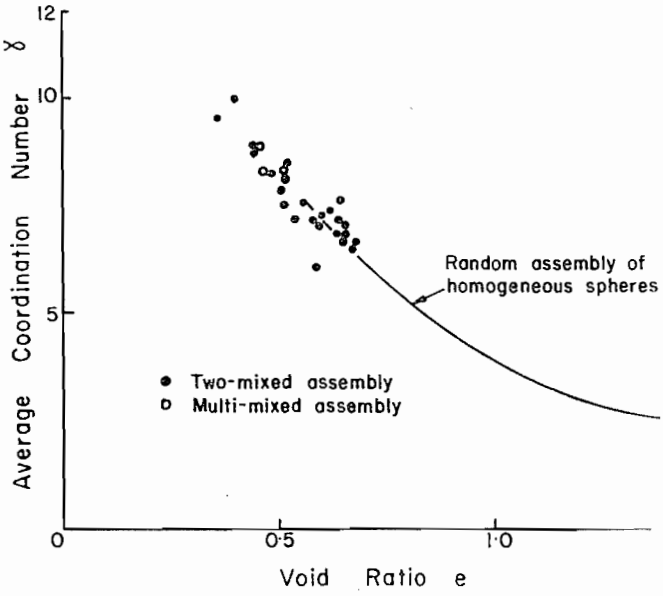

Figure 1.8 Experimental Relationship between Average Coordination Number γ and Void Ratio e
(Oda, 1977)

variety of granular media covering a range of grain-size distributions. The experimental work by these researchers is important because it shows that state parameters such as void ratio (which is a relatively easy parameter to determine in the laboratory) may be related to the average coordination number which, in turn, is considered to be a fundamental characterization of the microstructure of granular assemblies.

Satake (1978)

Satake (1978) pointed out that for plane systems of particles, the distribution of contact normals could be described by a second-order *anisotropy tensor* $\mathbf{C}$ which is defined by the following relationship:

$$\mathbf{C}_{ij} = 2\int_0^{2\pi} E(\theta) n_i^c n_j^c \, d\theta \qquad i,j = 1,2 \tag{1.8}$$

The tensorial description is independent of the form of $E(\theta)$ and reduces to the unit tensor for isotropic assemblies (i.e. for $E(\theta) = 1/2\pi$). Satake recognized that the tensorial description of fabric given by (1.8) is fundamental to the mechanics of granular media. Oda et al. (1982) and Mehrabadi et al. (1982) have proposed a three-dimensional tensorial quantity similar to (1.8) which they have called a *fabric tensor*.

1.6.3 Two-Dimensional Model Tests by Oda and Konishi

Oda and Konishi (1974a, 1974b) and Konishi (1978) report the results of laboratory simple shear and biaxial compression tests on two-dimensional assemblies of discs. The general test arrangement for the simple shear tests is shown on Figure 1.9.

The assemblies consisted of about 400 photo-elastic cylinders with diameters of 0.3, 0.4 or 0.5 cm. The discs were placed in a random manner between two glass plates in the ratio 25 : 15 : 8. Boundary loads and displacements were applied to the assembly through rigid platens. At the start of each test the assemblies were uniaxially loaded with no lateral expansion allowed followed by a shearing force applied through the lower platen. At intervals during shearing, photographs of the assembly were taken and the geometry of contacts and contact force intensity and orientation extracted from photo-elastic isochromatics in the vicinity of contacts.

Using the results of simple shear and biaxial compression tests, Konishi (1978) examined contact orientation anisotropy, contact force anisotropy and average stress in these assemblies. Contact anisotropy was quantified using a method first reported by Curray (1956) for analysis of two-dimensional orientation data. In this procedure an invariant measure of the intensity of preferred

tion $\overline{M}$ and the preferred direction ψ are calculated from:

$$\overline{M} = \frac{1}{\sum_{\theta_g} M_g(\theta_g)} \sqrt{\left(\sum_{\theta_g} M_g(\theta_g) \sin 2(\theta_g)\right)^2 + \left(\sum_{\theta_g} M_g(\theta_g) \cos 2(\theta_g)\right)^2} \tag{1.9}$$

$$\tan 2\psi = \frac{\sum_{\theta_g} M_g(\theta_g) \sin 2(\theta_g)}{\sum_{\theta_g} M_g(\theta_g) \cos 2(\theta_g)}$$

where $M_g(\theta_g)$ represents the number of contacts with the approximate orientation θ_g. Konishi (1978) has interpreted a value of $\overline{M} = 0$ as representing an isotropic assembly and $\overline{M} = 1$ as an assembly exhibiting maximum contact anisotropy.

The invariant stress ratio σ_t/σ_n was calculated from analysis of sub-assemblies of discs occupying approximately the middle two-thirds of the sample. Terms σ_t and σ_n are *deviatoric* and *normal* invariants of stress associated with the Mohr circle of stress.

The results of two simple shear tests using an initially loose assembly ($e_o = 0.26$) and an initially dense assembly of the same discs ($e_o = 0.22$) are given on Figure 1.10. The term *shear distortion* on Figure 1.10 is equal to the tangent angle formed by the upright platens with the vertical. Figure 1.11 shows polar histograms for contact normals at selected intervals during these tests. In a similar manner to the cylindrical samples of sand investigated by Oda (1972a,b,c), the two-dimensional assemblies of discs showed contact generation and loss in preferred directions under load.

Several important observations have been made by Oda and Konishi with respect to the results of their two-dimensional tests:

1) The quantity $\overline{M}$ describing contact normal anisotropy was strongly correlated to the invariant stress ratio σ_t/σ_n. In general, as the shear capacity of the system increased, the anisotropy of contact normals increased.

2) During principal stress rotation the major principal stress direction and the preferred direction of contact normals, ψ, appeared coincident.

3) Frequency distributions of mobilized interparticle friction angle $\phi_{mob} = \tan^{-1}(f_t^c/f_n^c)$ measured at stages in the two-dimensional tests were unimodal about $\phi_{mob} = 0$ (here f_t^c and f_n^c are tangential and normal contact forces respectively). As shown on Figure 1.12, the limiting interparticle friction angle $\phi_{mob} = \phi_\mu$ seldom occurred. The same phenomena have been reported in similar physical experiments employing *oval*-shaped photo-elastic particles (Oda, et al., 1983). These

observations together with frequency distributions of average (total) interparticle forces led Konishi (1978) to the conclusion that the primary mode of interparticle force transmission is through chains of contact forces which act normal to contact planes and in a direction which is essentially coincident with the maximum principal stress direction.

4) Oda and Konishi (1974b) and Konishi (1978) extracted average (total) contact force distributions with respect to orientation and showed that these distributions could be approximated by smooth trigonometric functions.

1.6.4 Rothenburg (1980), Rothenburg and Selvadurai (1981a,b,c)

Rothenburg (1980) reported the results of theoretical investigations into the micromechanical behaviour of idealized granular assemblies comprising discs or spheres.

In this study he showed that the average stress tensor $\overline{\sigma}$ for these systems has the properties of the stress tensor of continuum mechanics but is derived from consideration of discrete contact forces, contact geometry and principles of static equilibrium which together represent an approach foreign to classical continuum mechanics concepts.

A fundamental assumption in this study is that contact forces and contact vectors are *homogeneously* distributed through the granular assembly which contains a very large number of particles. The position independent nature of these parameters allows them to be approximated by continuous distributions representing averages of contact forces and contact vector lengths with respect to orientation. These distributions, which are a statistical description of internal load transmission and fabric, are related to the average stress tensor according to:

$$\overline{\sigma}_{ij} = m_v \int_\Omega \overline{f}_i^c(\Omega)\overline{l}_j^c(\Omega)E(\Omega)\,d\Omega \qquad i,j = 1,2,3 \tag{1.10}$$

where $E(\Omega)$ represents the distribution of contact normals and $d\Omega = \sin\beta\, d\beta\, d\theta$. The constant term in front of the integral expression is the assembly ***contact density*** $m_v = M_V/V$. A similar relationship to (1.10) has been reported by Mehrabadi et al. (1982). To further examine relation (1.10), Rothenburg has considered the two-dimensional analogue to this expression which is:

$$\overline{\sigma}_{ij} = m_v \int_0^{2\pi} \overline{f}_i^c(\theta)\overline{l}_j^c(\theta)E(\theta)\,d\theta \qquad i,j = 1,2 \tag{1.11}$$

Assuming assemblies of equal-sized discs with diameter d_o, expression (1.11) can be decomposed to:

$$\overline{\sigma}_{ij} = \frac{m_v d_o}{2} \int_0^{2\pi} \left(\overline{f}_n^c(\theta)n_i^c n_j^c + \overline{f}_t^c(\theta)t_i^c n_j^c\right) E(\theta)\,d\theta \qquad i,j = 1,2 \tag{1.12}$$

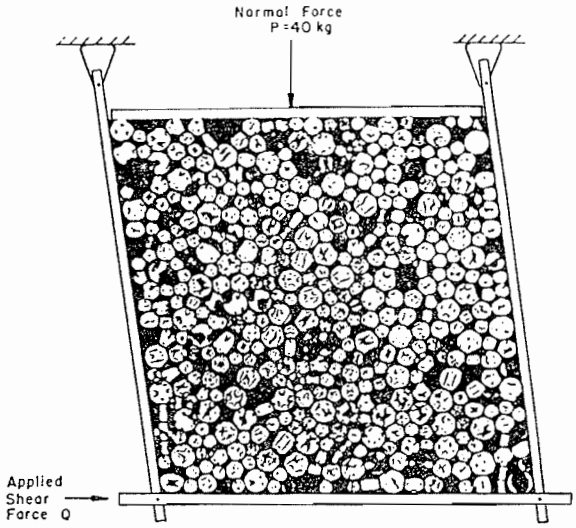

Figure 1.9 Two-Dimensional Simple Shear Test Apparatus
(after Oda and Konishi, 1974a)

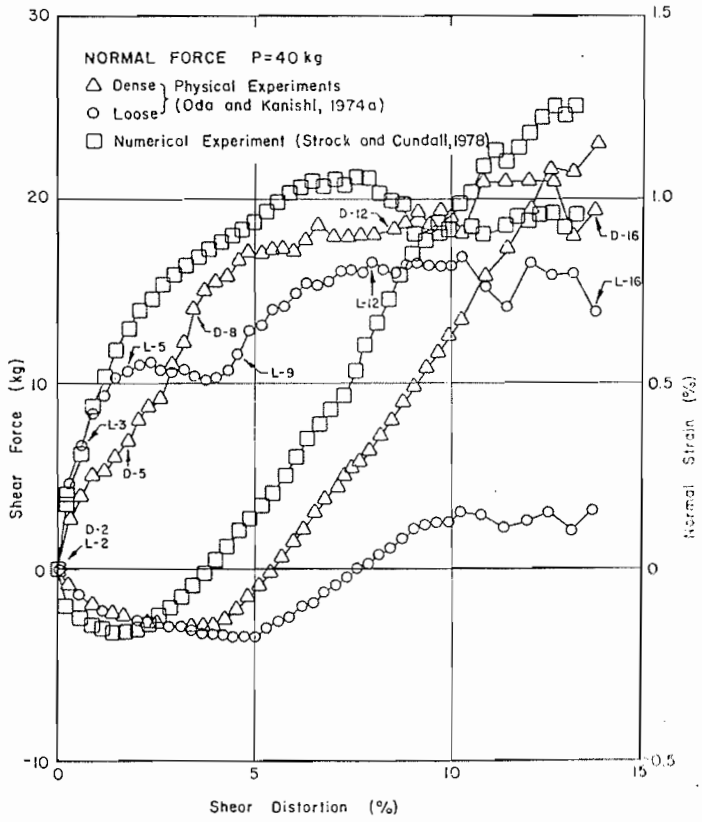

Figure 1.10 Comparison of Physical and Numerical Simple Shear Tests

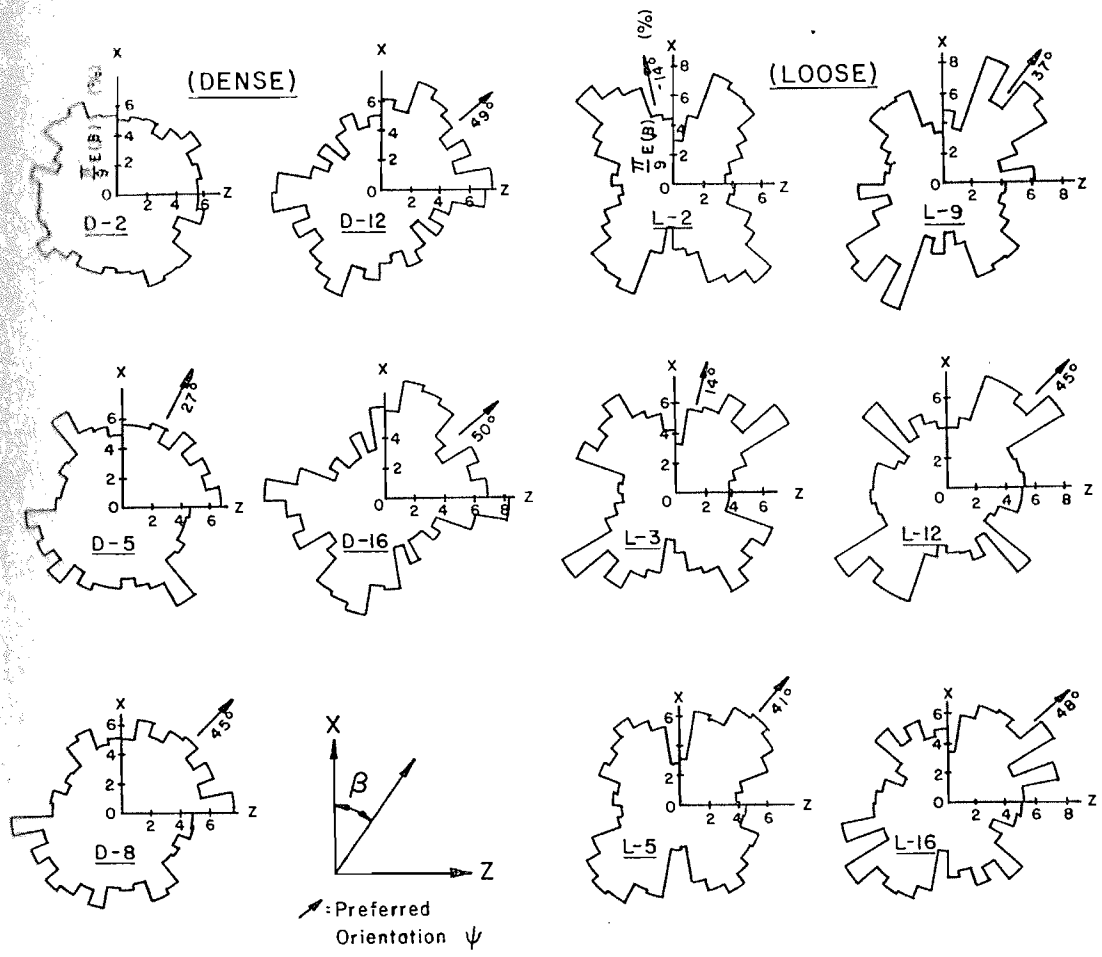

Figure 1.11 Fabric Changes during Simple Shear of Initially Dense and Loose Assemblies of Discs *(after Konishi, 1978)*

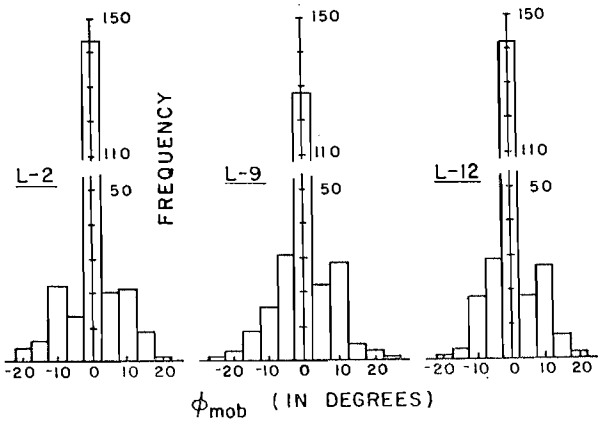

Figure 1.12 Frequency Distributions for Mobilized Interparticle Friction Angle *(after Oda and Konishi, 1974a)*

Here $\hat{n}^c = (\cos\theta, \sin\theta)$ and $\hat{t}^c = (-\sin\theta, \cos\theta)$ are normal and tangential components of contact vectors respectively. Rothenburg (1980) has proposed that the distribution functions $E(\theta)$, $\overline{f}_n^c(\theta)$ and $\overline{f}_t^c(\theta)$ can be described by truncated Fourier series expressions such as:

$$E(\theta) = \frac{1}{2\pi}\{1 + a\cos 2(\theta - \theta_o) + b\cos 4(\theta - \theta_o)\} \tag{1.13}$$

$$\overline{f}_n^c(\theta) = f_n^o\{1 + a_n\cos 2(\theta - \theta_f)\} \tag{1.14}$$

$$\overline{f}_t^c(\theta) = -f_n^o\{a_t\sin 2(\theta - \theta_t)\} \tag{1.15}$$

The non-dimensional parameters a, b, a_n and a_t are *coefficients of anisotropy* which are a measure of the intensity of these distributions in the *directions of anisotropy* denoted by θ_o, θ_f and θ_t respectively. Term f_n^o is the average normal contact force from all assembly contacts. Rothenburg has developed powerful relationships which equate the micromechanical parameters identified above to the macroscale shear capacity of the system. For example, if distributions for average contact force components and contact normals are assumed to have coaxial directions of anisotropy then:

$$\frac{\sigma_t}{\sigma_n} = \frac{1}{2}(a + a_n + a_t) \tag{1.16}$$

Relationship (1.16) shows that the shear capacity of the assembly is due directly to contributions of anisotropy from contact normals a, average normal contact force a_n, and average tangential contact force a_t.

Developments leading to the relationships described above have been summarized by Rothenburg and Selvadurai (1981a,b,c). Verification of relationship (1.16) developed by Rothenburg and Selvadurai for assemblies of equi-diameter discs is a major part of this investigation. It is shown that these relationships retain their form for assemblies comprising a range of disc diameters. Simplifying assumptions leading to this conclusion are carefully examined and their validity is assessed based on the results of numerical simulation.

In Chapter 5 of the current study, a similar relationship for three-dimensional assemblies of spheres or near-spherical particles is proposed. In a recent study by Rothenburg (1985), an equivalent expression has formed the basis of a continuum model for sands. Verification of two-dimensional analogues carried out in this study has proved to be an important step towards verifying the validity of the constitutive model.

1.6.4 Numerical Simulation of Idealized Granular Systems

Numerical simulation of media modelled as a collection of discrete particles is not restricted to granular assemblies. For example, fluids have been modelled as assemblages of *hard discs* or *hard spheres* in two and three dimensions (Bernal, 1964). Hard sphere models have also been used in computer simulation of crystal structure and in molecular dynamics (Ziman, 1979). Regardless of the application, these numerical techniques involve the solution of equations of motion for all particles comprising the system under study.

An explicit finite-difference numerical scheme called the Distinct Block Method (DBM) was first reported by Cundall (1971) as a numerical technique to solve equations of motion for granular assemblies. Specifically, the DBM was used to carry out numerical experiments on planar assemblies of discrete polygon-shaped blocks as an analogue to broken rock masses. The technique was subsequently modified by Strack and Cundall (1978) to simulate the behaviour of two-dimensional assemblies of discs representing idealized granular systems under conditions of loading and unloading. These researchers have developed a FORTRAN-code computer program called BALL which implements the Distinct Element Method (DEM) for assemblies of discs. Principal features of the program BALL and the results of numerical experiments have been reported by Cundall and Strack (1979a,b,c) and Cundall et al. (1982).

The major advantage of numerical simulation of granular media using techniques such as the DEM is that complete information on the system is available at any stage in a test. In addition, the influence of micromechanical properties such as interparticle friction angle and contact stiffness can be assessed more readily from these experiments than from comparable physical (photo-elastic) models.

The above researchers have attempted to validate the prototype program BALL as a useful tool for the investigation of the mechanical behaviour of idealized granular systems. The first validation exercise is reported by Strack and Cundall (1978) and was an attempt to reproduce the macroscale force-displacement response of the *dense* two-dimensional simple shear test reported by Oda and Konishi (1974a). The physical test has been described in the previous section. In the numerical simulation, the size distribution of discs was identical to the physical test but they were placed in an alternative random manner. With the exception of interparticle friction, disc properties were assumed by Strack and Cundall based on experience with the program BALL.

The results of the numerical simulation have been presented together with the physical test data on Figure 1.10. The numerical test, at least qualitatively, appears to behave in a similar manner to the dense assembly. The fact that the numerical test is more dilatant than the dense physical test

may be due in part to the greater initial density achieved by Strack and Cundall. By repeating the experiment with a less dense sample and different values of selected parameters, such as disc density and contact stiffness, Cundall and Strack believe that the laboratory results could be duplicated more closely.

The second validation attempt was to numerically duplicate a test on photo-elastic discs reported by De Josselin De Jong and Verruijt (1969). The results of this computer simulation can be found in Cundall and Strack (1979a). Some major differences exist between the laboratory investigation and the numerical simulation. For example, initial laboratory loading conditions are not reported by De Josselin De Jong and Verruijt and contact friction angles and contact stiffnesses had to be assumed in the computer simulation. In addition, the physical test was carried out under force-controlled boundary conditions while the numerical simulation employed strain-controlled boundaries. Nevertheless, the distribution and relative magnitude of contact forces from the numerical tests were qualitatively similar to those shown on Figure 1.1a.

The current investigation uses a heavily-modified version of the original program BALL called DISC but preserves the fundamental aspects of the DEM. Details of the DEM and its implementation using program DISC are given in Chapter 4.

CHAPTER 2

THEORETICAL DEVELOPMENTS

2.1 Introduction

Chapter 2 outlines the development of the fundamental relationship (1.6) proposed by Weber (1966) for discrete particulate systems in static equilibrium. This relationship equates a *macroscopic stress tensor* acting at the boundary of an infinitely large system to volume-additive quantities describing all assembly contact force and contact vector length components. The approach adopted in the current development follows very closely that used by Rothenburg and Selvadurai (1981b) for dynamic assemblies.

It is shown that the macroscopic stress tensor proposed by Weber (1966) is identical to the average stress tensor proposed by Hill (1963) and both quantities are considered to have the properties of the stress tensor used in continuum mechanics.

Next, theoretical developments are simplified by considering assemblies of spheres. A statistical mechanics approach is adopted which considers only certain averages of statically admissible contact force components together with average contact density and the distribution of contact normals. These average expressions are related in an integral form to the average stress tensor of the assembly in a development which is similar to Rothenburg (1980).

Finally, it is shown that assembly microstructure can be described by a *fabric tensor* of the same rank as the second-order stress tensor. The distribution of contact normals can be visualized as a three-dimensional surface described by a second-order equation.

2.2 Macroscopic Stress Tensor from External Applied Forces

Consider a three-dimensional assembly of rigid particles of arbitrary shape contained within a continuous smooth boundary. A two-dimensional analogue to such an assembly is shown in the Cartesian coordinate space on Figure 2.1. Tractions acting on the boundary S at $\tilde{R}$ may be specified in terms of a stress tensor σ_{ij}^{β} such that:

$$T_i^{\beta}(\tilde{R}) = \sigma_{ij}^{\beta} n_j(\tilde{R}) \qquad i,j = 1,2,3 \tag{2.1}$$

where $\tilde{n}$ denotes the exterior unit normal acting at $\tilde{R}$. Equation (2.1) corresponds to Cauchy's fundamental theorem for continuum. However, it should be noted that the tractions acting at the boundary of the *discontinuum* idealized on Figure 2.1 correspond to tractions which would act on the

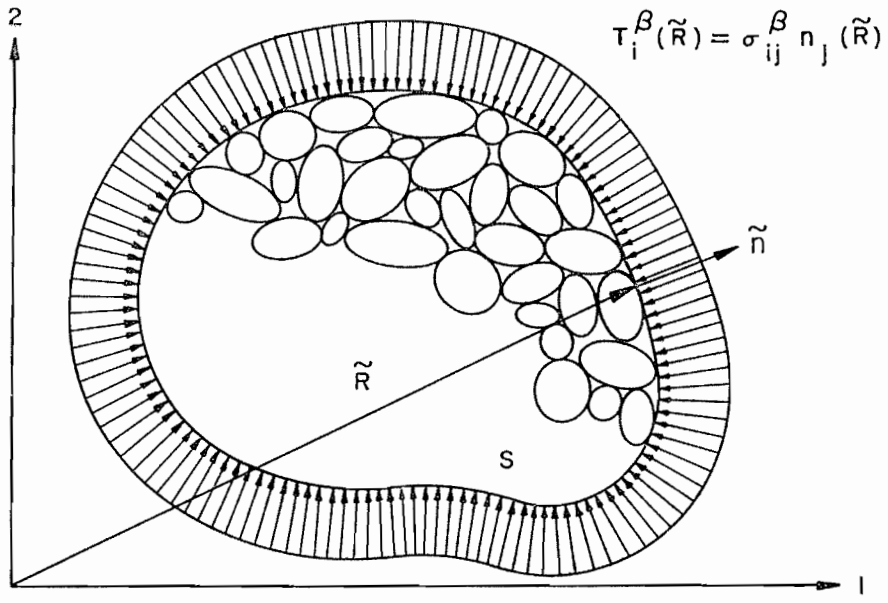

Figure 2.1 External Tractions Applied to a Smooth Boundary

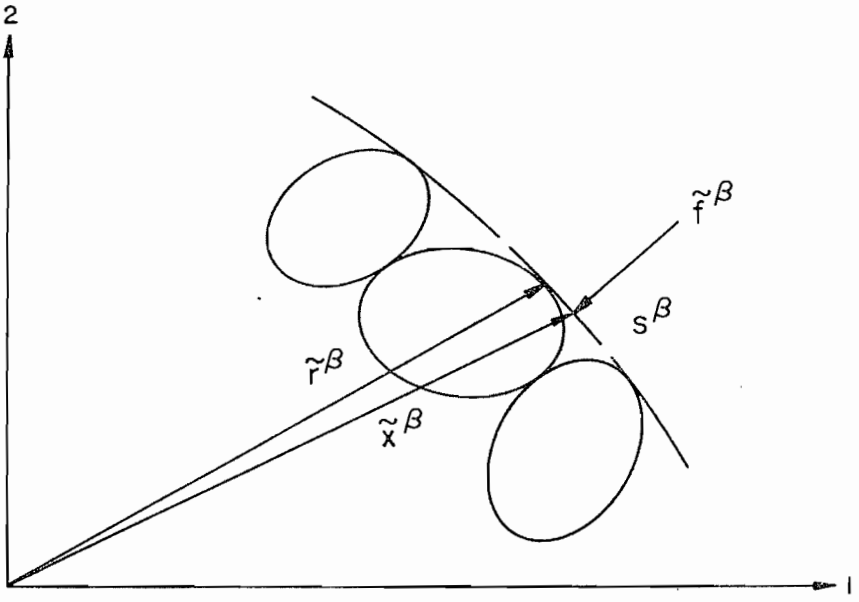

Figure 2.2 Equivalent Forces Applied to Partitioned Boundary

boundary of a similar uniformly stressed continuum. The tensor quantity σ_{ij}^{β} is introduced at this stage only to describe boundary tractions and cannot be identified as the stress tensor of continuum mechanics.

If the boundary surface S is partitioned into segment areas S^{β} as shown on Figure 2.2 then, the equivalent boundary force $\tilde{f}^{\beta}$ at the segment may be expressed in component form as:

$$f_i^{\beta} = \int_{S^{\beta}} T_i^{\beta}(\tilde{R})\, dS \tag{2.2}$$

Now let $\tilde{x}^{\beta}$ represent the location of the equivalent boundary force on S^{β} and $\tilde{r}^{\beta}$ the intersection point of the boundary particle with the boundary segment. For assembly volumes where $\tilde{x}^{\beta}$ and $\tilde{r}^{\beta}$ are large with respect to segment boundary areas and particle dimensions then, $x_j^{\beta} \simeq r_j^{\beta}$.

If a judicious choice of boundary partitioning is allowed then, the above approximation could be made exact and equivalent boundary forces could be applied directly to boundary contact points. Alternatively, a non-rigorous argument to justify an exact expression is that *on average* the expression holds and the global response of the assembly is insensitive to the approximation for large volumes and a great number of particles.

Using $x_j^{\beta} = r_j^{\beta}$, expression (2.2) can now be rewritten as:

$$f_i^{\beta} r_j^{\beta} = \int_{S^{\beta}} T_i^{\beta}(\tilde{R}) x_j^{\beta}\, dS \tag{2.3}$$

Substituting (2.1) into (2.3) leads to:

$$f_i^{\beta} r_j^{\beta} = \int_{S^{\beta}} \sigma_{ik}^{\beta} n_k(\tilde{R}) x_j^{\beta}\, dS \tag{2.4}$$

Addition of all contributing boundary contacts and integration of the right-hand side over the entire boundary surface, S, using the Gauss-Green theorem gives:

$$\sum_{\beta \epsilon S} f_i^{\beta} r_j^{\beta} = V \sigma_{ij}^{\beta} \tag{2.5}$$

Relationship (1.3) proposed by Hill (1963) can be recovered from expressions (2.3) and (2.5) assuming compensated boundary moments (i.e. $T_i^{\beta}(\tilde{R}) x_j^{\beta} = T_j^{\beta}(\tilde{R}) x_i^{\beta}$, $i \neq j$). Expression (2.5) has also been reported by Drescher and De Josselin De Jong (1972), Strack and Cundall (1978) and Mehrabadi et al. (1982) among others.

2.3 Macroscopic Stress Tensor Description from Internal Distribution of Contact Forces and Microstructure

Conditions of static equilibrium for a single particle k requires that:

$$\sum_{n=1}^{n_k} f_i^{n,k} = 0 \qquad i,j = 1,2,3 \tag{2.6}$$

where n_k represents the number of contacts associated with particle k. Terms $f_i^{n,k}$ in expression (2.6) refer to contact force components acting on particle k from particle n. In this development, contact forces are assumed to act at a point and, consequently, transfer of moments across physical contacts is not considered.

No loss in generality occurs if each force component in (2.6) is multiplied in turn by the r_j^k position component of the particle centroid. This operation leads to nine equations of the form:

$$\sum_{n=1}^{n_k} f_i^{n,k} r_j^k = 0 \tag{2.7}$$

The geometrical arrangement between contacting particles located at the interior of the assembly is shown on Figure 2.3. The geometrical arrangement of a boundary particle is given on Figure 2.4.

If the summation (2.7) is considered for all N particles in the assembly (interior and boundary particles) then:

$$\sum_{k=1}^{N} \sum_{n=1}^{n_k} f_i^{n,k} r_j^k = 0 \tag{2.8}$$

As shown on Figure 2.3, each interior physical contact contributes contact forces such that:

$$\tilde{f}^{n,k} + \tilde{f}^{k,n} = 0 \tag{2.9}$$

In addition, interior contact geometry gives:

$$r_j^k - r_j^n = l_j^{n,k} - l_j^{k,n} \tag{2.10}$$

where $\tilde{l}^{n,k}$ represents the *contact vector* directed from the centroid of particle n to the contact with particle k.

Terms contained within (2.8) representing non-boundary contacts can be collected together in pairs such as:

$$(f_i^{k,n} r_j^n + f_i^{n,k} r_j^k) \tag{2.11}$$

From (2.9) and (2.10) the above expression is equivalent to:

$$-(f_i^{k,n} l_j^{n,k} + f_i^{n,k} l_j^{k,n}) \tag{2.12}$$

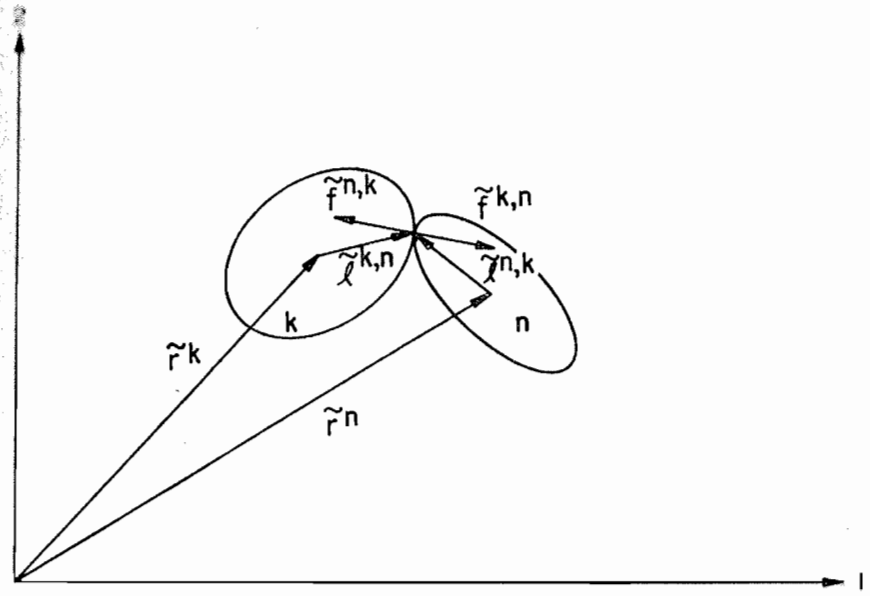

Figure 2.3 Geometry of Interior Contact

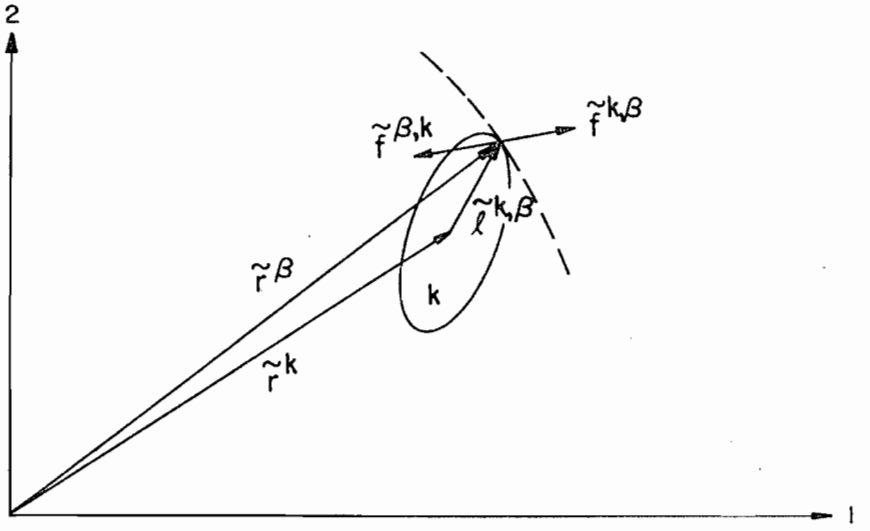

Figure 2.4 Geometry of Boundary Contact

Or, in general, contacts in the above summation (2.8) appear as:

$$-f_i^c l_j^c \tag{2.13}$$

Now consider the contribution of boundary contacts to the general expression (2.8). From Figure 2.4 these contributions will appear such as:

$$f_i^{k,\beta} r_j^k \tag{2.14}$$

Components of the contact vector $\tilde{l}^{k,\beta}$ for a boundary contact and the position vector $\tilde{r}^k$ for the boundary particle centroid are related by:

$$r_j^k + l_j^{k,\beta} = r_j^\beta \tag{2.15}$$

Terms (2.14) can now be expanded to:

$$-f_i^{k,\beta} l_j^{k,\beta} + f_i^{k,\beta} r_j^\beta \tag{2.16}$$

Hence, each boundary contact contributes an internal contact term of the form (2.13) and a boundary contact term of the form given by expression (2.5). Summation of all terms in (2.14) and expression (2.5) gives:

$$\sigma_{ij}^\beta = \frac{1}{V} \sum_{c \varepsilon V} f_i^c l_j^c \tag{2.17}$$

where $c \varepsilon V$ denotes summation with respect to contacts *within* and *on* the boundary of the assembly.

It can be noted that certain subsets of (2.8) must satisfy the condition of moment equilibrium for each particle. Specifically:

$$\sum_{n=1}^{n_k} (f_i^{n,k} l_j^{n,k} - f_j^{n,k} l_i^{n,k}) = 0 \qquad i \neq j \tag{2.18}$$

The development leading to equation (2.17) shows that the macroscopic stress tensor for an idealized granular system can be developed from consideration of statically admissible contact forces and microstructure described by contact vectors. This equation is a direct consequence of equations of static equilibrium in a system in which boundary tractions are specified in terms of σ_{ij}^β. Although the system is indeterminant, the sum of the combinations $f_i^c l_j^c$ is constrained by conditions of static equilibrium.

Expression (2.17) has also been reported by Weber (1966), Dantu (1968), Rothenburg (1980) and Christoffersen et al. (1981).

2.4 Average Stress Tensor for Discrete Particulate Systems

Tensor σ_{ij}^{β} was introduced here as a quantity specifying boundary loads on a statistically homogeneous discrete particulate system. If sums of force-contact vector components in (2.17) are evaluated for any subregion of the assembly then, it would fluctuate from volume to volume. However, as the subdomains increase in volume and number of particles, these fluctuations can be expected to become smaller and smaller. This tendency to a single representative *average stress tensor* is assured by the composition of the function where each term makes a small contribution to $\frac{1}{V} f_i^c l_j^c$. Only in the limit of an infinite assembly does σ_{ij}^{β} become volume independent and possess properties of the stress tensor of continuum mechanics. It should be noted that a continuum is an abstract entity that physically corresponds to a system comprising an infinite number of particles per unit volume. In any practical situation, physical volumes of interest indeed contain a large number of particles. Expression σ_{ij}^{β} as a stress tensor applied to finite but large volumes is an accurate analogue of the stress tensor used in continuum mechanics. Rothenburg and Selvadurai (1981b) have shown that for particulate systems, stress tensor (2.17) gives a gross traction $\tilde{T}$ acting on a plane with normal $\tilde{n}$ according to the Cauchy relationship (2.1). As a result of the arguments presented above, the average stress tensor $\overline{\sigma}$ and the boundary stress tensor σ^{β} are assumed equivalent in further discussions and $\sigma_{ij} = \overline{\sigma}_{ij} = \sigma_{ij}^{\beta}$.

Like the stress tensor of classical continuum mechanics, the quantity σ_{ij} is a second-order symmetric tensor. Symmetry is due to the condition of moment equilibrium for each particle (2.18) which, when considered over the entire assembly leads to:

$$\sigma_{ij} - \sigma_{ji} = \frac{1}{V} \sum_{c \epsilon V} (f_i^c l_j^c - f_j^c l_i^c) = 0 \qquad i \neq j \tag{2.19}$$

Unfortunately, calculation of the average stress tensor using relation (2.17) requires exact knowledge of contact forces and contact vector terms for all particles. However, as the next section shows, equivalent more manageable expressions for the average stress tensor can be developed by considering certain averages of contact forces and microstructural properties over assembly volumes approaching the infinite.

2.5 Average Stress Tensor from Averages of Contact Forces and Microstructure

Consider the unit spherical coordinate system shown on Figure 2.5 where $0 \leq \beta \leq \pi$ and $0 \leq \theta \leq 2\pi$. Imagine that average values of the product terms $f_i^c l_j^c$ are calculated from all contacts whose contact vectors fall within the elemental solid angle $\Delta\Omega = \sin\beta \, \Delta\beta \, \Delta\theta$. Product terms in the summation (2.17) corresponding to the same interval $\Delta\Omega$ can be approximated by group averages

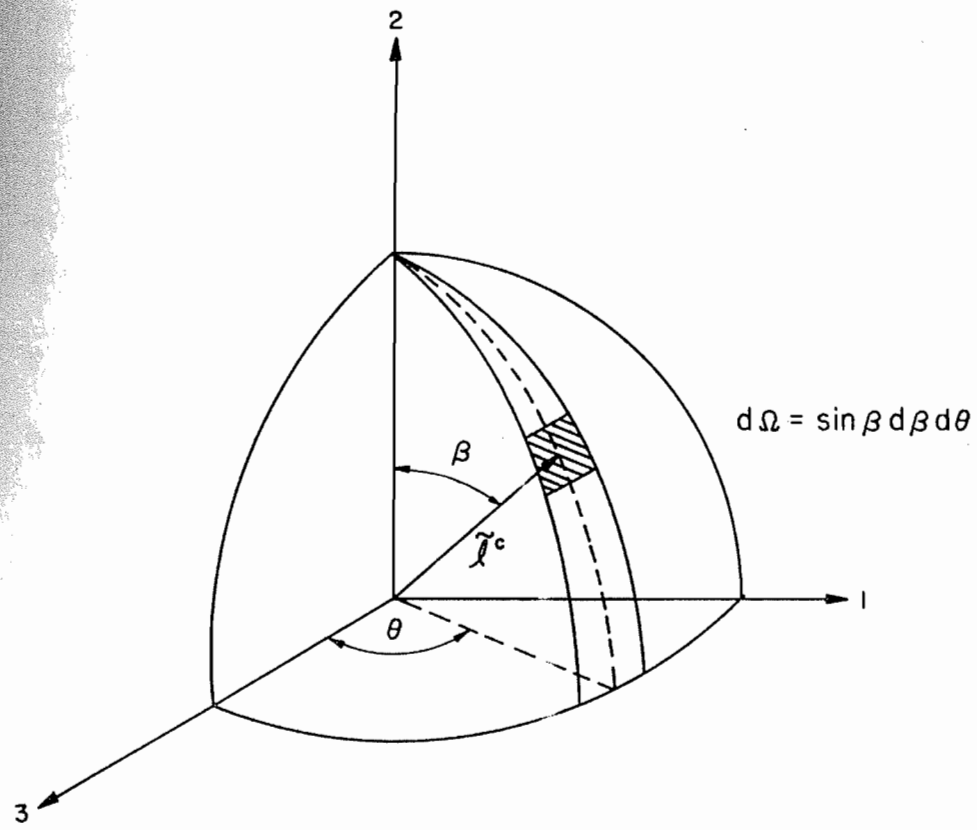

Figure 2.5 Contact Vector Orientation in Spherical Coordinate System (unit sphere radius = 1)

expressed as $\overline{f_i^c l_j^c}(\Omega_g)$ where Ω_g denotes the group orientation. Such a rearrangement is permissible since $f_i^c l_j^c$ terms are position independent. However, if group averages are used, a quantity representing the number of contacts in each group must be included to preserve relation (2.17). In similar developments by Rothenburg (1980) and Mehrabadi et al. (1982), a normalized discontinuous function $E(\Omega)$ has been used to describe the distribution of contacts with respect to contact vector orientation. The fraction of total assembly contacts (or contact vectors) associated with the group Ω_g is related to $E(\Omega)$ by:

$$M_g(\Omega_g) = M_V\, E(\Omega) \sin\beta\, \Delta\beta\, \Delta\theta \tag{2.20}$$

where M_V denotes the total number of assembly contacts. Summation over all assembly contacts gives:

$$\sum_{\Omega_g} E(\Omega)\, \Delta\Omega = 1 \tag{2.21}$$

It is now convenient to introduce a *contact density* term m_v, which is a measure of the average intensity of particle packing (Rothenburg, 1980), and is defined as:

$$m_v = \frac{M_V}{V} \tag{2.22}$$

The average stress tensor expression (2.17) can now be approximated by:

$$\sigma_{ij} = m_v \sum_{\Omega_g} \overline{f_i^c l_j^c}(\Omega) E(\Omega)\, \Delta\Omega \qquad i,j = 1,2,3 \tag{2.23}$$

Clearly, as the averaging interval approaches zero the exact relationship (2.17) is recovered.

The step from (2.17) to (2.23) presupposes that contacts or chains of contacts are distributed homogeneously over the considered volume. This spatially *random* distribution is then consistent with the concept that σ_{ij} represents an average stress condition for large systems.

Further study of the relationship between the average stress tensor, contact forces and microstructure is greatly facilitated if (2.23) can be rewritten as:

$$\sigma_{ij} = m_v \sum_{\Omega_g} \overline{f}_i^c(\Omega) \overline{l}_j^c(\Omega) E(\Omega)\, \Delta\Omega \tag{2.24}$$

For this step to be valid however, distributions of f_i^c and l_j^c must be uncorrelated.

Now consider an assembly with a large volume and a great number of particle contacts. The discontinuous function $E(\Omega)$ can be considered to approach a continuous distribution function similar to that proposed by Horne (1965). Expression (2.20) becomes:

$$M_g(\Omega_g) = M_V \int_{\Omega_g} E(\Omega)\, d\Omega \tag{2.25}$$

and satisfies the constraint:

$$\int_{\Omega} E(\Omega)\, d\Omega = 1 \tag{2.26}$$

For isotropic assemblies (i.e. assemblies with no preferred contact vector orientation) $E(\Omega) = 1/4\pi$.

Using a similar argument, distributions $\overline{f}_i^c(\Omega)$ and $\overline{l}_j^c(\Omega)$ can be expected to loose their discontinuous appearance and approach smooth distributions for assemblies comprising a great number of particles. Assuming an assembly with $\lim_{V\to\infty}$, $\lim_{M_V\to\infty}$ and $\lim_{\Delta\Omega\to 0}$, relation (2.24) can be expressed in integral form as:

$$\sigma_{ij} = m_v \int_{\Omega} \overline{f}_i^c(\Omega)\overline{l}_j^c(\Omega) E(\Omega)\, d\Omega \tag{2.27}$$

The limiting operations used above are required at this stage in order to approximate a large discrete mechanical system which is mathematically intractable, by an infinite continuous mechanical system which is mathematically manageable.

Relationship (2.27) is similar to expressions proposed by Rothenburg (1980), Rothenburg and Selvadurai (1981a,b) and Mehrabadi et al. (1982). At this point in the development, the form of the functions describing the distributions in (2.27) is unknown and their mutual independence is only assumed. It is likely, for example, that $\overline{l}_j^c(\Omega)$ is a complex expression since it must include the influence of particle shape and particle size-distribution.

Expression (2.27) can be simplified if an idealized granular assembly of equi-diameter spheres is considered. For spheres of constant diameter d_o, the distribution of contact vectors becomes:

$$\overline{l}_j^c(\Omega) = \frac{d_o}{2} n_j^c(\Omega) \tag{2.28}$$

where $\tilde{n}^c$ denotes the exterior unit normal to the (tangent) contact plane. In fact, for any size distribution of spheres, the contact geometry for these assemblies will be greatly simplified since contact normals will be coincident with contact vectors. For an assembly of equi-diameter spheres, equations (2.27) and (2.28) lead to:

$$\sigma_{ij} = \frac{m_v d_o}{2} \int_{\Omega} \overline{f}_i^c(\Omega) n_j^c(\Omega) E(\Omega)\, d\Omega \tag{2.29}$$

Expression (2.29) has been proposed in the same form by Rothenburg (1980) and can be recovered from general expressions reported by Mehrabadi et al. (1982).

While some mathematical simplicity is introduced by considering equi-diameter spheres, an assembly comprising equi-dimensional particles (of any shape) is a unique condition not found in natural granular systems.

For an idealized granular assembly comprising a range of particle diameters, equation (2.29) can be modified to:

$$\sigma_{ij} = m_v \bar{l}_o \int_\Omega \overline{f}_i^c(\Omega) n_j^c(\Omega) E(\Omega)\, d(\Omega) \tag{2.30}$$

where $\bar{l}_o$ represents the *average contact length* for the assembly. Implicit in (2.30) is the assumption that average contact length is independent of contact vector orientation over the range of particle diameters present in the system (i.e. $\overline{l}^c(\Omega) = \bar{l}_o$).

An additional simplification results from consideration of spherical particles. The contact distribution function is symmetrical with $E(\Omega) = E(-\Omega)$. This symmetry is a consequence of each physical contact contributing two contacts with opposite directions. It may be convenient to use $2E(\Omega)$ where integration is carried out over the half-unit sphere $\Omega_{1/2}$ corresponding to the limits $0 \leq \beta \leq \pi/2$ and $0 \leq \theta \leq 2\pi$. Hence (2.30) can be rewritten as:

$$\sigma_{ij} = 2m_v \bar{l}_o \int_{\Omega 1/2} \overline{f}_i^c(\Omega) n_j^c(\Omega) E(\Omega)\, d\Omega \tag{2.31}$$

2.6 Fabric Tensor

Satake (1978) and Rothenburg (1980) have pointed out that the distribution of contact normals in granular systems can be described by a certain second-order tensor. Oda et al. (1980) and Mehrabadi et al. (1982) have proposed a similar quantity which they have identified as a *fabric tensor*.

Consider expression (2.20) in the form:

$$\frac{M_g(\Omega_g)}{V} = m_v E(\Omega)\, \Delta\Omega \tag{2.32}$$

No loss in generality occurs if left and right-hand sides are multiplied by the scalar products $n_i^c(\Omega_g) n_j^c(\Omega_g)$ where $\tilde{n}^c(\Omega_g)$ represents the contact group orientation. The result of these operations is nine equations of the form:

$$\frac{M_g(\Omega_g)}{V} n_i^c(\Omega_g) n_j^c(\Omega_g) = m_v E(\Omega) n_i^c(\Omega_g) n_j^c(\Omega_g)\, \Delta\Omega \qquad i,j = 1,2,3 \tag{2.33}$$

Taking all contacts over Ω and $\lim_{M_V \to \infty}$, $\lim_{\Delta\Omega \to 0}$ for an infinite assembly gives:

$$\mathbf{R}_{ij} = \frac{1}{V} \sum_{c \varepsilon V} n_i^c n_j^c = m_v \int_\Omega E(\Omega) n_i^c n_j^c\, d\Omega \tag{2.34}$$

where $\tilde{n}^c$ is the contact normal orientation.

The quantity $\mathbf{R}_{ij}$ represents a three-dimensional second-order *fabric tensor*. Tensor $\mathbf{R}$ carries all essential information on the geometrical arrangement of assemblies comprising spheres or near-spherical particles. Examination of (2.34) shows that the fabric tensor is symmetrical with $\mathbf{R}_{ij} = \mathbf{R}_{ji}$

for $i \neq j$ and can be expressed either in terms of discrete information or, in terms of a suitably selected distribution function $E(\Omega)$. For an assembly with isotropic microstructure, the fabric tensor reduces to $\mathbf{R}_{ij} = m_v \delta_{ij}$ where δ_{ij} is the Kronecker delta (i.e. $\delta_{ij} = 1$ for $i = j$ and, $\delta_{ij} = 0$ for $i \neq j$).

A fabric tensor $\mathbf{F}$ proposed by Oda et al. (1980) and Mehrabadi et al. (1982) for assemblies of spheres is related to the fabric tensor $\mathbf{R}$ by:

$$\mathbf{F}_{ij} = \bar{l}_o \mathbf{R}_{ij} \tag{2.35}$$

In this study the fabric tensor $\mathbf{R}$ is preferred since use of this descriptor implies (correctly) that the micromechanical behaviour of systems differing only by a scaling term $\bar{l}_o$, is identical.

In an analogous manner to the stress tensor in continuum mechanics, *principal* fabric values can be associated with the fabric tensor. In the same way that the state of stress at a point can be described in *principal stress space*, the distribution of contacts can be described in a *principal fabric space*. Principal fabric tensor values $\mathbf{R}_1$, $\mathbf{R}_2$ and $\mathbf{R}_3$ can be found from the characteristic equation of $\mathbf{R}$. This equation is cubic and in determinant form can be written as:

$$|\mathbf{R}_{ij} - \mathbf{R}\delta_{ij}| = 0 \tag{2.36}$$

Invariant scalar quantities similar to the *octahedral normal stress* and *octahedral shear stress* of principal stress space can be defined for the contact density distribution. In this study these parameters are denoted as the *normal* $\mathbf{R}_n$ and *deviatoric* $\mathbf{R}_t$ invariant quantities of $\mathbf{R}$. The normal invariant is proportional to the first invariant of $\mathbf{R}$ and has constant value. Specifically:

$$\mathbf{R}_n = \frac{\mathbf{R}_{kk}}{3} = \frac{m_v}{3} \tag{2.37}$$

The deviatoric invariant is proportional to the square root of the second invariant of the *deviator* fabric tensor $\mathbf{R}'$ and can be calculated from:

$$\mathbf{R}_t = \sqrt{\frac{\mathbf{R}'_{ij}\mathbf{R}'_{ij}}{3}} = \frac{1}{3}\sqrt{(\mathbf{R}_1 - \mathbf{R}_2)^2 + (\mathbf{R}_2 - \mathbf{R}_3)^2 + (\mathbf{R}_1 - \mathbf{R}_3)^2} \tag{2.38}$$

The deviator fabric tensor $\mathbf{R}'$ is related to the fabric tensor $\mathbf{R}$ in the following manner:

$$\mathbf{R}'_{ij} = \mathbf{R}_{ij} - \frac{\mathbf{R}_{kk}}{3}\delta_{ij} \tag{2.39}$$

By virtue of the fabric tensor definition adopted in this development, the deviatoric invariant quantity $\mathbf{R}_t$ is considered to be a fundamental characterization of anisotropic microstructure in idealized granular systems.

2.7 Fabric Tensor and Contact Distribution Function from Laboratory Data

It is useful to consider expressions for $E(\Omega)$ which can be visualized as three-dimensional surfaces with certain axes of symmetry. The general form of equations describing these surfaces is:

$$\begin{aligned} E(\Omega) &= \frac{1}{4\pi}\{1 + a_{ij} n_i^c n_j^c\} \qquad i,j = 1,2,3 \\ a_{ij} &= a_{ji} \qquad i \neq j \\ a_{kk} &= 0 \end{aligned} \tag{2.40}$$

Contact normal components n_i^c are related to the unit spherical coordinate system on Figure 2.5 according to:

$$\begin{aligned} n_1^c &= \sin\beta \sin\theta \\ n_2^c &= \cos\beta \\ n_3^c &= \sin\beta \cos\theta \end{aligned} \tag{2.41}$$

Coefficient terms in (2.40) can be equated to tensorial quantities associated with the symmetrical fabric tensor **R**. Equation (2.40) is simplified if we assume that principal directions of the fabric tensor are coincident with the (orthogonal) axes on Figure 2.5. In this case, the normalized contact distribution function $E(\Omega)$ can be expressed as:

$$E(\Omega) = \frac{1}{4\pi}\left\{1 + a_1 (n_1^c)^2 + a_2 (n_2^c)^2 + a_3 (n_3^c)^2\right\} \tag{2.42}$$

Parameters a_1, a_2 and a_3 are called *coefficients of principal contact normal anisotropy* or *coefficients of contact anisotropy* for brevity. These coefficients are related to the intensity of contact normals in principal contact directions coincident with the base unit vectors e_1, e_2 and e_3. For an isotropic distribution of contacts, coefficients of contact anisotropy are zero. A positive coefficient term implies a contact density in the corresponding principal direction which is greater than that expected for an isotropic assembly. Conversely, $a_i < 0$ implies that contact density is reduced below the density associated with an isotropic sample. Figure 2.6 shows isotropic and anisotropic contact normal distributions generated using relationship (2.42). Among a small number of researchers in the field of micromechanics, the distinctive shape corresponding to an anisotropic distribution of contact normals has been affectionately identified as a *peanut*.

A contact distribution function of the form (2.42) and expressions (2.34) lead to the following relationships between principal values of the second-order fabric tensor **R** and coefficients of contact

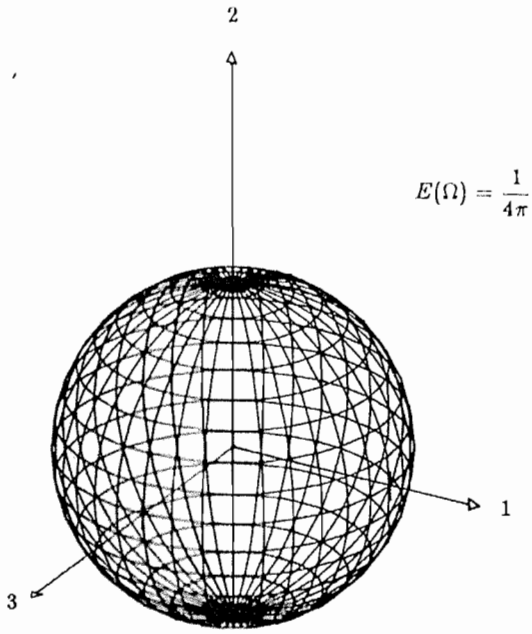

a) Isotropic Contact Normal Distribution

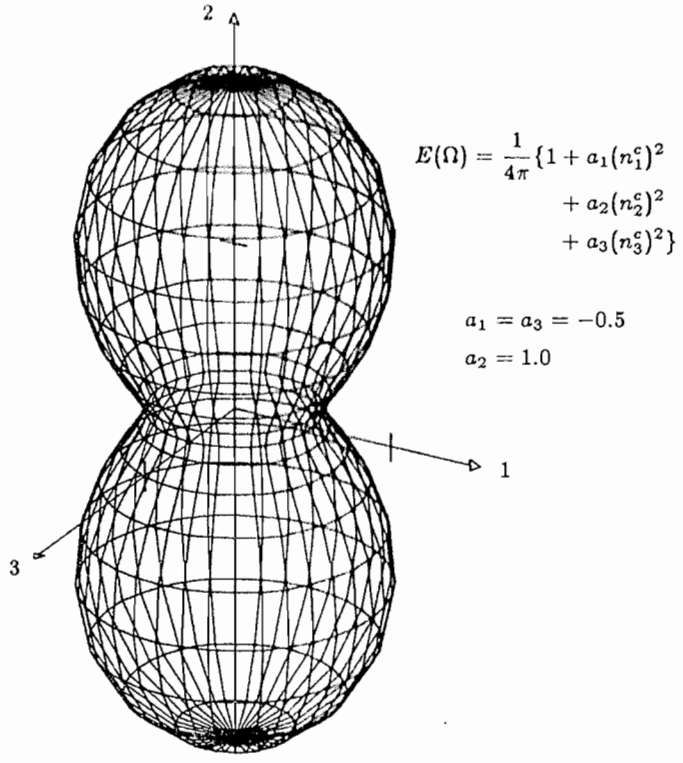

b) Anisotropic Contact Normal Distribution

Figure 2.6 Contact Normal Distributions as Three-Dimensional Surfaces

anisotropy:

$$\begin{aligned}\frac{\mathbf{R}_1}{\mathbf{R}_{kk}/3} &= 1 + (3a_1 + a_2 + a_3)/5 \\ \frac{\mathbf{R}_2}{\mathbf{R}_{kk}/3} &= 1 + (a_1 + 3a_2 + a_3)/5 \\ \frac{\mathbf{R}_3}{\mathbf{R}_{kk}/3} &= 1 + (a_1 + a_2 + 3a_3)/5\end{aligned} \tag{2.43}$$

Similarly, the deviatoric invariant fabric quantity $\mathbf{R}_t$ can be equated to coefficient terms from:

$$\frac{\mathbf{R}_t}{\mathbf{R}_{kk}/3} = \frac{2}{15}\sqrt{(a_1 - a_2)^2 + (a_1 - a_3)^2 + (a_2 - a_3)^2} \tag{2.44}$$

Oda (1972b) reports the results of a study directed at measuring fabric evolution in sand samples during drained triaxial compression testing. A reasonable assumption for these tests is that the distribution of contact normals is symmetrical about the vertical axis. Referring to Figure 2.5, this condition implies $E(\theta, \beta) = E(\beta)$ where axis 2 represents the vertical direction. For this axi-symmetric condition the contact distribution function reduces to:

$$E(\beta) = \frac{1}{4\pi}\{1 + a_2(2 + 3\cos\beta)/4\} \tag{2.45}$$

Principal fabric tensor terms $\mathbf{R}_i$ and the deviatoric invariant $\mathbf{R}_t$ are now uniquely related to a single coefficient of anisotropy a_2 by:

$$\frac{\mathbf{R}_2}{\mathbf{R}_{kk}/3} = 1 + 2a_2/5$$

$$\frac{\mathbf{R}_1}{\mathbf{R}_{kk}/3} = \frac{\mathbf{R}_3}{\mathbf{R}_{kk}/3} = 1 - a_2/5 \tag{2.46}$$

$$\frac{\mathbf{R}_t}{\mathbf{R}_{kk}/3} = \sqrt{2}a_2/5 \tag{2.47}$$

Fabric tensor terms can be extracted from axi-symmetric contact normal data using expressions (2.34) and a_2 calculated using relationships (2.46). This procedure has been applied to the test data shown on Figure 1.5 which has been reported by Oda (1972b).

Figures 2.7a and 2.7b show the macroscopic stress-strain behaviour of this test. Figure 2.7c shows a plot of coefficients of contact anisotropy a_1, a_2 and a_3 plotted against deviatoric strain ($\varepsilon_t = \varepsilon_{11} - \varepsilon_{22}$). Also presented on the figure are values of the invariant stress ratio $a_\sigma = (\sigma_{11} - \sigma_{22})/(\sigma_{11} + 2\sigma_{22})$ plotted against ε_t. The following observations can be made with respect to the evolution of second-order contact anisotropy under monotonic triaxial compression: The magnitude of contact anisotropy increases during both volumetric compression and sample dilation. Even at large strain, the data shows an increase in contact anisotropy between peak principal stress ratio and ultimate sample failure.

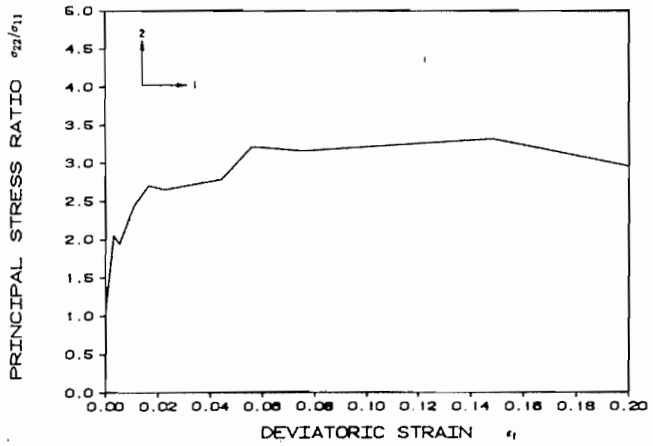

a) Principal Stress Ratio σ_{22}/σ_{11} versus Deviatoric Strain ε_t $(\varepsilon_t = \varepsilon_{11} - \varepsilon_{22})$

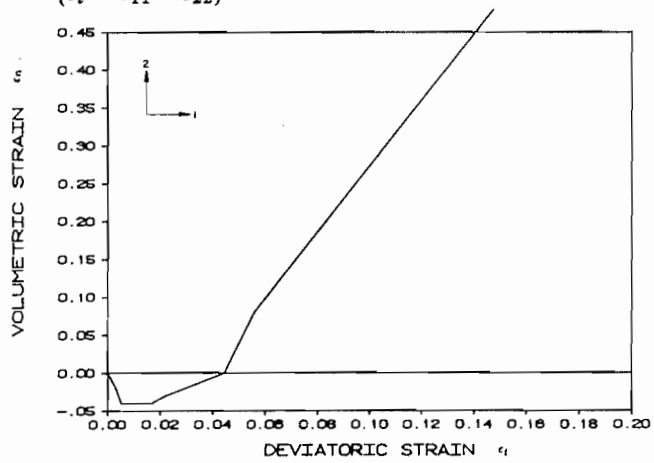

b) Volumetric Strain ε_n versus Deviatoric Strain ε_t $(\varepsilon_n = 2\varepsilon_{11} + \varepsilon_{22}$ versus $\varepsilon_t = \varepsilon_{11} - \varepsilon_{22})$

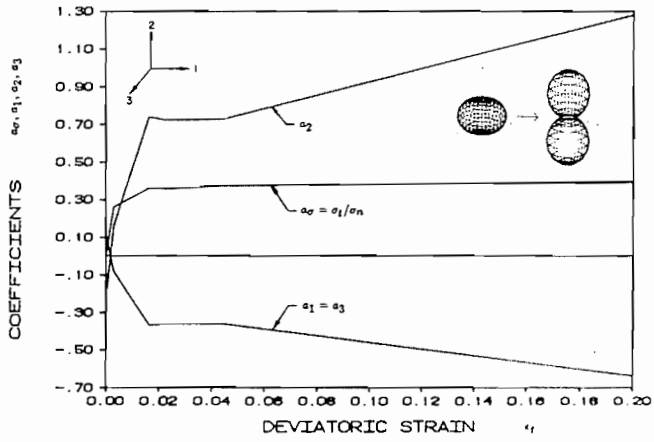

c) Invariant Stress Ratio a_σ and Coefficients of Anisotropy a_1, a_2 and a_3 versus Deviatoric Strain ε_t $(\varepsilon_t = \varepsilon_{11} - \varepsilon_{22})$

Figure 2.7 Results of Triaxial Compression Tests on Sand (*test reported by Oda, 1972b*)

The initial major principal direction of anisotropy for the sand sample was in the horizontal plane (i.e. the plane described by axes 1 and 3) and is a consequence of the non-spherical shape of the constituent sand particles and the vertical rodding action used to compact the sample. Upon loading, there occurred an almost instantaneous stress-induced rotation of the major principal direction of contact anisotropy through $\pi/2$ from the horizontal to vertical direction coincident with the direction of major principal stress.

Figures 2.8 and 2.9 show the distribution of second-order structure described by relationship (2.40) superimposed on directly measured $E(\beta)$ values extracted at the beginning and end of the triaxial compression test. The figures show that there are higher orders of structure apparent in the measured data which are not accounted for by the second-order contact distribution function assumed. Nevertheless, the visual impression given by the plots is that the predominant bias in the measured distribution of contacts is reflected by the approximating function having the form of equation (2.40).

2.8 Contact Density and Assembly Microstructure

Preceding sections have identified contact density as a fundamental parameter describing the average intensity of particle packing. If an idealized granular medium is considered, it can be shown that this parameter is related to the (macroscopic) density of the system ρ, (or void ratio e) and the average contact vector length $\bar{l}_o$.

The contact density for the system can be expressed as:

$$m_v = \frac{\gamma N}{V} \tag{2.48}$$

where N is the number of particles in the volume V and γ is the (average) coordination number for the assembly particles. If we consider an assembly of spheres with an average radius equal to the average contact vector length $\bar{l}_o$ then, the volume of solid material V_s may be assumed to be:

$$V_s = \frac{4N\pi\bar{l}_o^3}{3} \tag{2.49}$$

The total volume V of the assembly is related to the assembly void ratio e by virtue of:

$$V = V_s(1+e) \tag{2.50}$$

Substituting expressions (2.49) and (2.50) into (2.48) gives:

$$m_v = \frac{3\gamma}{4\pi\bar{l}_o^3(1+e)} \tag{2.51}$$

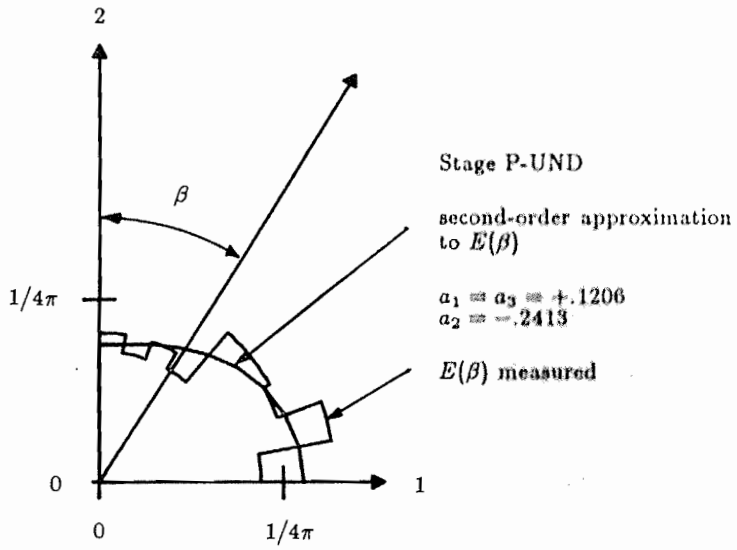

a) $E(\beta)$ in Plane $1-2$

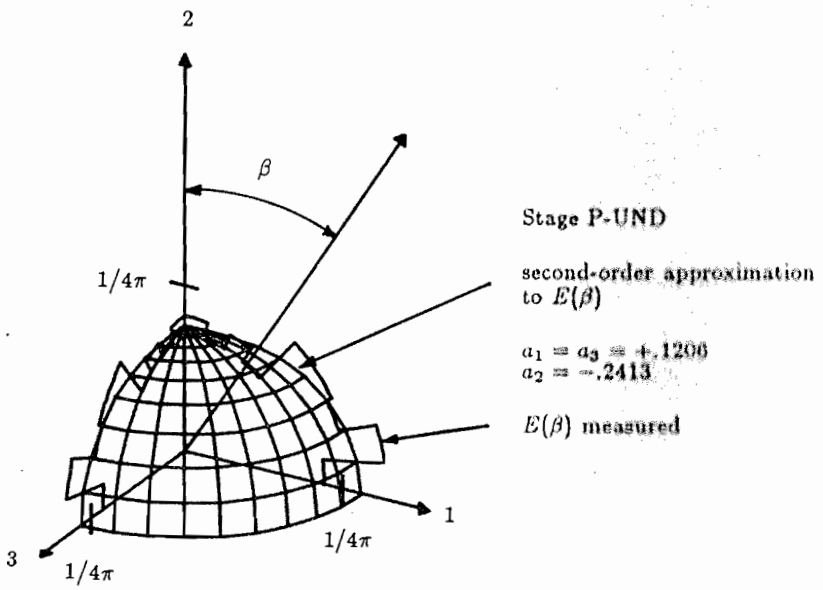

b) Three-Dimensional View of $E(\beta)$

Figure 2.8 Normalized Contact Distribution Function $E(\beta)$ for Sand at Start of Triaxial Compression Test *(from test data reported by Oda, 1972b)*

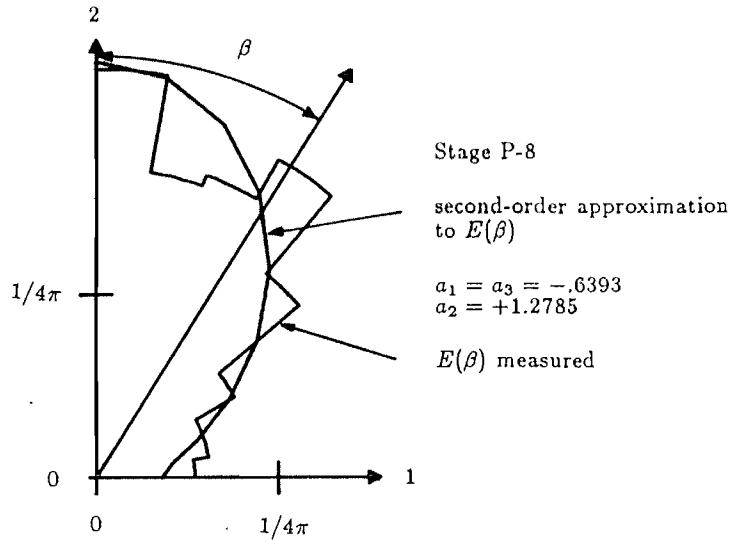

a) $E(\beta)$ in Plane $1-2$

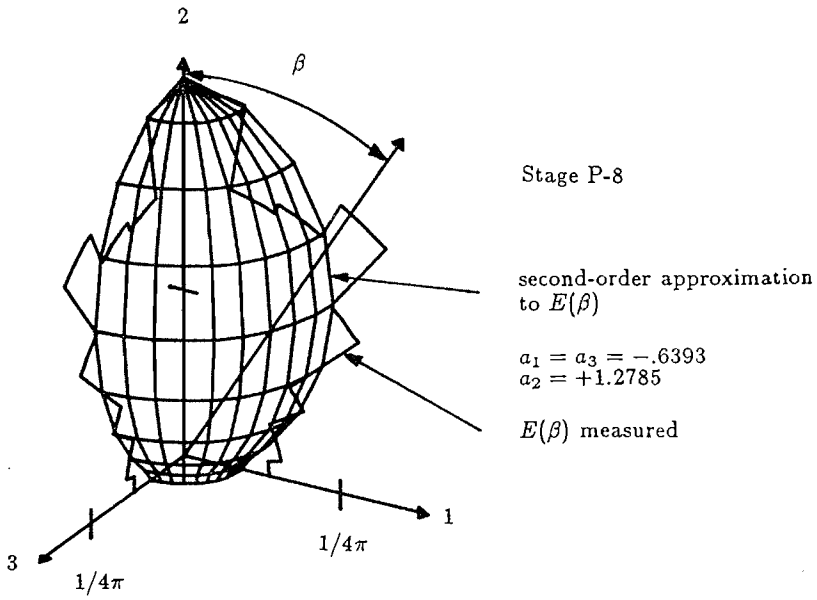

b) Three-Dimensional View of $E(\beta)$

Figure 2.9 Normalized Contact Distribution Function $E(\beta)$ for Sand at End of Triaxial Compression Test *(from test data reported by Oda, 1972b)*

Coordination number is related to the degree of redundancy in the system under conditions of static equilibrium. The range of average coordination numbers for stable assemblies of non-bonded particles will be a function of the size distribution and shape of the particles making up the assembly. Systematic packings of equi-diameter spheres have coordination numbers which range from 6 to 12 (Oda, 1977). For similar particle systems, the assembly with the lower coordination number will generally be more mobile and better able to develop contact normal anisotropy.

The minimum coordination number for a system of particles is dictated by the requirement for static determinancy (Horne, 1965). For example, consider a system containing N cohesionless particles with a total of M_V contacts. For this system, there are $3M_V/2$ unknown force components for each pair of contacts. Recognizing that there are $6N$ equations of static equilibrium for each particle then, the minimum requirement for static equilibrium is:

$$\frac{3M_V}{2} = 6N \tag{2.52}$$

Hence, the minimum coordination number must be:

$$\gamma_{min} = 4 \tag{2.53}$$

Similar calculations for two-dimensional assemblies give $\gamma_{min} = 3$.

It is interesting to note that frequency distributions calculated from physical assemblies of cohesionless granular media show individual particle coordination numbers as low as 3 (Oda, 1977). However, these particles do not contribute measurably to the average stress in the assembly according to expression (2.17) since the associated contact forces are due to particle self-weight and hence, negligibly small. In fact, as long as average stress is calculated according to the volume-additive expression (2.17), the distinction between a *passive* and *active* contact is not warranted. However, at a later stage in the current study it is desirable to isolate the contribution of microstructure, including the distribution of contact normals, to the assembly average stress. For example, a fundamental question in the study of stress and fabric in granular media is whether or not coaxiality of stress and fabric tensors is a valid assumption. Under conditions of static equilibrium a comparison of the fabric tensor $\mathbf{R}$ and the average stress tensor σ should only be based on those contacts which actively contribute to resist loads imposed at the system boundaries. As a result of the comments made above it is important to introduce an unambiguous definition of what constitutes a contact between particles. To this end it is proposed that a contact exists at any location between particles where loads greater than the self-weight of the contacting granules are transmitted.

2.9 Discussion

Using a statistical mechanics approach, which considers contact density together with certain averages of statically admissible contact forces, and distributions for average contact vector lengths, general expressions for the average stress tensor of idealized granular systems have been presented (2.27, 2.29 and 2.30).

However, despite simplifications introduced by considering assemblies of spheres, very little information concerning distributions for $E(\Omega)$ is available in the literature and none for $\overline{f}_i^c(\Omega)$. Based on limited experimental observation, second-order contact normal distributions may be approximated by equations describing second-order surfaces.

At this stage the only additional information on average stress tensor expressions for granular systems is that they must satisfy certain constraints. For example, symmetry of the second-order stress tensor dictates that:

$$\sigma_{ij} - \sigma_{ji} = m_v \bar{l}_o \left\{ \int_\Omega \overline{f}_i^c(\Omega) n_j^c(\Omega) E(\Omega)\, d\Omega - \int_\Omega \overline{f}_j^c(\Omega) n_i^c(\Omega) E(\Omega)\, d\Omega \right\} = 0 \quad i \neq j = 1,2,3 \tag{2.54}$$

An additional constraint is that the normalized distribution function $E(\Omega)$ satisfy the condition (2.26) and $E(\Omega) = 1/4\pi$ for isotropic assemblies.

The concepts and equations presented in this Chapter have a two-dimensional analogue. In Chapter 3 relationships between average stress quantities and distributions of contact forces and microstructure are developed by considering two-dimensional assemblies of discs as an analogue to idealized granular systems.

CHAPTER 3

TWO-DIMENSIONAL IDEALIZED GRANULAR SYSTEMS

3.1 Introduction

Theoretical developments presented in Chapter 2 lead to expressions for the average stress tensor of a discrete granular system in terms of certain functions describing the distribution of contact normals, average contact lengths and average contact forces with respect to orientation.

Expression (2.27) has the two-dimensional analogue:

$$\sigma_{ij} = m_v \int_0^{2\pi} \overline{f}_i^c(\theta)\overline{l}_j^c(\theta)E(\theta)d\theta \qquad i,j = 1,2 \tag{3.1}$$

Here the contact density term m_v is with respect to the area of the assembly defined by its boundary within a fixed plane cartesian coordinate space.

For an assembly of circular particles (discs) having a range of diameters, the two-dimensional equivalent to (2.30) is:

$$\sigma_{ij} = m_v \overline{l}_o \int_0^{2\pi} \overline{f}_i^c(\theta)n_j^c E(\theta)\, d(\theta) \tag{3.2}$$

Rothenburg (1980) has proposed that for systems of particles comprising discs with constant diameter d_o, expression (3.2) can be written as:

$$\sigma_{ij} = \frac{m_v d_o}{2} \int_0^{2\pi} \overline{f}_i^c(\theta)n_j^c E(\theta)d(\theta) \tag{3.3}$$

The developments which follow are similar to Rothenburg (1980) but the more general condition represented by expression (3.2) is considered together with the assumption of cohesionless discs.

3.2 Contact Normal Distribution Functions and Fabric Tensor

3.2.1 Fourier Series Contact Normal Distribution Functions

Fourier series expressions can always be considered as an approximation to a continuous distribution such as $E(\theta)$. Reference to Figure 1.11 taken from Konishi (1978) shows that the histogram data for contact normals has a periodic appearance which may be particularly well suited to this form of approximation. Rothenburg (1980) has suggested that for two-dimensional assemblies of discs, $E(\theta)$ may be represented by an even Fourier series expression of the form:

$$E(\theta) = \frac{1}{2\pi}\{1 + \sum_{n=1}^{\infty} a_{2n}\cos 2n(\theta - \theta_{2n})\} \tag{3.4}$$

Expression (3.4) satisfies the condition $E(\theta) = E(\theta - \pi)$ for assemblies of discs and when integrated over the limits $0 \leq \theta \leq 2\pi$ gives:

$$\int_0^{2\pi} E(\theta)\, d\theta = 1 \tag{3.5}$$

The constant terms θ_{2n} represent (major) principal directions of anisotropy for contact normals. Coefficients of anisotropy a_{2n} reflect the intensity of contact normals in these preferred directions. It can be seen that for isotropic assemblies $a_{2n} = 0$, for $n = 1, 2, 3 \ldots$ and, $E(\theta) = 1/2\pi$.

If Fourier expressions are restricted to second Fourier components then, equation (3.4) can be expressed equivalently as:

$$\begin{aligned} E(\theta) &= \frac{1}{2\pi}\{1 + a_{ij} n_i^c n_j^c\} \qquad i, j = 1, 2 \\ a_{ij} &= a_{ji} \qquad i \neq j \\ a_{kk} &= 0 \end{aligned} \tag{3.6}$$

Here $\tilde{n}^c = (\cos\theta, \sin\theta)$. Relationship (3.6) can be recognized as the two-dimensional analogue to the three-dimensional contact distribution function (2.40). In this study, contact distribution functions are expressed in Fourier series form because this format lends itself to instructive visual representation.

3.2.2 Fabric Tensor

The fabric tensor for two-dimensional assemblies is:

$$\mathbf{R}_{ij} = \frac{1}{V} \sum_{c \varepsilon V} n_i^c n_j^c = m_v \int_0^{2\pi} E(\theta) n_i^c n_j^c \, d\theta \qquad i, j = 1, 2 \tag{3.7}$$

In fact, relationship (3.7) is only strictly valid for infinite assemblies where the distribution function $E(\theta)$ is continuous. For any finite system of particles the equalities expressed above are approximate.

Invariant quantities can be associated with this symmetric tensor such as:

$$\mathbf{R}_n = \frac{\mathbf{R}_{kk}}{2} = \frac{m_v}{2} \tag{3.8}$$

$$\mathbf{R}_t = \sqrt{\frac{\mathbf{R}'_{ij}\mathbf{R}'_{ij}}{2}} = \sqrt{\left(\frac{\mathbf{R}_{11} - \mathbf{R}_{22}}{2}\right)^2 + \mathbf{R}_{12}{}^2} \tag{3.9}$$

The quantity $\mathbf{R}_n$ is defined as the *normal* invariant component (or *spherical* part) of $\mathbf{R}$ and is proportional to the first invariant of the fabric tensor. Term $\mathbf{R}_t$ is defined as the *deviatoric* component and is related to the second invariant of the *deviator* fabric tensor $\mathbf{R}'$. For two-dimensional assemblies of discs, the magnitude of fabric anisotropy is uniquely characterized by $\mathbf{R}_t$.

3.2.3 Coefficients of Contact Normal Anisotropy from Fabric Tensor

The following mathematical developments show how coefficients of contact anisotropy and directions of anisotropy can be calculated from expression (3.7) for two-dimensional assemblies of discs. The developments are given in some detail since the resulting equations are implemented in program DISC to extract parameters of anisotropy from numerical simulations and are also used to evaluate Fourier series functions of the form (3.4) as approximations to contact normal distribution data from physical tests.

Consider a contact distribution function $E(\theta)$ having no more than a second-order term, then:

$$E(\theta) = \frac{1}{2\pi}\{1 + a_2 \cos 2(\theta - \theta_2)\} \tag{3.10}$$

The above expression can be rewritten as:

$$E(\theta) = \frac{1}{2\pi}\{1 + a_2^c \cos 2\theta + a_2^s \sin 2\theta\} \tag{3.11}$$

where:

$$\begin{aligned} a_2^c &= a_2 \cos 2\theta_2 \\ a_2^s &= a_2 \sin 2\theta_2 \end{aligned} \tag{3.12}$$

and:

$$\tan 2\theta_2 = \frac{a_2^s}{a_2^c} \tag{3.13}$$

Substitution of (3.10) into (3.7) and integration of the right hand side leads to:

$$\begin{aligned} a_2^s &= \frac{4\mathbf{R}_{12}}{\mathbf{R}_{kk}} = \frac{2}{M_V}\sum_{c\epsilon V} \sin 2\theta \\ a_2^c &= \frac{2(\mathbf{R}_{11} - \mathbf{R}_{22})}{\mathbf{R}_{kk}} = \frac{2}{M_V}\sum_{c\epsilon V} \cos 2\theta \end{aligned} \tag{3.14}$$

From relations (3.9), (3.12) and (3.14) it can be seen that the second-order coefficient of contact anisotropy is proportional to the deviatoric invariant quantity $\mathbf{R}_t$ according to:

$$a_2 = \frac{4\mathbf{R}_t}{\mathbf{R}_{kk}} \tag{3.15}$$

In general, $2n - order$ terms or lower in (3.4) can be calculated from two-dimensional $2n - order$ fabric tensor expressions. For example, coefficient terms and directions of anisotropy for a fourth-order truncated Fourier series expression can be calculated from:

$$\mathbf{R}_{ijkl} = \frac{1}{V}\sum_{c\epsilon V} n_i^c n_j^c n_k^c n_l^c = m_v \int_0^{2\pi} E(\theta) n_i^c n_j^c n_k^c n_l^c \, d\theta \qquad i,j,k,l = 1,2,3,4 \tag{3.16}$$

Tedious calculations show that the fourth Fourier component of contact anisotropy is related to the second invariant of the deviator fourth-order fabric tensor.

In general, $2n - order$ coefficients of anisotropy a_{2n} and directions of anisotropy θ_{2n} can be calculated from:

$$a_{2n} = \sqrt{(a^c_{2n})^2 + (a^s_{2n})^2}$$
$$\tan 2\theta_{2n} = \frac{a^s_{2n}}{a^c_{2n}} \tag{3.17}$$

where:

$$a^c_{2n} = \frac{2}{M_V} \sum_{c \epsilon V} \cos 2n\theta$$
$$a^s_{2n} = \frac{2}{M_V} \sum_{c \epsilon V} \sin 2n\theta \tag{3.18}$$

In summary then, it can be seen that coefficients of anisotropy in (3.4) have important physical meaning since they represent invariant quantities of the deviator fabric tensor $\mathbf{R}'$. Similarly, terms θ_{2n} are principal directions (eigenvectors) for these tensors.

It can be noted that expressions (3.17) for $n = 1$ are essentially those proposed by Curray (1956) as a measure of the *degree of preferred orientation* and *preferred orientation direction* for two-dimensional geological data (see expressions (1.9)). While Curray recognized the invariant nature of a_2 (or $\overline{M}$), the connection to a tensor was not made at this time. The general expressions (3.17) and (3.18) can be used to extract coefficients of anisotropy and directions of anisotropy from contact distribution data such as that shown on Figure 1.11 which has been reported by Konishi (1978) from physical tests.

Fourier series expressions of the form (3.4) having up to four cosine terms were evaluated as approximations to this data. The *degree of fit* was evaluated by comparing the error expression $\sum |err_k|$ for each $E(\theta)$ function where err_k represents the error between the approximating function and the measured frequency for class intervals $k = 1, 2, 3...18$. Clearly the ability of this technique to resolve coefficient terms from the 18 interval histogram data will diminish with the order of the approximating function $E(\theta)$. However, analysis did show that fourth-order expressions were marginally more accurate than second-order expressions but that the degree of fit deteriorated rapidly for more than $n = 2$ terms. In addition, it was observed that coefficient terms became smaller with increasing order and directions of anisotropy were generally non-coincident.

Based on these observations for *real* data it is considered that the contact distribution function $E(\theta)$ for assemblies of discs with a narrow range of diameters may be approximated by:

$$E(\theta) = \frac{1}{2\pi}\{1 + a\cos 2(\theta - \theta_a) + b\cos 4(\theta - \theta_b)\} \tag{3.19}$$

The contact distribution function (3.19) is identical to that proposed by Rothenburg (1980) for assemblies of two-dimensional discs with the exception that coincidence of second-order directions of anisotropy θ_a and fourth-order directions θ_b is not *a priori* assumed. Components of the proposed function are represented by the distributions shown on Figure 3.1.

Figures 3.2 and 3.3 show replotted contact frequency data from Figure 1.11 together with superimposed functions of the form (3.19) extracted from this information. The corresponding macroscopic load-deformation stage for each plot can be taken from Figure 1.10. Figure 3.4 presents similar data from a biaxial compression test which comprised a disc size-distribution identical to the simple shear test assemblies (Konishi, 1978). The distribution of contact normals in this plot corresponds to the sample at about peak principal stress ratio σ_{22}/σ_{11} measured at the sample boundaries. The fully-mobilized interparticle friction angle between discs was measured by Konishi to be about $\phi_\mu = 20^o$.

It should be noted that Konishi does not report if he identified between passive and active contacts during frequency counts nor does he state whether or not disc-wall contacts were excluded in his analysis for compression tests. Nevertheless, the plots show that fourth-order distribution functions of the form (3.19) give a reasonable approximation to measured contact normal histogram data taken from two-dimensional assemblies of loaded photo-elastic discs.

3.3 Contact Force Distributions and Contact Force Tensors

3.3.1 Average Contact Force Distributions

The average contact force acting at contacts with orientation θ can be decomposed into an average *normal* force component $\overline{f}_n^c(\theta)$ and an average *tangential* (*or shear*) force component $\overline{f}_t^c(\theta)$. Contact force components for a single disc are shown on Figure 3.5.

Letting $\tilde{n}^c = (\cos\theta, \sin\theta)$ and $\tilde{t}^c = (-\sin\theta, \cos\theta)$ the average contact force term $\overline{f}_i^c(\theta)$ can be expressed as:

$$\overline{f}_i^c(\theta) = \overline{f}_n^c(\theta) n_i^c + \overline{f}_t^c(\theta) t_i^c \qquad i, j = 1, 2 \tag{3.20}$$

Subsequent theoretical development shows that the decomposition according to (3.20) facilitates examination of the contributions of interparticle tangential and normal force to the shear capacity of the assembly at the macroscale. A similar decomposition is possible in three dimensions except that the tangential direction $\tilde{t}^c$ is not uniquely related to $\tilde{n}^c$.

Normal contact forces are considered positive if they are tensile (only possible for bonded particles). Tangential contact forces are considered positive if they induce counter-clockwise rotation of the disc. Positive orientations are shown on Figure 3.5.

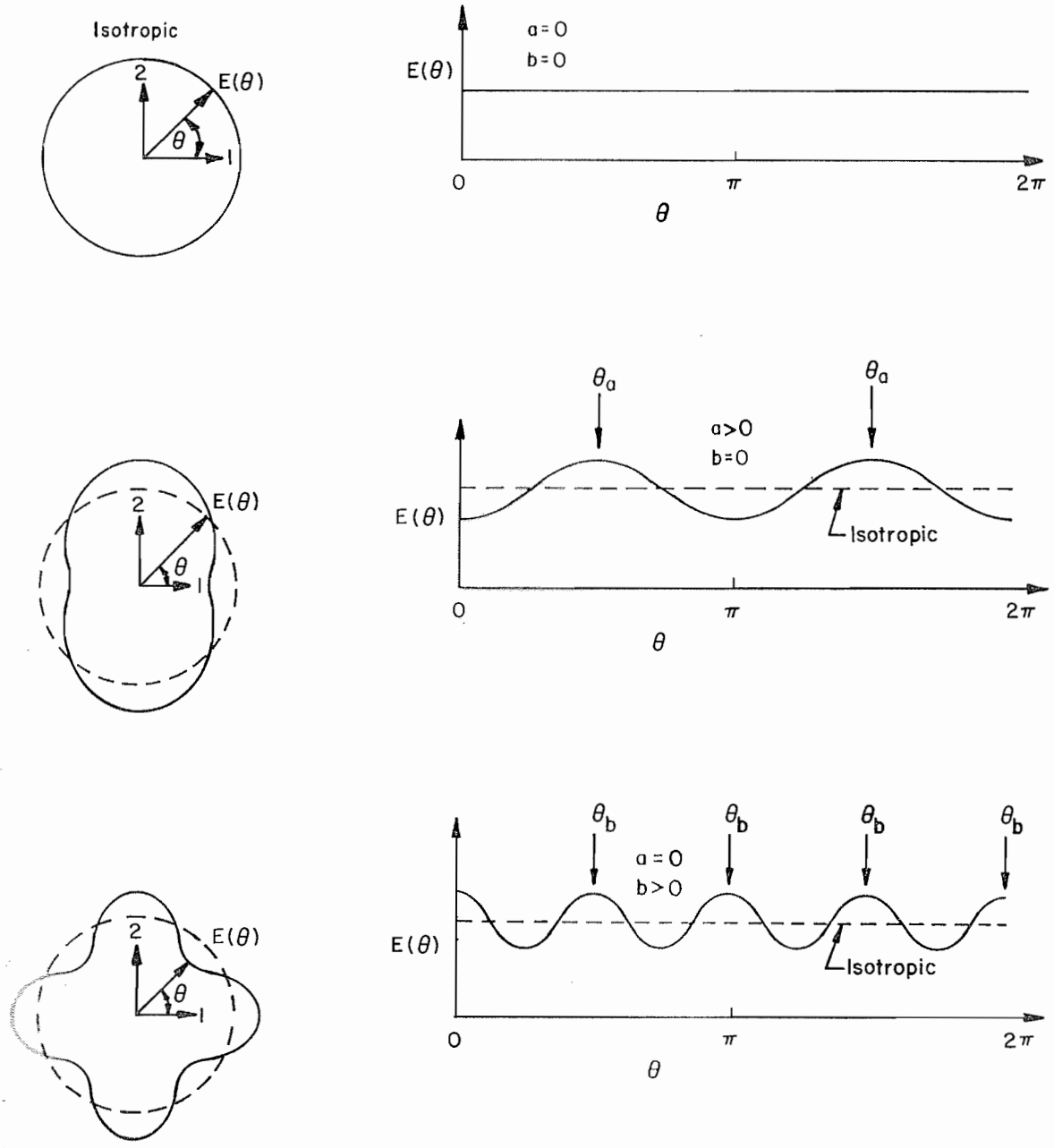

Figure 3.1 Contact Normal Distribution Function $E(\theta)$
$E(\theta) = \frac{1}{2\pi}(1 + a\cos 2(\theta - \theta_a) + b\cos 4(\theta - \theta_b))$

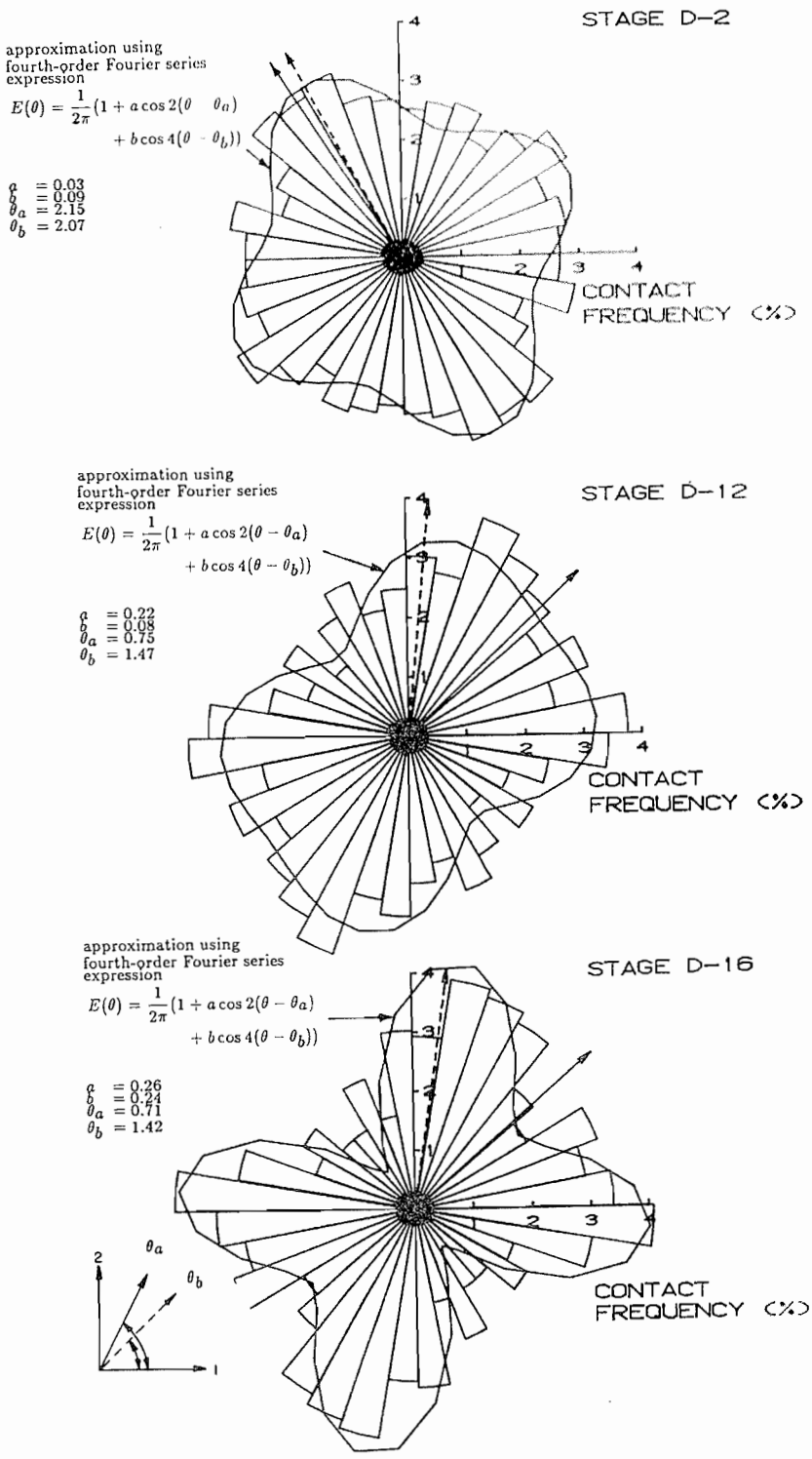

Figure 3.2 Contact Normal Distributions from (Dense) Two-Dimensional Simple Shear Tests *(data after Konishi, 1978)*

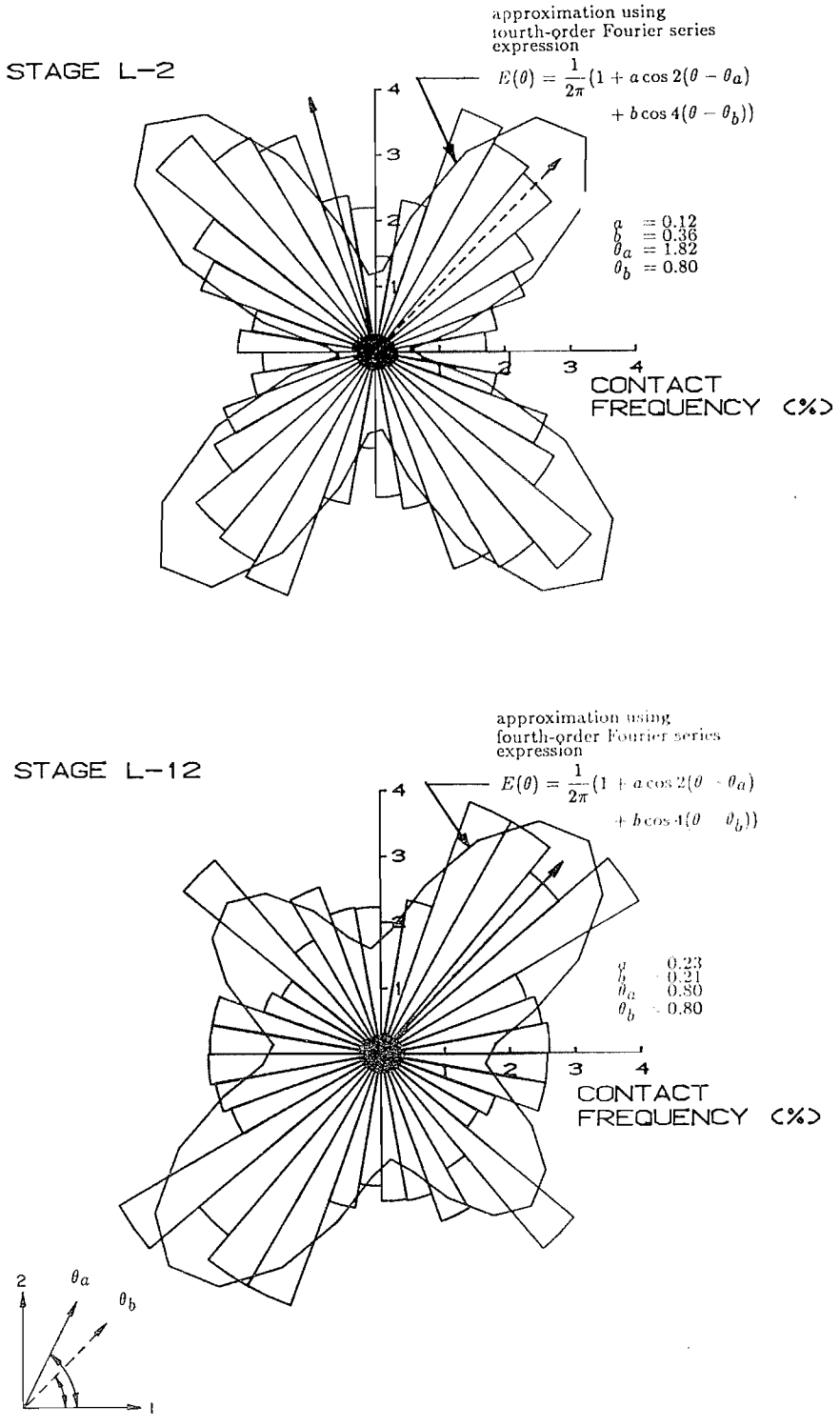

Figure 3.3 Contact Normal Distributions from (Loose) Two-Dimensional Simple Shear Tests *(data after Konishi, 1978)*

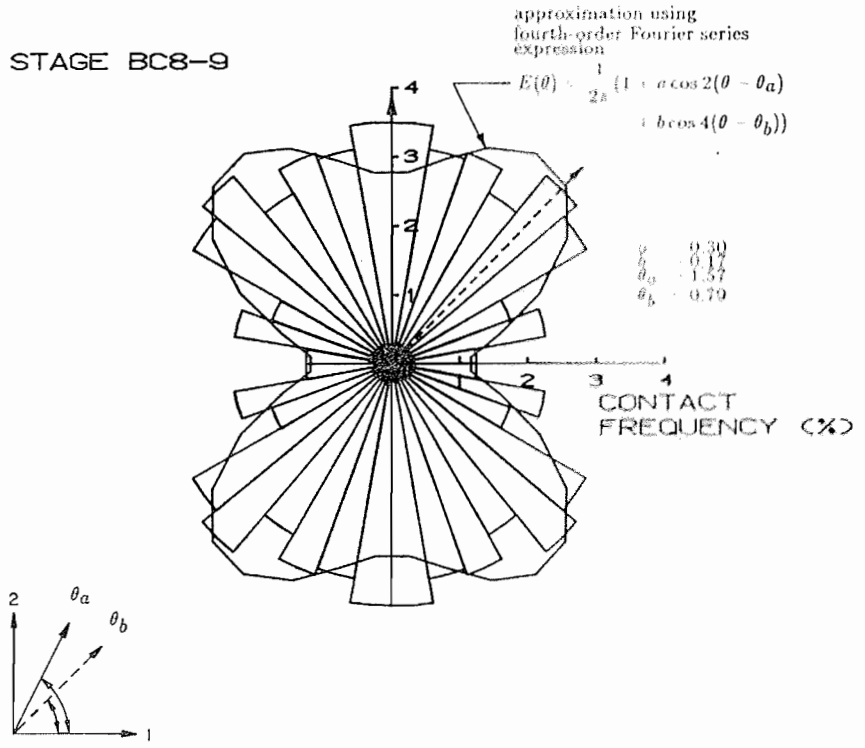

Figure 3.4 Contact Normal Distribution from Two-Dimensional Biaxial Compression Test *(data after Konishi, 1978)*

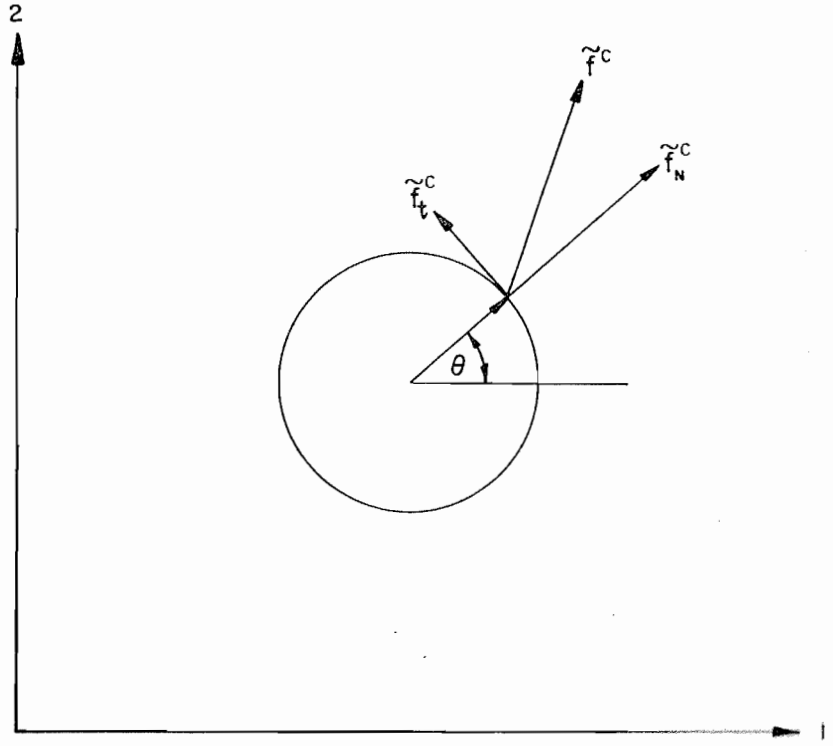

Figure 3.5 Normal and Tangential (Shear) Contact Force Components

The general expression for the average stress tensor (3.2) can now be rewritten as:

$$\sigma_{ij} = m_v \bar{l}_o \int_0^{2\pi} \left\{ \overline{f}_n^c n_i^c n_j^c + \overline{f}_t^c t_i^c n_j^c \right\} E(\theta)\, d\theta \tag{3.21}$$

Rothenburg (1980) has proposed that distributions for contact force components in two-dimensional particulate systems may be represented by Fourier series expressions of the form:

$$\overline{f}_n^c(\theta) = f_n^o \{1 + a_n \cos 2(\theta - \theta_f)\} \tag{3.22}$$

$$\overline{f}_t^c(\theta) = f_n^o \{a_\omega - a_t \sin 2(\theta - \theta_t)\} \tag{3.23}$$

The constant term f_n^o in (3.22) and (3.23) represents the average normal contact force from all assembly contacts and terms a_n, a_ω and a_t are non-dimensional *coefficients of contact force anisotropy*. Terms θ_f and θ_t represent certain preferred directions for contact force distributions and are called (*major*) *principal directions of contact force anisotropy*. The (major) principal direction of normal contact force anisotropy θ_f is chosen such that a_n always assumes a positive value. At this point no information is available to establish the relationship between θ_f and θ_t.

Average contact force distributions are shown on Figure 3.6 assuming $\theta_f = \theta_t$. Changing the sign of the coefficient term a_t results in distributions for average tangential contact forces which are orthogonal to those shown on the figure. For discussion purposes in the following text, the term *direction of contact force anisotropy* will refer to θ_f.

Expression (3.23) satisfies the constraint that distributions for tangential contact forces and contact normals $E(\theta)$ must result in moment equilibrium for assemblies comprising discs.

Consider that for all N discs, moment equilibrium requires:

$$\sum_{k=1}^{N} \sum_{n=1}^{n_k} f_t^n = 0 \tag{3.24}$$

If expressions for average tangential contact forces $\overline{f}_t^c(\theta)$ and contact distribution $E(\theta)$ are substituted into (3.24) and the assembly considered in the limit then, moment equilibrium requires that:

$$\int_0^{2\pi} \overline{f}_t^c(\theta) E(\theta)\, d\theta = 0 \tag{3.25}$$

The constant term a_ω is required in (3.23) to satisfy the general case of non-coincidence of tangential contact force anisotropy and anisotropy of contact normals. Physically, non-zero values of a_ω correspond to a situation in which a non-symmetrical distribution of shear contact forces is required to compensate for the lack of contact normals in the direction of maximum loading. The

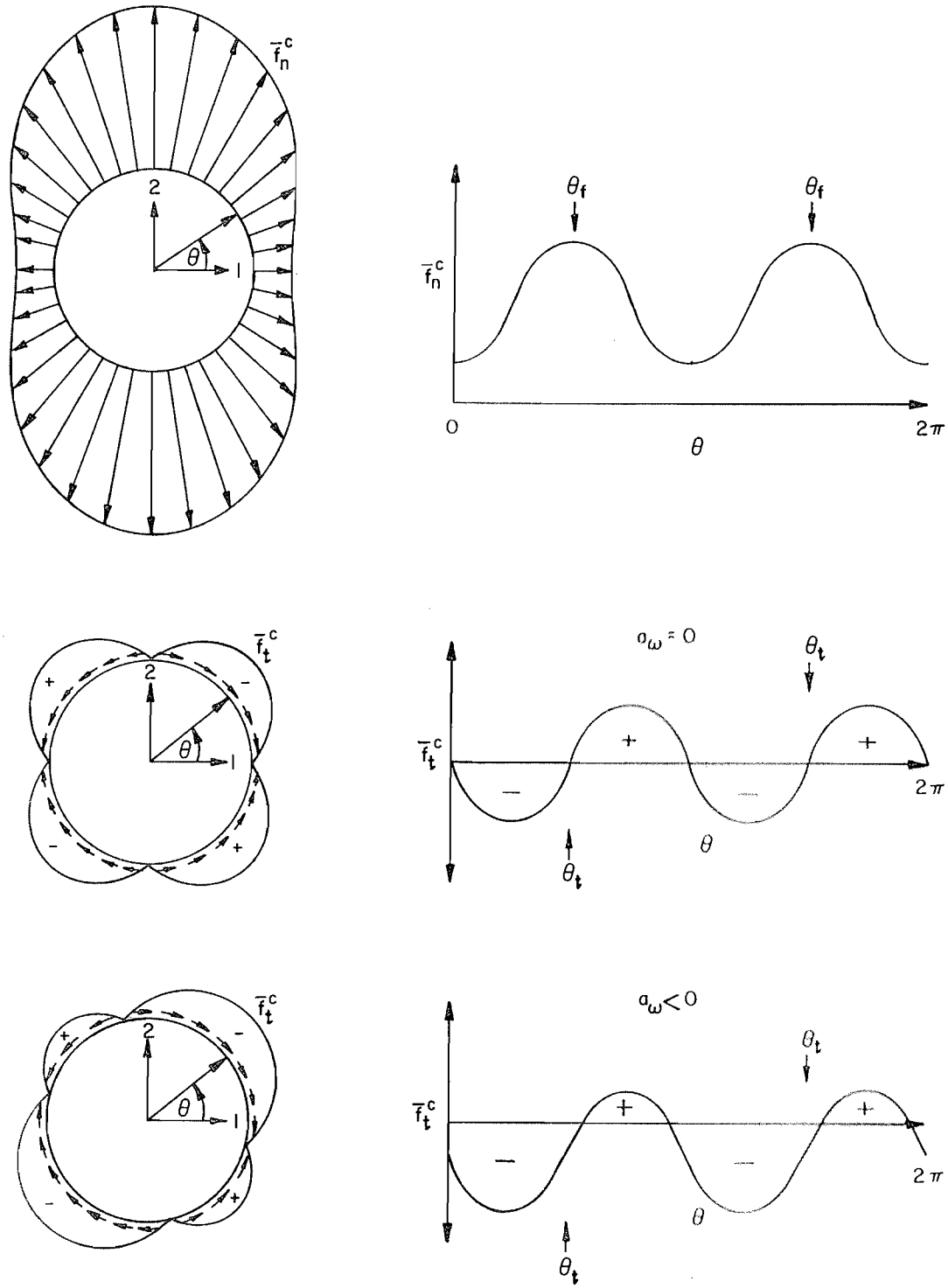

Figure 3.6 Normal and Tangential (Shear) Contact Force Distributions
$\bar{f}_n^c(\theta) = f_n^o(1 + a_n \cos 2(\theta - \theta_f))$, $\bar{f}_t^c(\theta) = f_n^o(a_\omega - a_t \sin 2(\theta - \theta_t))$

relative orientations of distributions describing tangential contact forces, contact normals and stress when this condition occurs are idealized on Figure 3.7.

Further examination of (3.23) and (3.25) reveals that a_ω is not an independent parameter but is related to coefficients a and a_t by:

$$a_\omega = \frac{-aa_t}{2} \sin 2(\theta_a - \theta_t) \tag{3.26}$$

It is easily seen that the coefficient term a_ω reduces to zero for $\theta_t = \theta_a$.

A simple model for limiting shear between cohesionless particles is a Coulomb friction law of the form:

$$\left| \frac{f_t^c}{f_n^c} \right|_{max} = \mu \tag{3.27}$$

where μ is the maximum interparticle friction coefficient. Relationships (3.22) and (3.23) together with simplifying assumptions can be used to predict the distribution of the average mobilized friction coefficient $\overline{\mu}_{mob}(\theta)$. For example, assuming $a_\omega = 0$ is reasonable for these systems, then:

$$\overline{\mu}_{mob}(\theta) = \left| \frac{a_t \sin 2(\theta - \theta_t)}{1 + a_n \cos 2(\theta - \theta_f)} \right| \tag{3.28}$$

If principal axes for $\overline{f}_n^c(\theta)$ and $\overline{f}_t^c(\theta)$ are coincident or orthogonal to each other (i.e. $\theta_t = \theta_f + n\pi/2$, for $n = 0, 1, 2, 3$) then, expression (3.28) implies that average tangential contact forces vanish in the direction of normal contact force anisotropy.

3.3.2 Contact Force Tensors

The distributions for average normal contact forces $\overline{f}_n^c(\theta)$ and average tangential contact forces $\overline{f}_t^c(\theta)$ are related to certain second-order symmetric tensors similar to the relationship between $E(\theta)$ and the second-order fabric tensor $\mathbf{R}$.

A normal contact force tensor $\mathbf{F}_N$ can be equated to the distribution of normal contact forces described by (3.22) according to:

$$\mathbf{F}_{N_{ij}} = \frac{f_n^o}{2\pi} \int_0^{2\pi} (1 + a_n \cos 2(\theta - \theta_f)) n_i^c n_j^c \, d\theta \qquad i, j = 1, 2 \tag{3.29}$$

The normal contact force tensor can be approximated from histogram data containing N_g intervals by:

$$\mathbf{F}_{N_{ij}} = \frac{1}{N_g} \sum_{\theta_g} \overline{f}_n^c(\theta) n_i^c n_j^c \tag{3.30}$$

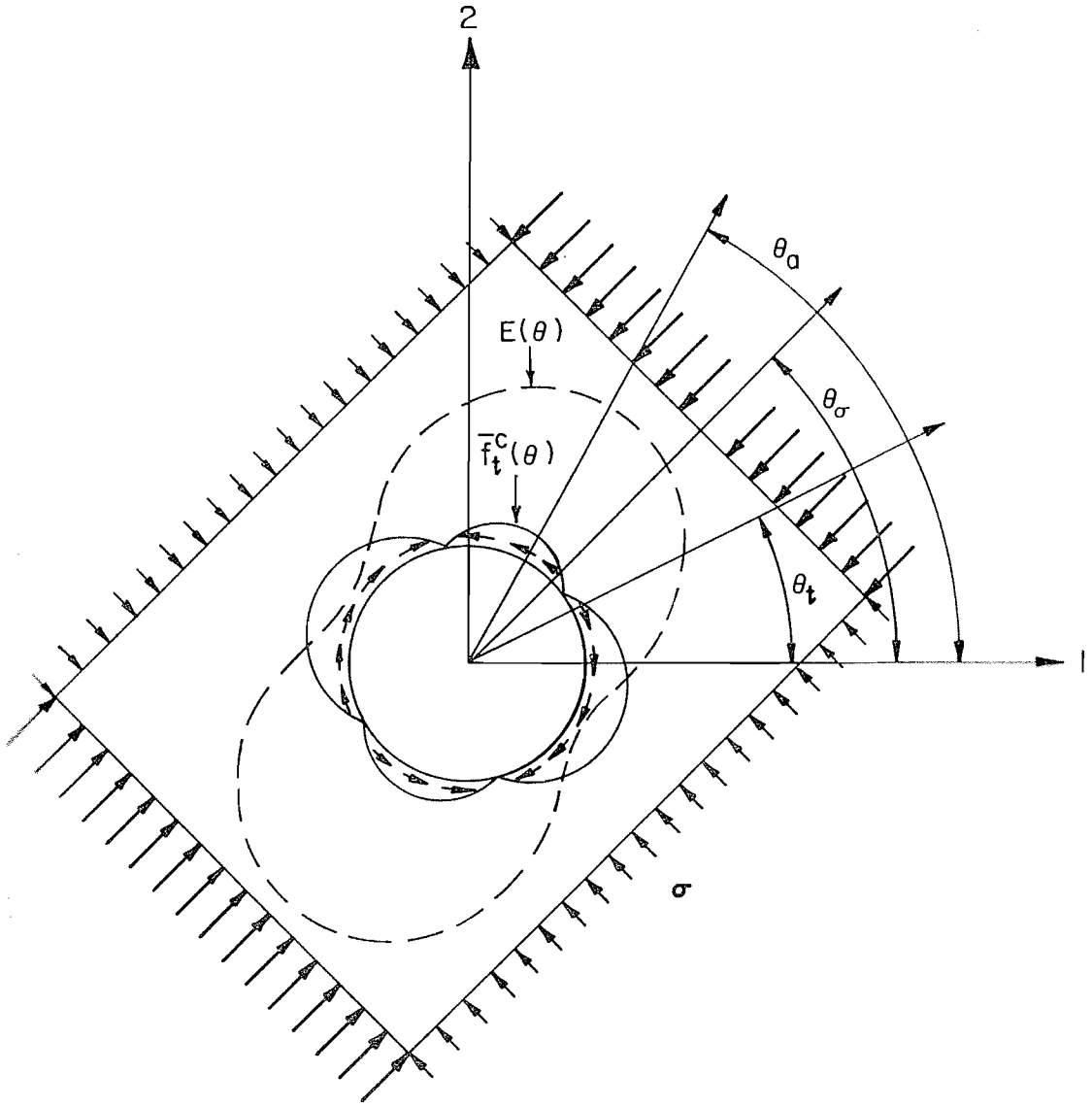

Figure 3.7 Relative Orientations of Distributions describing Tangential Contact Forces, Contact Normals and Assembly Stress for $a_\omega \neq 0$

The following relationships now emerge:

$$a_n = \frac{4\sqrt{\frac{\mathbf{F}'_{N_{ij}}\mathbf{F}'_{N_{ij}}}{2}}}{\mathbf{F}_{N_{kk}}} = \frac{4\sqrt{\left(\frac{\mathbf{F}_{N_{11}}-\mathbf{F}_{N_{22}}}{2}\right)^2+\left(\mathbf{F}_{N_{12}}\right)^2}}{\mathbf{F}_{N_{kk}}} \tag{3.31}$$

$$\tan 2\theta_f = \frac{2\mathbf{F}_{N_{12}}}{(\mathbf{F}_{N_{11}}-\mathbf{F}_{N_{22}})} \tag{3.32}$$

$$f_n^o = \mathbf{F}_{N_{kk}} \tag{3.33}$$

The above derivations confirm that a_n and θ_f have important physical meaning. The coefficient term a_n is related to the second invariant of the deviator normal force tensor. Term θ_f represents the (major) principal direction (or an eigenvector) for this tensor. An isotropic distribution of normal contact forces corresponds to tensor quantities having terms $f_n^o\delta_{ij}$.

Now consider the distribution of average tangential contact forces described by the relationship (3.23). In a similar manner, tensorial quantities can be related to this distribution according to:

$$\mathbf{F}_{T_{ij}} = \frac{f_n^o}{2\pi}\int_0^{2\pi}(a_\omega - a_t\sin 2(\theta-\theta_t))t_i^c n_j^c\, d\theta \tag{3.34}$$

Tangential contact force tensor quantities are estimated from measured data in numerical simulations as follows:

$$\mathbf{F}_{T_{ij}} = \frac{1}{N_g}\sum_{\theta_g}\overline{f}_t^c(\theta)t_i^c n_j^c \tag{3.35}$$

Inspection of expressions (3.34) and (3.35) shows that the tangential contact force tensor is a deviator tensor, hence $\mathbf{F}_T = \mathbf{F}'_T$. The coefficient term a_ω can be equated to contact force tensor quantities as follows:

$$a_\omega = \frac{\mathbf{F}_{T_{21}}-\mathbf{F}_{T_{12}}}{\mathbf{F}_{N_{kk}}} \tag{3.36}$$

Should $a_\omega = 0$ then, tensor $\mathbf{F}_T$ is a symmetric deviator tensor and coefficient term a_t and principal directions of tangential contact force anisotropy θ_t can be calculated from:

$$a_t = \frac{4\sqrt{\frac{\mathbf{F}'_{T_{ij}}\mathbf{F}'_{T_{ij}}}{2}}}{\mathbf{F}_{T_{kk}}} = \frac{4\sqrt{\left(\frac{\mathbf{F}_{T_{11}}-\mathbf{F}_{T_{22}}}{2}\right)^2+\left(\mathbf{F}_{T_{12}}\right)^2}}{\mathbf{F}_{N_{kk}}} \tag{3.37}$$

$$\tan 2\theta_t = \frac{2\mathbf{F}_{T_{12}}}{(\mathbf{F}_{T_{11}}-\mathbf{F}_{N_{22}})} \tag{3.38}$$

Expressions (3.30) and (3.35) show that tensorial quantities $\mathbf{F}_N$ and $\mathbf{F}_T$ are independent of the form of the average contact force distributions assumed. Relationships presented in this section can be used extract coefficients of contact force anisotropy and directions of anisotropy from contact force data for loaded assemblies of discs.

3.3.3 Contact Force Distributions from Laboratory Tests

Average (total) contact forces with respect to orientation have been reported by Oda and Konishi (1974b) and Konishi (1978) for simple shear and biaxial compression tests. Their data allows the ratio $\overline{f}^c(\theta)/f^o$ to be plotted against contact orientation. Here $\overline{f}^c(\theta)$ is the average total contact force for each group and f^o the average contact force from all assembly contacts. Frequency distribution data for the mobilized interparticle friction coefficient $\mu_{mob} = |f_t^c/f_n^c|$ showed that μ_{mob} was unimodal and peaked strongly at $\mu_{mob} = 0$ (see Figure 1.12). Consequently, the measured normalized contact force distribution data presented on Figures 3.8 and 3.9 is considered equivalent to $\overline{f}_n^c(\theta)/f_n^o$.

Coefficients of anisotropy and directions of anisotropy have been calculated from the frequency data using relationships from the previous section. The approximating curves are superimposed on the original data. The figures show that the second-order Fourier series expression for $\overline{f}_n^c(\theta)$ (3.22) gives a good approximation to the measured data. Unfortunately, Oda and Konishi have not reported the results of their tests in a manner which allows confirmation of the distribution function $\overline{f}_t^c(\theta)$ assumed for average tangential (shear) contact forces. However, the results of numerical simulations using two-dimensional assemblies of discs reported in Chapter 5 support both proposed expressions (3.22) and (3.23).

3.4 Assembly Stress and Anisotropy

3.4.1 Theoretical Developments

Distribution functions for average contact normal and tangential contact forces have been proposed in Section 3.3.1. These distribution functions together with a second-order contact distribution function of the form (3.10) lead to relatively simple relationships between invariant average stress quantities and invariant quantities describing anisotropy of contact forces and microstructure for assemblies of discs.

The following development is similar to that reported by Rothenburg (1980): Second-order Fourier series expressions for $\overline{f}_n^c(\theta)$, $\overline{f}_t^c(\theta)$ and $E(\theta)$ can be substituted into (3.21) and integration performed over the limits $0 \leq \theta \leq 2\pi$. Restriction of distribution functions to no more than second Fourier components is consistent with the observation that stress terms σ_{ij} are second-order tensorial quantities.

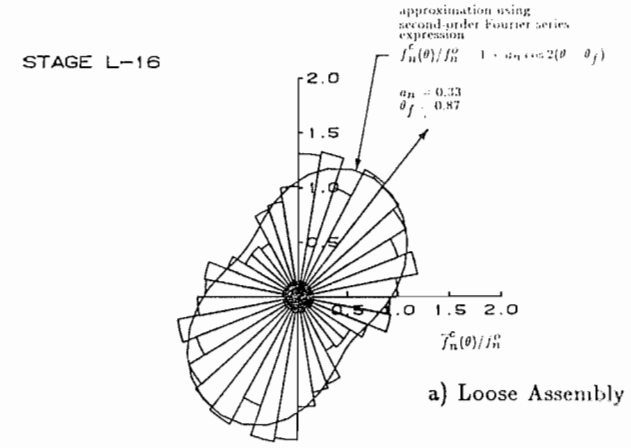

a) Loose Assembly

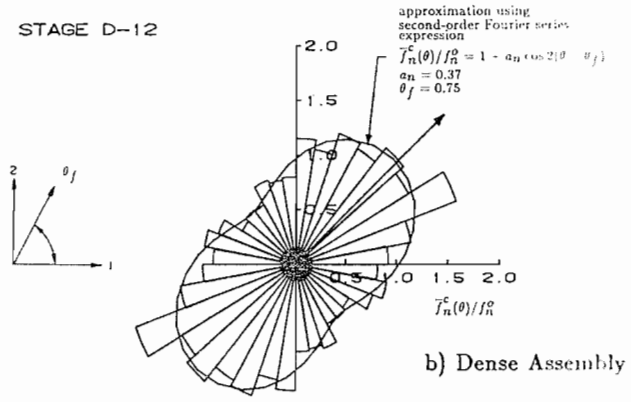

b) Dense Assembly

Figure 3.8 Contact Force Distributions from Two-Dimensional Simple Shear Tests *(data from Oda and Konishi, 1974b)*

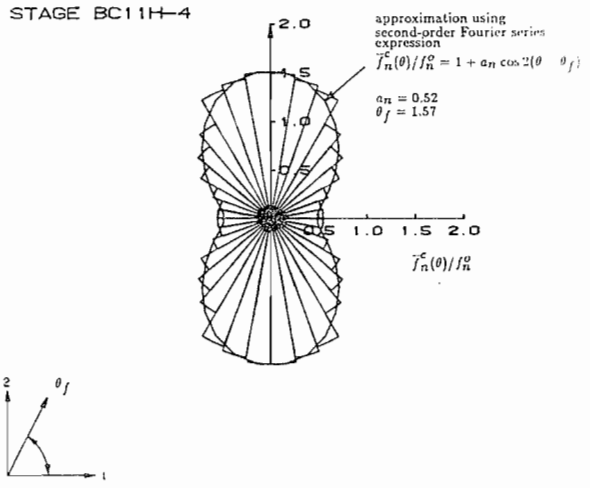

Figure 3.9 Contact Force Distribution from Two-Dimensional Biaxial Compression Test *(data from Konishi, 1978)*

Assuming $a_\omega = 0$, average stress quantities can now be approximated by the following relations:

$$\begin{aligned}
\sigma_{11} &= \frac{m_v \bar{l}_o f_n^o}{2}\left\{1 + \frac{1}{2}\left(a\cos 2\theta_a + a_n \cos 2\theta_f + a_t \cos 2\theta_t + aa_n \cos 2(\theta_a - \theta_f)\right)\right\} \\
\sigma_{22} &= \frac{m_v \bar{l}_o f_n^o}{2}\left\{1 - \frac{1}{2}\left(a\cos 2\theta_a + a_n \cos 2\theta_f + a_t \cos 2\theta_t - aa_n \cos 2(\theta_a - \theta_f)\right)\right\} \\
\sigma_{12} &= \frac{m_v \bar{l}_o f_n^o}{4}\left\{a\sin 2\theta_a + a_n \sin 2\theta_f + a_t \sin 2\theta_t\right\} \\
\sigma_{21} &= \sigma_{12}
\end{aligned} \tag{3.39}$$

Boundary stresses can be described by the following invariant quantities associated with the Mohr circle of stress:

$$\sigma_n = \left(\frac{\sigma_{11} + \sigma_{22}}{2}\right) \tag{3.40}$$

$$\sigma_t = \sqrt{\left(\frac{\sigma_{11} - \sigma_{22}}{2}\right)^2 + {\sigma_{12}}^2} \tag{3.41}$$

The term σ_n is the *normal* or *hydrostatic* component of stress and σ_t the *deviatoric* component.

Principal stress directions can be calculated from:

$$\cos 2\theta_\sigma = \frac{\sigma_{11} - \sigma_{22}}{2\sigma_t}, \qquad \sin 2\theta_\sigma = \frac{\sigma_{12}}{\sigma_t} \tag{3.42}$$

Relations (3.39) and (3.40) give:

$$\sigma_n = \frac{m_v \bar{l}_o f_n^o}{2}\left\{1 + \frac{aa_n}{2}\cos 2(\theta_a - \theta_f)\right\} \tag{3.43}$$

The results of tedious calculations show that relationship (3.43) is exact when integration of (3.21) is carried out using all fourier components in expressions for $\bar{f}_n^c(\theta)$, $\bar{f}_t^c(\theta)$ and $E(\theta)$. Second-order terms a and a_n extracted from experimental data suggests that these values are typically less than 0.5. Consequently, only a small error may be anticipated by considering the simplified expression for σ_n proposed by Rothenburg (1980):

$$\sigma_n = \frac{m_v \bar{l}_o f_n^o}{2} \tag{3.44}$$

Neglecting product terms aa_n in equations (3.39) and substitution into (3.41) leads to:

$$\sigma_t = \frac{m_v \bar{l}_o f_n^o}{4}\sqrt{a^2 + a_n^2 + a_t^2 + 2aa_n \cos 2(\theta_a - \theta_f) + 2aa_t \cos 2(\theta_a - \theta_t) + 2a_n a_t \cos 2(\theta_f - \theta_t)} \tag{3.45}$$

The collection of terms in front of the brackets can be eliminated if an *invariant stress ratio* parameter a_σ is introduced such that:

$$a_\sigma = \frac{\sigma_t}{\sigma_n} = \frac{1}{2}\sqrt{a^2 + a_n^2 + a_t^2 + 2aa_n \cos 2(\theta_a - \theta_f) + 2aa_t \cos 2(\theta_a - \theta_t) + 2a_n a_t \cos 2(\theta_f - \theta_t)} \tag{3.46}$$

If directions of anisotropy for contact normals and contact forces are coaxial (i.e. $\theta_o = \theta_a = \theta_f = \theta_t$) then (3.46) is simplified to:

$$a_\sigma = \frac{1}{2}\left(a + a_n + a_t\right) \tag{3.47}$$

The average stress ratio σ_{22}/σ_{11} can also be deduced from relationships (3.39). Specifically:

$$\frac{\sigma_{22}}{\sigma_{11}} = \frac{1 - \frac{1}{2}\left(a\cos 2\theta_a + a_n \cos 2\theta_f + a_t \cos 2\theta_t - a a_n \cos 2(\theta_a - \theta_f)\right)}{1 + \frac{1}{2}\left(a\cos 2\theta_a + a_n \cos 2\theta_f + a_t \cos 2\theta_t + a a_n \cos 2(\theta_a - \theta_f)\right)} \tag{3.48}$$

Again, expressions are simplified if coaxial directions are assumed and product terms aa_n considered to be negligible. For this condition, equation (3.48) reduces to:

$$\frac{\sigma_{22}}{\sigma_{11}} = \frac{1 - \frac{1}{2}\left(a + a_n + a_t\right)\cos 2\theta_o}{1 + \frac{1}{2}\left(a + a_n + a_t\right)\cos 2\theta_o} \tag{3.49}$$

Fundamental concepts relating average stress to fabric and contact force anisotropy are contained in expressions (3.44) and (3.47) which have been reported in the same form by Rothenburg (1980). For example, the hydrostatic component σ_n of the average stress tensor is proportional to the average normal contact force f_n^o within the assembly. However, the invariant stress ratio a_σ shows that the shear capacity of the assembly is due to contributions of contact anisotropy a, average normal contact force anisotropy a_n and, average tangential contact force anisotropy a_t.

The fundamental relationships introduced above can also be expressed in tensorial form. To simplify tensorial expressions it is convenient to introduce *reduced* deviator tensorial quantities for fabric and contact force tensors. These reduced tensors are related to tensors $\mathbf{R}$, $\mathbf{F}_N$ and $\mathbf{F}_T$ according to:

$$\overline{\mathbf{R}}'_{ij} = \frac{\mathbf{R}'_{ij}}{\mathbf{R}_{kk}/2} = \frac{\mathbf{R}_{ij}}{\mathbf{R}_{kk}/2} - \delta_{ij} \qquad i,j = 1,2 \tag{3.50}$$

$$\overline{\mathbf{F}}'_{N_{ij}} = \frac{\mathbf{F}'_{N_{ij}}}{\mathbf{F}_{N_{kk}}/2} = \frac{\mathbf{F}_{N_{ij}}}{\mathbf{F}_{N_{kk}}/2} - \delta_{ij} \tag{3.51}$$

$$\overline{\mathbf{F}}'_{T_{ij}} = \frac{\mathbf{F}'_{T_{ij}}}{\mathbf{F}_{N_{kk}}/2} = \frac{\mathbf{F}_{T_{ij}}}{\mathbf{F}_{N_{kk}}/2} - \delta_{ij} \tag{3.52}$$

Neglecting second-order products of these tensors, stress components σ_{ij} can now be expressed as:

$$\sigma_{ij} = \sigma_n\{\delta_{ij} + \overline{\mathbf{R}}'_{ij} + \overline{\mathbf{F}}'_{N_{ij}} + \overline{\mathbf{F}}'_{T_{ij}}\} \tag{3.53}$$

where:

$$\sigma_n = \frac{\bar{l}_o \mathbf{R}_{kk} \mathbf{F}_{N_{kk}}}{2} \tag{3.54}$$

Expressing coefficients of anisotropy in equivalent reduced tensorial form, and rearranging (3.47), leads to the following expression for the deviatoric stress component:

$$\sigma_t = \frac{\sigma_n}{\sqrt{2}}\{\sqrt{\overline{\mathbf{R}}'_{ij}\overline{\mathbf{R}}'_{ij}} + \sqrt{\overline{\mathbf{F}}'_{N_{ij}}\overline{\mathbf{F}}'_{N_{ij}}} + \sqrt{\overline{\mathbf{F}}'_{T_{ij}}\overline{\mathbf{F}}'_{T_{ij}}}\} \tag{3.55}$$

While mathematical developments leading to expressions (3.53) through (3.55) have been restricted to two-dimensional systems, the general form of these relationships is preserved for three-dimensional assemblies comprising spherical particles.

3.4.2 Contact Normal Anisotropy and Stress from Laboratory Tests

Some insight into the relationship between average stress and contact anisotropy can be gained from analysis of test data reported by Oda and Konishi (1974b) and Konishi (1978) for assemblies of photo-elastic discs.

Figures 3.10a and 3.10b show coefficients of contact anisotropy a, b and invariant stress ratio a_σ plotted against *shear distortion* measured at the sample boundaries. Coefficient terms a and b have been calculated from the histogram data on Figure 1.11 and a_σ from data reported by Oda and Konishi.

The following procedure was used by Oda and Konishi to estimate stresses acting over subregions of photo-elastic disc assemblies: A family of lines was drawn across the sample and normal and shear forces per unit length of line calculated from selected contact forces acting on particles intersected by the transect lines. Several lines were considered to arrive at a representative shear force F_T and normal force F_N per unit length of line. From two sets of orthogonal lines the average stress tensor for the subassembly was approximated from $F_N = \sigma_{ij}n_in_j$ and $F_T = \sigma_{ij}t_in_j$. The researchers restricted stress calculations and the determination of contact normal distributions to interior locations of the disc assemblies in order to minimize the influence of the rigid-wall boundaries. However, they do not indicate in the referenced literature if calculated stress quantities and contact distributions represent exactly the same subassembly volumes. In addition, a criterion to include only load-carrying (active) contacts in the calculation of the contact normal distribution is not mentioned. Nevertheless, assuming for the moment that a comparison of contact coefficient terms and a_σ is valid then, two important observations can be made from Figure 3.10 concerning the relationship between second-order tensors $\mathbf{R}$ and σ.

1) The behaviour of a and a_σ is similar. Generally, increases in contact anisotropy coincide with increases in sample strength as measured by a_σ. Similarly, where there is a drop in contact anisotropy, there is a corresponding loss in assembly shear capacity.

2) The major principal direction of contact anisotropy appears to *follow* the major principal stress direction. At relatively large strains both directions appear coincident.

The strong correlation between parameters equivalent to a and a_σ and coincidence of principal directions θ_a and θ_σ has been reported by Konishi (1978). The observation that a is less than a_σ and strongly correlated to assembly shear capacity is consistent with expression (3.46) which has been arrived at from theoretical considerations.

Oda and Konishi do not report distributions of normal and tangential contact forces for their tests. However, if the plots on Figure 3.8 are assumed to approximate normal contact forces during simple shear, then, the principal direction of contact normal force θ_f appears sensibly coincident with θ_σ. The same statement can be made based on distributions for contacts and contact forces shown on Figures 3.4 and 3.9 taken from the results of biaxial compression tests (major principal stress direction at $\theta_\sigma = \pi/2$).

The relationship of the fourth-order coefficient of anisotropy b to the shear capacity of the system is less clear. Figure 3.10 shows that as the initial dense assembly *dilates*, b increases in value. Conversely, the initially *loose* assembly shows that the early contact geometry associated with b is attenuated with increasing sample distortion. The following interpretation is offered which is due in part to insight gained from numerical simulations of assemblies of discs reported in Chapter 5:

Theoretical developments leading to expression (3.47) pointed out that b is, in fact, an invariant quantity of a *fourth-order contact* tensor. As a result, the evolution of higher-order contact geometry such as that described by b is likely an indirect response to imposed boundary disturbances which are described by a *second-order* average (stress) tensor. Changes in b are likely due to (as yet) undefined stability requirements which are pronounced when the system has a high degree of mobility. Significant changes in b and/or relatively large values comparable to a only occur if the sample is initially *loose* or reaches a lower contact density through dilation. In contrast, dramatic changes in a occur in both tests irrespective of assembly density.

Principal directions plotted on Figure 3.10c and 3.10d show that in general, θ_a and θ_b are non-coincident.

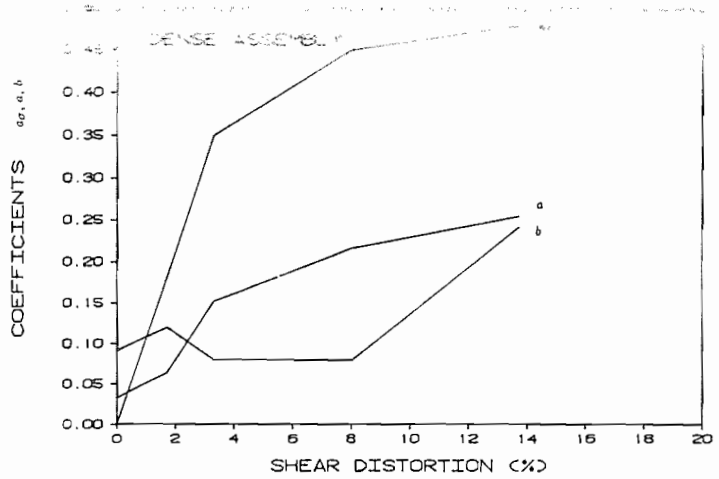

a) Coefficients of Anisotropy a_σ, a, and b versus *Shear Distortion*

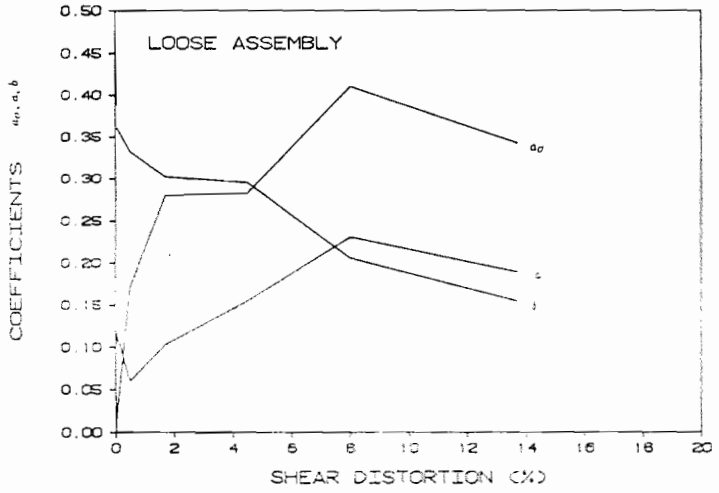

b) Coefficients of Anisotropy a_σ, a, and b versus *Shear Distortion*

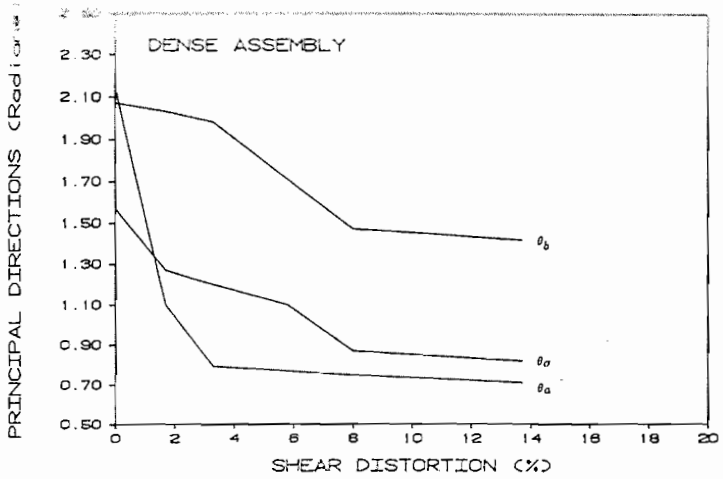

c) Principal Stress Direction θ_σ and Contact Normal Directions θ_a, θ_b versus *Shear Distortion*

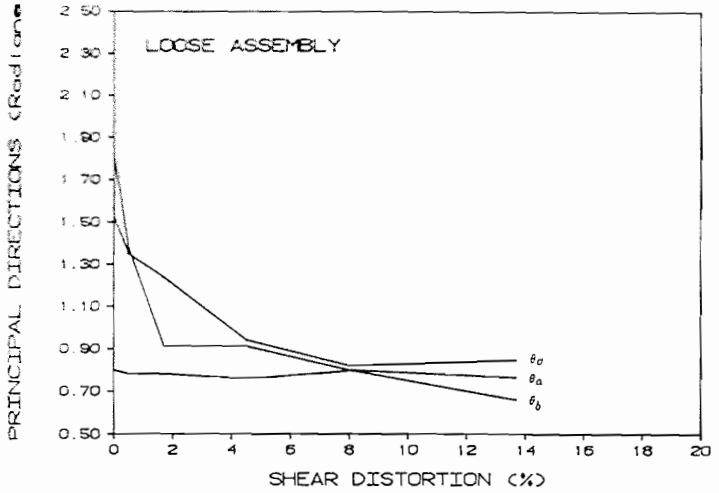

d) Principal Stress Direction θ_σ and Contact Normal Directions θ_a, θ_b versus *Shear Distortion*

Figure 3.10 Assembly Shear and Contact Normal Anisotropy from Two-Dimensional Simple Shear Tests *(data from Oda and Konishi, 1974b, and Konishi, 1978)*

CHAPTER 4

NUMERICAL SIMULATION OF TWO-DIMENSIONAL ASSEMBLIES OF DISCS

4.1 Introduction

The Distinct Element Method and its computer implementation to numerically simulate assemblies of discs have been reported by Strack and Cundall (1978), Cundall (1979), and Cundall and Strack (1979a,b,c). These researchers developed the computer program BALL and attempted to validate its usefulness as a research tool to study the mechanical behaviour of idealized granular systems. A description of the validation exercises has been briefly outlined in Section 1.6.5.

The numerical simulation of two-dimensional assemblies of discs has some important advantages over comparable physical experiments such as those reported by Oda and Konishi (1974a, 1974b). These advantages include the following:

1) Tests can be performed which examine assemblies having a range of particle sizes and particle properties.

2) Parametric studies can be undertaken which allow parameters describing particle interactions to be isolated and their contribution to the macroscopic behaviour of these systems evaluated.

3) Tests which are difficult to perform in the laboratory, such as reversal of principal stress axes, can be easily accommodated in these simulations.

4) Data extraction, including distributions of contact normals and contact force components and the like, is easily automated.

5) Assembly configurations can be stored at any stage in a test and restarted at a later date without disturbing the original condition of the sample.

6) Boundary conditions imposed on test assemblies are perfectly controlled.

An important advantage of the numerical experiments reported in this study over other simulations, such as finite element models representing continua, is that the macroscopic response of the system is dictated by the micromechanical behaviour of the discrete media. Other analytical

approaches have the drawback that macroscale hypotheses, including constitutive relations and associated flow rules, must be assumed and their implementation may obscure or misrepresent actual physical behaviour.

The current investigation uses a heavily-modified version of the prototype program BALL, called DISC.

4.2 The Distinct Element Method (DEM)

4.2.1 General

The following sections outline the fundamental aspects of the Distinct Element Method (DEM) as reported by Strack and Cundall (1978), Cundall and Strack (1979a,c).

The DEM employs an explicit time-finite-difference scheme in which each calculation cycle includes the application of Newton's Second Law to the centroid of each disc followed by application of two simple force-displacement laws at all disc contacts. By keeping the time-step Δt small, disturbances initiating at the assembly boundaries will propagate at a rate not greater than the distance between contacting disc centres during a calculation cycle. The disc accelerations and velocities calculated from Newton's Second Law are assumed to be constant over Δt and the net forces and moment acting on each disc are updated from force-displacement laws applied at the contacts with neighbouring discs.

In actual fact, the DEM models a dynamic transient mechanical system. It can be imagined as a network of lumped-mass-dashpot elements in which linear springs connect disc shaped masses. Although the system is dynamic, the transient state approaches a static equilibrium condition if loading rates at the sample boundaries are kept low enough that inertial disc forces are always a small fraction of the average contact forces acting through the assembly. Kinetic energy is dissipated through the introduction of artificial damping, without which, the approximation to a static equilibrium condition would not be achieved.

4.2.2 Disc Geometry

Consider the two contacting discs shown on Figure 4.1 having radii R_A and R_B. A physical contact exists when $D < R_A + R_B$. The contact between discs A and B is considered to be at point C located equi-distant from the points P_A and P_B along the branch length connecting the centroid of disc A to the centroid of disc B. If very stiff contacts are considered then, the overlap between particles is very small compared to the diameters of the contacting discs.

The geometry of contacting particles is completely described by the location of the disc centroids x_{Ai}, x_{Bi}, disc rotations θ_A, θ_B and disc radii (indicial operations are with respect to $i = 1, 2$). A finite-difference scheme is used to relate changes in geometry at the end of each time-step to current translational and angular velocities $\dot{x}_{Ai}$, $\dot{x}_{Bi}$, $\dot{\theta}_A$ and $\dot{\theta}_B$. Contact displacements for the overlapping discs are calculated based on the relative velocities of point P_A with respect to point P_B.

It is convenient to resolve incremental contact displacements which occur over each time-step into normal and tangential components referenced to the normal and tangential contact vectors for disc A. As before, these contact vectors are denoted as $\tilde{n}^c = (\cos\theta, \sin\theta)$ and $\tilde{t}^c = (-\sin\theta, \cos\theta)$.

4.2.3 Equations of Motion from Newton's Second Law

Newton's Second Law applied to a disc can be written as:

$$\begin{aligned} m(\ddot{x}_i)_N &= (F_i)_N \qquad i = 1, 2 \\ I(\ddot{\theta})_N &= (M)_N \end{aligned} \tag{4.1}$$

Here m and I represent the mass and moment of inertia of the disc and $(F_i)_N$ and $(M)_N$ the net force components and moment acting at the disc centroid at the beginning of the time-step corresponding to t_N. Net force components F_i and the total moment M acting at a disc centroid are shown on Figure 4.2. The figure shows positive orientations for these parameters. Forces F_n and F_s represent normal and tangential (shear) contact forces.

Assuming that disc accelerations $\ddot{x}_i$ and $\ddot{\theta}$ at t_N are constant over the interval $t_{N-1/2}$ to $t_{N+1/2}$ then, disc velocities can be calculated from:

$$\begin{aligned} (\dot{x}_i)_{N+1/2} &= (\dot{x}_i)_{N-1/2} + \frac{(F_i)_N \Delta t}{m} \\ (\dot{\theta})_{N+1/2} &= (\dot{\theta})_{N-1/2} + \frac{(M)_N \Delta t}{I} \end{aligned} \tag{4.2}$$

The coordinates of the disc centroid and disc rotation are then calculated at the end of the time-step t_{N+1} according to:

$$\begin{aligned} (x_i)_{N+1} &= (x_i)_N + \left((\dot{x}_i)_{N+1/2}\right)\Delta t \\ (\theta)_{N+1} &= (\theta)_N + \left((\dot{\theta})_{N+1/2}\right)\Delta t \end{aligned} \tag{4.3}$$

The finite-difference scheme employed to implement changes in geometry without considering damping is summarized on Figure 4.3.

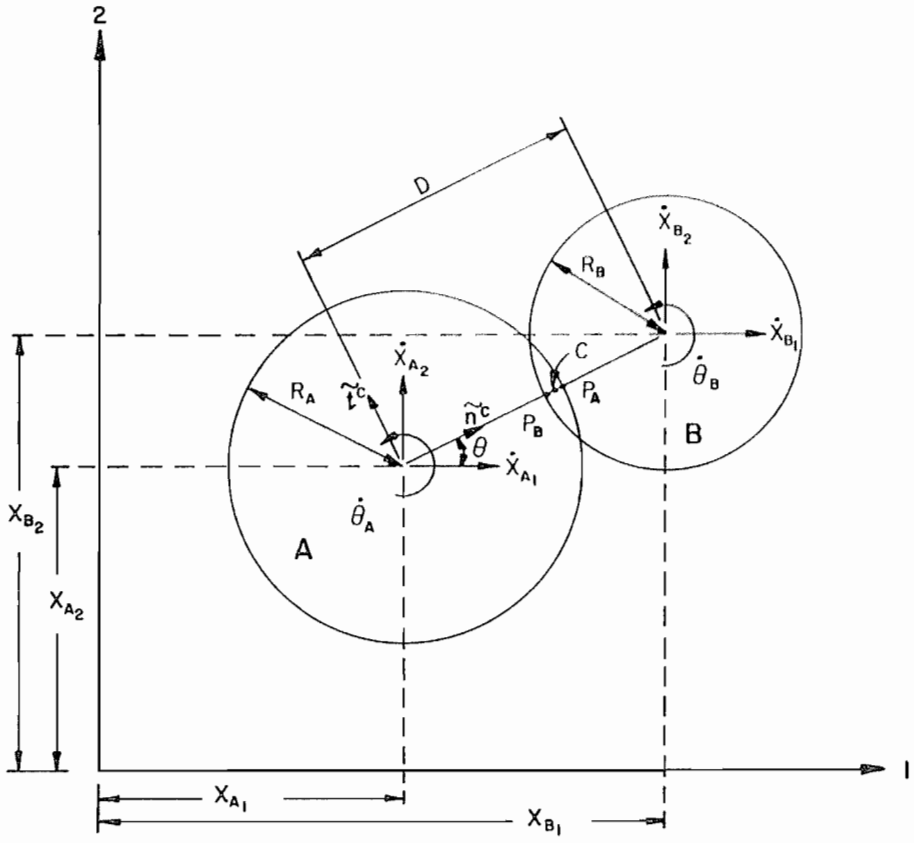

Figure 4.1 Geometry of Contacting Discs

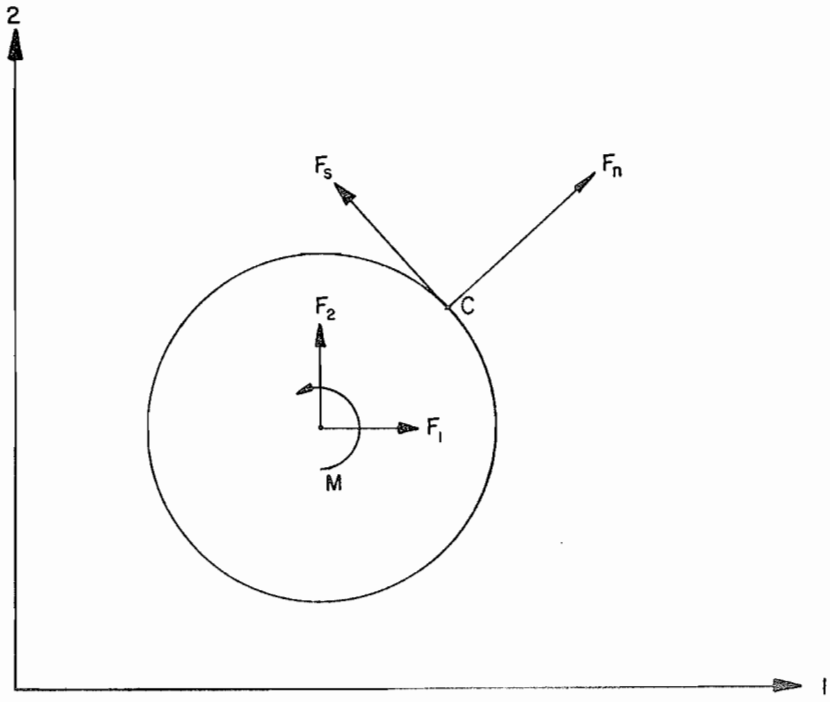

Figure 4.2 Disc Forces and Moment

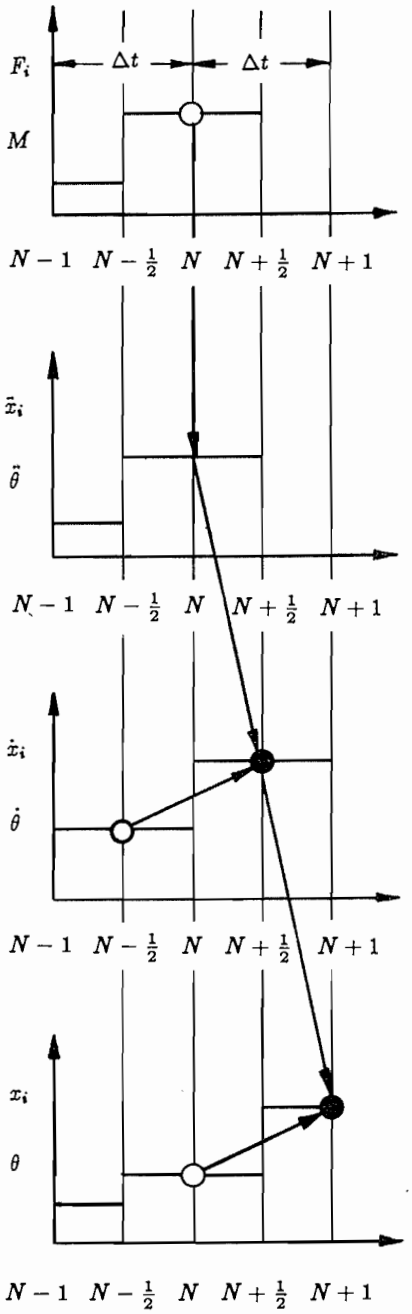

$$m(\ddot{x}_i)_N = (F_i)_N \qquad i = 1, 2$$
$$I(\ddot{\theta})_N = (M)_N \tag{4.1}$$

$$(\dot{x}_i)_{N+1/2} = (\dot{x}_i)_{N-1/2} + \frac{(F_i)_N \Delta t}{m}$$
$$(\dot{\theta})_{N+1/2} = (\dot{\theta})_{N-1/2} + \frac{(M)_N \Delta t}{I} \tag{4.2}$$

$$(x_i)_{N+1} = (x_i)_N + \left((\dot{x}_i)_{N+1/2}\right)\Delta t$$
$$(\theta)_{N+1} = (\theta)_N + \left((\dot{\theta})_{N+1/2}\right)\Delta t \tag{4.3}$$

○ stored value at start of calculation cycle

● stored value at end of calculation cycle

Figure 4.3 Finite-Difference Scheme for Changes in Disc Location and Rotation

4.2.4 Force-Displacement Laws

Following application of Newton's Second Law to all discs, contact force components are updated using:

$$\begin{aligned}(F_n)_{N+1} &= (F_n)_N + (\Delta F_n)_N = (F_n)_N + k_n(\Delta n)_{N+1/2} \\ (F_s)_{N+1} &= (F_s)_N + (\Delta F_s)_N = (F_s)_N + k_s(\Delta s)_{N+1/2}\end{aligned} \tag{4.4}$$

Here Δn and Δs refer to incremental normal and tangential contact displacements at a contact with normal and tangential contact stiffnesses k_n and k_s. Contact displacements are calculated from the current relative disc velocities (4.2) using the following finite-difference notation:

$$\begin{aligned}(\Delta_n)_{N+1/2} &= \Big((\dot{x}_{B_i} - \dot{x}_{Ai})_{N+1/2}\Big) n_i^c \Delta t \qquad i = 1,2 \\ (\Delta_s)_{N+1/2} &= \Big(\Big((\dot{x}_{Bi} - \dot{x}_{Ai})_{N+1/2}\Big) t_i^c - (\dot{\theta}_A R_A + \dot{\theta}_B R_B)_{N+1/2}\Big) \Delta t\end{aligned} \tag{4.5}$$

The finite-difference scheme for the application of the force-displacement laws is shown on Figure 4.4 without damping.

A Coulomb-type friction law is employed in order to allow particles to slip once a threshold tangential force level is achieved. The friction criterion for cohesionless contacts can be expressed as $|(F_s)|_{max} = |F_n \mu|$. Term μ refers to the maximum interparticle friction coefficient. If two discs with different μ values are encountered the minimum value is used in the computation. If calculations show that the magnitude of the critical tangential shear force has been exceeded, then $|(F_s)|_{max}$ is used together with the sign of the computed excess shear force. Should contacting discs have different stiffnesses for k_n and k_s then, the contact stiffnesses in (4.4) are calculated assuming that stiffness components act in series.

The final step in any calculation cycle is updating of disc forces F_i and moment M which is done by summing all contact force components and moments in the following manner:

$$\begin{aligned}(F_i)_{N+1}^k &= \sum_{n=1}^{n_k} \Big((F_n)_{N+1} n_i^c + (F_s)_{N+1} t_i^c\Big) \\ (M)_{N+1}^k &= r^k \sum_{n=1}^{n_k} \Big((F_s)_{N+1}\Big)\end{aligned} \tag{4.6}$$

In the above relationship, n_k refers to the contacts associated with disc k having radius r^k.

The cycle procedure is then repeated with the updated disc forces and moments substituted into the expressions for changes in disc geometry described in Section 4.2.3.

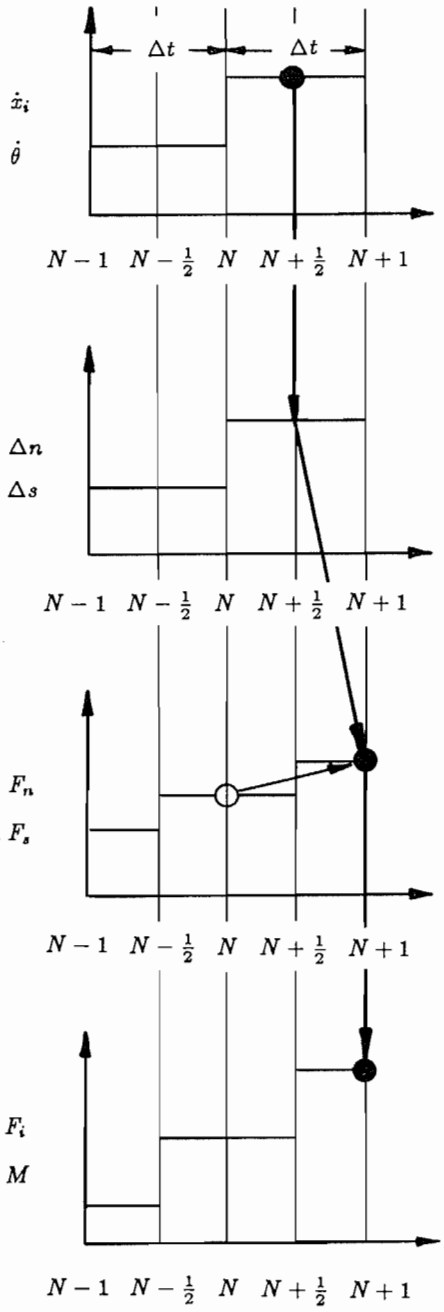

$$(\dot{x}_i)_{N+1/2} = (\dot{x}_i)_{N-1/2} + \frac{(F_i)_N \Delta t}{m}$$
$$(\dot{\theta})_{N+1/2} = (\dot{\theta})_{N-1/2} + \frac{(M)_N \Delta t}{I} \qquad (4.2)$$

$$i = 1, 2$$

$$(\Delta_n)_{N+1/2} = \left((\dot{x}_{B_i} - \dot{x}_{A_i})_{N+1/2}\right) n_i^c \Delta t$$
$$(\Delta_s)_{N+1/2} = \left(\left((\dot{x}_{B_i} - \dot{x}_{A_i})_{N+1/2}\right) t_i^c - (\dot{\theta}_A R_A + \dot{\theta}_B R_B)_{N+1/2}\right) \Delta t \qquad (4.5)$$

$$(F_n)_{N+1} = (F_n)_N + (\Delta F_n)_N = (F_n)_N + k_n(\Delta n)_{N+1/2}$$
$$(F_s)_{N+1} = (F_s)_N + (\Delta F_s)_N = (F_s)_N + k_s(\Delta s)_{N+1/2} \qquad (4.4)$$

$$(F_i)^k_{N+1} = \sum_{n=1}^{n_k} \left((F_n)_{N+1} n_i^c + (F_s)_{N+1} t_i^c\right)$$
$$(M)^k_{N+1} = r^k \sum_{n=1}^{n_k} \left((F_s)_{N+1}\right) \qquad (4.6)$$

○ stored value at start of calculation cycle

● stored value at end of calculation cycle

Figure 4.4 Finite-Difference Scheme for Application of Force-Displacement Laws

4.2.5 Damping

The DEM must include a provision for damping in order that the assembly of discs can approach a state of static equilibrium under all conditions.

Three forms of damping have been introduced by Strack and Cundall (1978) and are included in the prototype program BALL and the current version DISC. They are:

1) Contact damping which acts on the relative velocities at disc contacts in both normal and tangential directions. Contact damping may be envisaged as dashpots which act in parallel with the linear springs describing contact stiffnesses.

2) GIobal damping which acts on the absolute velocities of the discs and can be envisaged as dashpots which connect each disc to a fixed frame of reference.

3) Friction damping: Tangential contact forces are restricted according to the interparticle friction criterion described in Section 4.2.4. Consequently, whenever this value is substituted into the force-displacement expressions it represents a damping mechanism on interparticle tangential displacements. In order not to cause excessive tangential damping when $|(F_s)|_{max}$ is achieved, the tangential contact damping is not applied during sliding.

Contact damping coefficients are related to the contact stiffnesses k_n and k_s through a coefficient of proportionality β :

$$\begin{aligned} c_n &= \beta k_n \\ c_s &= \beta k_s \end{aligned} \tag{4.7}$$

Normal and tangential contact damping forces are calculated from:

$$\begin{aligned} (D_n)_N &= c_n \left[\left((\dot{x}_{Bi} - \dot{x}_{Ai})_{N-1/2} \right) n_i^c \right] \qquad i = 1, 2 \\ (D_s)_N &= c_s \left[\left((\dot{x}_{Bi} - \dot{x}_{Ai})_{N-1/2} \right) t_i^c - (\dot{\theta}_A R_A + \dot{\theta}_B R_B)_{N-1/2} \right] \end{aligned} \tag{4.8}$$

Contributions of contact damping are resolved into components D_i and added to the force term in (4.2). Tangential contact force damping is also included in the moment M. Hence expressions (4.2) now become:

$$\begin{aligned} (\dot{x}_i)_{N+1/2} &= (\dot{x}_i)_{N-1/2} + \left[\left(\frac{F_i + D_i}{m} \right)_N \right] \Delta t \\ (\dot{\theta})_{N+1/2} &= (\dot{\theta})_{N-1/2} + \left[\left(\frac{M}{I} \right)_N \right] \Delta t \end{aligned} \tag{4.9}$$

It should be noted that there is a half time-step error between the force and moment sums in (4.9) and terms $(D_n)_N$ and $(D_s)_N$. The original authors consider this error negligible.

Global damping coefficients are related to the mass and moment of inertia of each disc through a coefficient of proportionality α:

$$\begin{aligned} c_m &= \alpha m \\ c_I &= \alpha I \end{aligned} \tag{4.10}$$

The original equation of motion can now be rewritten to include both contact and global damping contributions:

$$\begin{aligned} m(\ddot{x}_i)_N &= (F_i + D_i)_N - c_m(\dot{x}_i)_N \\ I(\ddot{\theta})_N &= (M)_N - c_I(\dot{\theta})_N \end{aligned} \tag{4.11}$$

Letting:

$$\begin{aligned} (\dot{x}_i)_N &= \frac{1}{2}\Big((\dot{x}_i)_{N+1/2} + (\dot{x}_i)_{N-1/2}\Big) \\ (\dot{\theta})_N &= \frac{1}{2}\Big((\dot{\theta})_{N+1/2} + (\dot{\theta})_{N-1/2}\Big) \end{aligned} \tag{4.12}$$

and

$$\begin{aligned} (\ddot{x}_i)_N &= \frac{(\dot{x}_i)_{N+1/2} - (\dot{x}_i)_{N-1/2}}{\Delta t} \\ (\ddot{\theta})_N &= \frac{(\dot{\theta})_{N+1/2} - (\dot{\theta})_{N-1/2}}{\Delta t} \end{aligned} \tag{4.13}$$

leads to revised equations of motion in the form:

$$\begin{aligned} (\dot{x}_i)_{N+1/2} &= \frac{(\dot{x}_i)_{N-1/2}(1 - \alpha\Delta t/2) + (F_i + D_i)_N \Delta t/m}{1 + \alpha\Delta t/2} \\ (\dot{\theta})_{N+1/2} &= \frac{(\dot{\theta})_{N-1/2}(1 - \alpha\Delta t/2) + (M)_N \Delta t/m}{1 + \alpha\Delta t/2} \end{aligned} \tag{4.14}$$

It is easily seen that setting $\alpha = 0$ and $\beta = 0$ leads to the original equations of motion (4.2) without the option of damping.

The lumped-mass linear spring and dashpot system which is used in the current version of DISC to model the behaviour of cohesionless discs is summarized on Figure 4.5.

4.2.6 Additional Comments on the DEM

The contact force-displacement laws described in Section 4.2.4 have been adopted because they are simple. It should be noted that the principal purpose of using the DEM technique in this investigation is to verify formulations developed in earlier chapters which are independent of the contact model employed. However, it is of interest to note that other contact models, such as those that incorporate non-linear contact stiffnesses, could easily be used in the numerical technique. The use of linear (or non-linear) springs is not unreasonable if one considers that contact behaviour between *real* granular

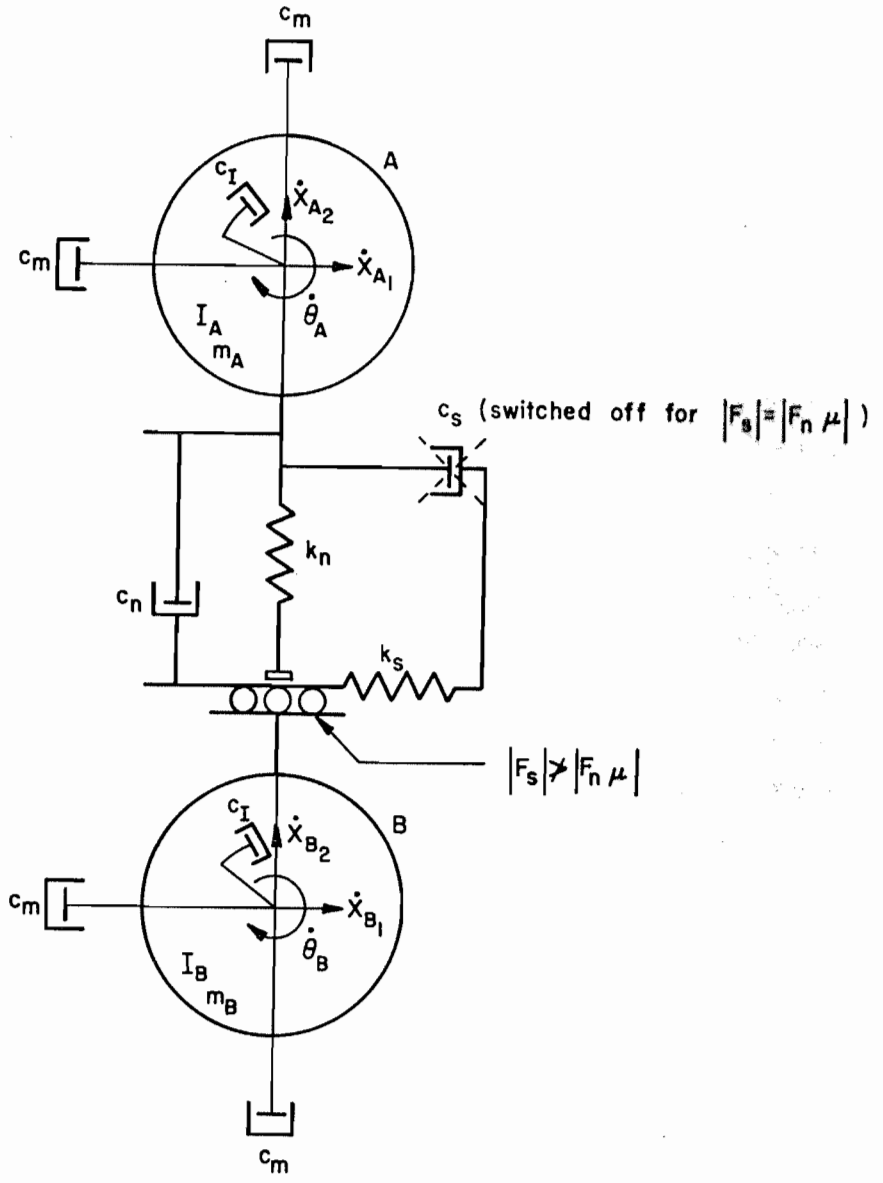

Figure 4.5 Schematic Showing Principal Rheological Elements of the Distinct Element Method for Cohesionless Discs

particles is likely to be governed by surface asperities and consequently is unrelated to the dimensions of the particles (as would be the case of truly *elastic* particles).

The finite-difference expressions presented in this chapter can also be modified to include body forces (i.e. gravity). These forces can be added to the right-hand side of equation (4.1). For simplicity, gravity forces were not considered in this study since, for the small assemblies considered, self-weight could be assumed to be negligible compared to the stresses imposed on the system. In addition, weightless particles eliminate the need to differentiate between active and passive contacts in program DISC during contact distribution data extraction.

The DEM technique can also be formulated to consider *bonded* assemblies of discs. For these systems the Coulomb-type interparticle friction criterion can be modified to include a very large cohesion term.

The description of the DEM method presented in this Chapter must raise the question of the validity of the mechanisms through which energy imparted at the system boundary is dissipated internally. In real systems, low frequency damping (which is a necessary part of the DEM technique) is not present. Consequently, the results of numerical simulations using this technique to propose micromechanical models relating global stress and strain through energy considerations must be undertaken with caution. In the current investigation the DEM technique and its implementation through program DISC is restricted to validating aspects of micromechanical behaviour which depend only on laws of static equilibrium.

4.3 Program DISC

4.3.1 Introduction

The current investigation uses a heavily-modified version of the program BALL originally developed by Strack and Cundall (1978). The modifications were made for two principal reasons:

First, the original program BALL was developed for execution on 32 bit mini-computers with restricted internal core (i.e. 64K words). Consequently, the original FORTRAN code and algorithm structure were written to preserve CPU memory and minimize floating-point arithmetic operations. The program DISC has been written in FORTRAN but operates on mainframe computers (in this study a 36 bit Honeywell DPS/8). As a result, the program DISC has a much simpler structure since memory requirements (typically 170K words) were not a constraint and no execution-time savings are realized by incorporating the integer arithmetic operations found in the prototype BALL.

The second major reason for modifying the original program was to extract data which would provide an independent verification of the theories proposed in Chapter 3.

Other major differences between the programs should be mentioned: For example; to eliminate rigid-wall boundary effects on assemblies of discs, program DISC considers only near-circular assemblies of particles whose boundaries are defined by perimeter discs. In addition, the application of prescribed boundary disturbances to these assemblies differs from the prototype program BALL in order to improve execution time.

Nevertheless, while *bookkeeping*, data extraction and boundary control in program DISC are very different from program BALL, the implementation of the DEM, as reported by Strack and Cundall (1978), has been essentially preserved in the current version of DISC.

A computèr listing of program DISC can be found in Appendix A together with program AUTODISC which is a separate program used to generate initial uncompacted disc assemblies.

The following sections summarize important aspects of both programs.

4.3.2 Description of Program DISC

4.3.2.1 General

Program DISC models the mechanical behaviour of a near-circular assembly of two-dimensional discs using the DEM numerical technique. A visual representation of a small assembly of discs generated by program DISC is shown on Figure 4.6.

The assembly is contained within a series of *boundary* discs identified by the dark discs in the figure. The centre of each boundary disc represents the vertex of a convex polygon compriaing straight-line segments joining boundary disc centres. At the beginning of each calculation cycle, velocity or force components are applied to the centre of each boundary disc in response to prescribed boundary stress and/or strain-rate conditions. As the system deforms, the assembly boundary discs are updated. For example, should the centre of an interior located disc intercept any straight-line boundary segment then, it becomes a boundary disc.

4.3.2.2 Disc Generation

Prior to initial execution of program DISC it is necessary to generate an assembly of discs and to locate these discs with respect to a fixed-rectangular coordinate space. Disc generation is accomplished through the execution of a separate program called AUTODISC. This program contains a random number generator which is used to place non-overlaping discs at random radial locations within a

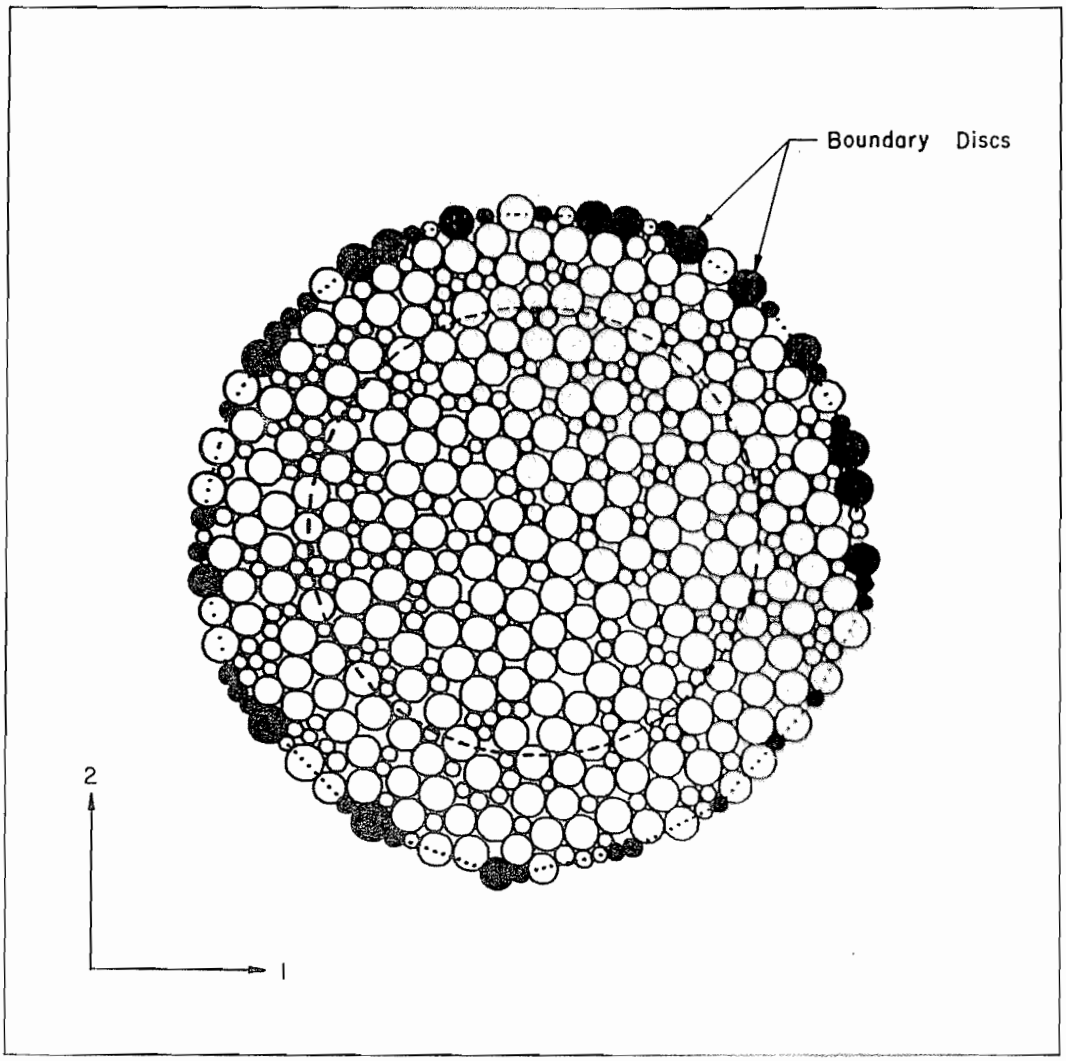

Figure 4.6 Two-Dimensional Assembly of Compacted Discs

circular region. The selection of disc sizes is taken from a prescribed particle size-distribution. The result of the operations just described is a very loose assembly of discs whose density diminishes with distance from the sample centre. An example of such an assembly is given on Figure 4.7. The nonhomogenous sample generation was adopted purposely so that during the subsequent compaction stage, a relatively homogenous assembly was created. The problem with a disc generating scheme which locates discs with respect to randomly selected coordinates x_i is that, during compaction, the outer *layers* of the assembly are compacted to a greater extent than interior located discs and a significant density gradient through the sample results.

Also shown on Figure 4.7 is the grid of *boxes* generated by program AUTODISC as part of the *bookkeeping* scheme used to trace the movement of discs and identify contacting neighbours and discs in close proximity to each other during execution of program DISC. Following disc generation, the assembly is compacted using program DISC which implements the numerical scheme described in Section 4.2. It is this compacted assembly which is the starting point for the majority of tests reported in this study.

4.3.2.3 General Organization of Program DISC

The main algorithm flow chart for program DISC is illustrated on Figure 4.8.

Program initialization is carried out through Subroutine INITP which does the following:

1) Input contents of the *configuration file* containing current assembly data. Included in this file are all current disc values for x_i, $\dot{x}_i$, θ, $\dot{\theta}$, F_i and M and a list of all contacts together with their associated contact forces F_n, F_s and total contact normal and tangential displacements.

2) Input contents of a file describing disc properties.

3) Input damping coefficients α and β.

4) Calculate certain fixed parameters such as the time-step Δt.

5) Input test program details including number of execution cycles, cycle interval for data extraction and prescribed boundary conditions.

The DEM as outlined in previous sections is implemented in Subroutine CYCLE. Each calculation cycle begins with the Subroutine SRVMOT which applies velocities or forces to each boundary disc according to the prescribed boundary conditions. Next, Subroutine MOTION is executed which applies expressions (4.14) and (4.3) to each disc in the assembly. Subroutine FORD follows during which the force-displacement laws (4.4 and 4.5) are applied to each disc and disc forces and moment

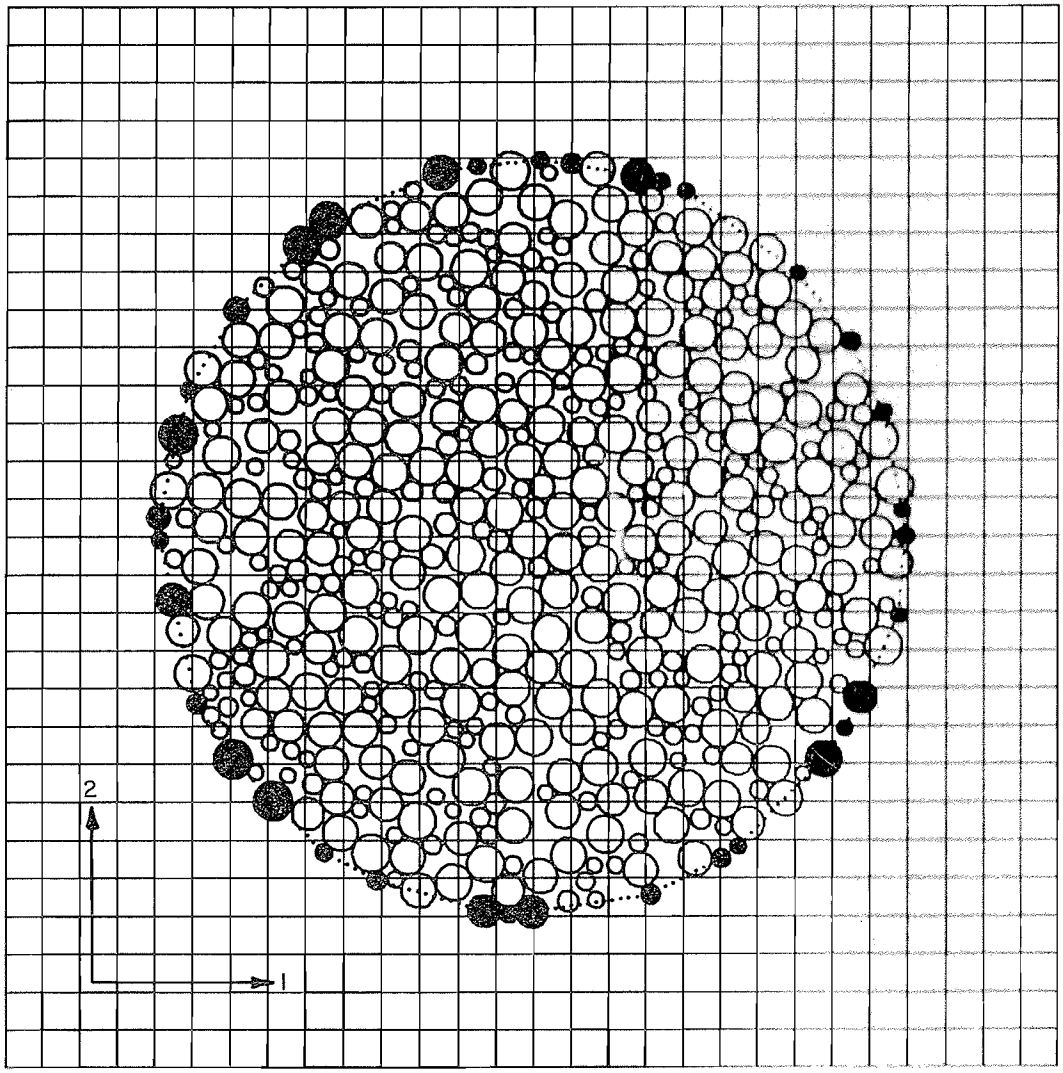

Figure 4.7 Disc Generation

updated according to (4.6). If the cycle count corresponds to a prescribed value then, Subroutine EXTRACT is executed which loads a data file with assembly information at that particular stage of the test.

Once the total number of calculation cycles has been completed, the assembly configuration file is updated and becomes the data source for subsequent execution(s) of program DISC.

4.3.2.4 Disc Properties and Units

Program DISC accommodates up to 50 disc types. Each disc type identifies a set of disc properties which include a radius r, density ρ, normal and tangential contact stiffnesses k_n and k_s, and coefficient of interparticle friction μ. The intensity of contact and global damping is determined by the single set of damping constants α and β described in Section 4.2.5.

The magnitude of the values describing disc radii, density, stiffnesses, and damping constants are similar to those reported by Strack and Cundall (1978) and *do not* represent any physical units. The values assigned to these parameters were chosen to ensure that disc overlaps during program execution were very small and numerical results were stable and accurate.

4.3.2.5 Calculation of Time-Step

As a consequence of the explicit nature of the numerical scheme employed in program DISC, a time-step must be selected which is small enough that the numerical simulation is stable. The time-step Δt is calculated as a fraction of a critical time-step Δt_c which in turn is estimated from a single degree-of-freedom mass-spring model according to:

$$\Delta t_c = 2\sqrt{m_{min}/k_n} \tag{4.15}$$

Here, m_{min} represents the mass of the smallest disc in the assembly and k_n the corresponding normal linear contact stiffness.

4.3.2.6 Average Stress

Program DISC allows the investigator to trace changes in the average stress tensor σ for the entire assembly and for selected interior sub-assemblies at any number of stages in the test.

The average stress tensor is conveniently calculated from:

$$\sigma_{ij} = \frac{1}{V}\sum_{c \epsilon V} f_i^c r_j^c \qquad i,j = 1,2 \tag{4.16}$$

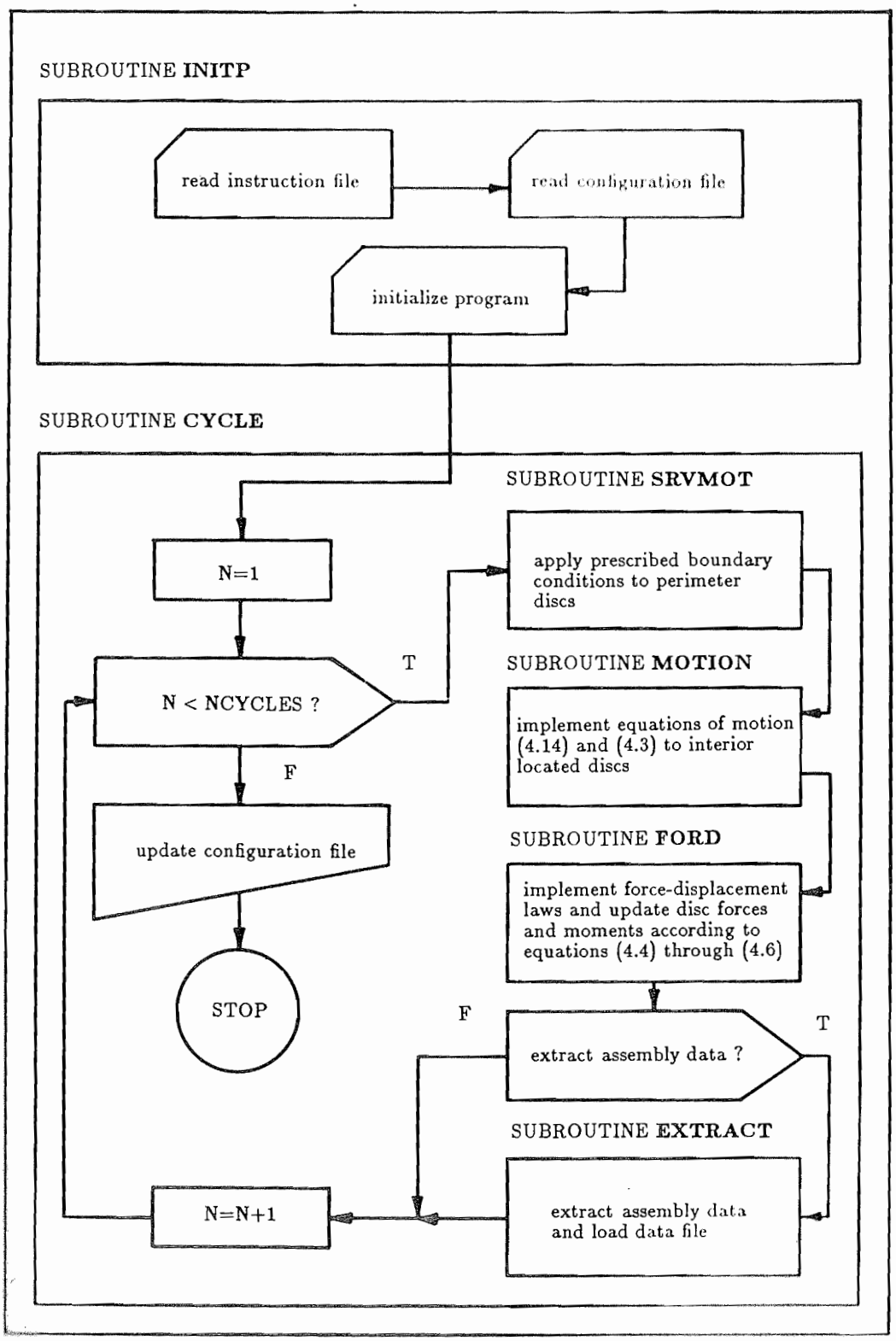

Figure 4.8 Program DISC Flow Chart

which follows from (2.17). In the above expression, r^c represents the disc radius corresponding to the contact c. The volume term V in (4.16) corresponding to the entire assembly is approximated by the area contained by the convex-polygon of line segments connecting adjoining boundary disc centroids. Sub-assemblies comprise discs which fall within and on a specified circle (such as the dashed circle on Figure 4.6). The volume term V for these sub-assemblies is approximated by the area of the circle.

To minimize the influence of boundary discs on the calculation of σ, contacts between discs which are located on the perimeter of the entire assembly are not considered in expression (4.16).

Normal and deviatoric invariant stress values are calculated according to (3.40) and (3.41) respectively. Principal stress directions are calculated from expressions (3.42).

4.3.2.7 Average Strain

A measure of sample deformation is required to complete the macroscopic description of the stress-strain behaviour of the assembly. Program DISC monitors the (total) displacement of boundary discs at pre-selected cycle intervals and converts these displacements into an *average strain tensor* ε using:

$$\varepsilon_{ij} = \frac{1}{V}\sum_{\beta=1}^{n^\beta}\left[\frac{1}{2}\left\{\Delta x_j^\beta + \Delta x_j^{\beta+1}\right\}e_i^\beta S^\beta\right] \qquad i,j = 1,2 \tag{4.17}$$

The above expression can be referenced to Figure 4.9. Term V represents the area contained by the polygon described by the scalar line segments S^β connecting boundary discs. Each line segment is defined by the coordinates of adjacent boundary discs β and $\beta+1$ having displacements Δx^β and $\Delta x^{\beta+1}$ respectively. Term e_i^β refers to components of the unit vector acting normal to the line segment S^β.

Invariants of the average strain tensor are calculated in the program using the following expressions:

$$\begin{aligned}\varepsilon_n &= \varepsilon_{11} + \varepsilon_{22}\\ \varepsilon_t &= \sqrt{(\varepsilon_{11} - \varepsilon_{22})^2 + (\varepsilon_{12} + \varepsilon_{21})^2}\\ \varepsilon_\omega &= \varepsilon_{21} - \varepsilon_{12}\end{aligned} \tag{4.18}$$

Here ε_n is the *volumetric strain* and ε_t the *deviatoric strain* or shear strain. Term ε_ω represents *rigid body rotation* with a positive sign indicating counter-clockwise body rotation. Principal strain directions are calculated according to:

$$\sin 2\theta_\varepsilon = \frac{\varepsilon_{21} + \varepsilon_{12}}{\varepsilon_t}, \qquad \cos 2\theta_\varepsilon = \frac{\varepsilon_{11} - \varepsilon_{22}}{\varepsilon_t} \tag{4.19}$$

It should be noted that the term *average strain tensor* does not imply that deformations measured at the sample boundaries reflect deformation fields observed at interior locations. A continuous

displacement profile is imposed on the boundary of the entire test assembly but discontinuities are invariably observed within the assembly following peak shear. Clearly, a strain tensor description such as ε is an inadequate description of deformations which are characterized by discontinuities. The principal purpose of ε in this investigation is to provide a familiar description of the extent of total sample deformation over the course of each test.

4.3.2.8 Boundary Control

Boundary control is implemented in Subroutine SRVMOT. Three different boundary control modes were used in the current investigation and may be summarized as follows.

Mode 1 (Constant Boundary Strain-rate Test)

Mode 1 applies velocity components $\dot{x}_i^\beta$ to the centre of each boundary disc according to a prescribed strain-rate tensor $\dot{\varepsilon}_{ij}^b$. The velocities are calculated as follows:

$$\dot{x}_i^\beta = \dot{x}_{\varepsilon i}^\beta = \dot{\varepsilon}_{ij}^b (x_j^\beta - x_j^c) \qquad i,j = 1,2 \tag{4.20}$$

where $\tilde{x}^\beta$ represents the disc location at the beginning of the calculation cycle and x_j^c the centre coordinates of the assembly. Boundary control Mode 1 was used in this investigation to compact selected samples by setting off-diagonal strain-rate tensor terms to zero and imposing boundary disc velocities corresponding to $\dot{\varepsilon}_{11}^b = \dot{\varepsilon}_{22}^b$.

Mode 2 (Constant σ_{11} Test)

Mode 2 models a biaxial compression or extension test in which the boundary stress component σ_{11} and the strain-rate component $\dot{\varepsilon}_{22}^b$ are kept constant. The boundary disc velocity $\dot{x}_2^\beta$ corresponding to the prescribed strain-rate component is calculated from expression (4.20). The constant stress component σ_{11} at the sample boundaries is maintained using a strain-controlled boundary which functions in the manner of a servo-mechanism. At the end of each calculation cycle the average stress tensor σ_{ij} for the entire assembly is calculated from expression (4.16). In the next calculation cycle, σ_{11} is compared against the prescribed boundary stress component σ_{11}^b and the boundary disc velocity $\dot{x}_1^\beta$ updated from:

$$\dot{x}_i^\beta = \dot{x}_{bi}^\beta = \frac{g(\sigma_{ij}^b - \sigma_{ij})(x_j^\beta - x_j^c)}{\sigma_{ij}^b} \qquad i = j = 1 \tag{4.21}$$

Here the term g represents the servo gain.

Mode 4 (Servo Strain-controlled Test)

Mode 4 allows a prescribed strain-rate tensor $\dot{\varepsilon}_{ij}^b$ to be applied to the assembly boundary simultaneously with prescribed boundary stress σ_{ij}^b. Alternatively, by setting prescribed strain-rate tensor components to zero, the boundary is stress-controlled using only the servo-mechanism.

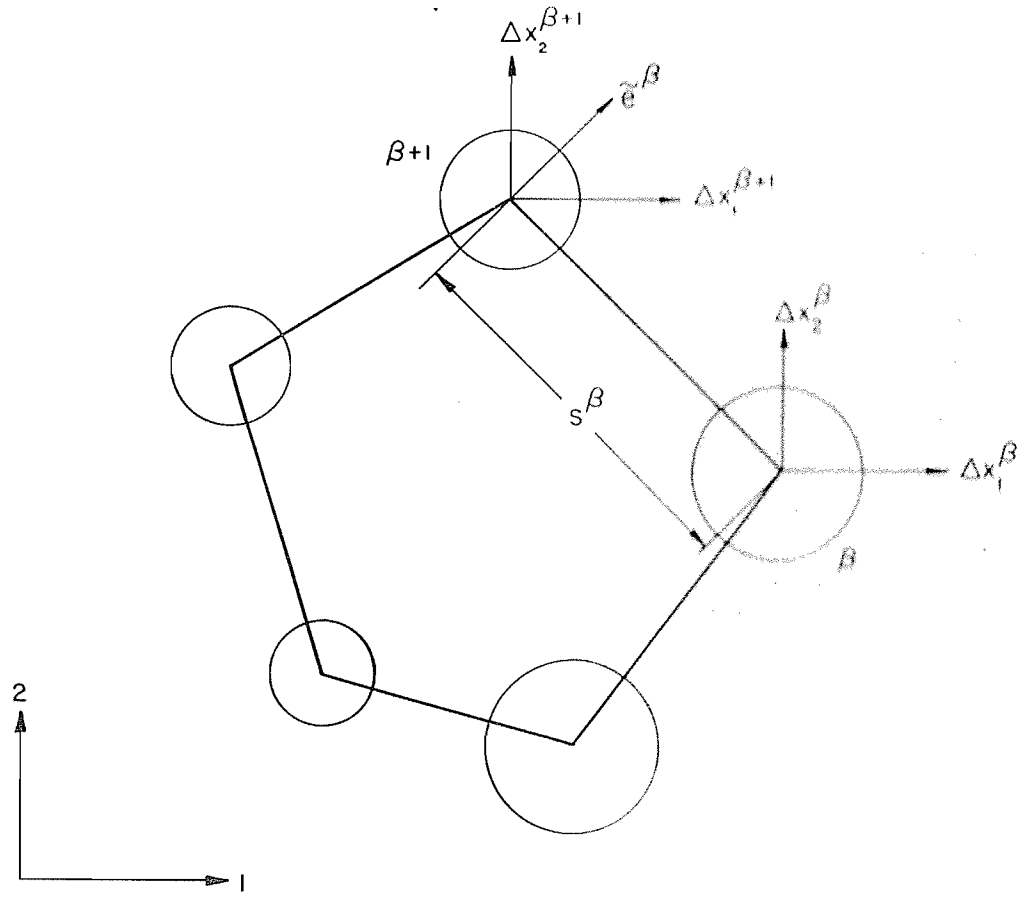

Figure 4.9 Boundary Disc Displacements for Calculation of Average Strain

The resultant boundary disc velocities are calculated as the sum of contributions from the strain-rate boundary control and the servo-mechanism boundary control. The contribution of the prescribed strain-rate tensor is calculated from expression (4.20). The contribution of the prescribed boundary stress tensor σ^b_{ij} is calculated from (4.21) with $i, j = 1, 2$. The resultant boundary disc velocities $\dot{x}^\beta_i$ are then calculated from:

$$\dot{x}^\beta_i = \dot{x}^\beta_{\varepsilon i} + \dot{x}^\beta_{bi} \tag{4.22}$$

The Mode 4 boundary control option was used in this investigation to create compacted isotropic ($K_o = 1$) and anisotropic ($K_o \neq 1$) assemblies under conditions of zero shear. In addition, this boundary control mode was used to shear compacted samples under conditions of constant normal stress.

4.3.2.9 Data Extraction

At prescribed numbers of cycles, information on the assembly is loaded to a data file which is used to trace the history of the test. Data extraction is done by Subroutine EXTRACT.

Information contained in the file includes average stress and strain tensor components, coordination number, contact density and assembly density for the entire sample. In addition, histogram data is extracted for distributions $\overline{f}^c_n(\theta)$, $\overline{f}^c_t(\theta)$ and also for the average contact vector length $\overline{l}^c(\theta)$. Parameters such as a, b, θ_a, θ_b, a_n, a_t, θ_f and θ_t are also calculated in order to examine system contact and force anisotropy. Similar information is included for selected circular sub-assemblies located within the interior of the assembly. The algorithms employed to calculate parameters of anisotropy are based on the numerical techniques developed in Sections 3.2.3 and 3.3.2.

The data file is constructed so that each record contains all of the above information at prescribed addresses in a one-dimensional binary array. Each record in the extract file then contains a complete description of the assembly at a particular cycle count. The data file is configured in this manner to facilitate test interpretation. Separate plotting routines, written by the author, were used to plot up to ten dependent variables against any one independent variable by simply identifying the addresses of the parameters to be investigated and the number of times data was extracted from the assembly during a test.

4.3.3 Comments on Program DISC

Several practical problems associated with the implementation of the DEM in program DISC for large assemblies should be noted.

The current version of DISC executes on a Honeywell DPS/8 mainframe at about one calculation cycle per second per 1000 discs and requires about 170K words internal memory. The amount of internal core required increases with the number of discs and also with the range of disc diameters in the assembly. In the current investigation most tests comprised 1000 disc assemblies. To ensure that these assemblies were always close to static equilibrium, rates of loading were kept to small values. Typically, tests were run to 200,000 cycles in order to achieve boundary deviatoric strains of 10 to 20 percent. Corresponding execution times for these 1000 disc tests were about 50 to 60 CPU hours! Clearly the use of this type of simulation has to be restricted to situations (such as the authors) where computer resources are virtually unrestricted. It should be noted that the CPU time consumed is largely due to those portions of the computer code devoted to keeping track of the location, forces and moments acting on the assembly discs and tracing existing and potential contacts between discs in proximity to one another. In addition, a great deal of computer time is spent on executing code devoted to identifying boundary discs. A substantial portion of program development by the author was concerned with development of algorithms which optimize the *bookkeeping* associated with keeping track of the current status of all discs and contacts in the assembly during a test.

Numerous trial runs were undertaken by the writer to arrive at a combination of boundary control parameters which resulted in satisfactory assembly behaviour- specifically minimum inertial effects. Optimal rates of loading and magnitude of the servo-gain were established by trial and error such that the prescribed boundary control mode did not result in a sluggish servo-mechanism nor generate disturbances leading to excessive inertial effects.

CHAPTER 5

TEST PROGRAM AND RESULTS

5.1 Introduction

In this chapter the results of a test program carried out on two-dimensional assemblies of discs using program DISC are reported.

The principal purpose of the tests was to independently verify the theoretical relationships between average stress, contact density and coefficients of anisotropy developed in Chapter 3.

Program DISC allows the investigator to subject an assembly of discs to a range of boundary conditions resulting in stress-induced changes in the microstructure and distribution of contact forces. The average stress acting on the assembly at any stage in a test can be compared to the microstructure and contact force anisotropies which develop to maintain the sample in static equilibrium. Additional understanding of the micromechanical behaviour of two and three-dimensional idealized granular systems is also possible from interpretation of the test results reported in this chapter

5.2 Organization

A description of the test program is given in Section 5.3. Test results are presented in Section 5.4 which in turn is divided into the following subsections:

Section 5.4.1 describes typical macroscopic behaviour of initially dense assemblies under various loading paths. The purpose of this section is to show that the response of these systems to controlled boundary disturbances is qualitatively similar to that which may be expected for analogous tests carried out on physical samples.

Section 5.4.2 considers the micromechanical response of these systems using the statistical mechanics descriptions introduced in the earlier chapters. General relationships between contact density, coordination number, void ratio and average contact vector length are investigated. Distributions for contact normals, contact force components and contact lengths are examined.

Section 5.4.3 examines the relationship between average assembly stress and parameters describing contact normal and contact force anisotropies. Fundamental equations which relate microstructure and contact force distributions to the measured average stress in an assembly are evaluated.

Section 5.4.4 investigates the influence of the magnitude of disc interparticle stiffness and friction coefficient on the global behaviour of these systems and the associated statistical descriptions of microstructure and interparticle forces.

Section 5.4.5 examines relationships between second and fourth-order coefficients of contact normal anisotropy and coordination number. Qualitative features of the evolution of microstructure under different loading conditions are also identified.

Section 5.5 summarizes essential features of the micromechanical performance of assemblies of discs based on the interpretation of test results given in preceding sections.

Finally, Section 5.6 proposes fundamental relationships for three-dimensional systems of cohesionless spherical or near-spherical particles which are analogous to the relationships established for two-dimensional assemblies of discs.

5.3 Test Program

5.3.1 Disc Size-Distribution and Properties

With the exception of a single 500 disc test, the numerical experiments reported in this investigation consist of 1000 particle systems having 20 different disc radii. The number of discs in each interval was chosen to approximate a log-normal distribution as shown on Figure 5.1. A log-normal size-distribution is considered typical for many well-graded granular media. It should be noted that the range of disc radii was made as wide as possible without reducing computational efficiency and accuracy. The number of discs (i.e. 1000) was a compromise between a desire to have as large an assembly as possible, to ensure a statistically representative system but, at the same time, ensure that computation time was not excessive.

Normal and tangential contact stiffnesses were chosen such that $k_n/k_s = 1$ which is a convenient value and represents a lower limit on the ratio of tangential to normal compliances for elastic spheres in contact according to Mindlin (1949).

Contact stiffnesses were chosen for each test such that the quantity $k_n r$ assumed a constant value for all disc sizes. Here, term r represents the disc radius. Appendix B describes the approach used to estimate realistic magnitudes for contact stiffnesses for numerical experiments in this study. For the majority of tests, a value of $k_n r = 3.75 \times 10^{10}$ was used. This value ensured that disc overlaps were very small, with respect to disc radii, but of a magnitude which may be anticipated for relatively

compressible photo-elastic materials. In fact, disc overlaps from these tests were similar to those reported by Strack and Cundall (1978) for their verification tests involving numerical simulation of photo-elastic disc assemblies. A limited number of tests were carried out with $k_n r = 3.75 \times 10^{11}$ to examine the influence of stiffer contacts on the global and micromechanical response of disc assemblies.

In the current study, a number of tests were also undertaken to evaluate the influence of the magnitude of the interparticle friction coefficient μ on test results. Tests were carried out on assemblies comprising discs with friction coefficients of 0, 0.10, 0.25 and 0.5. This range of interparticle friction coefficients is considered reasonable based on measured values reported for (dry) spheres manufactured from glass or steel materials (Skinner, 1969) and discs constructed from photo-elastic materials (Oda and Konishi, 1974a)

5.3.2 Assembly Generation

Disbursed assemblies of discs were initially generated using program AUTODISC. *Dense* isotropic assemblies were then created by compacting these initially disbursed assemblies in two stages using program DISC: First, the assembly was compressed hydrostatically (using modes 1 or 4) while temporarily assigning a friction coefficient of zero to all discs. Next, the assembly was allowed to come to equilibrium under hydrostatic boundary stresses (e.g. mode 4 and $\dot{\varepsilon}^b_{ij} = 0$, $\sigma^b_{11} = \sigma^b_{22}$, $\sigma^b_{12} = \sigma^b_{21} = 0$) with the desired friction coefficient assigned to all discs. The compacted dense isotropic assembly which was the starting configuration for a majority of the tests reported in this study is shown on Figure 5.2. The initial void ratio of this assembly is $e_o = 0.16$ and the initial coordination number $\gamma_o \approx 4.0$.

Dense *anisotropic* assemblies were created in the same way with the exception that during the second compaction stage, mode 4 was applied with $\sigma^b_{22}/\sigma^b_{11} > 0$.

It should be noted that the starting configurations for numerical assemblies were isotropic (or anisotropic) with respect to second-order expressions for contact normals $E(\theta)$, and contact force components $\overline{f}^c_n(\theta)$ and $\overline{f}^c_t(\theta)$. Discussions in Section 5.4.5 show that the b term in $E(\theta)$ (i.e. fourth-order microstructure) was not directly controlled through application of a prescribed boundary stress tensor.

Figure 5.3 shows the influence of sample size on assembly density. The assembly volumes on the plots are described by a normalized radial distance $r/\overline{r}_o$ from the centre of the selected circular region. Here r is normalized with respect to the average disc radius $\overline{r}_o$.

A number of important observations can be made from Figure 5.3: First, a large sample (say

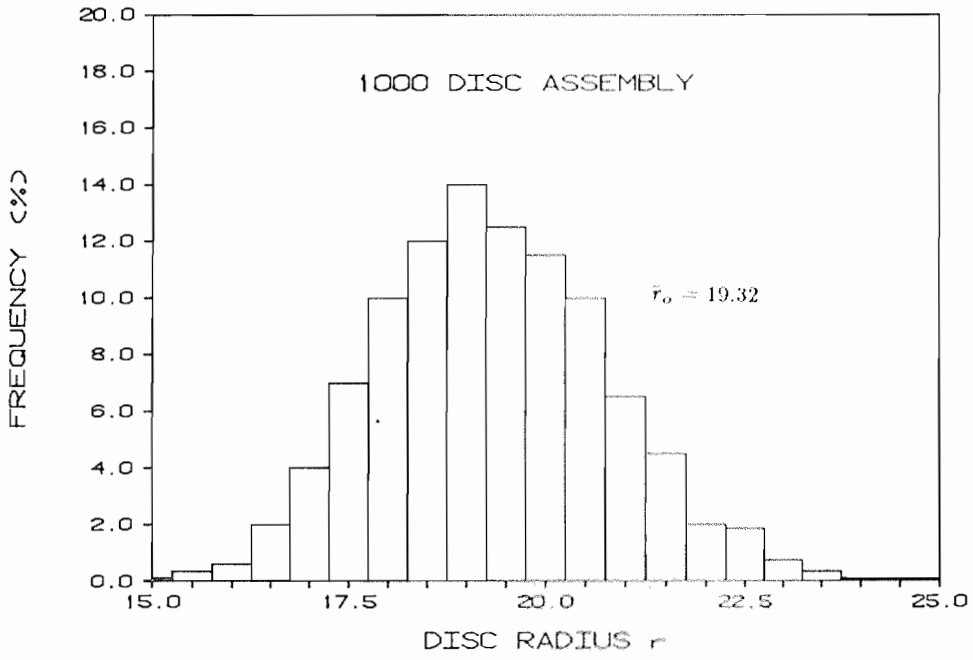

Figure 5.1 Disc Size-Distribution for 1000 Disc Tests

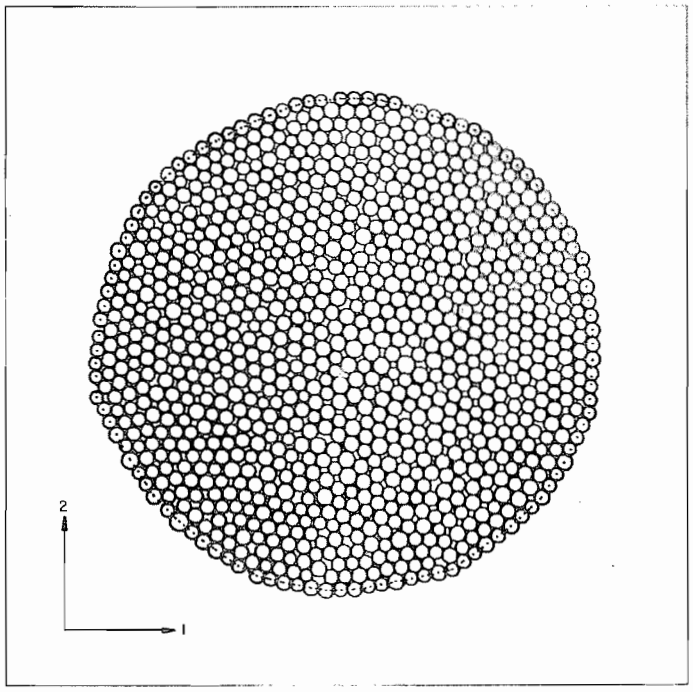

Figure 5.2 Compacted Isotropic Assembly (1000 Discs)

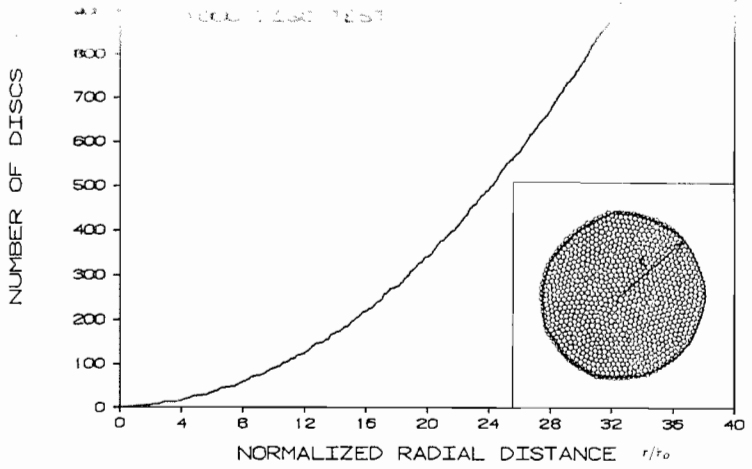

a) Number of Discs N versus Normalized Radial Distance $r/\bar{r}_o$

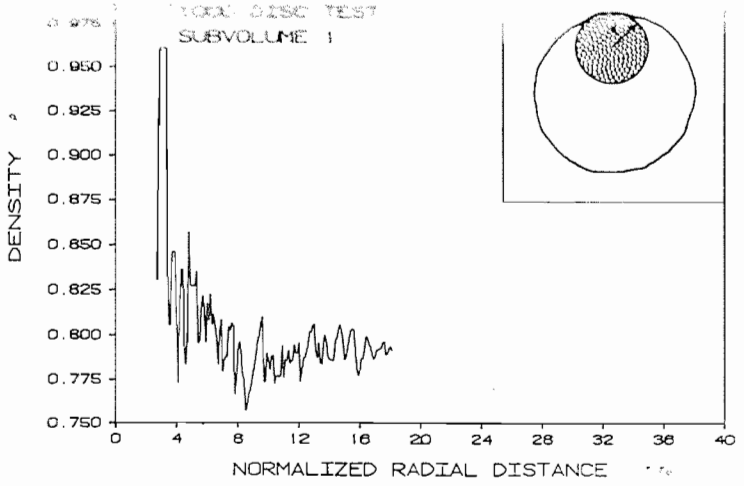

c) Assembly Density ρ versus Normalized Radial Distance $r/\bar{r}_o$

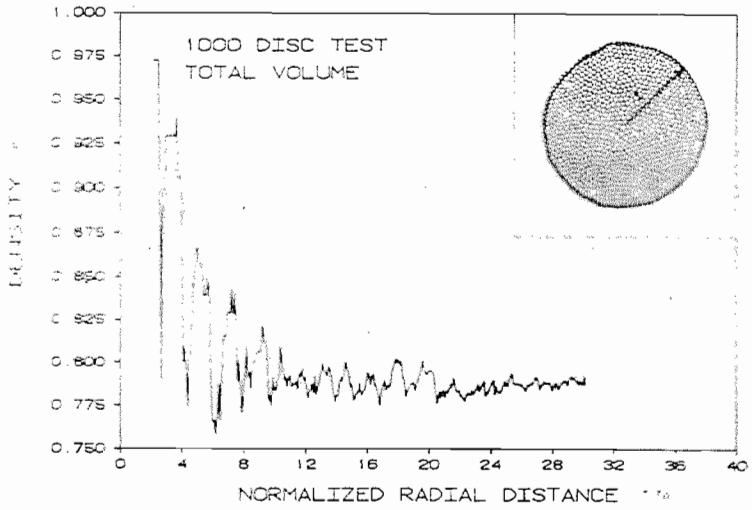

b) Assembly Density ρ versus Normalized Radial Distance $r/\bar{r}_o$

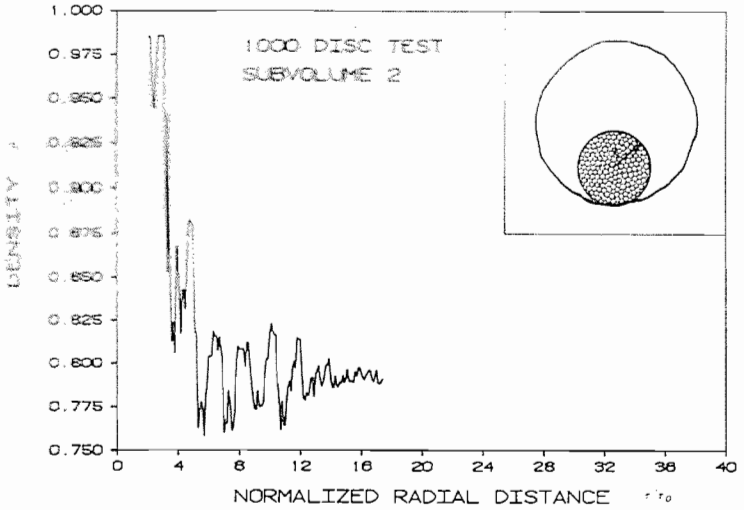

d) Assembly Density ρ versus Normalized Radial Distance $r/\bar{r}_o$

Figure 5.3 Influence of Sample Size and Location on Assembly Density

$N \geq 500$) is required in order to minimize fluctuations in measured density. Comparisons between tests comprising smaller samples may be compromised by fluctuations in (macroscale) physical properties which obscure the relative performance of these samples under otherwise identical loading conditions. The plots suggest that a 1000 disc sample affords protection against significant fluctuations in sample properties and they also indicate that separate subregions of the assembly exhibit densities which converge to a similar representative average value. While not shown, the same statement can be made with respect to other physical properties such as coordination number and contact density.

5.3.3 Summary of Test Parameters and Loading Paths

Table 5.1 summarizes the test program for initially dense compacted assemblies of discs. The table shows that the principal parameters which were varied between tests were the loading path and disc properties.

The loading/stress paths which resulted from specified boundary control conditions are idealized in the invariant stress space shown on Figure 5.4. The normal stress level corresponding to the origin of loading paths on the figure was set at $\sigma_n = -2.0 \times 10^6$. The boundary conditions which were used to generate the loading paths are shown on Figure 5.5. For selected samples, one or more unloading cycles were included in the loading program. The compression and extension loading paths which were applied to test assemblies are analogous to those which may be expected for drained triaxial tests in conventional soil mechanics laboratory practice.

5.3.4 Program Stability

In Chapter 4 it was explained that the Distinct Element Method (DEM) numerical technique models a transient problem in which static equilibrium is assumed whenever inertial forces or velocities are negligible.

Boundary strain-rates and servo-gain for the various boundary control modes and damping coefficient values were selected (after many trial runs) so that at any stage in a test the maximum disc force F_i was less than one percent of the maximum total contact force. In addition, samples were deemed unstable if absolute translational ball velocities were greater than 1×10^{-2}. Similar criteria were adopted by the original developers of the prototype program BALL. These criteria are necessary in order to make valid comparisons between tests and to assess the validity of theories which have been developed on the premise of statically admissible forces within particulate systems. Tests were discontinued when inertial effects became significant. Invariably this condition occurred at a

TABLE 5.1

SUMMARY OF TEST PROGRAM

1000 DISC TESTS

Test No.	Load Path	Disc Properties μ	Disc Properties $k_n r$	Remarks
1003	1	0.50	3.75×10^{10}	
1005	2	0.50	3.75×10^{10}	
1006	1	0	3.75×10^{10}	
1007	1	0.25	3.75×10^{10}	
1008	2	0.25	3.75×10^{10}	
1009	2	0	3.75×10^{10}	
1011	1	0.50	3.75×10^{10}	including unload/reload cycle
1013	1	0.50	3.75×10^{10}	initial anisotropic assembly
1015	4	0.50	3.75×10^{10}	unload at large strain
1017	4	0.50	3.75×10^{10}	unload/reload
1018	3	0.50	3.75×10^{10}	
1022	4	0.50	3.75×10^{11}	unload/reload
1024	1	0.50	3.75×10^{11}	
1025	2	0.50	3.75×10^{11}	
1031	1	0.10	3.75×10^{10}	

500 DISC TEST

Test No.	Load Path	Disc Properties μ	Disc Properties $k_n r$	Remarks
501	1	0.50	3.75×10^{10}	disc size-distribution from Figure 5.18

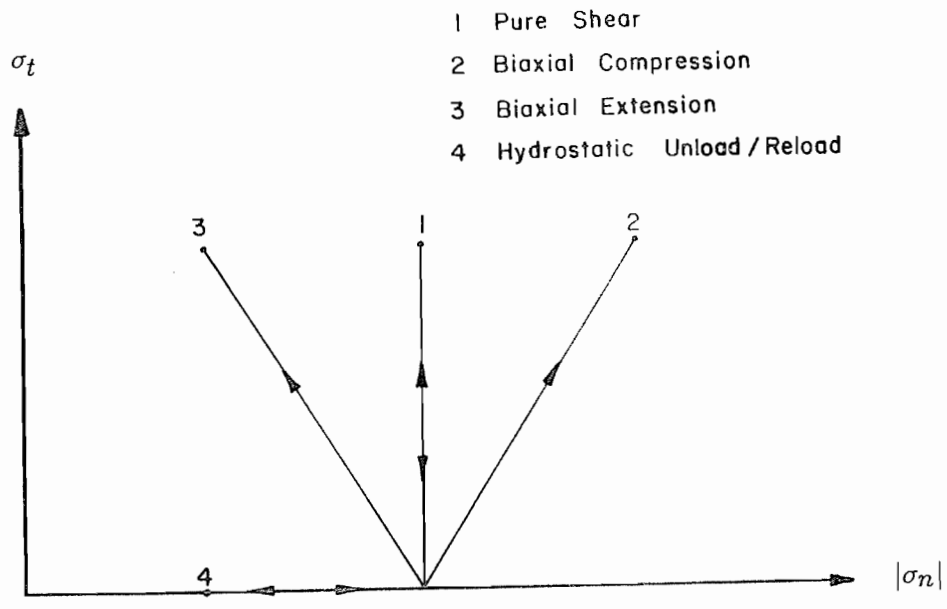

Figure 5.4 Loading Paths in Invariant Stress Space

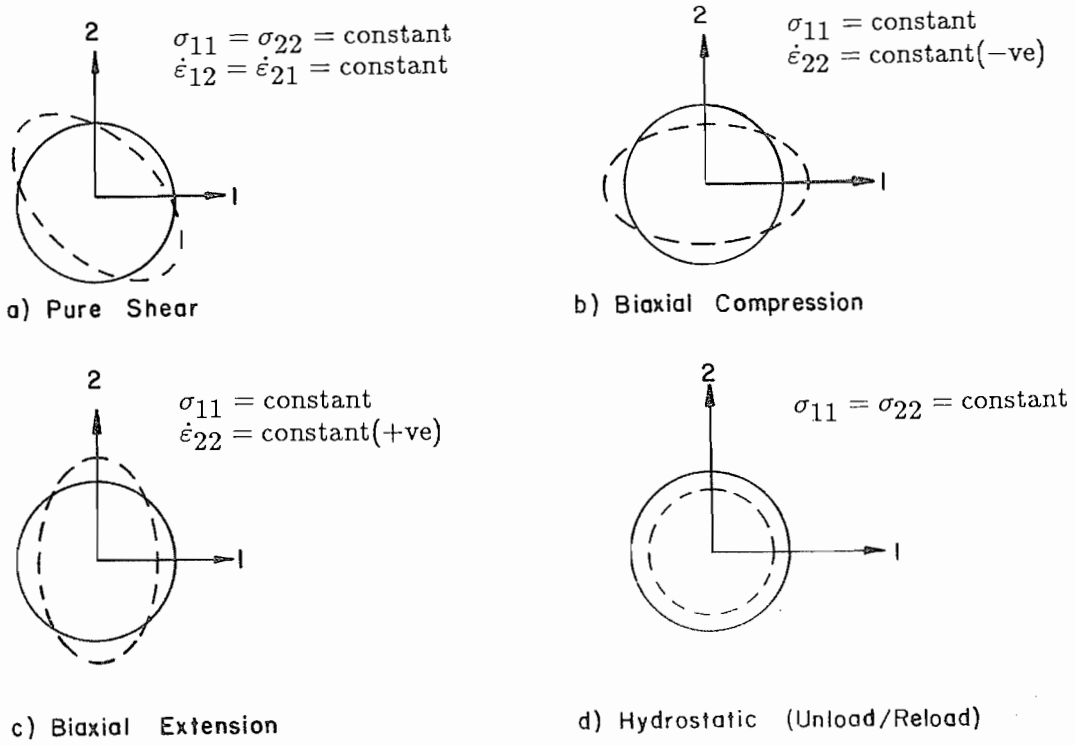

Figure 5.5 Applied Boundary Conditions

limiting minimum sample density analogous to the *critical state* for granular media in soil mechanics terminology.

While attempts were made to test initially *loose* assemblies of discs, these tests proved unsatisfactory. Loose isotropic samples were easily created by unloading any dense assembly once it had achieved a dilated state. However, on reloading, these samples proved to be unstable according to the criteria outlined above. This observed instability is not unexpected since these loose assemblies were close to, or at, a metastable condition. Nevertheless, the principal purpose of this study was well served by carrying out tests on dense assemblies. During shearing deformations, a wide range of stress-induced changes in microstructure and contact force anisotropy was observed as assemblies dilated from a dense to loose condition.

5.4 Test Results

5.4.1 Macroscopic Behaviour

The global stress-strain-void ratio behaviours measured at the boundaries of selected tests are shown on Figures 5.6 and 5.7. Test results presented on these figures refer to assemblies with disc properties set to $\mu = 0.5$ and $k_n r = 3.75 \times 10^{10}$. Each test was started from a dense isotropic condition and loaded along stress paths described in the previous section. While void ratio has been introduced in previous sections as a measure of microstructure, it is included here in the description of macroscale behaviour because it is often measured in the soil mechanics laboratory along with boundary stress and strain quantities.

Qualitative features of the plots on Figures 5.6 and 5.7 are not unlike what may be expected from dense three-dimensional granular systems based on conventional soil mechanics experience. The following observations can be made from Figure 5.6:

1) Under monotonic loading, peak shear strength increases with increasing normal stress levels. A macroscopic Mohr-Coulomb friction coefficient of about 0.4 can be calculated from the invariant stress quantities measured at peak shear for tests shown on the figure. Similar calculations give an apparent cohesion of zero for the total assembly.

2) At large strains, all three samples reached an ultimate state (failure) characterized by constant shear strength and constant volume with further distortion. In conventional soil mechanics terminology this condition is often called *critical state*.

3) Samples with constant or increasing normal stress levels are seen to *harden* to peak shear strength values and then *soften* to a reduced ultimate shear capacity. For the pure shear and biaxial compression tests, the dilatancy rate $\dot{\varepsilon}_n/\dot{\varepsilon}_t$ falls to zero and the void ratio tends to a limiting *critical void ratio* value e_{cr} as the ultimate state of the samples is approached. This phenomenon is less clear with the biaxial extension test which was not able to sustain a gradual approach to critical state before becoming numerically unstable.

4) All samples exhibited dilatancy rate and critical void ratio values which were suppressed with increasing normal stress level.

Figure 5.7 shows the stress-strain-void ratio response of tests which included unloading to a hydrostatic stress state at stages in the loading program. The plot shows that, while in a relatively dense state (stages 1 and 2), the sample behaved in a linear elastic manner during the unload/reload cycle.

5.4.2 Micromechanical Behaviour

5.4.2.1 General

An overall impression of the microstructure and distribution of interparticle forces which has evolved at stages in the loading history of Test #1003 can be made from Figures 5.8 through 5.10. In this test the average deviatoric invariant stress acting through the sample was increased monotonically while maintaining the (maximum) principal stress direction at an orientation of $\theta_\sigma = \pi/4$.

Figure 5.8a shows the spatial arrangement of disc contacts for the dense isotropic assembly at the start of the test. Contact orientations are represented by the branch lengths connecting the centres of discs which are in physical contact (i.e. contacts which transmit load). Dotted lines at the sample perimeter connect the centres of discs defining the boundary of the assembly. The isotropic distribution of contact forces on Figure 5.8b for the initial compacted assembly clearly reflects the hydrostatic stress state under which it was created. In this plot, the orientation of each line corresponds to the line of action of interparticle forces between discs and the thickness of each line is proportional to the intensity of the contact force between particles. The contact force pairs act at the midpoint of each line segment.

The dilatant response of this assembly during shear is apparent from the visually less-dense distributions of contacts on Figures 5.9a and 5.10a. However, the distribution of contacts with respect to orientation is not visually apparent from plots of this type but can be shown from contact frequency distribution data presented in Section 5.4.2.3.

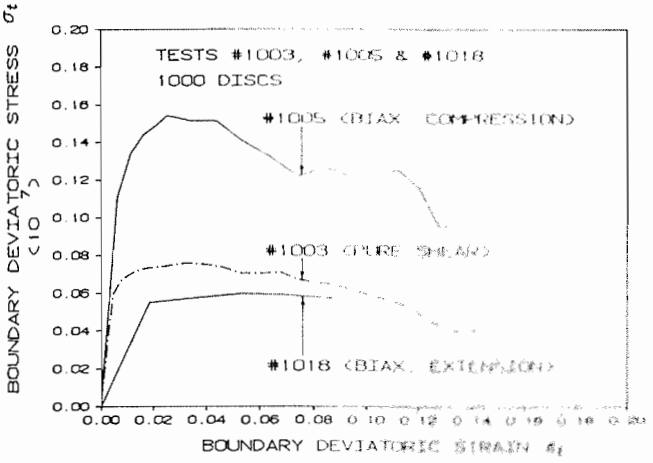

a) Deviatoric Stress versus Deviatoric Strain

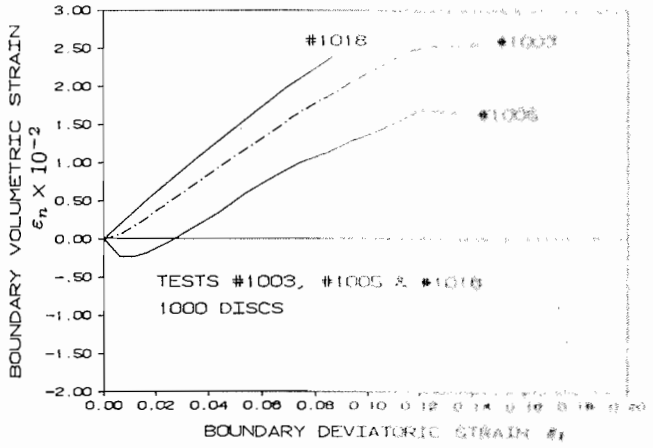

b) Volumetric Strain versus Deviatoric Strain

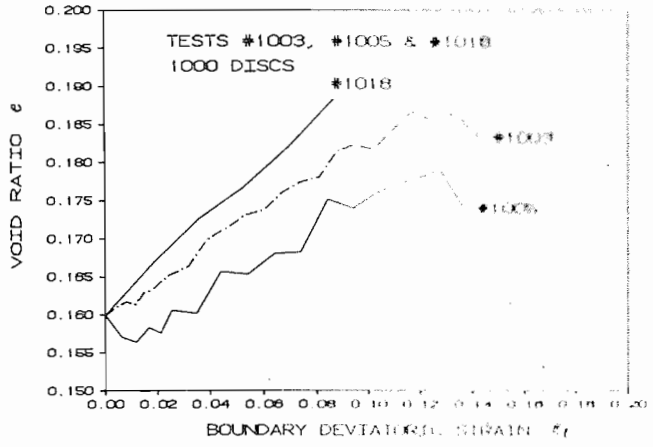

c) Void Ratio versus Deviatoric Strain

Figure 5.6 Stress-Strain-Void Ratio Behaviour from Selected Tests

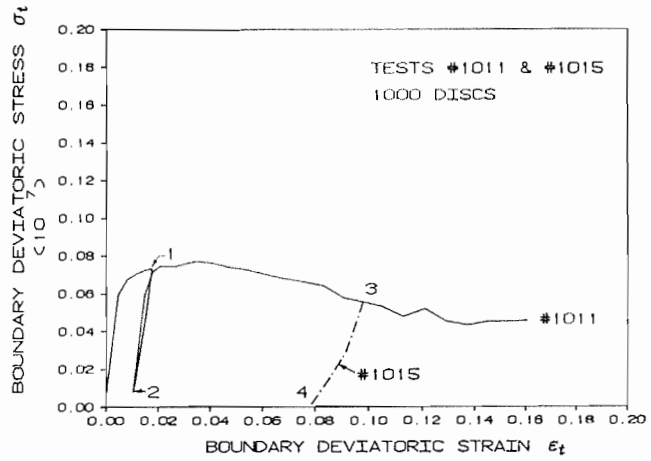

a) Deviatoric Stress versus Deviatoric Strain

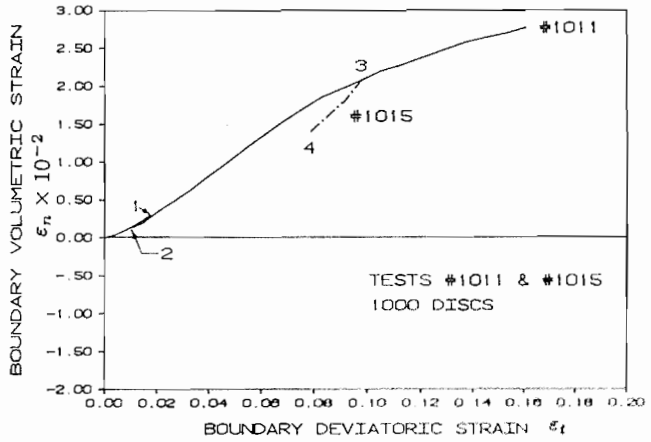

b) Volumetric Strain versus Deviatoric Strain

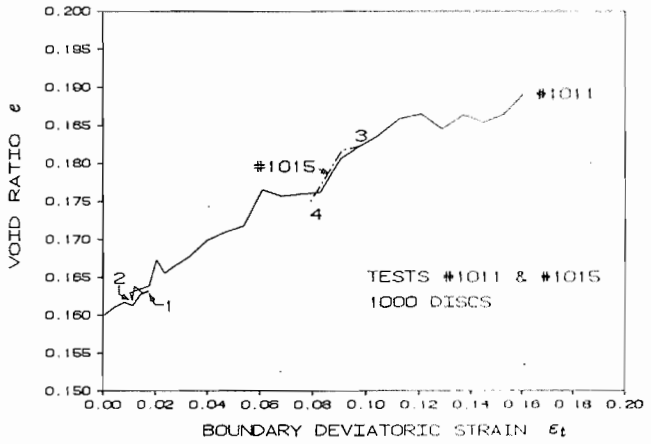

c) Void Ratio versus Deviatoric Strain

Figure 5.7 Stress-Strain-Void Ratio Behaviour from Selected Tests

In contrast, the redistribution of contact forces during shearing deformations is readily apparent from Figures 5.9b and 5.10b. At peak and ultimate states the orientation and intensity of contact force chains is clearly biased in the direction of the maximum principal stress. Similar visual patterns were observed for all tests in this investigation in which samples were subjected to increasing shearing deformations.

Figure 5.10a and 5.10b show the test assembly at an ultimate state characterized by limiting values of statistical quantities describing microstructure and contact force anisotropy. Typical of all tests in the current study, further incremental shearing deformations led to numerical instability (i.e. the assemblies became dynamic). However, under conditions of constant confining stress, it was possible to sustain the ultimate (stable) condition over a small range of deviatoric strain in some tests. When this delicate balance was achieved, the growth and collapse of predominant load-carrying chains could be observed while noting that statistical parameters describing microstructure and contact forces remained unchanged. This condition corresponds to a *steady state* of sample micromechanical behaviour under shearing deformations. Hypothetically, the steady state condition could be preserved indefinetly by increasing assembly size and reducing the rate of deformations associated with the boundary control mechanisms found in program DISC. In view of the comments just made, it is convenient to denote parameters measured at the steady state condition by the subscript ∞. Functionally, the term *steady state* corresponds to the familiar concept of *critical state* in soil mechanics terminology. The concept of steady state will be developed more fully later in this chapter.

5.4.2.2 Contact Density, Coordination Number and Void Ratio

The global response recorded from numerical tests on dense assemblies of discs was characterized by increasing volumetric strains and an increase in void ratio up to steady state. Associated decreases in microstructure were seen as reductions in coordination number and contact density. Steady state values for coordination number, void ratio and contact density are denoted as γ_∞, e_∞ and m_{v_∞} in the following text.

Figure 5.11 shows the change in coordination number with deviatoric strain for the numerical experiments described in previous sections. These samples showed an early dramatic reduction in the number of contacts followed by a reduced rate of contact loss up to failure. At large strain, each test tended to a *steady state* coordination number γ_∞.

The early dramatic reduction in coordination number recorded for these tests can be misleading.

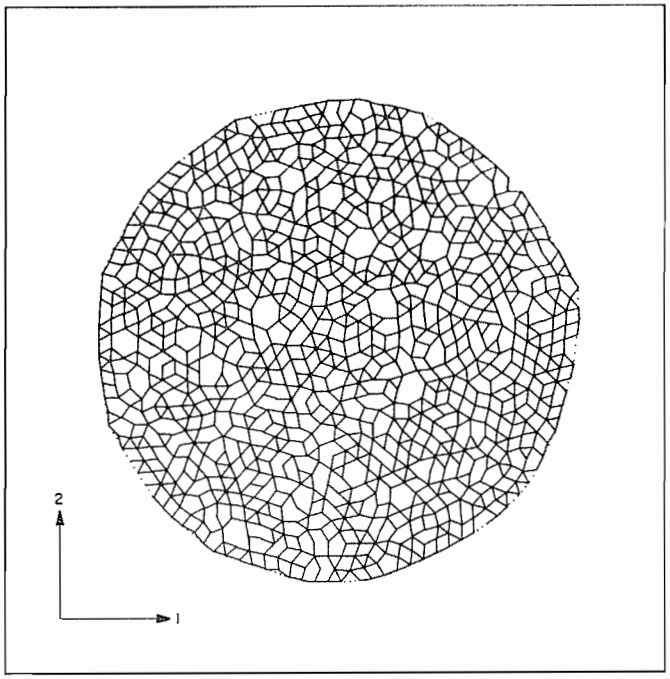

a) Distribution of Branch Lengths (Contacts)

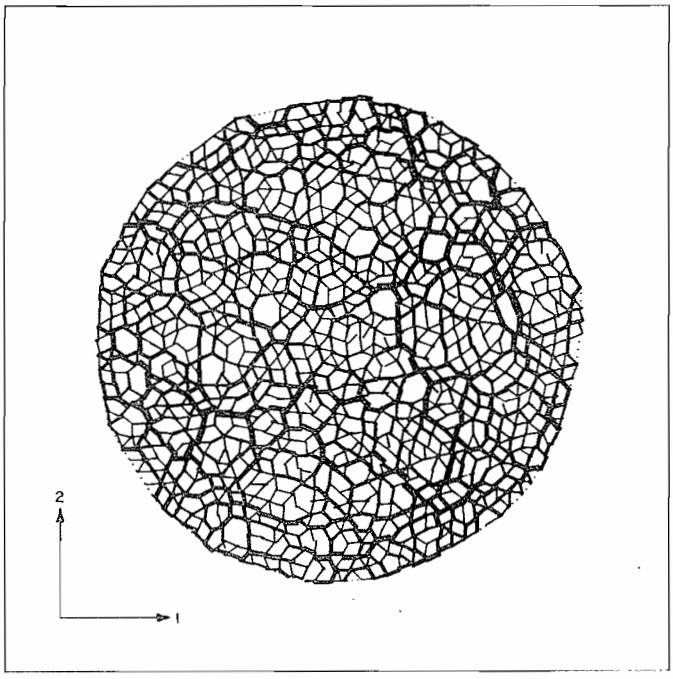

b) Distribution of Contact Forces

Figure 5.8 Distribution of Branch Lengths (Contacts) and Contact Forces from Initial Isotropic 1000 Disc Assembly

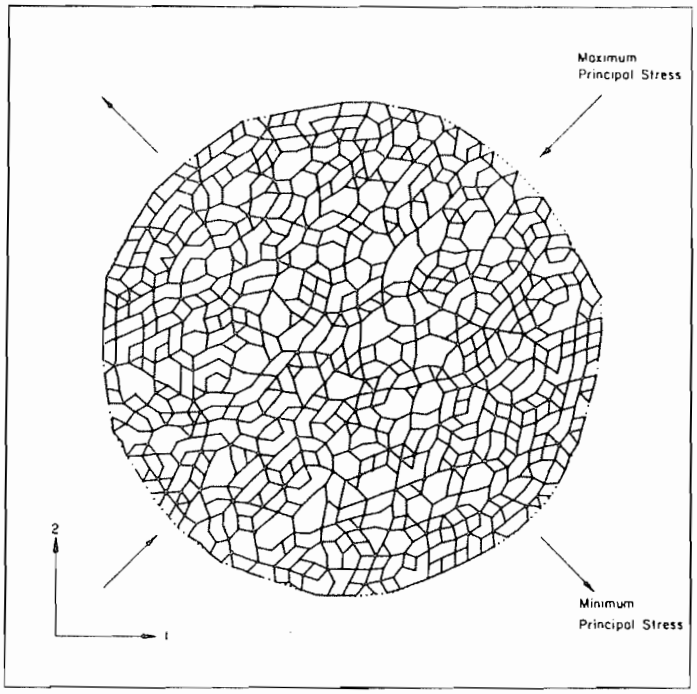

a) Distribution of Branch Lengths (Contacts)

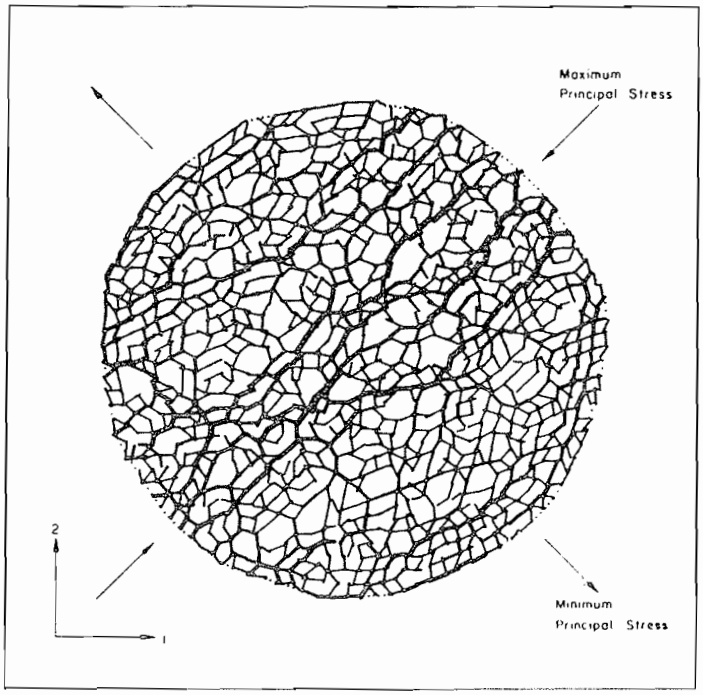

b) Distribution of Contact Forces

Figure 5.9 Distribution of Branch Lengths (Contacts) and Contact Forces from Test #1003 at Peak Shear (1000 Disc Assembly)

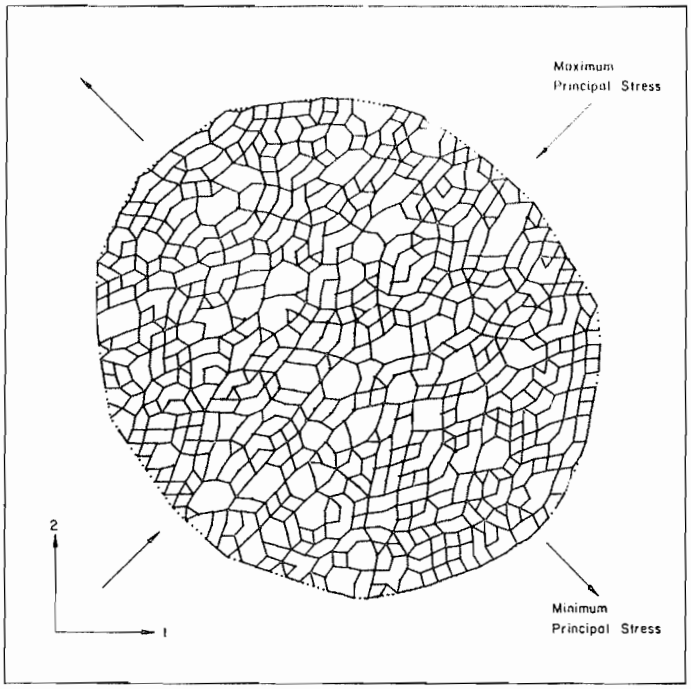

a) Distribution of Branch Lengths (Contacts)

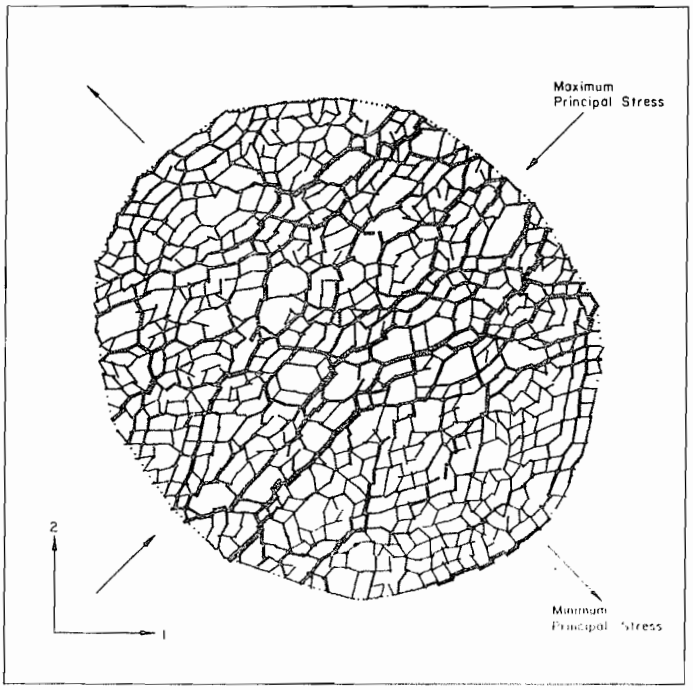

b) Distribution of Contact Forces

Figure 5.10 Distribution of Branch Lengths (Contacts) and Contact Forces from Test #1003 at Ultimate State (1000 Disc Assembly)

It should be noted that a contact is recorded only if it transmits load. Elastic unloading of many contacts while the assembly is *locked* in a dense configuration is responsible for the rapid decrease in coordination number. Hence, this early reduction in γ does not reflect a significant spatial rearrangement of the particles. If contacts were included which represented discs in *close* proximity then, a shallower $\gamma - e$ curve would be anticipated. However, the criterion that a contact carry load in order to be counted has been adopted in the current study because it is unambiguous.

Figure 5.12 summarizes $\gamma - e$ data taken from Tests #1003, #1005 and #1018. This plot shows that the initial reduction in coordination number does not correspond to a rapid reduction in density, which is consistent with the comments made above. The range of coordination numbers corresponding to a given void ratio e appears to be sensitive to the magnitude of the average normal contact force acting at assembly contacts. For example, over the relatively shallow portion of the plot, the highest values of γ correspond to the biaxial compression test and the lower values to the biaxial extension test. The biaxial extension test #1018 is considered to have failed prematurely due to numerical instability; consequently, the tendency to a unique pressure independent value for γ_∞ over the full range of normal stress shown on Figure 5.11 cannot be discounted on the basis of these three tests. Pressure sensitivity of coordination number under hydrostatic loading is examined in Section 5.4.4.

The sensitivity of coordination number to normal stress level has important consequences to three-dimensional systems. It is interesting to note that data reported in the literature (such as Oda, 1977) does not include the effect of stress level or particle stiffness on the $\gamma - e$ relationship for granular media. In addition, it is doubtful whether experimental techniques used to identify contacts in physical tests (such as those reported by Oda, 1977 and others) are able to distinguish between loaded contacts and points at which particles are close to touching.

In Section 2.8 it was shown that contact density may be expressed as a function of coordination number, void ratio and the average contact vector length for assemblies comprising spheres. For two-dimensional assemblies of discs the equivalent expression to (2.51) is:

$$m_v = \frac{\gamma}{\pi \bar{l}_v^2 (1+e)} \tag{5.1}$$

A summary of data presented on Figure 5.13 shows that the measured data supports equation (5.1). While expression (5.1) is independent of interparticle friction angle, test results reported in Section 5.4.4 show that values for m_{v_∞}, γ_∞ and e_∞ are sensitive to the magnitude of interparticle stiffness and interparticle friction.

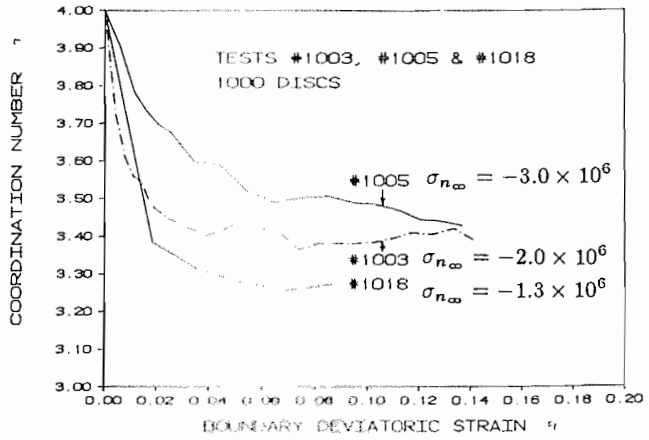

Figure 5.11 Coordination Number γ versus Deviatoric Strain ε_t from Selected Tests

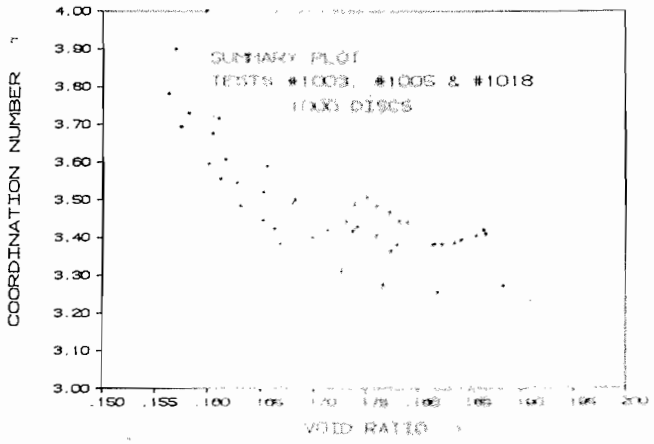

Figure 5.12 Coordination Number γ versus Void Ratio e from Selected Tests

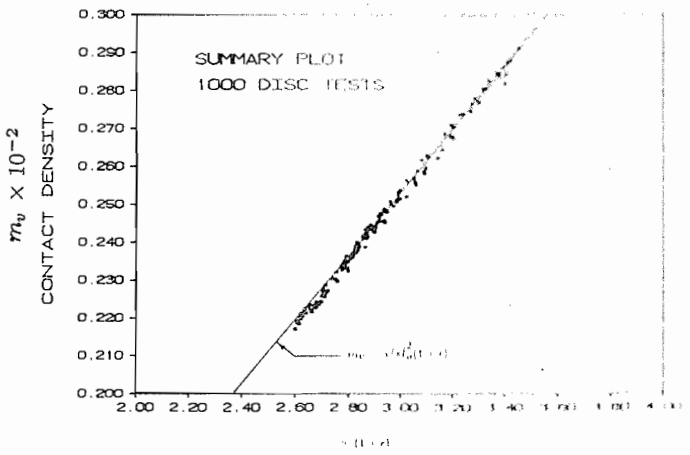

Figure 5.13 Contact Density m_v versus $\gamma/(1+e)$

5.4.2.3 Distribution of Contact Normals and Fabric Tensor

The fabric or microstructure which evolves to maintain a granular assembly in static equilibrium with the forces imposed at the system boundaries can also be characterized by the distribution of contact normals.

Figure 5.14 shows the initial distribution of contact normals which was taken from the 1000 disc assembly used as the starting configuration for dense isotropic tests with $k_n r = 3.75 \times 10^{10}$. Superimposed on the figure is the fourth-order Fourier series approximation $E(\theta)$ to this distribution according to expression (3.19). Section 3.2.3 has shown that the coefficients of anisotropy a and b contained in this expression are proportional to deviatoric invariant quantities of the fabric tensor $\mathbf{R}$. This relationship allows the coefficient terms and principal directions of contact anisotropy θ_a and θ_b to be extracted directly from the measured contact normal data using expressions (3.17) and (3.18).

Figure 5.14 shows that the second-order distribution of contact normals is essentially isotropic (i.e. $a \approx 0$) under the hydrostatic boundary stress conditions employed to create the assembly. In addition, the initial test configuration recorded a very low value for fourth-order microstructure represented by coefficient term b.

Figure 5.15 presents contact normal distributions recorded for Tests #1011 and #1015. These tests included unloading to a hydrostatic stress state at two stages in the loading program. The plots show that concurrent with increasing deviatoric stress and dilatancy there was an increase in contact anisotropy. However, at the end of each unloading stage, there was a stress-induced return to an essentially second-order isotropic distribution of contact normals. In addition, comparison of approximating curves for initial and stage 4 contact frequencies shows an irrecoverable loss of contacts.

An important observation from Figures 5.14 and 5.15 is that the distribution function $E(\theta)$, in the form (3.19), gives a reasonable visual approximation to the predominant trends in measured data at all stages. Nevertheless, isolated peaks are apparent on the contact distribution plots which cannot be accounted for by a fourth-order Fourier series expression. These peaks may represent higher-order microstructure and/or isolated chains of contacts which span the assembly diameter. For larger samples, it is likely that a smoother distribution of measured contact normals would result. However, from theoretical considerations (and as subsequent sections verify), only second-order microstructure described by coefficient term a is important for the prediction of assembly shear strength.

Comparison of the distributions on Figures 5.15 suggests that contact anisotropy is generated primarily by a reduction in the number of contact normals with orientations close to the minor principal stress direction. The relatively greater loss of contacts in the minor principal stress direction

(as compared to the maximum principal direction $\theta_\sigma = \pi/4$) can be seen on Figure 5.16. The curves on the figure represent the number of contacts falling within 5 degrees of principal stress directions. Similar phenomena have been reported in the literature from the results of physical tests on dense planar systems of discs subject to increasing shear stress (Oda and Konishi, 1974a) and numerical experiments on assemblies of discs reported by Cundall et al. (1982).

5.4.2.4 Distribution of Contact Lengths

Expressions (2.30) and (3.2) in Chapters 2 and 3 show that the relationship between average stress and distributions for average contact force components and microstructure is simplified if the distribution of contact lengths is independent of contact vector orientation (i.e. for two-dimensional assemblies $\overline{l}^c(\theta) = \overline{l}_o$).

Figure 5.17 shows polar histogram data for the distribution of average contact lengths at a post-peak condition for a typical test comprising 1000 discs with the size-distribution given on Figure 5.1. In fact, the data from all tests reveals that the distribution of average contact lengths with respect to orientation was isotropic over the entire range of shearing deformations. Furthermore, Figure 5.19 illustrates that the average contact length for the 1000 disc tests remained constant at about the average disc radius (i.e. $\overline{r}_o \approx \overline{l}_o$). This result is not surprising considering the particle size-distribution adopted for these tests.

A similar test using 500 discs with a *gap-graded* distribution of disc radii (Figure 5.18) was carried out to confirm the independence of average contact lengths from orientation and to investigate the hypothesis that a bimodal distribution of particle radii will bias the distribution of average contact lengths in favour of larger particle sizes under deviatoric loading. Histogram data for this test revealed, once again, that for the range of disc radii considered, the distribution of average contact lengths was independent of the orientation of contact vectors but that the average contact length $\overline{l}_o$ is biased towards the larger disc sizes (Figure 5.19).

It may be concluded that for assemblies of discs (or spheres in three-dimensional systems) with smooth unimodal size-distributions, the average contact length $\overline{l}_o$ may be usefully approximated by the average particle radius $\overline{r}_o$.

5.4.2.5 Contact Force Distributions and Contact Force Tensors

Figure 5.20a and 5.20b show the distribution of normal and tangential (shear) contact force components for the initial dense isotropic assembly which was used as the starting configuration for

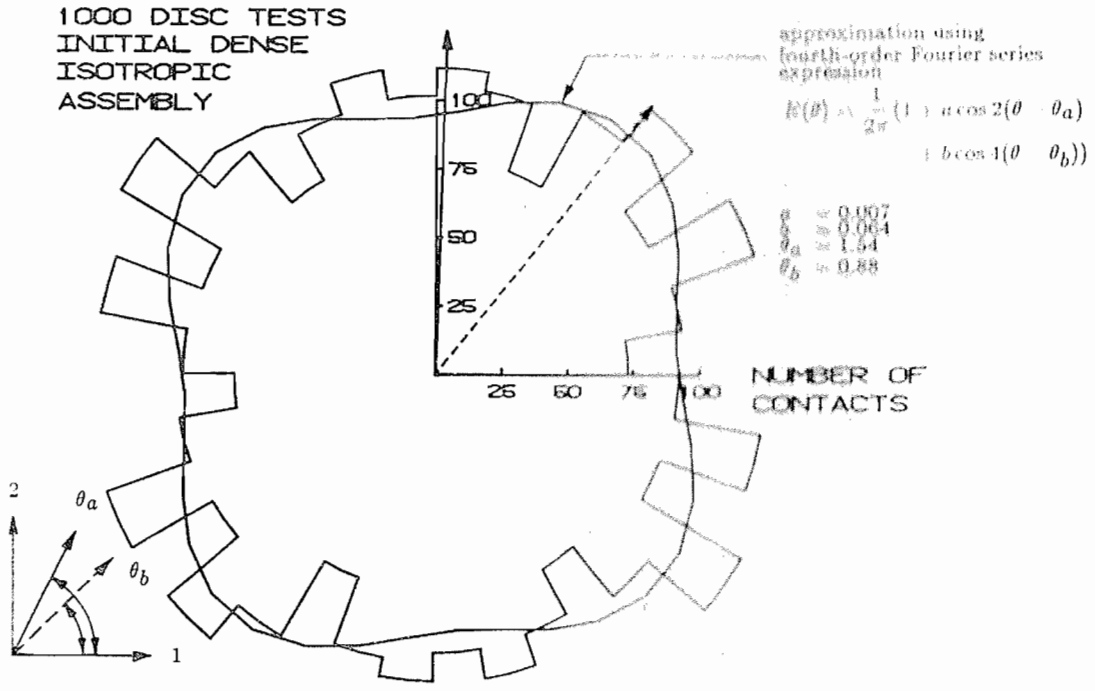

Figure 5.14 Distribution of Contact Normals from Initial Dense Isotropic Assembly

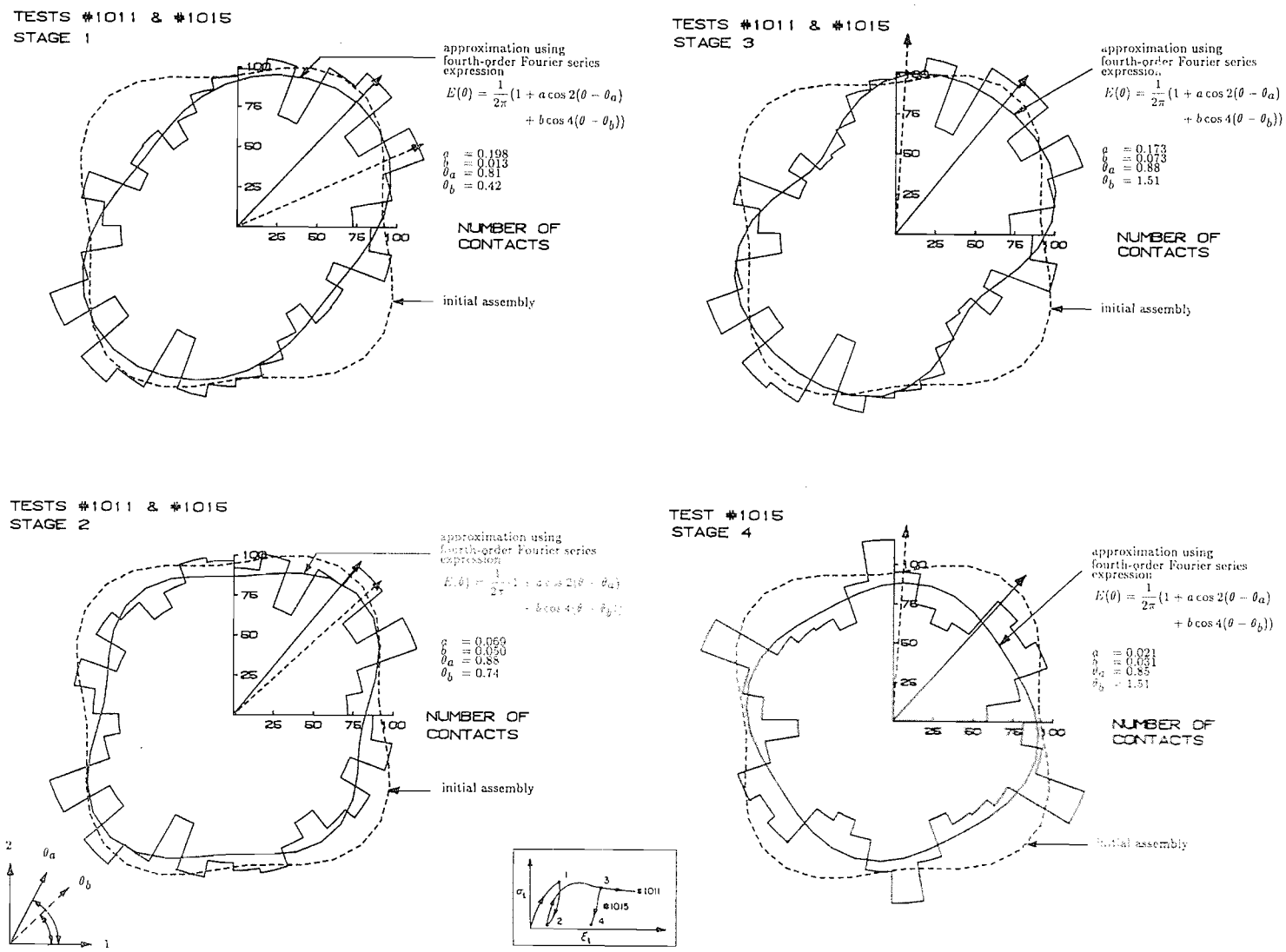

Figure 5.15 Distribution of Contact Normals from Tests #1011 and #1015

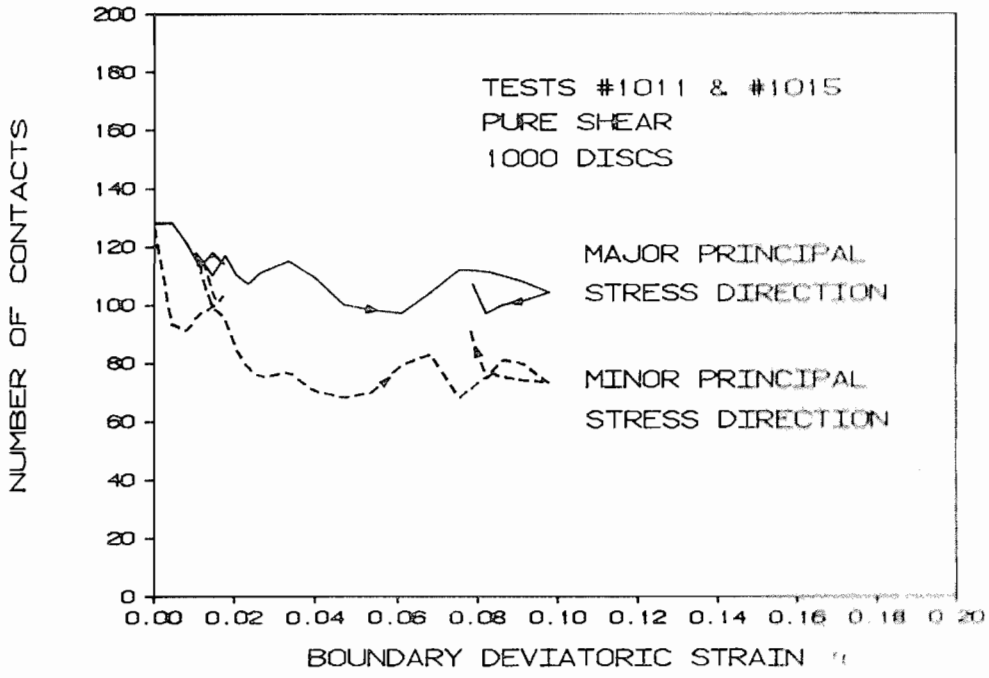

Figure 5.16 Contact Loss/Regeneration at Orientations close to Principal Stress Directions

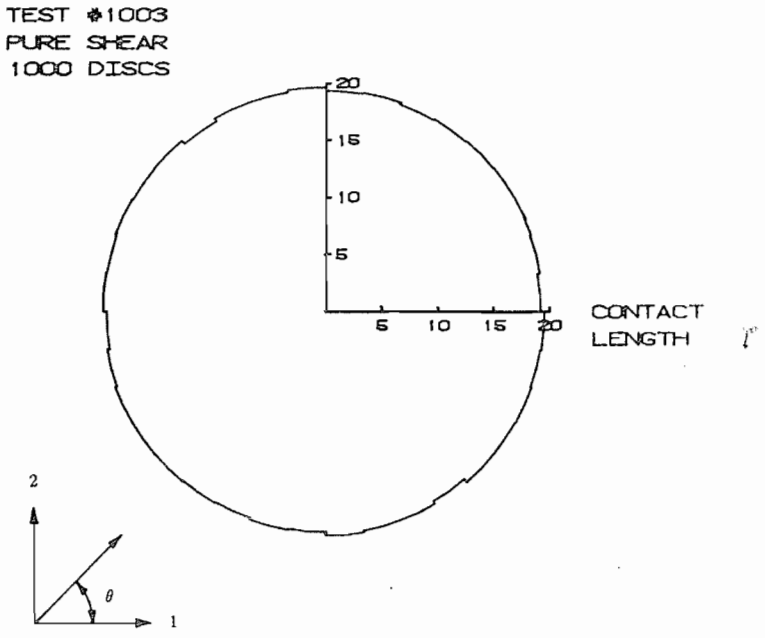

Figure 5.17 Distribution of Contact Lengths $\bar{l}^c(\theta)$ at Peak Shear

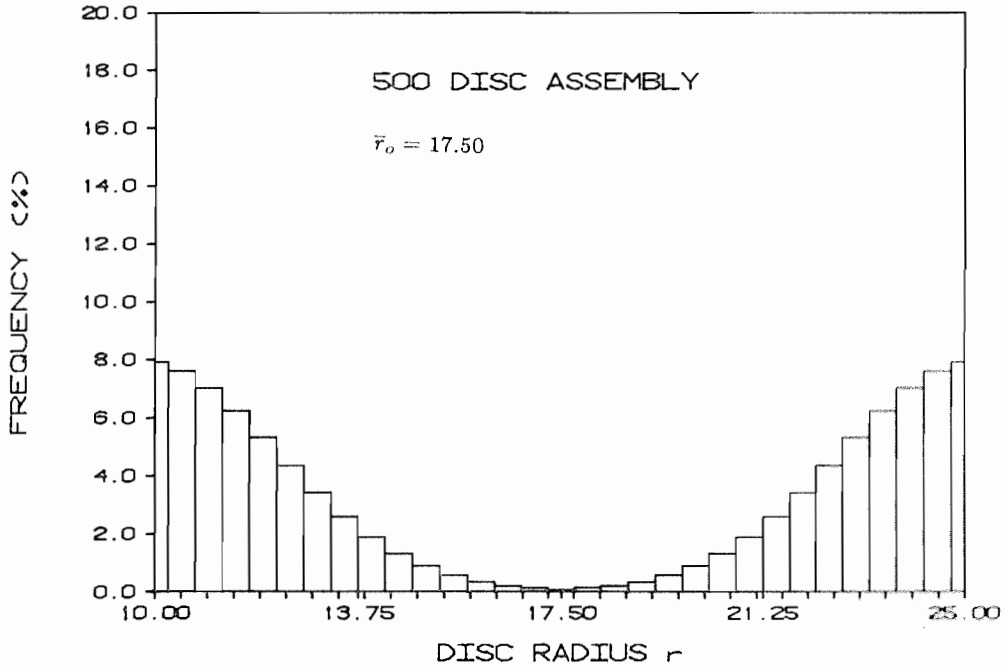

Figure 5.18 Disc Size-Distribution for 500 Disc Test

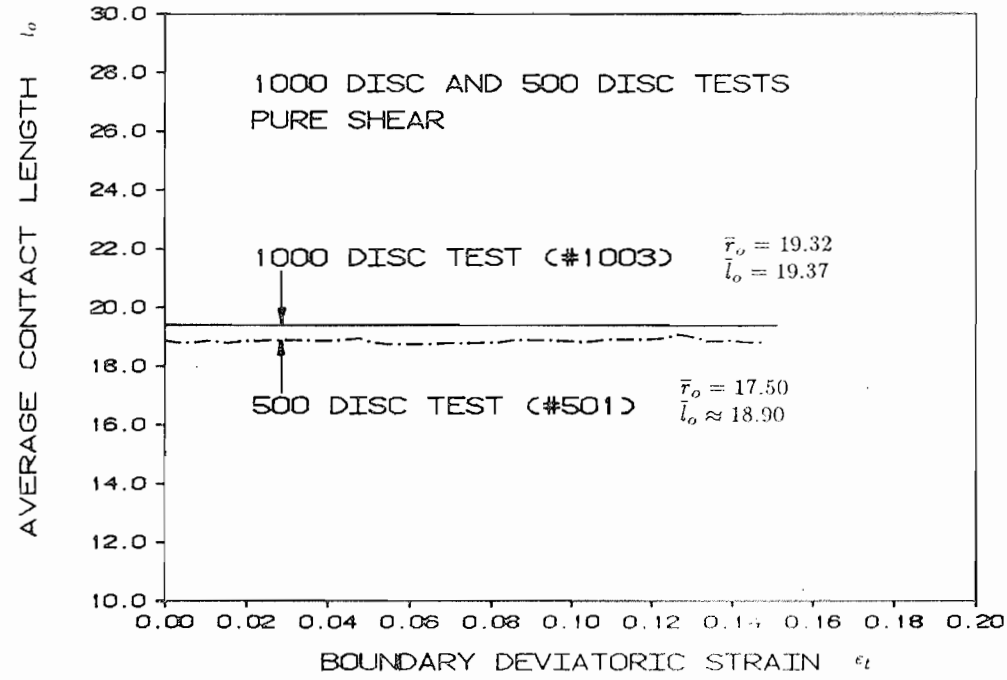

Figure 5.19 Average Contact Length $\bar{l}_o$ versus Deviatoric Strain from 1000 Disc and 500 Disc Tests

the majority of the 1000 disc tests in this study. The contact force distributions correspond to the interparticle forces shown on Figure 5.8b. The distribution of contact forces is clearly isotropic. Fourier series approximations to these distributions in the form (3.22) and (3.23) are also superimposed on the figures.

Developments in Section 3.3.2 have shown that the coefficient terms in the approximating functions $\overline{f}_n^c(\theta)$ and $\overline{f}_t^c(\theta)$ are, in fact, invariant quantities of the contact force tensors $\mathbf{F}_N$ and $\mathbf{F}_T$. Similarly, directions of contact force anisotropy θ_f and θ_t are principal directions (eigenvectors) for these same tensors.

Normal and tangential (shear) contact force distributions at stages during loading and unloading of Tests #1011 and #1015 are shown on Figures 5.21 and 5.22. Expressions presented in Section 3.3.2 have been used to extract f_n^o, coefficients of contact force anisotropy a_n, a_t, a_ω and principal contact force directions θ_f and θ_t from the histogram data on the figures.

Perhaps the first observation which can be made from these plots is that the Fourier series expressions of the form (3.22) and (3.23) appear to well represent the measured data. It may also be noted that principal contact force directions for loaded stages (1 and 3) were coincident and in the approximate direction of the maximum load (or maximum principal stress direction $\theta_\sigma = \pi/4$).

During unloaded stages 2 and 4 the contact force distributions returned to a near-isotropic form consistent with a return to a hydrostatic stress state.

The loading program for the tests presented on Figures 5.21 and Figure 5.22 corresponded to a pure shear stress path. Hence the assembly was under constant normal stress during loading and unloading stages. Expression (3.44) predicts that under conditions of constant normal stress, a reduced contact density must be compensated by an increase in average normal contact force. Comparison of approximating curves at stage 4 on Figure 5.21 supports this relationship.

In all tests the magnitude of the shear contact force coefficient a_ω was sensibly zero and hence it can be neglected in the equation (3.23) for the distribution of contact shear forces.

Distributions for average mobilized interparticle friction coefficient $\mu_{mob}(\theta)$ are shown on Figure 5.23 at two stages in Tests #1011 and #1015. Measured distributions have been calculated directly from:

$$\overline{\mu}_{mob}(\theta) = |\overline{f}_t^c(\theta)/\overline{f}_n^c(\theta)| \tag{5.2}$$

Superimposed on the plots are the approximations to $\overline{\mu}_{mob}(\theta)$ using the theoretically derived relation (3.28). For coaxial contact force tensors, expression (3.28) predicts that the mobilized contact friction coefficient must be zero in the direction of contact force anisotropy. The measured data in the figure

supports this hypothesis. Physically, this means that at orientations close to $\theta_\sigma + n\pi/2$, $n = 0, 1, 2, 3$, the resultant interparticle forces comprise essentially normal components with little contribution from the interparticle shear capacity at the contact.

The relatively low amplitude of these curves, even at the early stages of loading, shows that $\overline{\mu}_{mob}(\theta) << \mu = 0.5$. In fact, the (average) operative contact friction was always less than about 30 percent of interparticle shear capacity at all contact orientations. The absence of fully-mobilized friction in sheared two-dimensional assemblies of discs has been remarked upon by Oda and Konishi (1974a) from the results of their physical experiments (see Figure 1.12). A conspicuous absence of oblique contact forces between discs is also apparent from physical experiments by De Josselin De Jong and Verruijt (1969) as shown on Figure 1.1a.

5.4.3 Average Stress and Anisotropy

5.4.3.1 General Observations

Relationships which equate average stress in planar assemblies of discs to contact density and invariant quantities describing the distribution of contact normals and contact force components have been proposed in Section 3.4.1.

The observations made in this subsection are restricted to assemblies with the disc properties $\mu = 0.5$ and $k_n r = 3.75 \times 10^{10}$. These values were used for the majority of tests in the current study and reflect properties which are considered reasonable for physical discs constructed from photo-elastic materials (Strack and Cundall, 1978). The influence of disc properties on the global and micromechanical response of numerical disc assemblies is examined in subsequent sections.

Figure 5.24a shows the measured invariant stress ratio $a_\sigma = |\sigma_t/\sigma_n|$ recorded from Test #1003 together with coefficients of anisotropy a, a_n and a_t. Superimposed on the figure is the predicted curve for a_σ using expression (3.47). The predicted curve appears to be a reasonable approximation to the measured invariant stress ratio. From the same figure it is possible to trace the relative contributions of assembly anisotropies to the shear capacity of the system.

At the very initial stage of sample loading, before particles had a chance to *unlock*, rapid increases in all three anisotropies were recorded as the sample behaved in a linear elastic manner. However, only a small further reduction in contact density was required before the magnitude of tangential (shear) contact force anisotropy a_t dropped substantially and remained low for the remainder of the test. In contrast, normal contact force anisotropy a_n and contact normal anisotropy a peaked later at about the maximum shear capacity recorded for the system. With further distortion, both terms

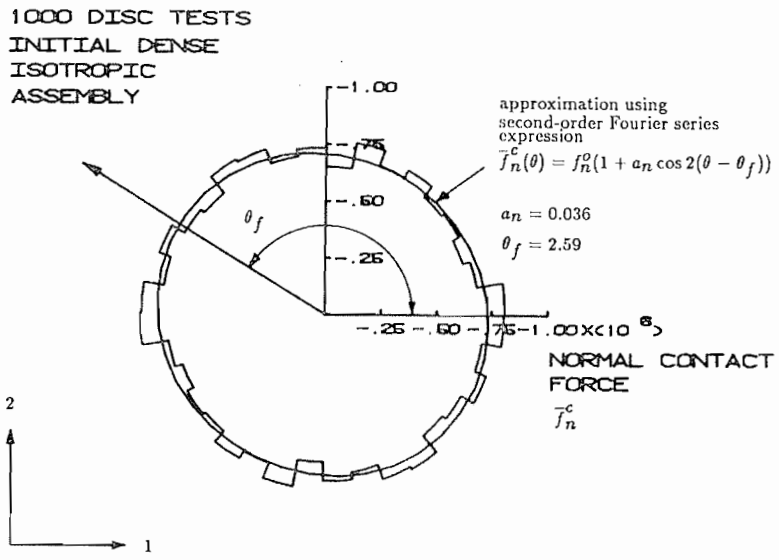

a) Distribution of Normal Contact Forces

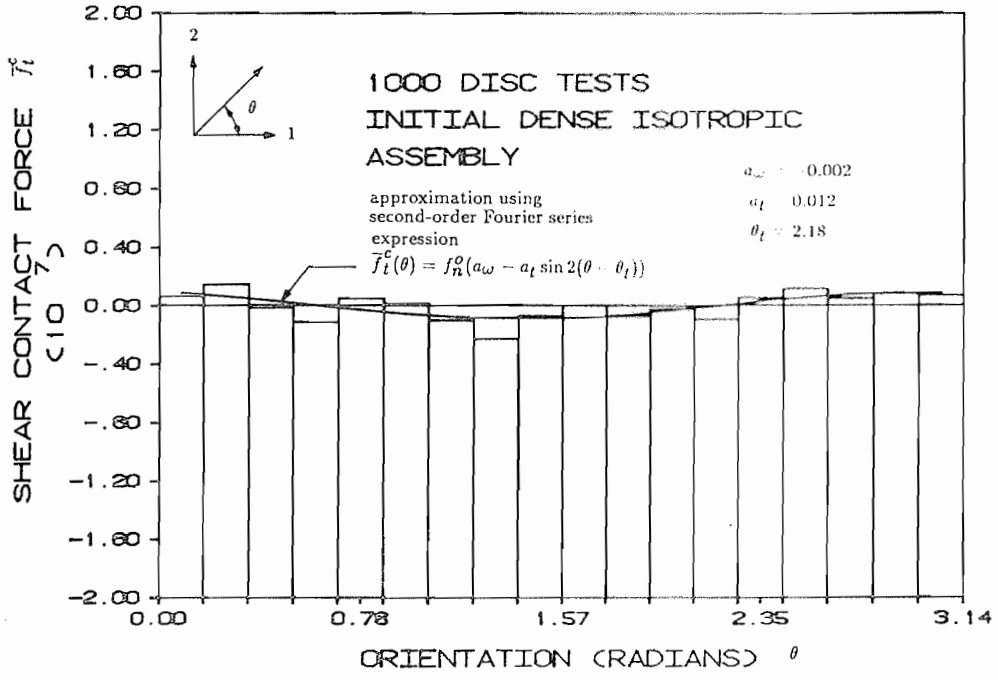

b) Distribution of Tangential (Shear) Contact Forces

Figure 5.20 Contact Force Distributions from Initial Dense Isotropic Assembly

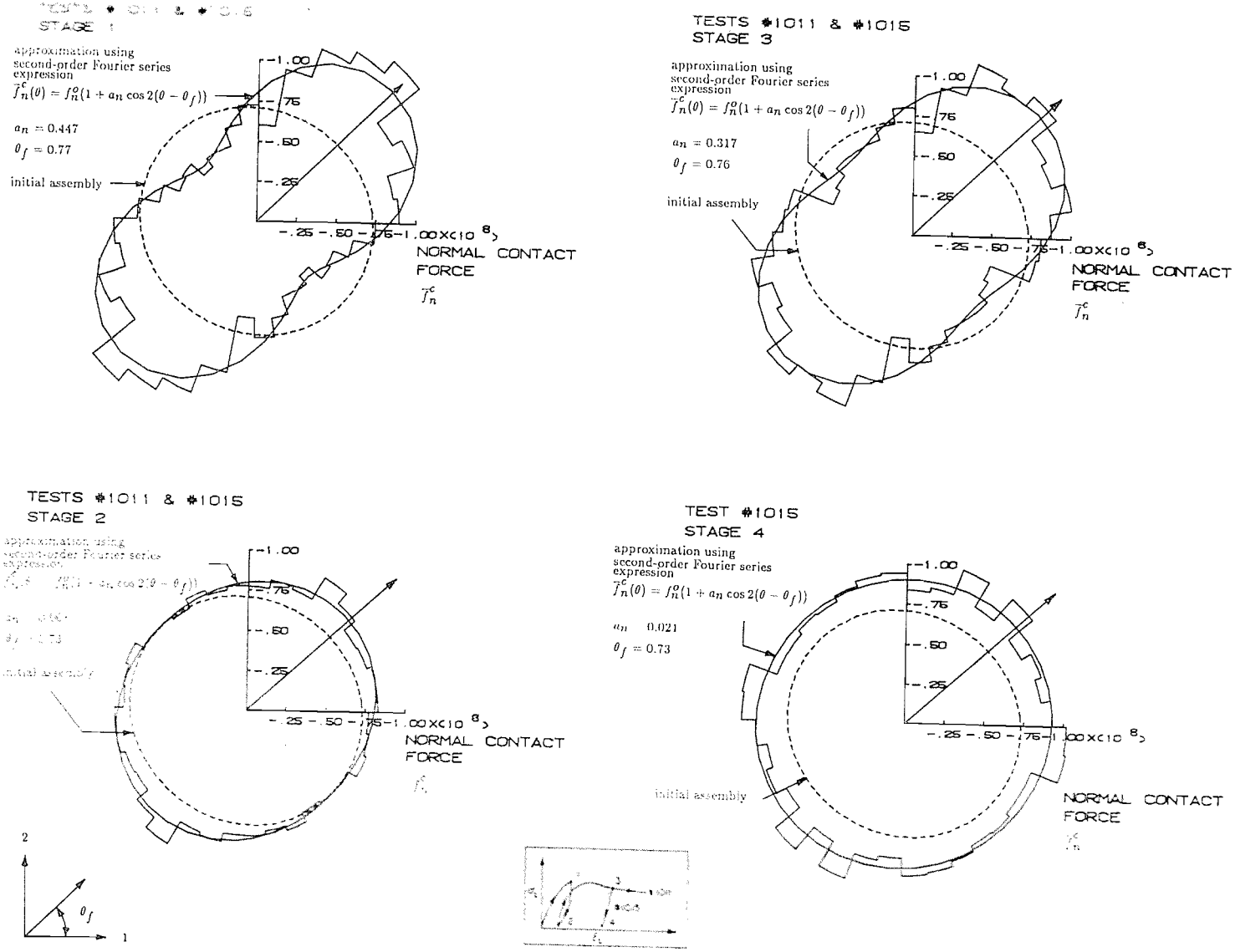

Figure 5.21 Normal Contact Force Distributions from Tests #1011 and #1015

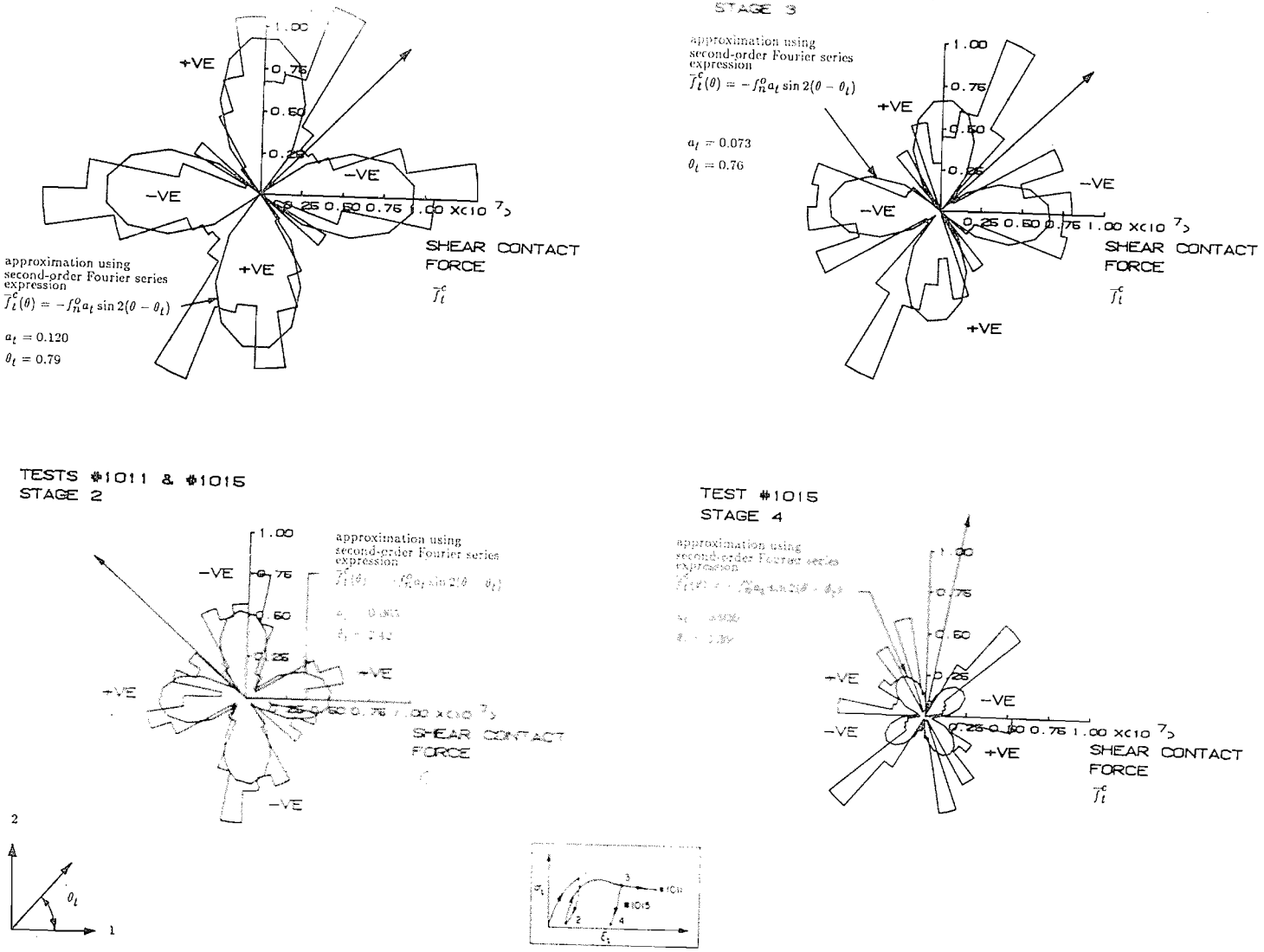

Figure 5.22 Tangential (Shear) Contact Force Distributions from Tests #1011 and #1015

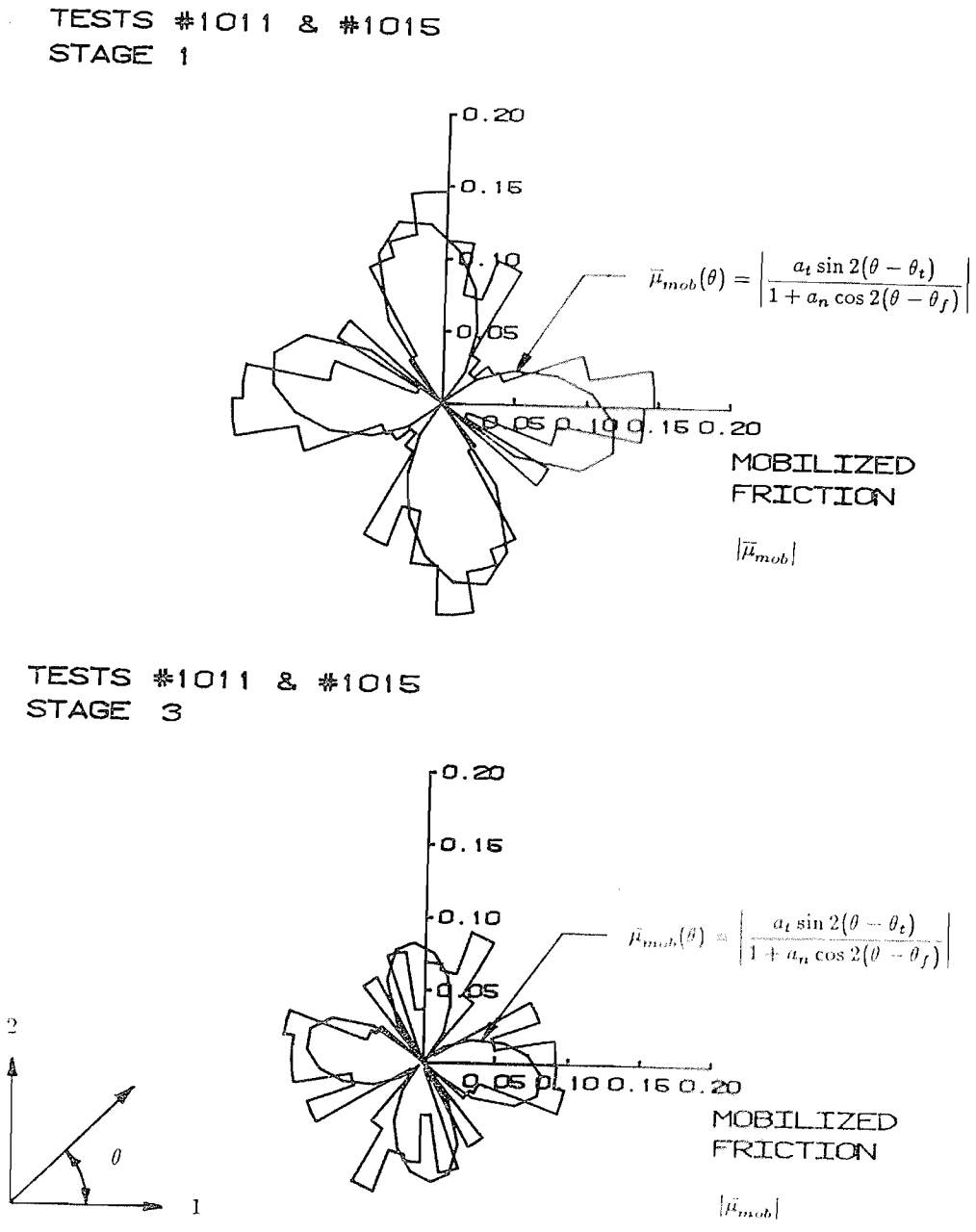

Figure 5.23 Distributions for Mobilized Friction Coefficient from Tests #1011 and #1015

diminished in value leading to macroscopic *softening* of the assembly. The reduction of normal contact force anisotropy a_n was particularly pronounced following peak shear.

Comparison of Figures 5.24a and 5.24b shows that the post-peak reduction of coefficient terms a and a_n occurred close to, or at about, the *steady state* coordination number for the test (i.e. $\gamma_\infty \approx 3.40$). However, ultimate failure did not occur until coordination number, void ratio *and* coefficients of anisotropy had achieved steady state values (Figures 5.24a through 5.24c).

Figure 5.24d shows some minor fluctuations from coaxiality of stress, contact force and contact tensors. While insignificant, these fluctuations illustrate how contact distributions and tangential contact force distributions compensate each other to maintain the assembly of discs in moment equilibrium. For example, when the direction of contact anisotropy fluctuates to $\theta_a < \theta_\sigma$, the contact forces compensate in the opposite direction (i.e. $\theta_t > \theta_\sigma$) to ensure that the moment equilibrium criterion described by equation (3.25) is preserved. The relative orientations of contact and tangential contact force tensors with respect to the (major) principal stress direction are idealized on Figure 3.7. However, it should be noted that fluctuations from coincidence of contact normal and contact force tensors are not great enough to invalidate the fundamental relationship described by equation (3.47)

The results of Tests #1011 and #1015 are presented on Figure 5.25. At all stages, expression (3.47) gave a good approximation to the directly measured invariant stress ratio. An important observation from these unload/reload tests is that microstructure anisotropy measured by parameter a is stress-induced. Unloading to a hydrostatic stress state results in a return to an essentially second-order isotropic distribution of contact normals. During unloading, these numerical systems of discs have no *memory* from previous anisotropic microstructure. This behaviour is considered to be a feature of particulate assemblies comprising *discs*. Similar tests carried out with non-circular particles (such as elliptical-shaped particles) may be expected to exhibit microstructural *memory* which is stress-path dependent.

Figure 5.26 shows the results of a biaxial compression test started from an initially dense isotropic condition. Predicted principal stress ratios and invariant stress ratios σ_{22}/σ_{11} and a_σ from expressions (3.49) and (3.47) compare favorably to the measured data. Coaxiality of principal directions θ_a, θ_f, θ_t and θ_σ was also observed in this test. Unlike the pure shear tests, a dramatic reduction in contact anisotropy was not observed for the biaxial compression test following peak shear. The sustained contact anisotropy is thought to be due to the generally higher coordination number (or contact density) which was observed for this system at a post-peak shear condition. A similar sustained level of contact anisotropy can be observed from data reported by Biarez and Wiendieck (1963) for

two-dimensional biaxial compression tests (refer to Figure 1.5).

Figure 5.27 shows the results of a pure shear test which was started from an initially dense *anisotropic* condition ($K_o = 1.5$) in order to investigate the assumption of coaxiality of assembly tensors. The plots in this figure show that, even for initially anisotropic assemblies, expression (3.47) is valid and principal directions are coincident. Another interesting observation which can be made from this test is that the reorientation of microstructure described by contacts is essentially instantaneous under rotation of principal stress directions. The rapid reorientation of microstructure due to changes in principal stress directions for this two-dimensional numerical experiment has also been observed in two-dimensional physical tests (see Figure 3.10) and in three-dimensional assemblies of sand (see Figure 2.7).

The results of the numerical experiments in the current study lead to the important conclusion that the shear capacity of these systems, at all loading stages, is largely due to contact and normal contact force anisotropies a and a_n which are generated in the major principal stress direction. Physically, this means that assembly microstructure evolves so that the capacity of the system is due to contact orientations and interparticle forces which attempt to align themselves with the direction of maximum load. Relatively little *direct* system capacity is generated through interparticle shear.

Oda and Konishi (1974a) have come to essentially the same conclusion based on physical experiments but were not able to quantify the contributions of contact force components to the shear capacity of their assemblies. Interestingly, the maximum values for a and a_n extracted from their data in Sections 3.2.3 and 3.3.3 are reasonably close to those recorded for the numerical experiments.

5.4.3.2 Accuracy of Theoretical Expressions for Average Stress Quantities

Figure 5.24a, for example, shows that the theoretical expression for a_σ using equation (3.47) overestimates the measured values by several percent. However, while the discrepancy does not appear unacceptable, it is important to trace the source of the error in order to locate which assumption(s) leading to theoretically developed expressions, such as (3.47), is responsible. In addition, it is desirable to identify the error in the predicted values of σ_t and σ_n to ensure that the close agreement between predicted and measured values of a_σ is not due to a fortuitous over-estimation of σ_t and σ_n terms.

Figures 5.28 and 5.29 present simple error analyses of data from typical tests. On Figure 5.28a the percent error between values from theoretically derived expressions (3.44), (3.45) and (3.47) and directly measured data is shown. Directly measured values follow from expressions (4.16) and invariant stress quantities (3.40) and (3.41) associated with the Mohr circle of stress. The figure shows that

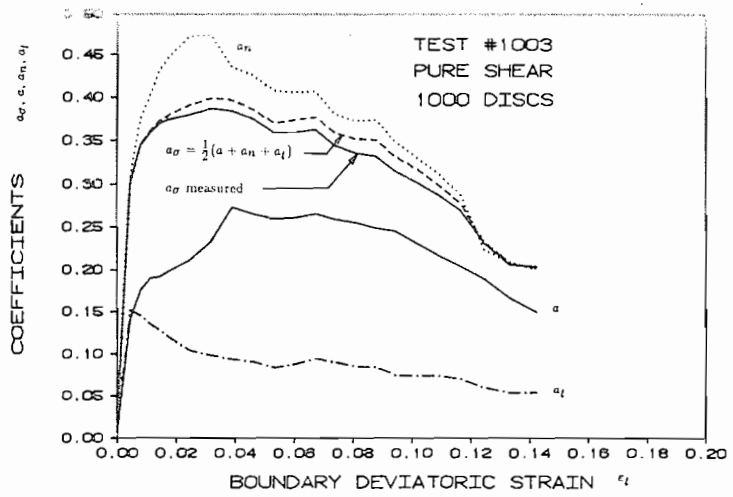

a) Coefficients of Anisotropy a_σ, a, a_n, a_t versus Deviatoric Strain ε_t

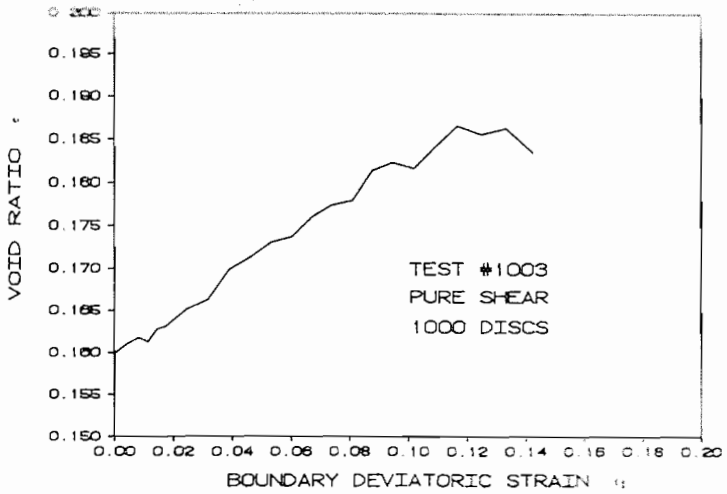

c) Void Ratio e versus Deviatoric Strain ε_t

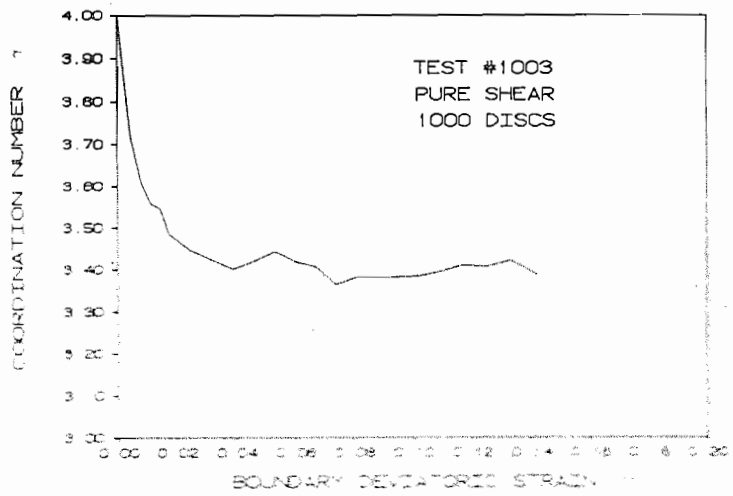

b) Coordination Number γ versus Deviatoric Strain ε_t

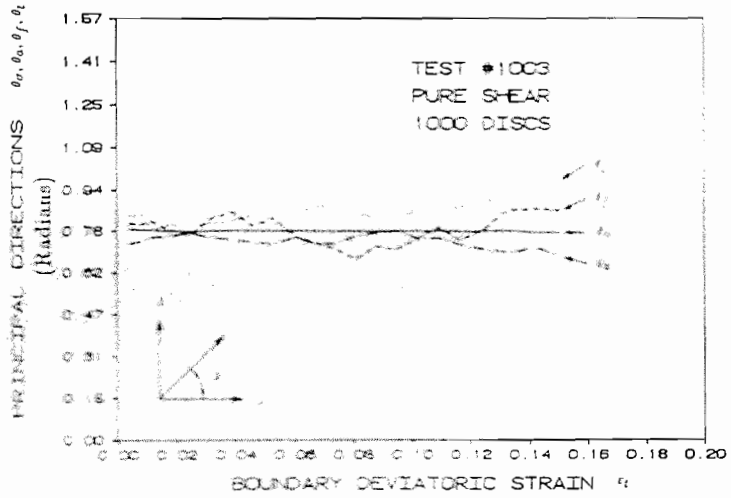

d) Principal Directions of Anisotropy θ_σ, θ_a, θ_f, θ_t versus Deviatoric Strain ε_t

Figure 5.24 Micromechanical Behaviour from Test #1003

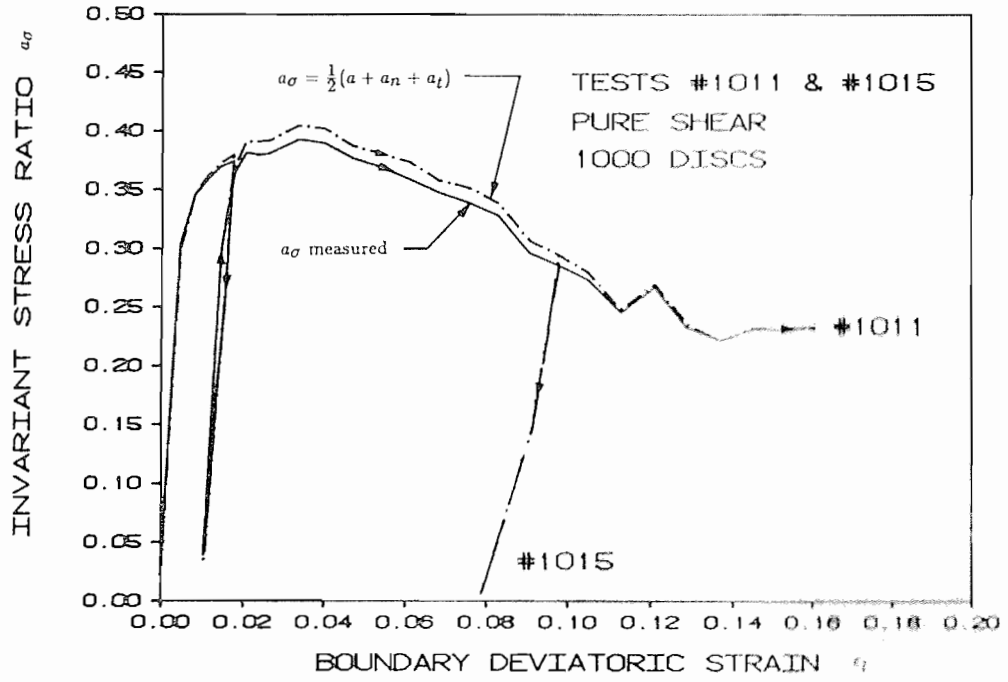

a) Invariant Stress Ratio a_σ versus Deviatoric Strain ε_t

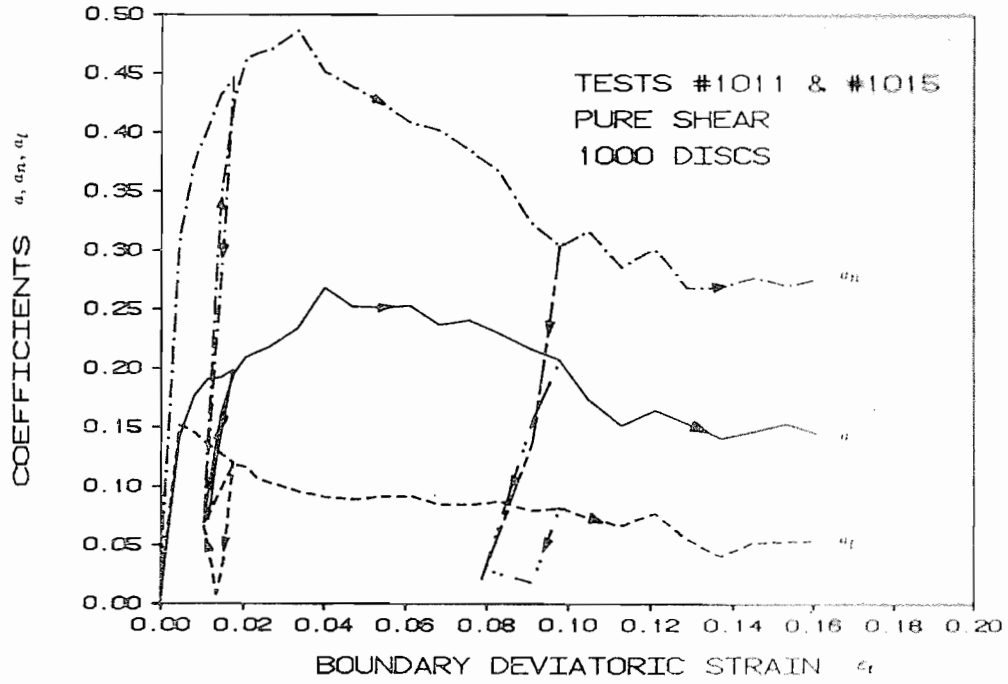

b) Coefficients of Anisotropy a, a_n, a_t versus Deviatoric Strain ε_t

Figure 5.25 Micromechanical Behaviour from Tests #1011 and #1015

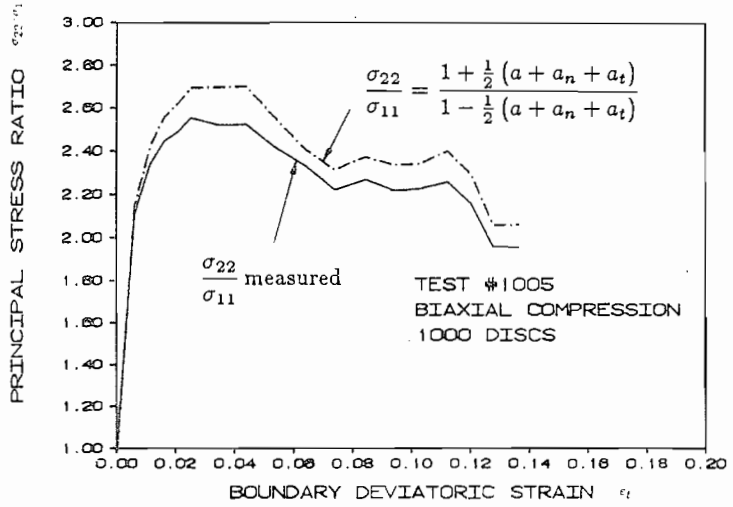

a) Principal Stress Ratio σ_{22}/σ_{11} versus Deviatoric Strain ε_t

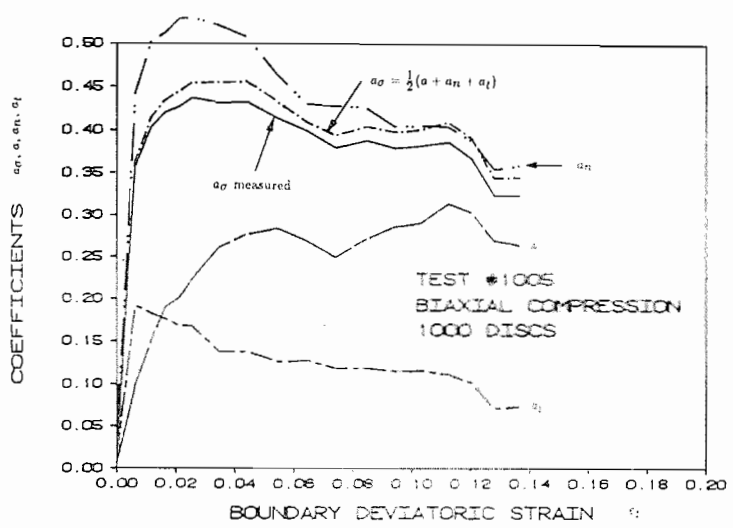

b) Coefficients of Anisotropy a_σ, a, a_n, a_t versus Deviatoric Strain ε_t

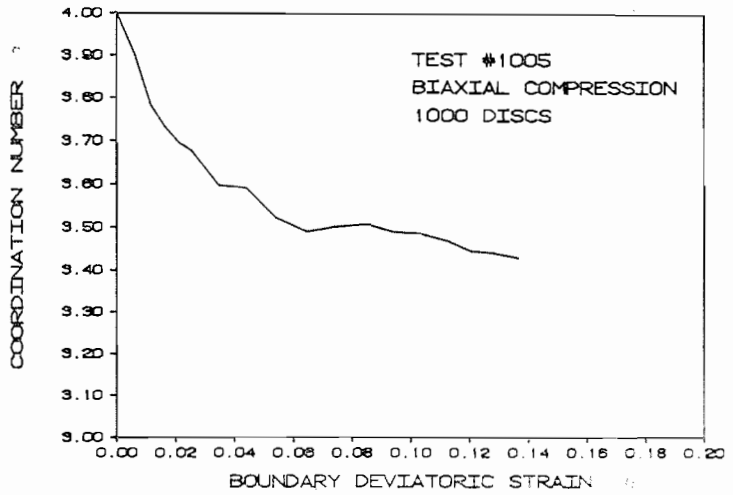

c) Coordination Number γ versus Deviatoric Strain ε_t

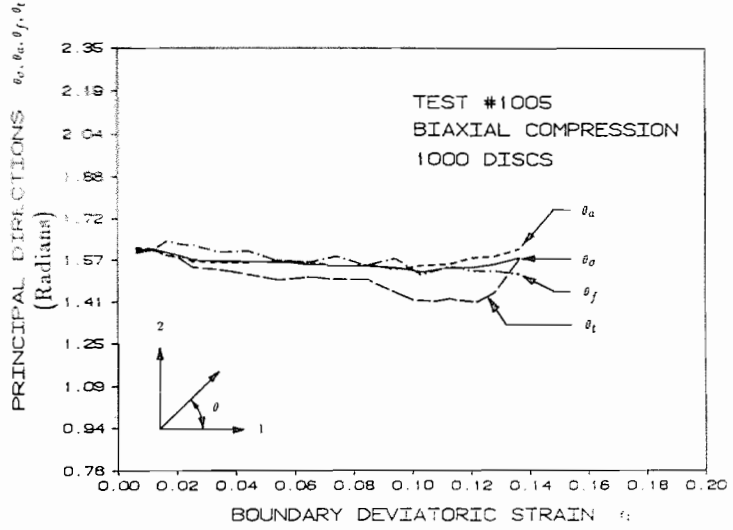

d) Principal Directions of Anisotropy θ_σ, θ_a, θ_f, θ_t versus Deviatoric Strain ε_t

Figure 5.26 Micromechanical Behaviour from Test #1005

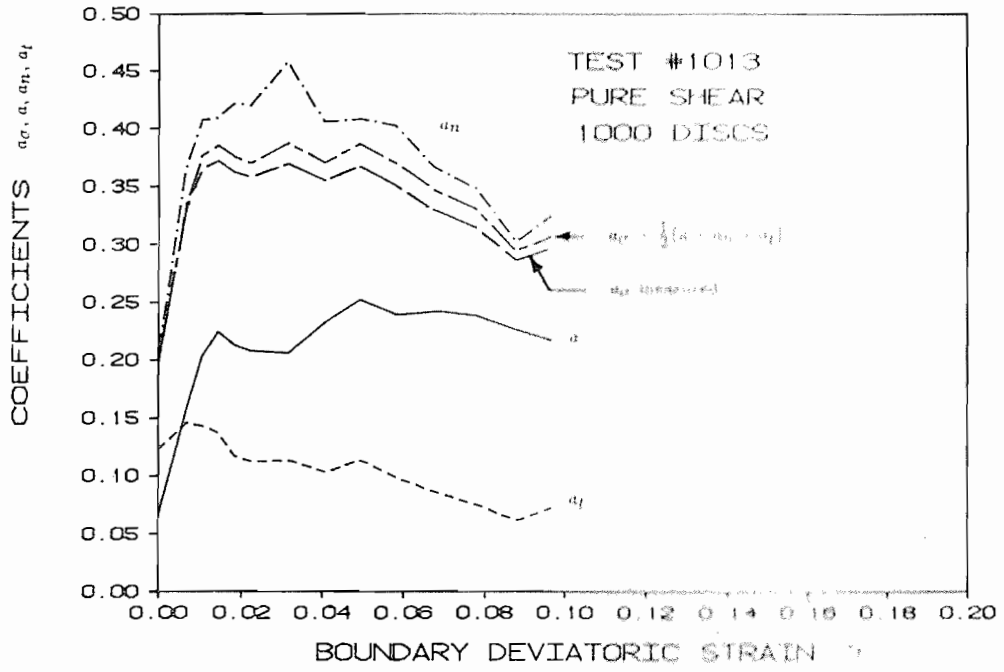

a) Coefficients of Anisotropy a_σ, a, a_n, a_t versus Deviatoric Strain ε_t

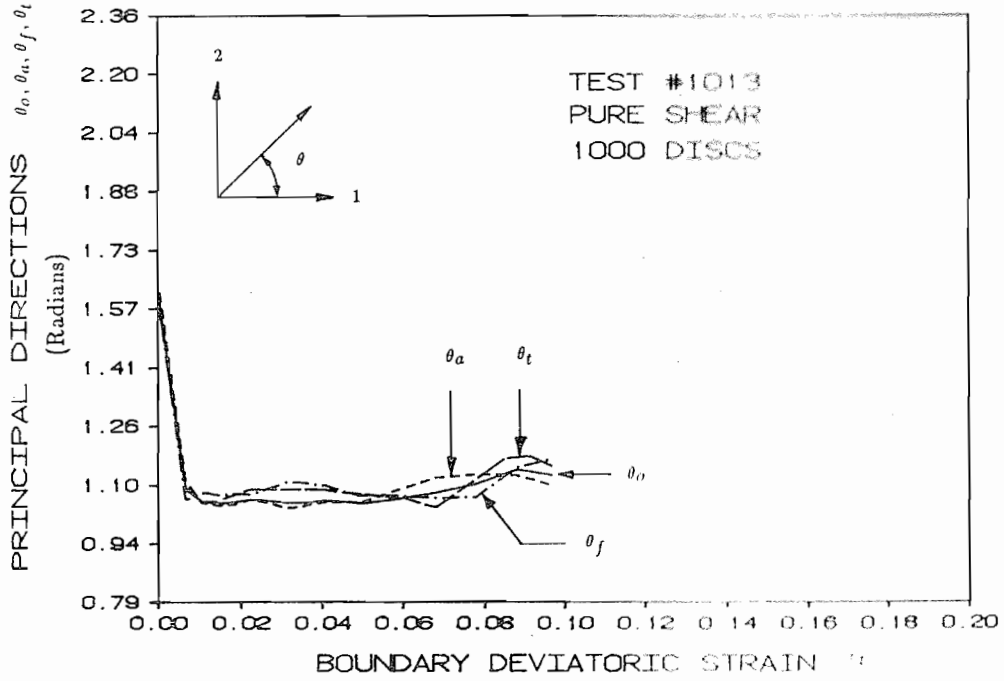

b) Principal Directions of Anisotropy θ_σ, θ_a, θ_f, θ_t versus Deviatoric Strain ε_t

Figure 5.27 Micromechanical Behaviour from Test #1013 (Initial Dense *Anisotropic* Assembly)

the percent error in a_σ is largely due to an over-estimation of the deviatoric stress component σ_t. Nevertheless, the predicted value for σ_t is within 10 percent of the measured value.

Figure 5.28b shows predicted values for the same invariant stress quantities calculated directly from 36 interval histogram data for $\overline{f}_n^c(\theta)$, $\overline{f}_t^c(\theta)$, $\overline{l}^c(\theta)$ and $M_g(\theta)$ over the range $0 \leq \theta \leq 2\pi$. Term $M_g(\theta)$ represents the number of contacts falling within the class boundaries with mid-interval orientation θ_g. Invariant stress values were calculated using the following approach: Average stress quantities σ_{ij} can be approximated from histogram data according to:

$$\sigma_{ij} = \frac{1}{V} \sum_{\theta_g} \left\{ \overline{f}_i^c(\theta) \overline{l}_j^c(\theta) M_g(\theta) \right\} \quad i,j = 1,2 \tag{5.3}$$

Expression (5.3) can be recognized as the two-dimensional analogue to relationship (2.24). Letting $\tilde{n}^c = (\cos\theta, \sin\theta)$ and $\tilde{t}^c = (-\sin\theta, \cos\theta)$ be normal and tangential contact vector components corresponding to histogram intervals, then:

$$\sigma_{ij} = \frac{1}{V} \sum_{\theta_g} \left\{ \left(\overline{f}_n^c(\theta) n_i^c + \overline{f}_t^c(\theta) t_i^c \right) \overline{l}^c(\theta) n_j^c M_g(\theta) \right\} \tag{5.4}$$

The percent error from measured values using these expressions is relatively small. The largest errors occur for the initial isotropic assembly but may be misleading since the magnitude of σ_t for the assembly at this stage is very small (e.g. two orders of magnitude lower than σ_n).

The results of a similar error analysis are presented on Figure 5.29 for a biaxial compression test (#1005). Figure 5.29a shows that the error between theory and measured values for the stress ratio σ_{22}/σ_{11} is due to σ_{22} but the discrepancy is still within 10 percent. Again, approximations using histogram data and relation (5.4) give essentially the directly measured values (Figure 5.29b).

Similar error analyses were carried out for all numerical experiments in the current investigation. Irrespective of test details, including the magnitude of disc parameters μ and $k_n r$, the maximum error between stress quantities calculated from parameters of anisotropy and directly measured stress quantities was never greater than 10 percent.

The accuracy with which theoretical expressions can be expected to predict assembly stress quantities is related to sample size and homogeneity. It was observed during the trial runs of program DISC that near-circular assemblies of less than about 500 discs resulted in *continuous* branch length *chains* which extended across the sample diameter. The corresponding histogram for contact normals when this occurred showed isolated peaks which could not be reproduced by a fourth-order Fourier series distribution function. Similar peaks are apparent from the physical test data taken from Konishi (1978) and reproduced on Figures 3.2 through 3.4 for assemblies of 400 discs. However, for the 1000

disc tests in the current investigation, unbroken chains of contacts propagating through the sample were less frequent. In these tests the chains tended to form and dissipate within the sample resulting in a larger number of dispersed chains and a smoother distribution of contact normals. While the larger assemblies comprising 1000 discs improved the accuracy of the Fourier series distribution function, occasional predominant chains of contacts are responsible for the discontinuous appearance of the contact normal histogram data reported in Section 5.4.2.3. Ignoring for the moment the prohibitive amount of computer time required to carry out tests on even larger assemblies, it is considered that second-order Fourier series expressions would produce more accurate approximations to contact normal distributions for larger sample sizes.

In summary, the results of the error analyses show that stress quantities can be calculated directly from position-independent average quantities $\overline{f}_n^c(\theta)$, $\overline{f}_t^c(\theta)$, $\overline{l}^c(\theta)$ and $M_g(\theta)$ according to (5.4). This is an important statement because relationship (5.4) is a two-dimensional analogue to expression (2.24) which is a fundamental postulate for three-dimensional systems.

In addition, the results of numerical experiments reported in this section show that the principal stress ratio, invariant stress ratio, normal stress and deviatoric stress acting through the assembly can be usefully approximated by expressions presented in Section 3.4.1 which contain invariant quantities of second-order contact and contact force tensors. Since stress quantities σ_{ij} expressed as (3.53) retain their form in three dimensions, it may be inferred that similar fundamental expressions for invariant stress ratio, principal stress ratio etc. are equally valid for three-dimensional granular media.

5.4.4 Influence of Disc Properties

5.4.4.1 Contact Stiffnesses

The test results presented at this stage have been largely restricted to experimental results from assemblies of discs with linear elastic contacts having the constant product term $k_n r = 3.75 \times 10^{10}$. From Appendix B, it is reasonable to expect that photo-elastic materials exhibit normal compliances which may be one order of magnitude greater than similar particles comprising stiffer elastic materials such as steel or quartz.

Three tests were carried out to examine the influence of the magnitude of contact stiffness on the global and micromechanical response of assemblies of discs. The experiments performed were identical to tests already described with the exception that $k_n r = 3.75 \times 10^{11}$. Unfortunetly, assemblies with higher stiffnesses impose a time-step penalty which can be appreciated from equation (4.15). This relation shows that to achieve the same amount of deformation as recorded in previous tests, program

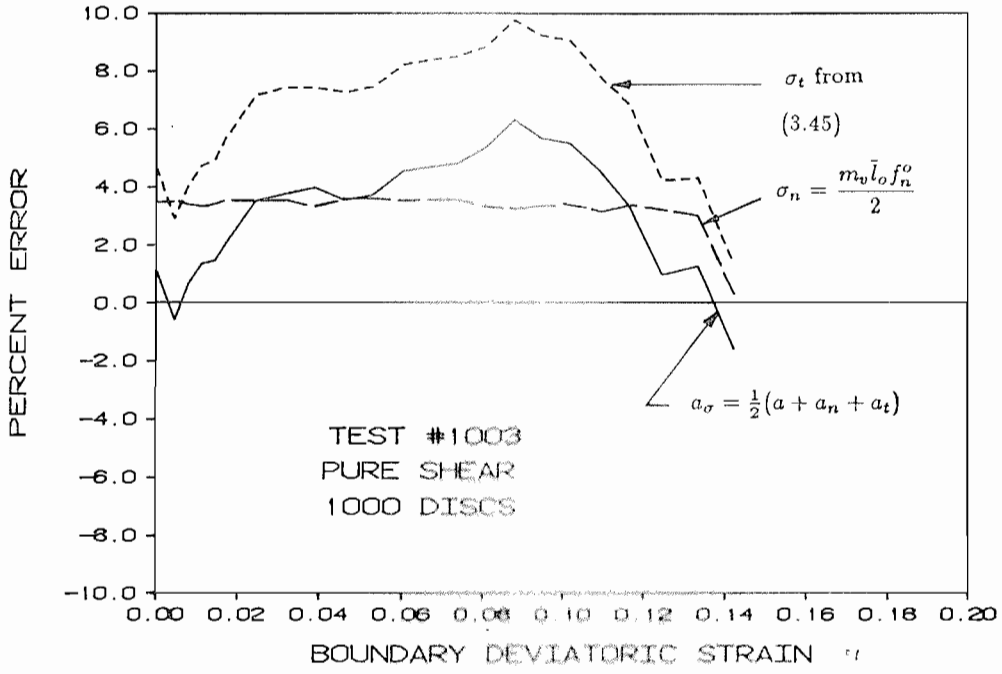

a) Percent Error from Measured Stress Quantities using Theoretical Expressions

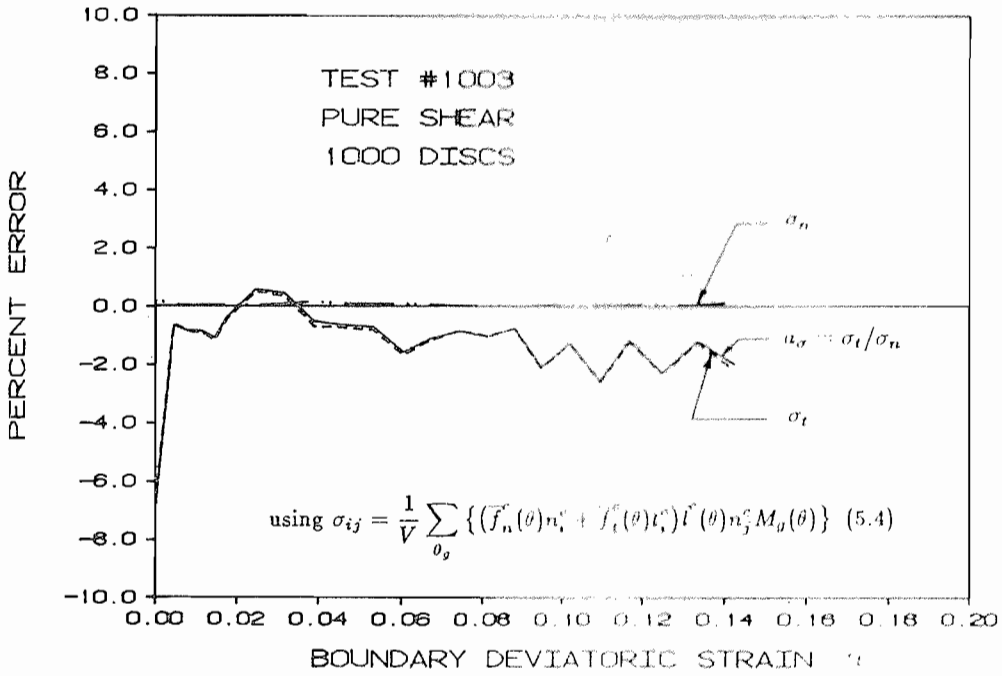

b) Percent Error from Measured Stress Quantities using Histogram Data

Figure 5.28 Error Analysis for Test #1003

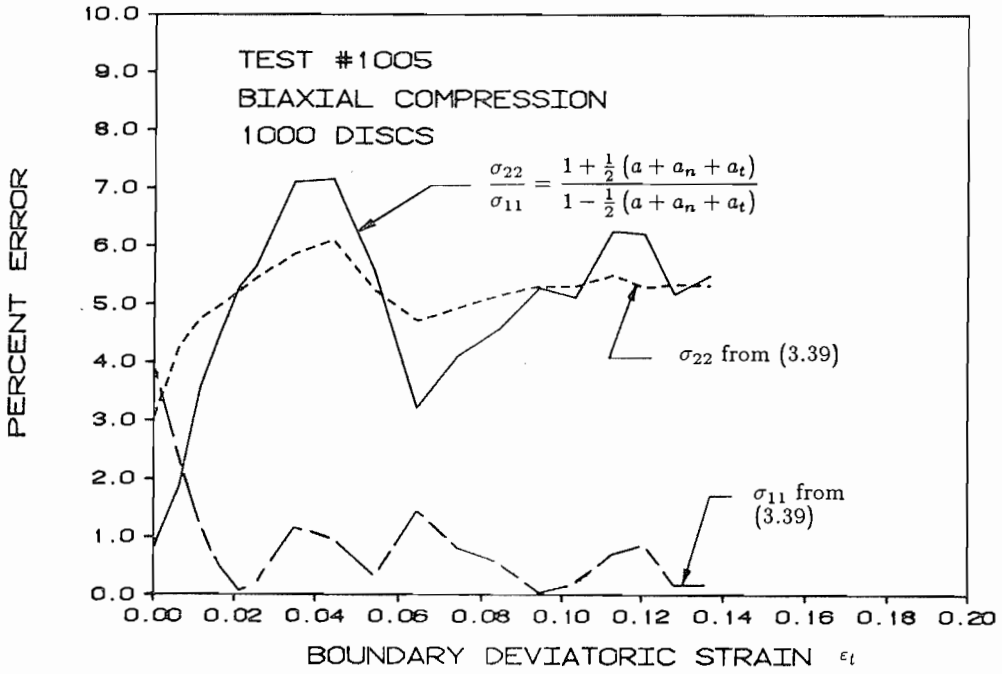

a) Percent Error from Measured Stress Quantities using Theoretical Expressions

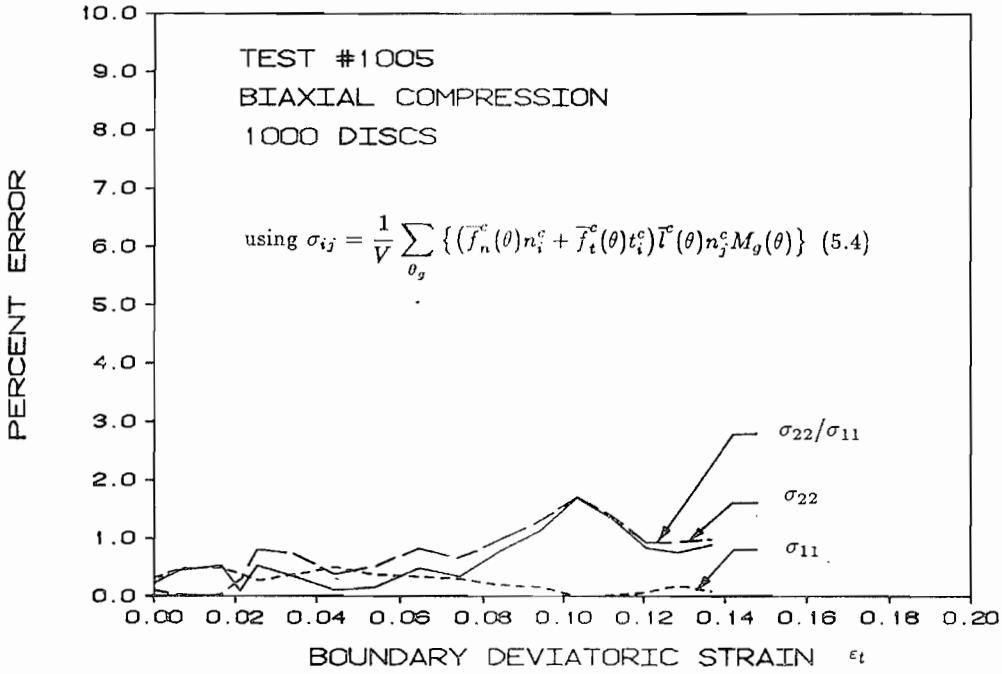

b) Percent Error from Measured Stress Quantities using Histogram Data

Figure 5.29 Error Analysis for Test #1005

DISC had to run $\sqrt{10}$ times longer for assemblies with high contact stiffnesses. Consequently, fewer of these tests were performed even though they may be considered more representative of actual granular materials.

Figure 5.30 shows the normal stress-volumetric strain response for two hydrostatic unload/reload tests. As may be anticipated, the system with the lower contact stiffnesses showed a lower bulk modulus B where $B = \Delta\sigma_n/\Delta\varepsilon_n$.

Figure 5.31 illustrates the sensitivity of coordination number to average contact force level. Specifically, the figure shows that there is an essentially linear relationship between coordination number γ and average normal contact force f_n^o during hydrostatic tests. The sensitivity of coordination number to contact force level is more pronounced for sytems with *low* stiffness contacts. The source of the performance difference between these two tests can be identified from frequency distributions for contact normal forces as shown on Figures 5.32a and 5.32b. The frequency data on the figures has been taken over 40 intervals. These figures show that during hydrostatic unloading, the frequency distributions shift to the left corresponding to lower average contact normal force f_n^o. However, the increase in contacts with low interparticle forces is less for the low stiffness assembly and this system experiences a greater net loss in contacts. If the assemblies under study were to comprise *bonded* discs (i.e. contacts which could take tension) then, one would expect a significant number of contacts to change from transmitting compressive forces to transmitting tensile forces under hydrostatic unloading. However, because the assemblies investigated are cohesionless, these contacts are lost. This loss does not represent a significant rearrangement in structure, but is a consequence of the unambiguous requirement that a contact must carry load before it is recorded in these numerical experiments.

The observations made above with respect to the frequency distribution of contact forces for cohesionless systems have interesting ramifications for *bonded* assemblies. The implication from these tests is that significant numbers of tensile contact forces are possible in bonded granular assemblies even when these systems are loaded under (compressive) hydrostatic conditions.

Differences in the behaviour of pure shear tests with dissimilar contact stiffnesses are shown on Figure 5.33. Test #1024 shows an initially greater global elastic stiffness and an overall higher shear capacity as compared to Test #1003. In addition, larger volumetric strains were sustained for the stiffer sample before becoming unstable (Figure 5.35b). Associated micromechanical behaviour for the stiffer assembly can be seen from Figures 5.34a and 5.34b. Consistent with the generally higher invariant stress ratio values a_σ recorded for Test #1024, there were higher values for coefficients of anisotropy a_n and a (compare Figure 5.34a with Figure 5.24a). On the other hand, a_t was not observed

to vary significantly between tests with different contact stiffnesses.

Figure 5.35 and 5.36 show the results of Test #1025 which is a biaxial compression test conducted with $k_n r = 3.75 \times 10^{11}$. Figure 5.35 compares the global stress-strain response of Tests #1025 and #1005. The stiffer sample shows an initially steeper $\sigma_a - \varepsilon_t$ curve and relatively little initial elastic volumetric compression. The peak and post-peak shear capacities recorded for these tests are similar and show comparable coefficients of anisotropy a, a_n and a_t (compare Figures 5.36a and 5.26b). However, like the pure shear tests, assembly anisotropies in Test #1025 are generated at significantly lower coordination numbers as shown on Figure 5.36b.

5.4.4.2 Interparticle Friction Coefficient

The stress-strain-void ratio response of pure shear tests with interparticle friction coefficient μ set to of 0, 0.10, 0.25 and 0.50 is shown on the plots from Figure 5.37. Tests with zero friction values represent a hypothetical condition which is not possible for real systems. However, valuable lessons are gained from examination of test results carried out under the limiting condition represented by frictionless particles.

The following observations can be made: The peak deviatoric stress, dilatancy rate $\dot{\varepsilon}_n/\dot{\varepsilon}_t$ and void ratio increase with increasing magnitude of μ. Importantly, for assemblies with $\mu = 0$, there is essentially no change in sample volume or void ratio with increasing deviatoric strain. Nevertheless, despite the inability of these systems to generate tangential contact forces, a small amount of shear capacity is still measured for these assemblies. It is possible that a portion of the shear capacity recorded for $\mu = 0$ assemblies is due to the artificial damping introduced as part of the DEM numerical scheme to dissipate kinetic energy. This contribution (should it exist) can be likened to the small additional stability afforded granular particles by immersing the assembly in a *viscous* medium.

The micromechanical response of tests shown on Figure 5.37 is presented on Figure 5.38. The steady state coordination number for these assemblies is greatly influenced by interparticle friction. In general, increasing μ results in lower coordination numbers (Figure 5.38a). Similarly, reduced μ values correspond to lower coefficients of anisotropy a, a_n and a_t. As expected, assemblies with $\mu = 0$ exhibit no tangential (shear) contact force anisotropy. Similar observations can be made from the data presented on Figures 5.39 and 5.40 taken from the results of biaxial compression tests with variable friction coefficients.

The observations made above give important insight into the contribution of interparticle friction to the shear capacity of these systems observed at the macroscale. The *direct* contribution of tangen-

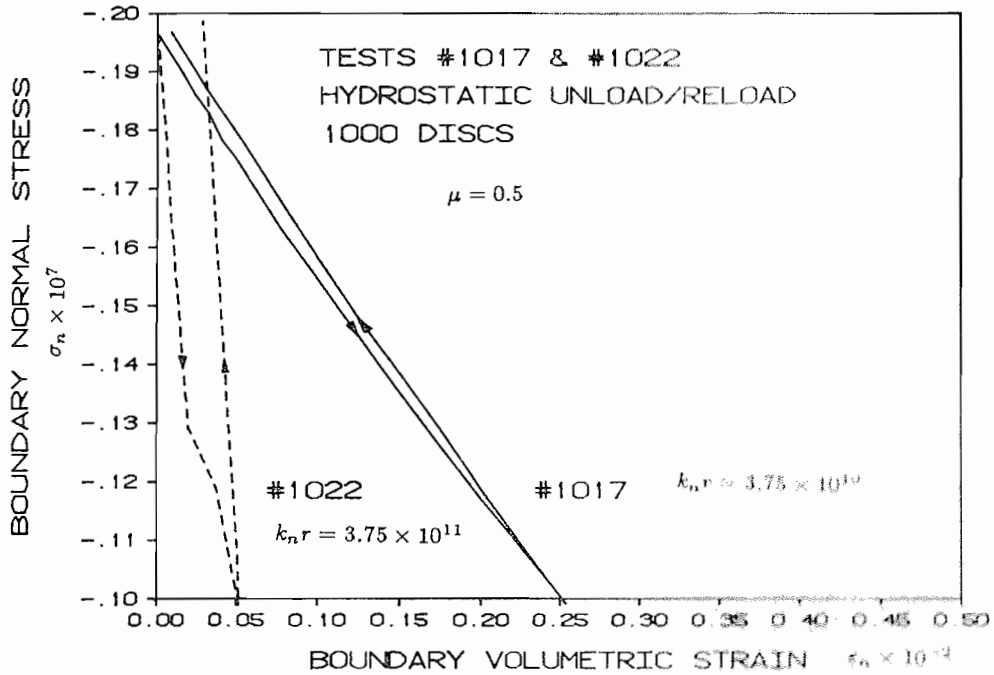

Figure 5.30 Stress-Strain Response from Hydrostatic Unload/Reload Tests with Variable Interparticle Stiffness

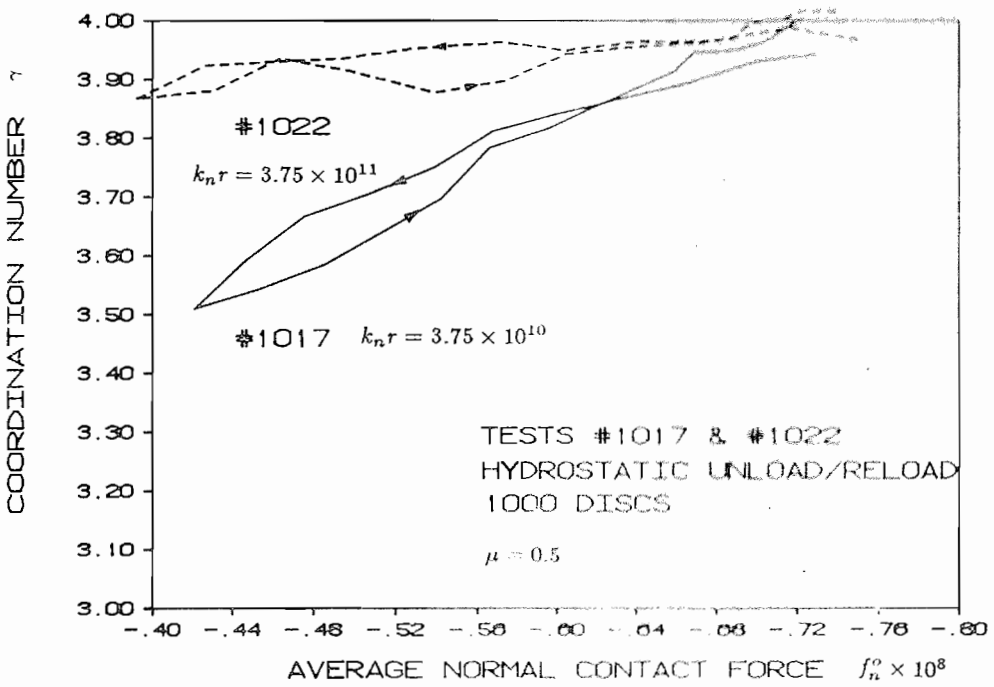

Figure 5.31 Coordination Number versus Average Normal Contact Force from Hydrostatic Unload/Reload Tests with Variable Interparticle Stiffness

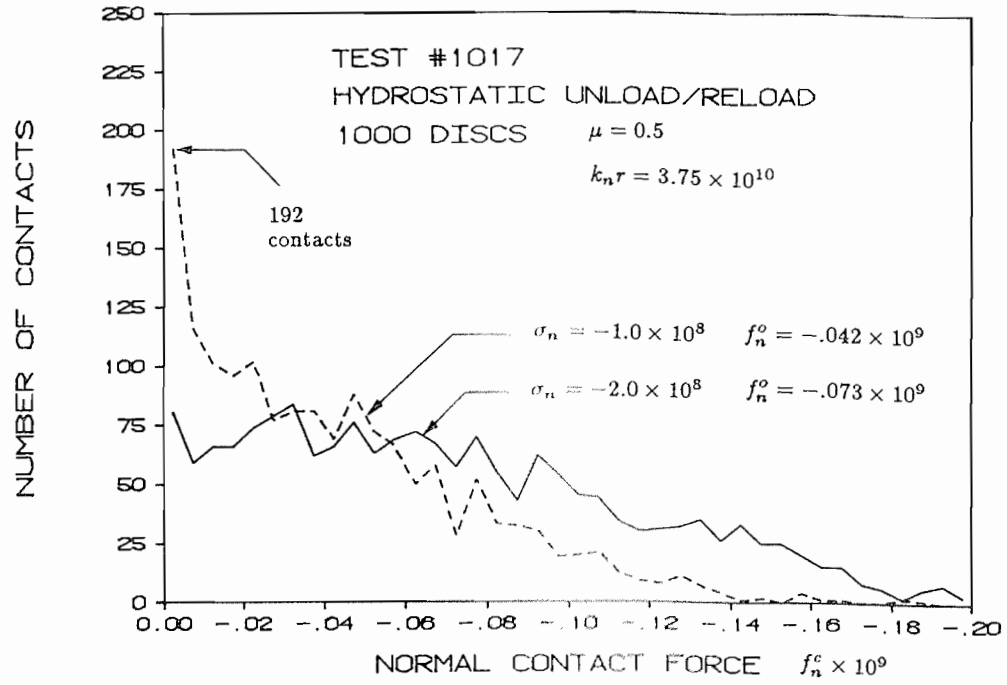

a) Assembly with *Low* Contact Stiffness

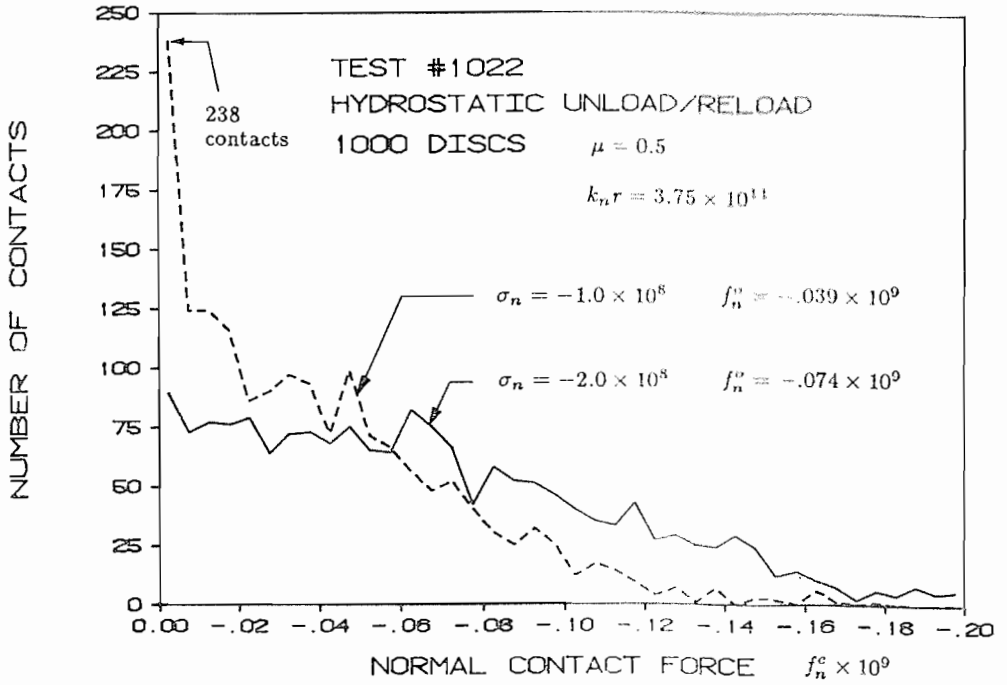

b) Assembly with *High* Contact Stiffness

Figure 5.32 Normal Contact Force Frequency Distributions from Hydrostatic Unload/Reload Tests with Variable Interparticle Stiffness

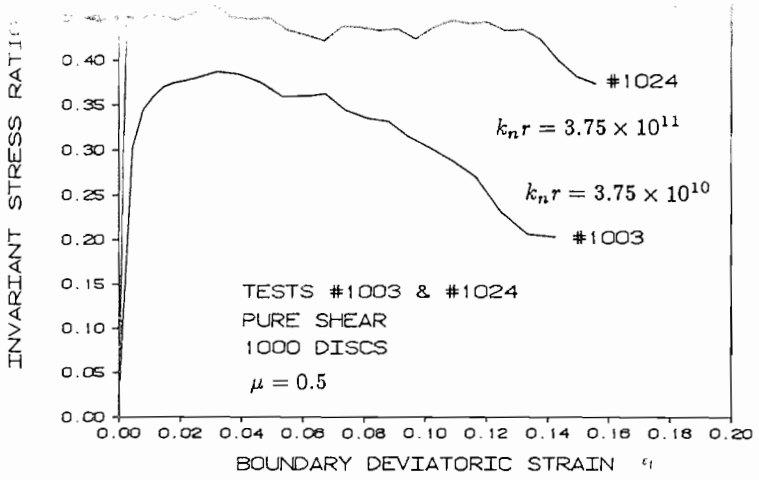

a) Invariant Stress Ratio a_σ versus Deviatoric Strain ε_t

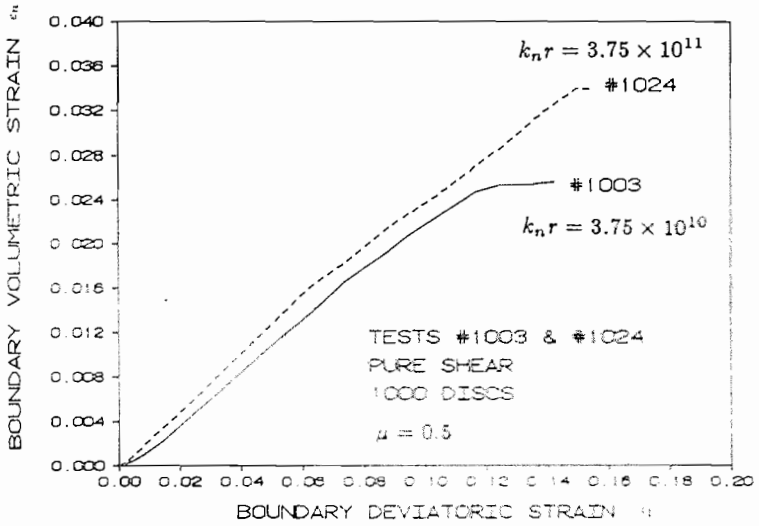

b) Volumetric Strain ε_n versus Deviatoric Strain ε_t

Figure 5.33 Stress-Strain Response from Tests with Variable Interparticle Stiffness

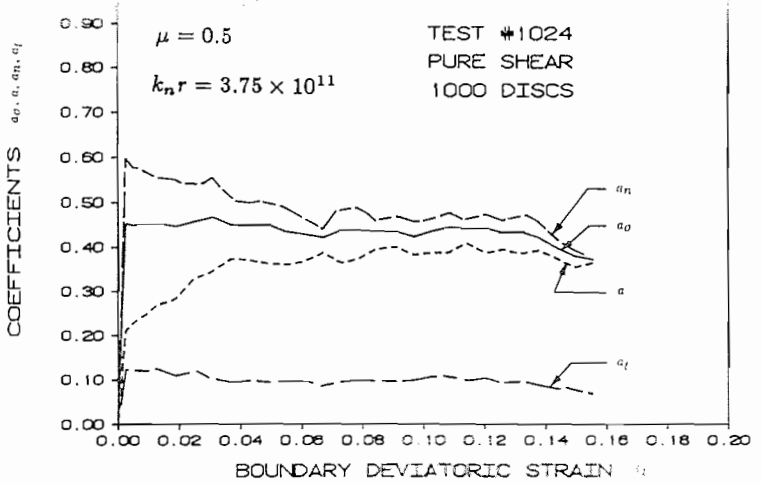

a) Coefficients of Anisotropy a_σ, a, a_n, a_t versus Deviatoric Strain ε_t

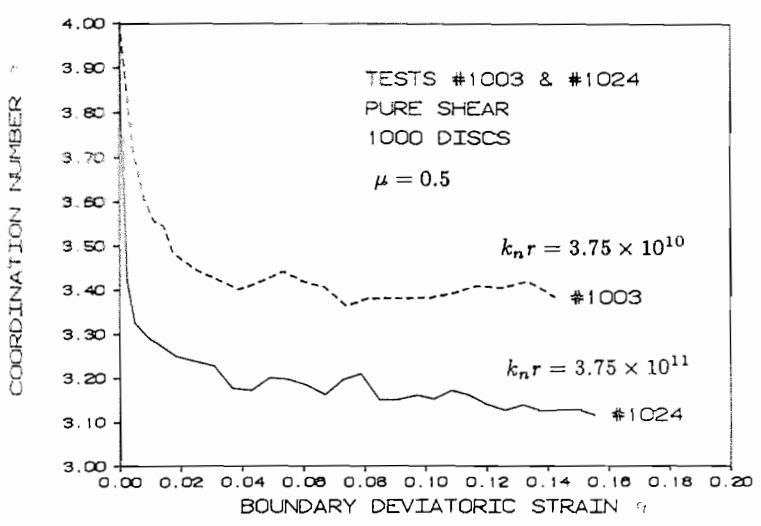

b) Coordination Number γ versus Deviatoric Strain ε_t

Figure 5.34 Micromechanical Behaviour from Tests with Variable Interparticle Stiffness

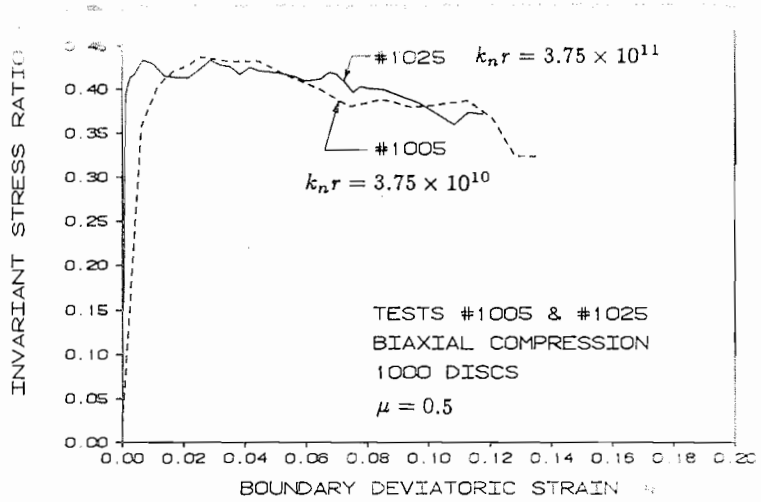

a) Invariant Stress Ratio a_σ versus Deviatoric Strain ε_t

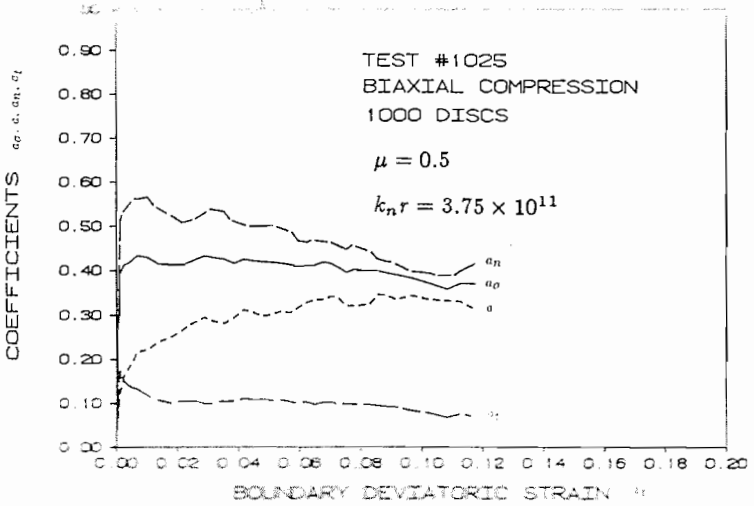

a) Coefficients of Anisotropy a_σ, a, a_n, a_t versus Deviatoric Strain ε_t

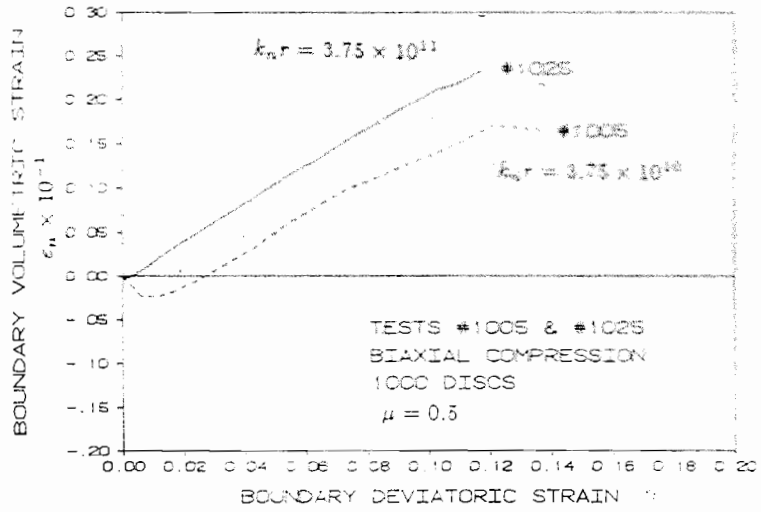

b) Volumetric Strain ε_n versus Deviatoric Strain ε_t

Figure 5.35 Stress-Strain Response from Tests with Variable Interparticle Stiffness

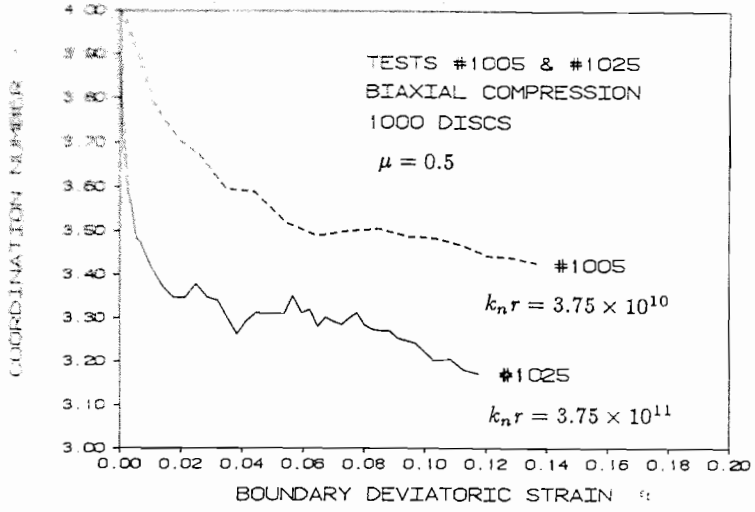

b) Coordination Number γ versus Deviatoric Strain ε_t

Figure 5.36 Micromechanical Behaviour from Tests with Variable Interparticle Stiffness

tial contact force anisotropy described by the coefficient a_t is observed to be small when compared to a_n and a. However, interparticle friction dictates the extent to which the microstructure can dilate and anisotropies a_n and a evolve. In general, assemblies with lower coordination numbers are more mobile and have the potential for greater anisotropy as described by parameters a_n and a. However, in order to generate stable configurations at reduced coordination numbers it is necessary that assemblies of discs be capable of transmitting tangential contact forces. As the test data show, without interparticle friction, it is not possible for these assemblies to dilate under deviatoric strain because only the initial (dense) packing arrangement with $\gamma \approx 4$ is stable. The test results suggest that only a modest frictional capacity is required during sample distortion to allow the microstructure to develop the oblique interparticle forces which are required to maintain the assembly in static equilibrium at coordination numbers less than four.

Skinner (1969) reported that for shear box tests with ballotini having variable interparticle friction angle, the measured macroscopic assembly friction angles at peak shear and at critical void ratio do not increase monotonically with increasing magnitude of interparticle friction. It is interesting to compare Skinner's observations with the results of numerical tests in the current study. Assuming that numerical assemblies at the macroscale obey a Coulomb friction law then, the macroscopic assembly friction angle ϕ at any stage can be calculated from:

$$\sin \phi = |\sigma_t / \sigma_n| \tag{5.5}$$

The results of calculations for ϕ_{max} and ϕ_{cv} (or ϕ_{∞}) are plotted against ϕ_μ on Figure 5.41. Figure 5.41 shows that the curve for pure shear tests at the ultimate state gives the same trend as reported by Skinner for three-dimensional assemblies of spherical particles (see Figure 1.6c). Like Skinner's results, the numerical pure shear tests showed ϕ_{cv} (or ϕ_{∞}) to be independent of interparticle friction angle for $\phi_\mu > 5$ degrees. For all other data on Figure 5.41, there is a distinct non-linear appearance to the curves. Indeed, for all curves there is a threshold value of ϕ_μ beyond which macroscopic shear capacity is essentially independent of interparticle friction angle. This threshold value varies from 5 to (say) 25 degrees depending on the loading path and whether the system under consideration is at peak or ultimate condition. This range of values is well within directly measured values of ϕ_μ for actual granular media.

5.4.5 Coefficients of Contact Anisotropy and Coordination Number

Examination of parameters a, b and coordination number γ gives some qualitative understanding of how the microstructure of assemblies comprising discs evolves during shear.

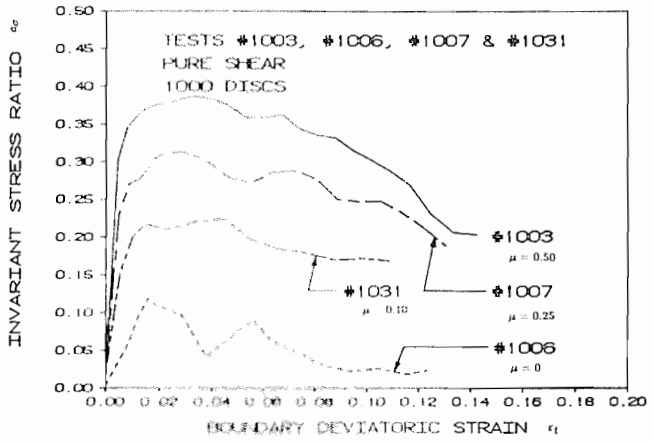

a) Invariant Stress Ratio a_σ versus Deviatoric Strain ε_t

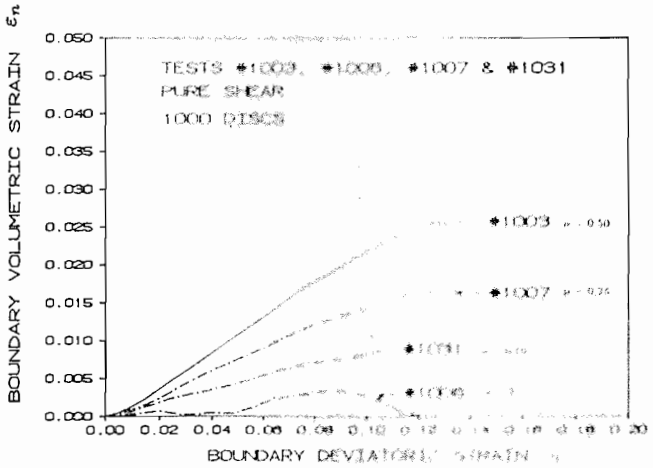

b) Volumetric Strain ε_n versus Deviatoric Strain ε_t

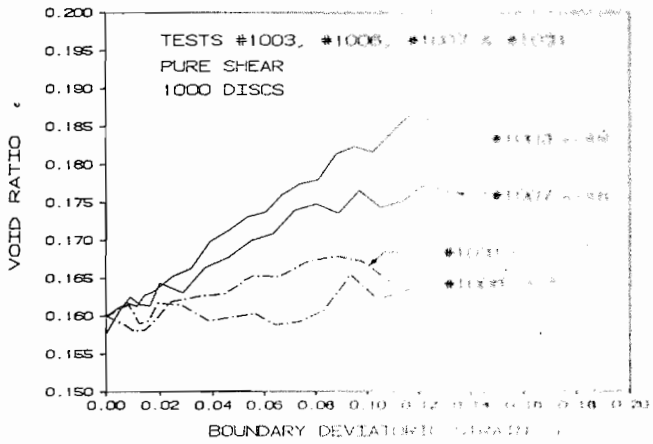

c) Void Ratio e versus Deviatoric Strain ε_t

Figure 5.37 Stress-Strain-Void Ratio Behaviour from Tests with Variable Interparticle Friction Coefficient and $k_n r = 3.75 \times 10^{10}$

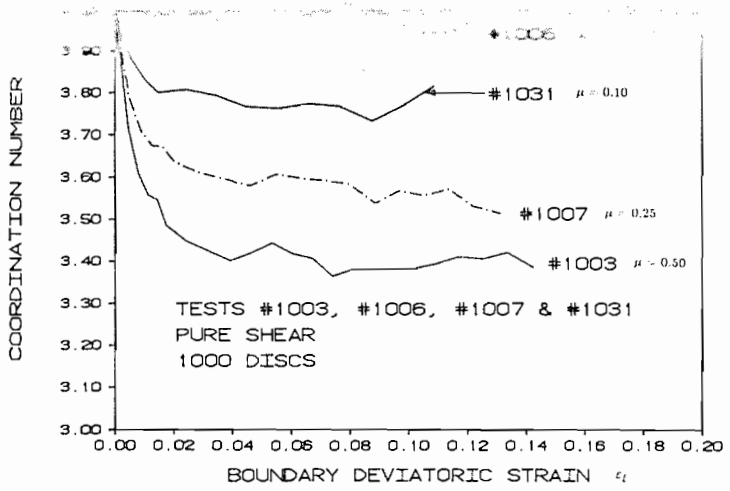

a) Coordination Number γ versus Deviatoric Strain ε_t

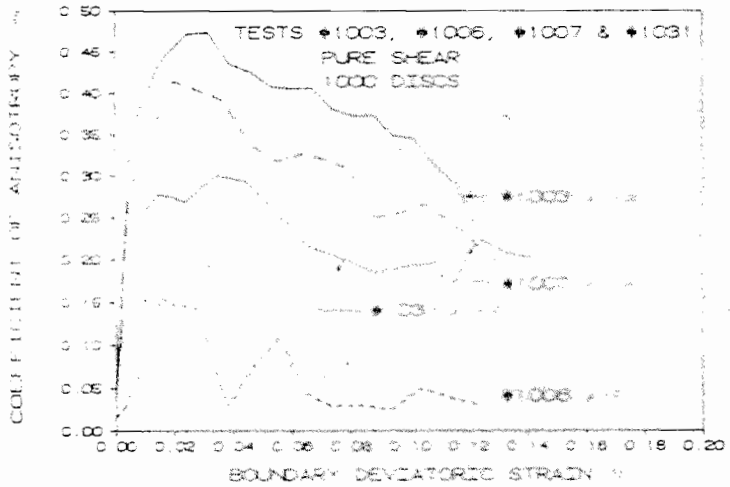

b) Normal Contact Force Anisotropy a_n versus Deviatoric Strain ε_t

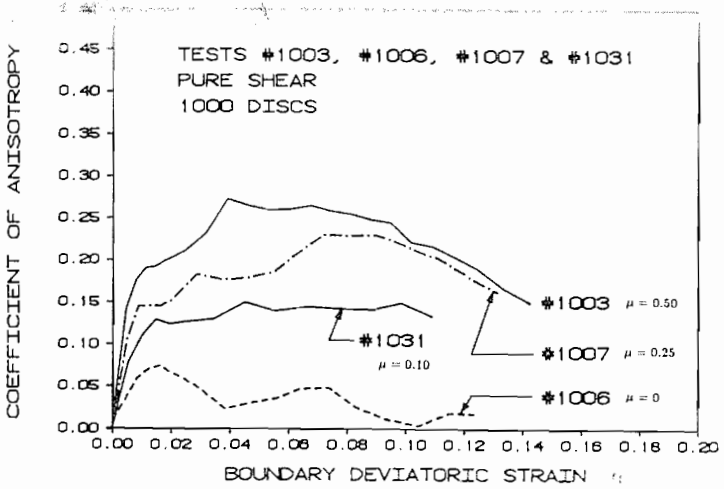

c) Contact Normal Anisotropy a versus Deviatoric Strain ε_t

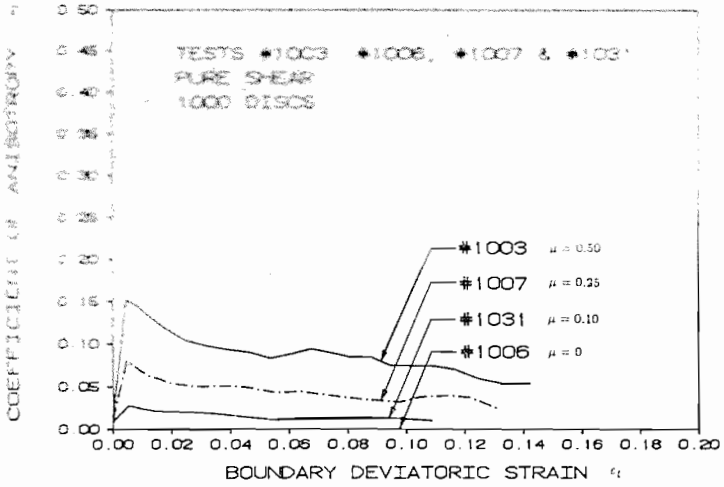

d) Tangential (Shear) Contact Force Anisotropy a_t versus Deviatoric Strain ε_t

Figure 5.38 Micromechanical Behaviour from Tests with Variable Interparticle Friction Coefficient and $k_n r = 3.75 \times 10^{10}$

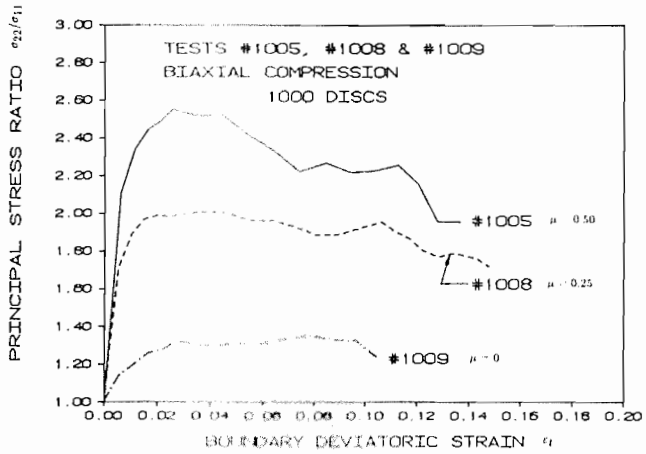

a) Principal Stress Ratio σ_{22}/σ_{11} versus Deviatoric Strain ε_t

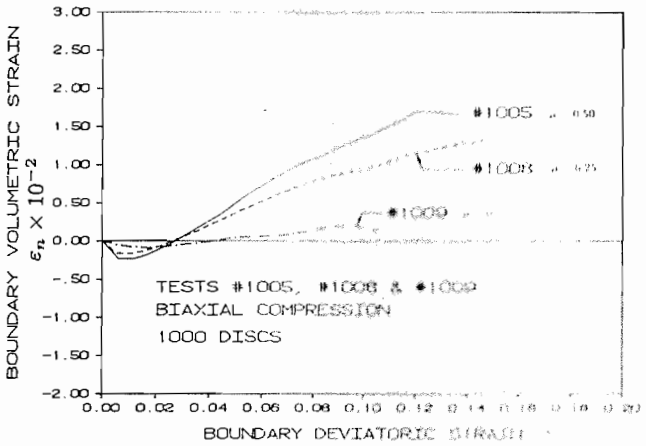

b) Volumetric Strain ε_n versus Deviatoric Strain ε_t

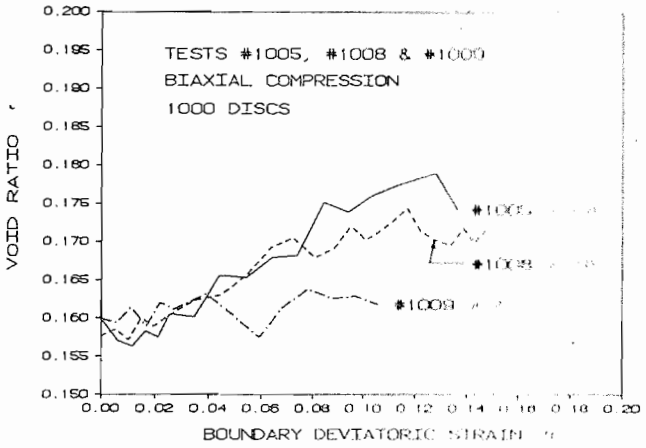

c) Void Ratio e versus Deviatoric Strain ε_t

Figure 5.39 Stress-Strain-Void Ratio Behaviour from Tests with Variable Interparticle Friction Coefficient and $k_n r = 3.75 \times 10^{10}$

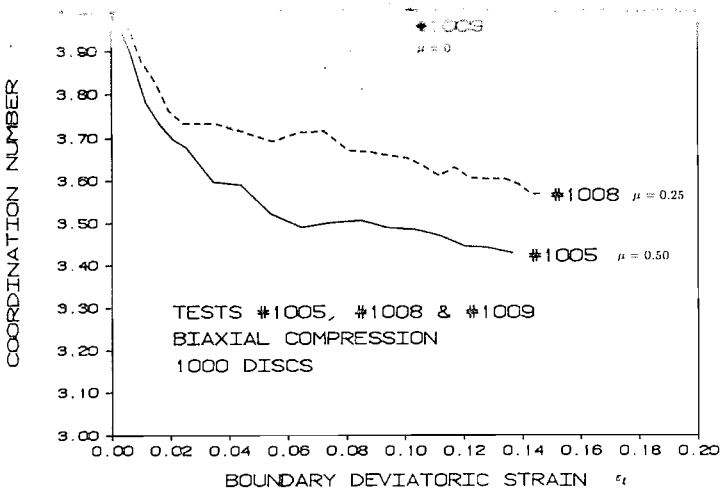

a) Coordination Number γ versus Deviatoric Strain ε_t

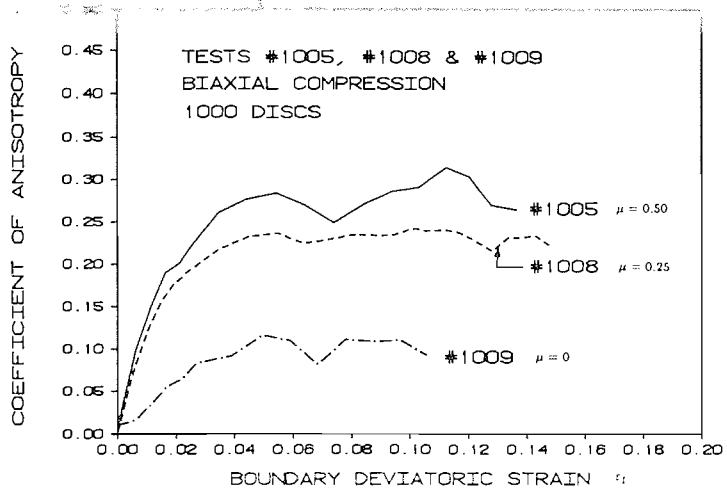

c) Contact Normal Anisotropy a versus Deviatoric Strain ε_t

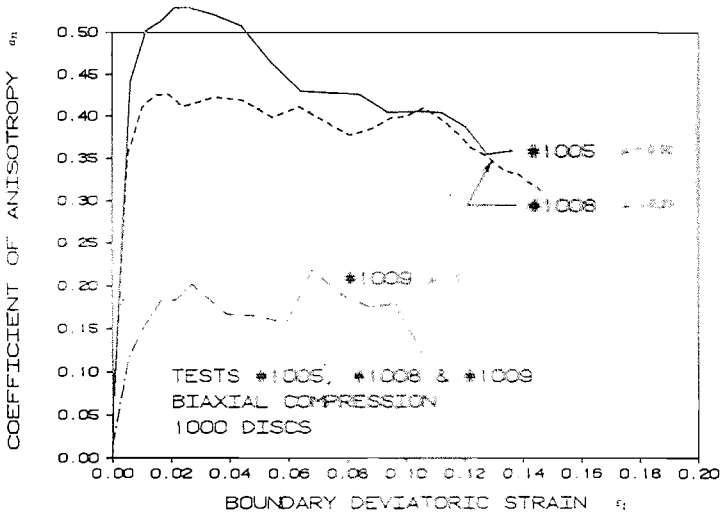

b) Normal Contact Force Anisotropy a_n versus Deviatoric Strain ε_t

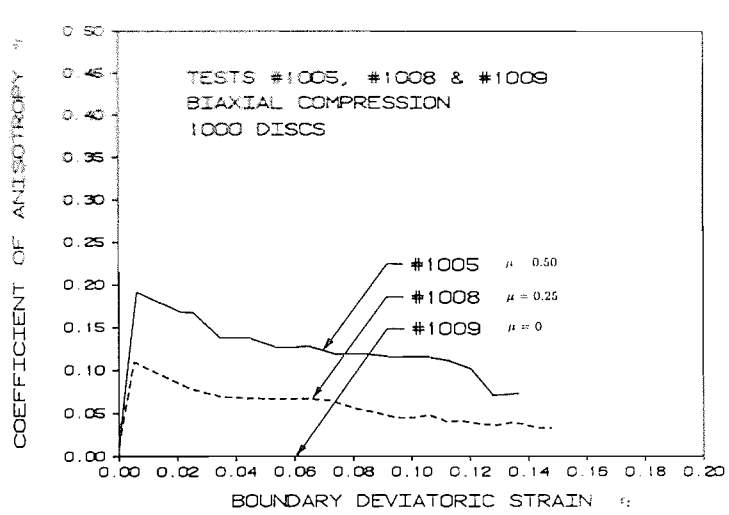

d) Tangential (Shear) Contact Force Anisotropy a_t versus Deviatoric Strain ε_t

Figure 5.40 Micromechanical Behaviour from Tests with Variable Interparticle Friction Coefficient and $k_n r = 3.75 \times 10^{10}$

Figure 5.41

Macroscopic Assembly Friction Angles ϕ_{max}, ϕ_∞ versus Interparticle Friction Angle ϕ_μ

1000 Disc Tests
$k_n r = 3.75 \times 10^{10}$

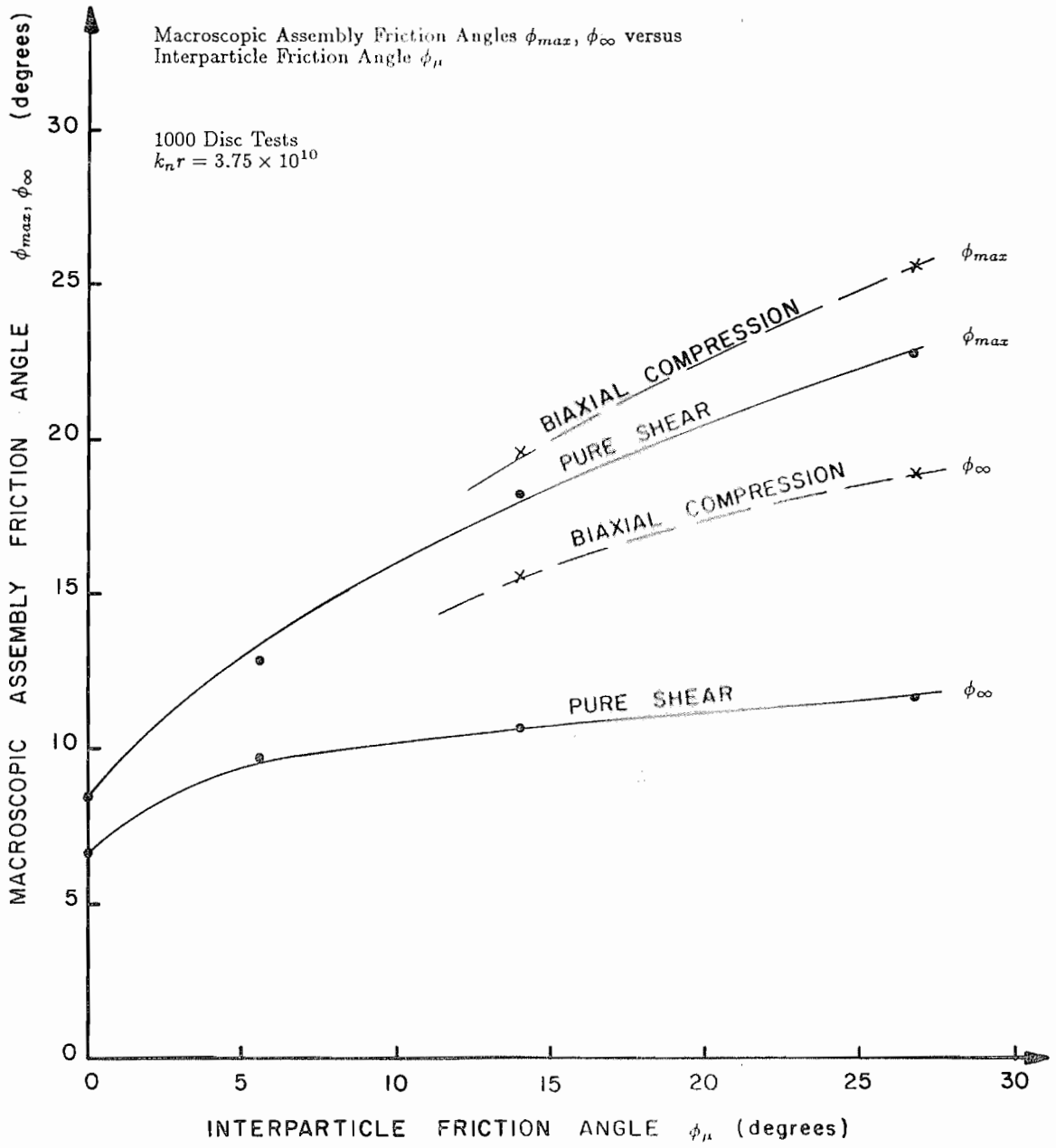

In general, the invariant quantity a, which is related to the second-order deviator fabric tensor $\mathbf{R}$, was observed to increase in magnitude with decreasing coordination number. Typical test results in support of this statement are shown on Figure 5.42. The plots on this figure show that a limiting maximum value of a is achieved only after the assembly reaches a minimum or ultimate coordination number equal in magnitude to the steady state value. Microstructure collapse manifest as a reduction in a was observed in pure shear tests with $\mu \neq 0$ and *soft* contacts ($k_n r = 3.75 \times 10^{10}$) once these assemblies had achieved a coordination number $\gamma_\infty \approx 3.4$. All other tests in the current investigation did not exhibit significant structural collapse (i.e. reduced a values) at large strains. For example, high contact stiffness assemblies corresponding to Tests #1024 and #1025 (Figures 5.42c and 5.42d), did not exhibit significant reductions in a even after achieving lower steady state coordination numbers ($\gamma_\infty \approx 3.12$). Biarez and Wiendieck (1963) report the results of physical two-dimensional biaxial tests taken to large strains (see Section 1.6.1). Similar qualitative observations were made by these researchers concerning the evolution of contact anisotropy (parameter A) with increasing sample distortion. For these tests they noted that peak contact anisotropy was sustained at large strains and that the intensity of contact anisotropy increased with increasing void ratio.

Based on limited data for *high* stiffness assemblies, it is possible to identify the area falling below the $a - \gamma$ curves as a region containing admissible combinations of a, γ quantities. Assemblies with microstructure described by a, γ values falling below the $a - \gamma$ curves on the plots are attainable by unloading assemblies with coordination numbers $\gamma_\infty < \gamma < \gamma_{max} \approx 4.0$. However, because of the sensitivity of microstructure parameters to contact force levels, the upper boundary on this region may vary between tests subjected to other stress paths. Further testing of high stiffness assemblies is required to determine if a unique *state geometry* defined by admissible combinations of a, γ does indeed exist for numerical systems with stiffnesses comparable to actual granular media.

The relationship between a and γ_∞ is easy to understand from the results of the current study. The overall minimum intensity of particle packing, which is described in part by γ, offers the most mobile yet stable condition in which contacts can arrange themselves in preferred directions. However, the magnitude of the steady state coordination number for a given test is dependent largely on the magnitude of disc properties assigned to the assembly discs. Data presented in the previous section shows that, in general, the steady state coordination number decreases with increasing interparticle friction coefficient and increasing contact stiffness.

On Figure 5.42 the fourth-order structure described by the coefficient of contact anisotropy b is also plotted. These figures show that the magnitude of b is generally less than a. In addition, the

increase in b is not as progressive as that recorded for a. In most tests a rapid increase in b was observed only after the assembly was at or about the value of the steady state coordination number. Similar qualitative performances can be observed from the results of a laboratory two-dimensional simple shear test reported by Konishi (1978) using a *dense* assembly of discs (Figure 3.10a).

It is interesting to note that second-order isotropic assemblies of discs (i.e. $a = 0$) were easily created by setting applied boundary stresses to $\sigma^b_{11} = \sigma^b_{22}$ and $\sigma^b_{12} = \sigma^b_{21} = 0$. In other words, a second-order isotropic distribution of contact normals was directly controlled by the second-order *isotropic* average stress condition imposed on the samples to create the initial compacted assemblies. The relationship between the fourth-order term b (which is related to the fourth-order deviator fabric tensor) and the second-order stress tensor is more subtle. Initial b values for compacted isotropic assemblies were greater than zero indicating that some higher-order structure was created for these assemblies despite the isotropic distribution of tractions applied at the sample boundaries. Examination of second and fourth-order directions of contact anisotropy θ_a and θ_b from selected tests gives some insight into the relationship between second and fourth-order microstructure for these numerical experiments (refer to Figure 5.43). The plots show that for the initial compacted assemblies $\theta_b = \pi/4, 3\pi/4$ over the interval $0 \leq \theta \leq \pi$. This fourth-order direction of anisotropy is at $\pm\pi/4$ to the principal stress directions (directions 1 and 2) which in turn are coaxial with the two directions along which the servo-mechanism acts in program DISC to create an isotropic stress condition in the sample. The initial fourth-order orientation of contact normals was preserved in biaxial compression and extension tests (Figure 5.43b). As a result, there was no destruction of this higher-order microstructure as the samples were loaded as shown by the test data presented on Figures 5.42b and 5.42d. In contrast, the fourth-order contact structure in assemblies subjected to pure shear loading paths evolved in a different manner. Before the fourth-order microstructure in these tests could develop significantly, it was necessary for this structure to rotate through $\pi/4$ and in the process be completely destroyed. However, after rotation, there was a dramatic increase in b once the limiting coordination number for the assembly was reached.

The two histories described above are idealized on Figure 5.44. The initial contact normal arrangement is shown on Figure 5.44a. The microstructure at the ultimate state for biaxial compression and pure shear tests is shown on Figures 5.44b and 5.44c respectively.

It appears from these tests that second and fourth-order contact normal arrangements are related. The ultimate contact arrangement which an assembly of discs attempts to achieve under monotonic loading with constant principal stress direction is characterized by second-order and fourth-order

directions of anisotropy related by $|\theta_a - \theta_b| = \pi/4$. Similar observations can be made from physical tests on dense assemblies of discs reported Oda and Konishi (refer to Figure 3.10c).

An additional observation from Figure 5.43a can be made concerning the transition of the assembly from a *locked* to relatively mobile condition. The curve for θ_b on this figure shows a distinct break at about $\varepsilon_t = 0.015$ which can be interpreted as the deviatoric strain at which the assembly packing is sufficiently *loose* to allow fourth-order contact normal rearrangement.

The rather detailed examination of fourth-order microstructure may be of academic interest considering that theoretical developments presented in Chapter 3 show that its contribution to shear capacity is likely small. While the development of fourth-order structure defined by coefficient b is pronounced in the numerical experiments at large strain, the presence of this microstructural component is considered a unique feature of two-dimensional systems. While it cannot be verified in the current investigation, it is likely that the greater geometric freedom available to three-dimensional granular media will minimize the development of fourth-order (or greater) anisotropic microstructure for these systems.

5.5 Essential Features of the Micromechanical Behaviour of Two-Dimensional Assemblies of Discs

5.5.1 General

The results of numerical simulations using two-dimensional assemblies of discs have shown that fundamental relationships proposed in Chapters 2 and 3 relating average stress to statistical descriptions of fabric and contact forces are valid for the systems investigated.

In addition, the experimental results provide a catalogue of observations which together give a qualitative understanding of the influence of particle properties, microstructure and boundary loading conditions on the macroscopic behaviour of these idealized systems. The following sections summarize these observations in a manner which may be useful to those researchers proposing constitutive models for granular systems which adopt the statistical mechanics framework employed in the current study.

5.5.2 Steady State and Processes of Order and Disorder

Any attempt to synthesize observed micromechanical behaviour of granular media emphasizes the complex mechanical nature of these materials. Their complex behaviour is due, in part, to the observation that they exhibit properties of both solids and fluids. For example, under hydrostatic compression, a dense sand will behave as a solid. Under large shearing strains the same system will flow similar to a fluid.

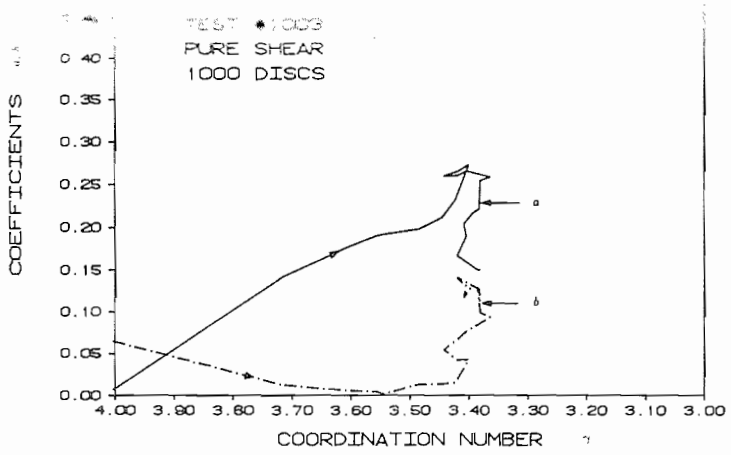

a) *Low* Stiffness Test ($k_n r = 3.75 \times 10^{10}$)

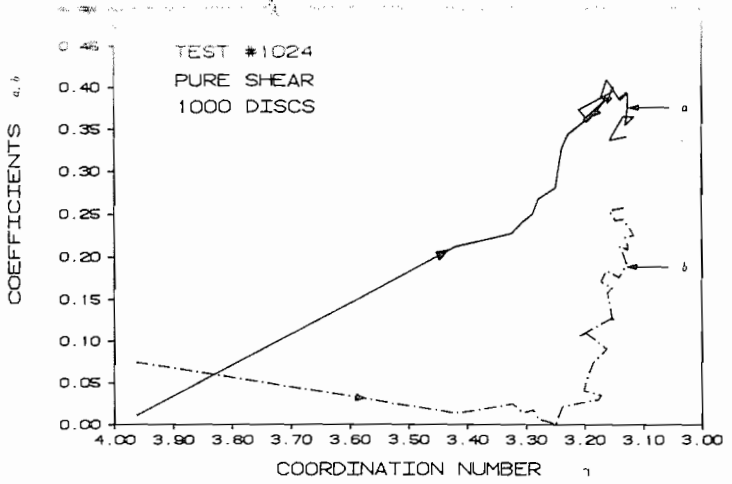

c) *High* Stiffness Test ($k_n r = 3.75 \times 10^{11}$)

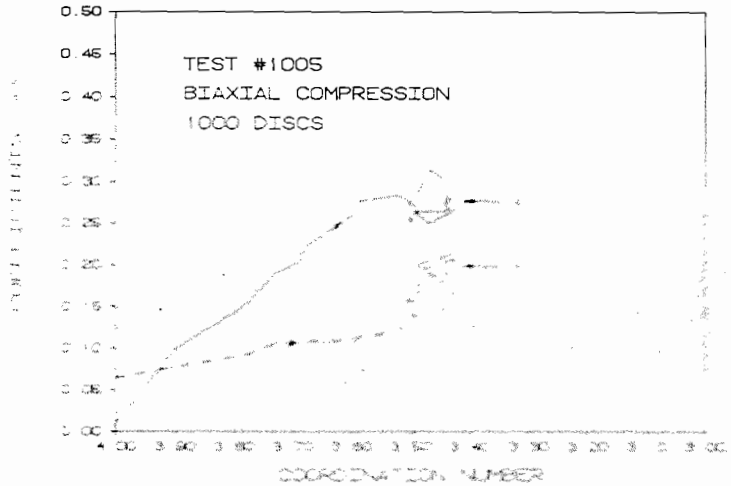

b) *Low* Stiffness Test ($k_n r = 3.75 \times 10^{10}$)

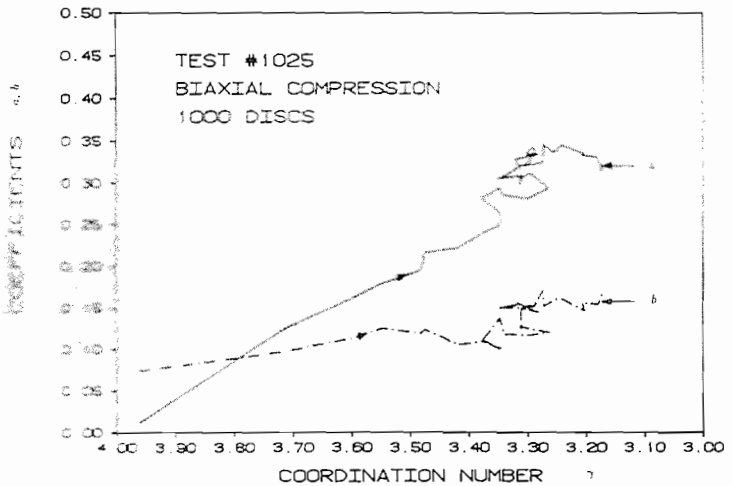

d) *High* Stiffness Test ($k_n r = 3.75 \times 10^{11}$)

Figure 5.42 Coefficients of Contact Normal Anisotropy a, b versus Coordination Number γ from Selected Tests

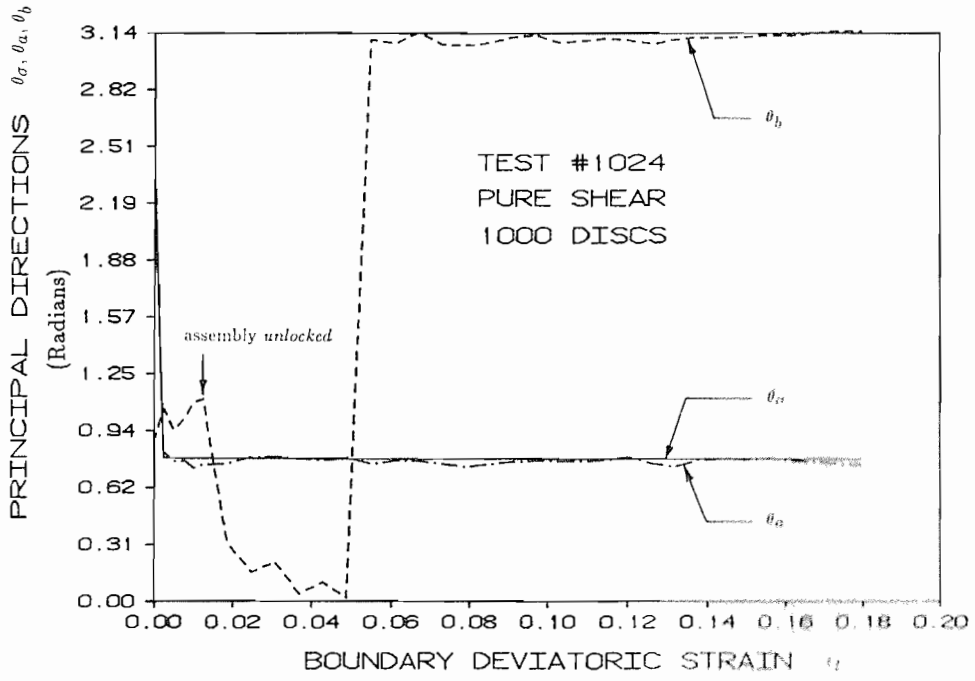

a) Pure Shear Test with $\mu = 0.5$ and $k_n r = 3.75 \times 10^{11}$

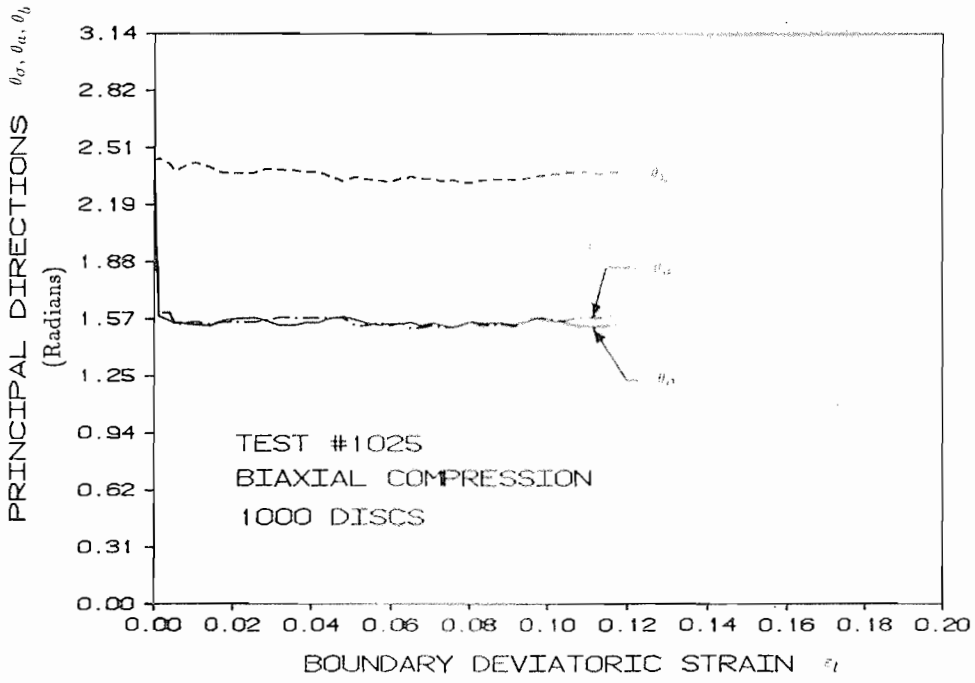

b) Biaxial Compression Test with $\mu = 0.5$ and $k_n r = 3.75 \times 10^{11}$

Figure 5.43 Second and Fourth-Order Principal Contact Normal Directions from Selected Tests

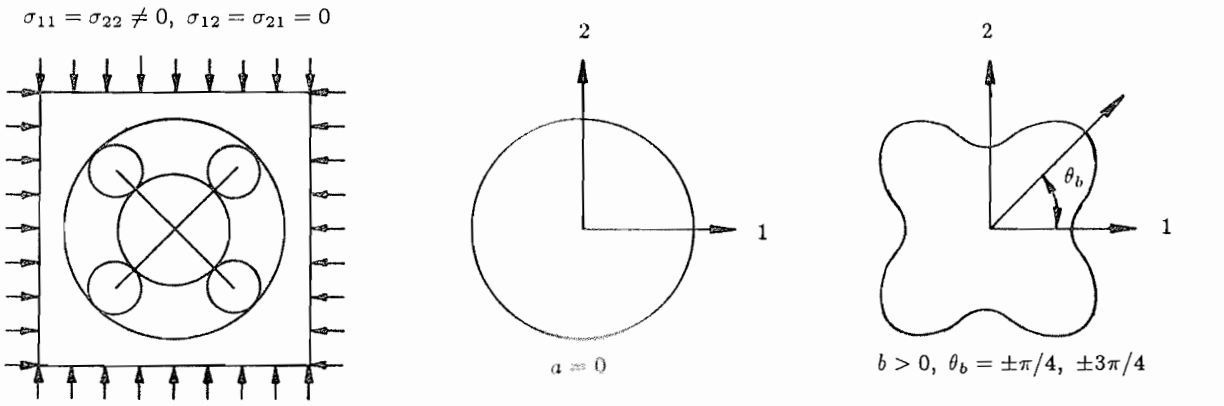

a) Contact Normal Anisotropy for Initial Compacted Dense Assembly

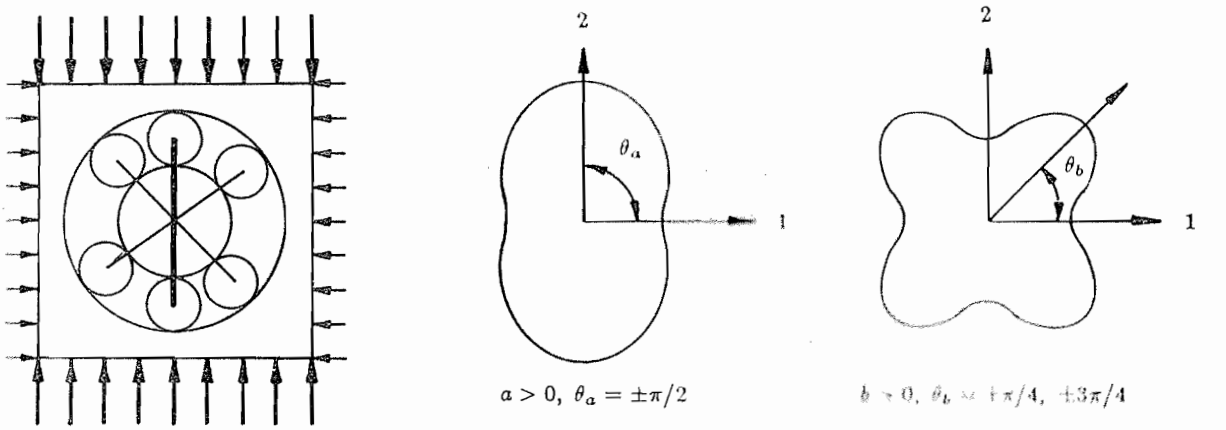

b) Contact Normal Anisotropy during Biaxial Compression ($\Delta\theta_b = 0$)

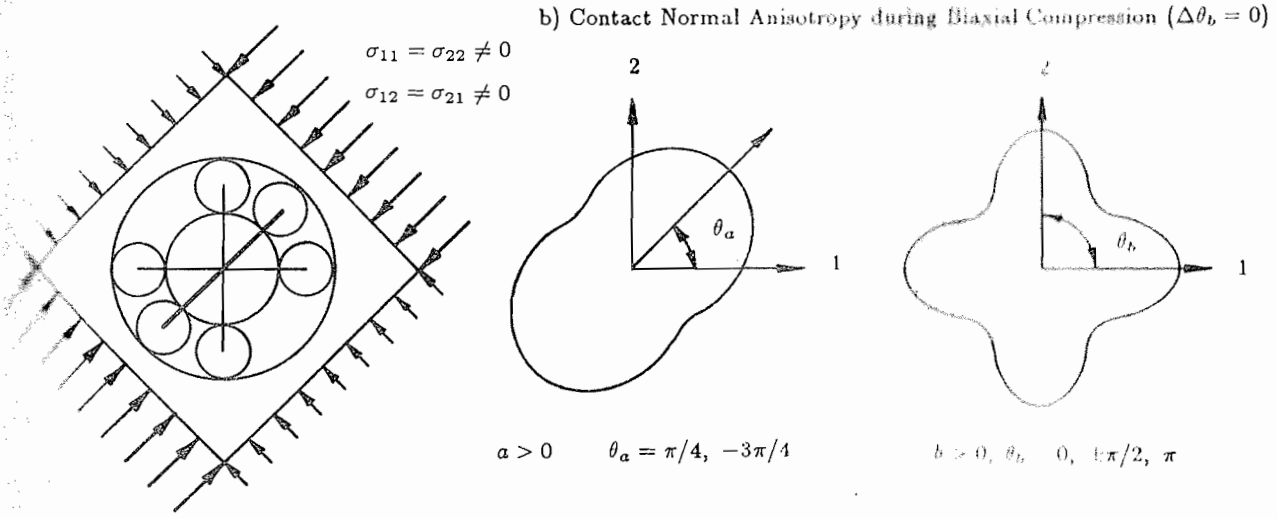

c) Rotation of Fourth-Order Contact Normal Anisotropy during Pure Shear ($\Delta\theta_b = \pm\pi/4$)

Figure 5.44 Evolution of Second and Fourth-Order Contact Normal Anisotropy during Numerical Two-Dimensional Tests

In many respects, the microscopic processes occurring in granular materials during shear are analogous to mechanisms accompanying melting of solids. Although mechanisms of thermally-activated melting are somewhat different from shear-activated flow, both lead to increased mobility of particles in the respective systems.

During melting of solids, particles (molecules) receive sufficient kinetic energy to increase the volume of the system and to reduce geometrical constraints to the point that the system becomes mobile and can flow. In granular systems, subject to shearing deformations, reduction of geometrical constraints is associated with loss of interparticle contacts during dilation. *Flow* occurs under sufficiently advanced shearing deformations.

Unlike molecular systems, granular materials never reach a ***fluid phase*** under low deviatoric strain rates. Their state is to some extent comparable to a state of liquid-solid phase transition when both phases coexist. At this point, the molecular motions for these systems are just sufficient to initiate melting but, the material is still able to sustain shearing at a reduced capacity from the solid phase. The liquid-solid phase transition state for molecular systems is thermodynamically unstable and virtually impossible to observe in laboratory. Consequently, this state of matter has not been explored in physical experiments on molecular systems and researchers have resorted to numerical simulations of molecular systems represented by assemblies of *discs* or *spheres*. In fact, the entire problem of liquid-solid phase transition is considered to be one of the most challenging in contemporary physics. Granular assemblies, on the other hand, can be maintained in the analogous state due to dissipation of energy during shearing deformations.

The above mentioned analogies between the behaviour of molecular systems in the area of solid-phase transition and granular material during shearing deformations leads naturally to the concept of *steady state* of deformations. In very general terms, steady state occurs when the limit of material anisotropy is achieved under shearing deformations and no further changes in microstructure are evident at the macroscale. Functionally, the term steady state corresponds to the familiar concept of *critical state* in soil mechanics terminology; the former is preferred however, since it suggests a clearer notion of the internal processes which are occurring when a granular system achieves an ultimate condition under shearing deformations.

The results of numerical simulations suggest that there are two competing processes at work during transition to steady state. The first process is a tendency to *disorder* which is manifest as local dilation at the microscale (micro-softening) and volumetric expansion at the macroscale. The degree of disorder can be observed as a reduction in coordination number γ and a corresponding increase

in void ratio e. A fundamental parameter which quantifies the average state of packing is contact density m_v, which for idealized systems comprising a unimodal size-distribution of spheres or discs, is a function of γ, e and average particle radius $\bar{r}_p$. Superimposed on this process is a tendency to *order* (creation of anisotropic structure) which is manifest as the development of *chains* of contacts, carrying higher than average contact forces, which align themselves with the principal direction of loading. The formation of chains can be viewed as local densification or contraction in preferred directions. In soil mechanics, this localized contraction is referred to as *interlocking* or micro-hardening. For the planar systems under study, the stress-induced tendency to anisotropic structure has been quantified using a fabric tensor $\mathbf{R}$ and deviatoric invariant quantities associated with this tensor.

A fundamental premise is that these competing stabilizing and destabilizing processes are always present during deformations but the rates at which they occur varies. In the numerical experiments reported in this study, the stabilizing and destabilizing processes can be observed as erratic fluctuations in parameters describing microstructure (e.g. a, γ and e). For analogous three-dimensional assemblies of granular media consisting of a very large number of particles, stabilizing/destabilizing processes occur but fluctuations in parameters of interest are obscured and their curves appear smooth. Steady state represents the limiting condition when both stabilizing and destabilizing processes are in equilibrium. At steady state, the rate at which local contractions are occurring through the growth of new chains is just equal to the rate at which existing chains are disintegrated by the destabilizing effect of local dilation. At the macroscale, steady state is manifest as a no net change in volume and also no change in statistical quantities describing fabric (such as γ, e and a).

The growth-decay cycle of predominant chains can be appreciated by the analogy of these microfeatures as load-bearing columns. The capacity of each column of particles is dictated by the degree of lateral support offered by contacting particles not forming the chain. Local dilation reduces this support and, if continued, leads to collapse of the chain. The analogy of microstructure as containing load-bearing columns can be extended to include the influence of disc properties on the capacity of load-carrying chains. Similar to *columns*, increasing the stiffness of interparticle contacts improves the capacity of the load-bearing chains; increasing interparticle tangential forces is analogous to increasing lateral support to these microfeatures.

The numerical simulations showed that, during shearing deformations, the predominant micromechanical response up to steady state was dilatancy characterized by a direction-independent loss of contacts. Superimposed on this process were contractions in the direction of maximum load and generation of load-bearing chains of discs. Together, these two processes resulted in the generation of

contact anisotropy primarily through net contact loss in directions orthogonal to the applied load.

At the early stages during numerical simulations, the ability to generate anisotropy (as measured by coefficient a) was suppressed until the samples became *unlocked*. The greatest anisotropy was recorded after the assemblies had achieved a threshold contact density which afforded these systems sufficient mobility to develop anisotropy in contact distribution yet, adequate density to support load-bearing chains.

5.5.3 Fabric Tensor

Statistical quantities describing fabric can be associated with each of the stabilizing and destabilizing processes identified above. The second-order fabric tensor $\mathbf{R}$ carries all essential information on the geometrical arrangement of assemblies comprising discs. Qualitative insight is gained by describing this fabric tensor as the sum of spherical and deviator tensor parts ($\mathbf{R}^*$ and $\mathbf{R}'$). Hence:

$$\mathbf{R}_{ij} = \mathbf{R}^*_{ij} + \mathbf{R}'_{ij} \qquad i,j = 1,2 \tag{5.6}$$

The destabilizing processes which are associated with assembly dilatancy are measured by the spherical tensor:

$$\mathbf{R}^*_{ij} = m_v \delta_{ij} \tag{5.7}$$

Processes which result in the generation of anisotropic structure in response to shearing deformations can be measured by the deviator fabric tensor:

$$\mathbf{R}'_{ij} = \mathbf{R}_{ij} - m_v \delta_{ij} \tag{5.8}$$

or the *reduced* deviator fabric tensor:

$$\overline{\mathbf{R}}'_{ij} = \frac{\mathbf{R}'_{ij}}{\mathbf{R}_{kk}/2} - \delta_{ij} \tag{5.9}$$

The fabric tensor and its decomposition to spherical and deviator parts represents more than a quantitative measure of microstructure. Both are physical quantities which enter directly into expressions which predict the hydrostatic resistance offered by these assemblies and the assembly shear capacity (i.e. equations (3.44) and (3.47)).

5.5.4 Contact Forces and Fabric

It is clear that the ability of anisotropic structure to sustain load is due to the distribution of contact forces which evolves directly as a result of loads imposed at the system boundaries. Correct interpretation of micromechanical behaviour must recognize the interrelation between distribution of forces and the evolution of microstructure which develops *as a result of* forces. Perhaps the fundamental shortcoming of theories which have attempted to relate fabric to assembly stress has been to neglect the contribution of interparticle forces. The intimate relation between anisotropy in contact forces and fabric has been obvious from the results of current study. Distributions of both quantities are visually similar (e.g. they are *peanut*-shaped under deviatoric load) and can be described by second-order tensors with coaxial orientations.

Similarities in tensorial quantities can be anticipated if simpler systems comprising bonded discs are examined: For example, consider first an unloaded two-dimensional continuum bounded by a surface S as shown on Figure 5.45. Imagine that the body is subject to a smooth displacement field described by the symmetric strain tensor ε. From strain compatibility, the internal displacement vector $\Delta\tilde{L}$ is related to the original undeformed vector $\tilde{L}_o$ by virtue of:

$$\Delta L_i = |L_o|\varepsilon_{ij}n_j \qquad i,j = 1,2 \tag{5.10}$$

Relative normal and tangential displacements δ_n and δ_t can be calculated from:

$$\begin{aligned} \delta_n &= \frac{\Delta L_i n_i}{|L_o|} = \varepsilon_{ij}n_i n_j \\ \delta_t &= \frac{\Delta L_i t_i}{|L_o|} = \varepsilon_{ij}t_i n_j \end{aligned} \tag{5.11}$$

Expressions (5.11) can also be written in terms of the invariant quantities and principal directions associated with tensor ε (equations (4.18) and (4.19)). Hence:

$$\begin{aligned} \delta_n &= \frac{1}{2}\{\varepsilon_n + \varepsilon_t \cos 2(\theta - \theta_\varepsilon)\} \\ \delta_t &= \frac{1}{2}\{\varepsilon_\omega - \varepsilon_t \sin 2(\theta - \theta_\varepsilon)\} \end{aligned} \tag{5.12}$$

Now imagine that the continuum is replaced by a large assembly of *elastic* discs and that $\tilde{L}_o$ represents an undeformed contact vector for the dashed disc shown on the figure. The normal and tangential contact forces acting at the contact associated with $\tilde{L}_o$ may be assumed proportional to the relative displacements components. If relative displacement components for all contacts are grouped according to orientation then, average contact forces may be described by:

$$\begin{aligned} \overline{f}_n^c(\theta) &= K_n\overline{\delta}_n(\theta) = \frac{K_n}{2}(\varepsilon_n + \varepsilon_t \cos 2(\theta - \theta_\varepsilon)) \\ \overline{f}_t^c(\theta) &= K_t\overline{\delta}_t(\theta) = \frac{K_t}{2}(\varepsilon_\omega - \varepsilon_t \sin 2(\theta - \theta_\varepsilon)) \end{aligned} \tag{5.13}$$

Here, K_n and K_t are coefficients of proportionality which depend on particle stiffness and assembly microstructure (Rothenburg, 1980). The distributions above have the same functional form as the assumed distributions for $\overline{f}_n^c(\theta)$ and $\overline{f}_t^c(\theta)$ given by relationships (3.22) and (3.23). In fact, the arguments just presented have been taken from Rothenburg (1980), who used the same non-rigorous approach to intuitively justify contact force distributions for planar systems as second-order Fourier series expressions. The results of numerical simulations show that the form of these contact force distribution functions is preserved for cohesionless assemblies of discs.

Bonded assemblies cannot change their structure under deviatoric loading (i.e. Δa remains zero) hence, any increase in load-carrying capacity under shearing deformations may be equated to deviator tensor quantities describing only contact forces. The distribution function $\overline{f}_n^c(\theta)$ predicts that at contact orientations close to the minor principal strain direction, average normal contact forces $\overline{f}_n^c(\theta)$ will be reduced below the average (compressive) normal contact force level $\overline{f}_n^c$ and the number of individual tensile contact forces will be higher. If our hypothetical assembly was suddenly made cohesionless, by disrupting interparticle bonds, then contacts with tensile contact normal force would be lost. Consequently, generation of tensile contact forces which would otherwise occur in bonded systems translates to loss of contacts in cohesionless assemblies where rearrangement of particles is possible. Using the non-rigorous arguments above, it is not surprising that distribution functions describing contact density with respect to orientation have a visually similar shape and orientation to the distribution of normal contact forces.

The lack of fully-mobilized tangential contact forces in physical and numerical experiments on cohesionless two-dimensional particulate systems is well established. The inability for these systems to generate and sustain significant tangential interparticle forces is due to the local cycles of *locking* and *unlocking* or (*micro-hardening* and *micro-softening*). These processes, which occur at the microscale, are obscured in large samples but are manifest in smaller samples as low amplitude fluctuations superimposed on macroscale stress-strain curves. These fluctuations are readily apparent in numerical simulations. Similar fluctuations have been observed in shear box tests carried out on glass ballotini by Skinner (1969) (Figures 1.6a and 1.6b).

As a result of observations which show that tensorial quantities describing fabric $\mathbf{R}$ and normal contact forces $\mathbf{F}_N$ are similar and coaxial and the direct contribution of tangential contact forces $\mathbf{F}_T$ is small, it appears that it is the distribution of contact normal forces which is primarily responsible for the generation of fabric anisotropy. In simple terms, incremental shearing deformations which are initiated at the sample boundary generate a new set of normal contact forces which cause local

instabilities within load-carrying chains. These local instabilities cause movement of particles, generation and loss of contacts in preferred directions, and redistribution of load between existing and newly-created chains such that static equilibrium is preserved. Granular systems are always close to static equilibrium under the low rates of strain familiar to most soil mechanics applications and consequently, by tracing the contributions to static equilibrium, powerful constraints to assembly stress can be formulated.

The intimate relationship between fabric and normal contact force anisotropy can be appreciated from Figure 5.46. The figure shows the ratio a_n/a plotted against γ for numerical assemblies which have achieved sufficient mobility to allow contact anisotropy to develop freely in response to contact forces (i.e assemblies are *unlocked*). Together, the curves from all tests show that under shearing deformations, the ratio of normal contact force anisotropy to contact normal anisotropy a_n/a tends to unity at *steady state*. The steady state value for a_n/a can only be achieved once the assemblies have achieved limiting values for void ratio and coordination number. The steady state coordination number is sensitive to the magnitude of disc properties defined by contact stiffness and interparticle friction coefficient. In general, as the magnitude of these parameters increase, curves shift to the left. For two-dimensional assemblies of discs with relatively high stiffness and friction (Tests #1024 and #1025), the steady state coordination number approaches the minimum value of three predicted for static redundancy. For frictionless discs (e.g. Test #1006), the admissible combinations of a_n/a and γ are restricted to $a_n/a = 1$ and $\gamma_o \approx 4.0$. The fluctuations in a_n/a recorded for this test are a consequence of the relatively small values of a generated in this experiment. A systematic investigation of the pressure sensitivity of coefficients of anisotropy was not undertaken in the current study. However, based on limited data, it is interesting to note that at steady state, assemblies with identical disc properties converge to about the same coordination number γ_∞ irrespective of normal stress levels.

If we neglect the contribution of tangential contact forces, these disc assemblies may be modelled in their steady state condition as Coulomb-type materials with shear capacity approximated by:

$$\sin\phi_\infty = \left|\frac{\sigma_t}{\sigma_n}\right|_\infty \approx a_\infty \qquad (5.14)$$

Again, terms $\sin\phi_\infty$ and the more familiar expression $\sin\phi_{cv}$ are equivalent.

Values of $a_n/a < 1$ are considered inadmissible for assemblies of cohesionless discs. However, while it cannot be verified from the results of the current study, it is likely that two dimensional systems of cohesionless *non-spherical* particles will be able to achieve this condition. The additional

geometrical freedom afforded these systems may result in a larger portion of shear capacity derived from microstructural anisotropy as compared to contact force anisotropy.

5.6 Implications to Three-Dimensional Systems

Fundamental expressions, shown to be accurate for two-dimensional systems, have three- dimensional equivalents. Many of the comments made in preceding sections are valid for three-dimensional systems with qualifications. For example, expressions for the second-order fabric tensor and contact force tensors are equally valid for three-dimensional systems comprising spheres or assemblies with near-spherical particles.

The contribution of tangential contact forces to shear capacity at the macroscale is impossible to measure but localized lock-unlock processes must also be present which will inhibit the development of these forces in a true granular media such as sand. In fact, it is possible that the topological constraint imposed by a two-dimensional system is responsible for the level of tangential contact force anisotropy which was observed in numerical experiments. For three-dimensional systems, the greater freedom available for particle interactions may likely diminish this contribution even further.

Neglecting tangential contact forces, the calculation of stress tensor for three-dimensional assemblies comprising spherical or near-spherical particles can be formulated starting with expression (2.30) in a simplified form:

$$\sigma_{ij} = m_v \bar{l}_o \int_\Omega \overline{f}_n^c(\Omega) E(\Omega) n_i^c n_j^c \, d\Omega \qquad i,j = 1,2,3 \tag{5.15}$$

Derivation of an equivalent tensorial expression for σ_{ij} terms can be carried out using relation (2.40) for $E(\Omega)$ and a similar function for $\overline{f}_n^c(\Omega)$ expressed as:

$$\begin{aligned} \overline{f}_n^c(\Omega) &= f_n^o\{1 + f_{ij} n_i n_j\} \\ f_{ij} &= f_{ji} \qquad i \neq j \\ f_{kk} &= 0 \end{aligned} \tag{5.16}$$

If products of coefficients are neglected after substituting (2.40) and (5.16) into (5.15) the following expression emerges:

$$\sigma_{ij} = \sigma_n\{\delta_{ij} + \overline{\mathbf{R}}'_{ij} + \overline{\mathbf{F}}'_{N_{ij}}\} \tag{5.17}$$

Again, $\overline{\mathbf{R}}'$ and $\overline{\mathbf{F}}'_N$ are *reduced* deviator tensors and are introduced for mathematical convenience.

The normal or hydrostatic invariant of average stress becomes:

$$\sigma_n = \frac{m_v \bar{l}_o f_n^o}{3} = \frac{\bar{l}_o \mathbf{R}_{kk} \mathbf{F}_{N_{kk}}}{3} \tag{5.18}$$

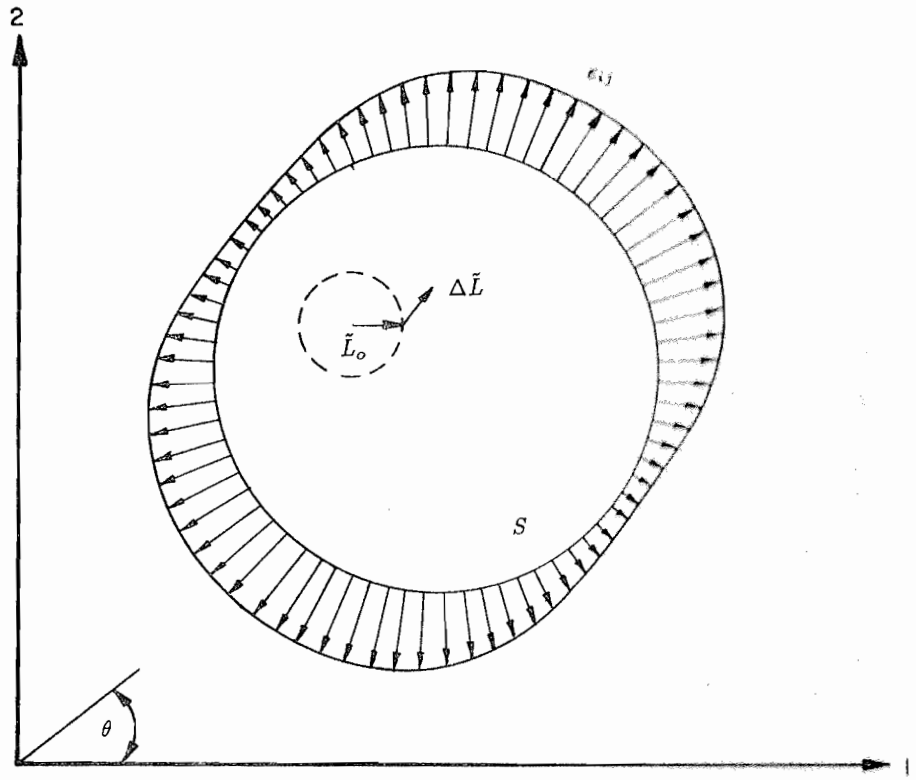

Figure 5.45 Contact Vector Displacements within a Continuum

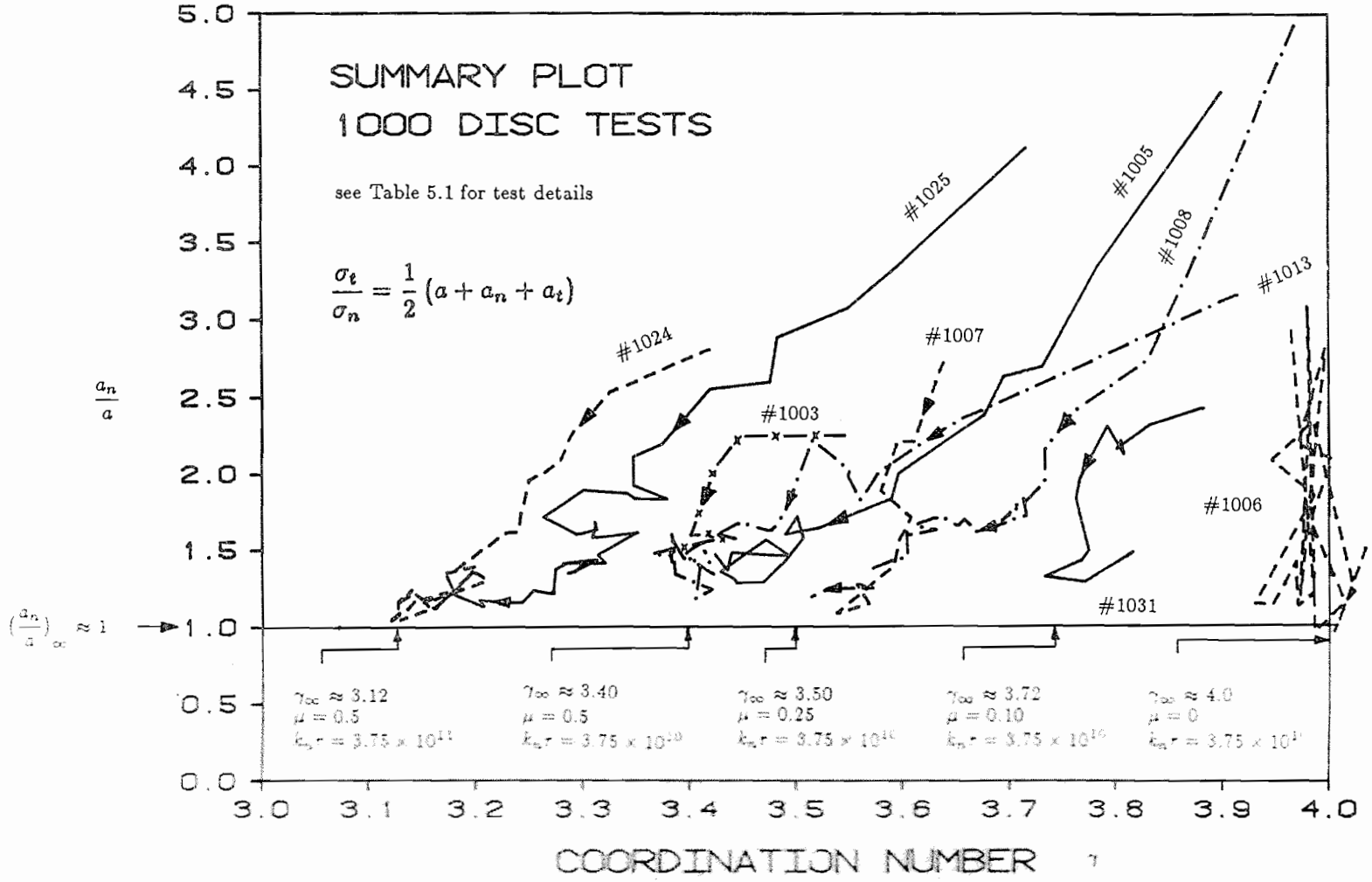

Figure 5.46 Summary Plot for a_n/a versus Coordination Number γ under Shearing Deformations

Similarly, neglecting tangential contact force contributions, the invariant stress ratio a_σ for assemblies of spheres or near-spherical particles may be expressed as:

$$a_\sigma = |\frac{\sigma_t}{\sigma_n}| = \left(\sqrt{\frac{\overline{\mathbf{R}'_{ij}\mathbf{R}'_{ij}}}{3}} + \sqrt{\frac{\overline{\mathbf{F}'_{N_{ij}}\mathbf{F}'_{N_{ij}}}}{3}}\right) \tag{5.19}$$

Here, the deviatoric stress invariant σ_t is defined as:

$$\sigma_t = \sqrt{\frac{\sigma'_{ij}\sigma'_{ij}}{3}} \tag{5.20}$$

Assuming that the steady state condition for assemblies of cohesionless spherical or near-spherical particles is characterized by equal contact normal and normal contact force anisotropies then, the following relationship is a useful approximation for these granular media at their ultimate state under deviatoric loading:

$$|\frac{\sigma_t}{\sigma_n}|_\infty = 2\left(\sqrt{\frac{\overline{\mathbf{R}'_{ij}\mathbf{R}'_{ij}}}{3}}\right)_\infty \tag{5.21}$$

If it were possible to carry out numerical experiments on assemblies of spheres then, a plot analogous to Figure 5.46 could be generated. This figure would comprise an ordinate axis defined by the ratio $\sqrt{\overline{\mathbf{F}'_{N_{ij}}\mathbf{F}'_{N_{ij}}}}/\sqrt{\overline{\mathbf{R}'_{ij}\mathbf{R}'_{ij}}}$ and the abscissa by a range of coordination numbers with $z_{min} = 4$ and a maximum value dependent on the size-distribution for the assembly particles. Qualitative features identified on Figure 5.46 for two-dimensional systems would also be anticipated for the equivalent data extracted from hypothetical tests on three-dimensional systems.

CHAPTER 6

CONCLUSIONS AND RECOMMENDATIONS FOR FURTHER RESEARCH

6.1 Introduction

The principal objective of the current study has been to investigate relationships between stress and parameters characterizing microstructure and load transmission in idealized granular systems. The theoretical basis of the study has been an approach originally reported by Rothenburg (1980) and Rothenburg and Selvadurai (1981b). Fundamental relationships developed for three-dimensional systems have a limited two-dimensional analogue. Verification of fundamental relationships for two-dimensional granular media has been undertaken primarily through numerical simulation of assemblies of discs.

The following sections summarize major conclusions drawn from the results of the current study into the micromechanical behaviour of idealized two-dimensional granular systems. Fundamental relationships originally proposed for three-dimensional systems are refined based on the experience gained from numerical experiments. Recommendations for further research along the lines adopted in the current study are also presented.

6.2 Conclusions

6.2.1 Verification of Fundamental Relationships

1) Developments presented in Chapter 2 showed that a stress tensor for granular systems could be formulated from consideration of contact vector lengths and contact forces between particles in static equilibrium. For three-dimensional systems this fundamental relationship is:

$$\sigma_{ij} = \frac{1}{V} \sum f_i^c l_j^c \qquad i,j = 1,2,3 \tag{6.1}$$

This fundamental expression has the same form for two-dimensional systems with $i, j = 1, 2$. The results of numerical experiments on 1000 disc assemblies showed that expression (6.1) could be approximated with essentially no error by an expression containing averages of contact forces and contact vector lengths over groups of contacts with similar orientations. The equivalent expression can be written as:

$$\sigma_{ij} = \frac{1}{V} \sum_{\theta_g} \overline{f}_i^c(\theta) \overline{l}_j^c(\theta) M_g(\theta) \qquad i,j = 1,2 \tag{6.2}$$

Mathematically tractable expressions were obtained by considering both three-dimensional and two-dimensional systems in the limit of infinite, spatially homogeneous granular assemblies. Under these conditions, the average stress tensor for three-dimensional systems can be written as:

$$\sigma_{ij} = m_v \int_\Omega \overline{f}_i^c(\Omega)\overline{l}_j^c(\Omega)E(\Omega)\,d\Omega \qquad i,j = 1,2,3 \tag{6.3}$$

The two-dimensional analogue to this expression is:

$$\sigma_{ij} = m_v \int_0^{2\pi} \overline{f}_i^c(\theta)\overline{l}_j^c(\theta)E(\theta)\,d\theta \qquad i,j = 1,2 \tag{6.4}$$

Assemblies of discs with contact vector length distributions which are independent of orientation (i.e. $\overline{l}^c(\theta) = \overline{l}_o$) can be described by a simplified equation of the form:

$$\sigma_{ij} = m_v \overline{l}_o \int_0^{2\pi} \left\{ \overline{f}_n^c n_i^c n_j^c + \overline{f}_t^c t_i^c n_j^c \right\} E(\theta)\,d\theta \tag{6.5}$$

2) Truncated Fourier series expressions of the form originally proposed by Rothenburg (1980) describing distributions of contact normal orientations $E(\theta)$ and distributions of average contact force components $\overline{f}_n^c(\theta)$ and $\overline{f}_t^c(\theta)$ were shown to be reasonable approximations to measured data from physical tests and the results of numerical experiments in the current study. These expressions are as follows:

$$E(\theta) = \frac{1}{2\pi}\left\{1 + a\cos 2(\theta - \theta_a) + b\cos 4(\theta - \theta_b)\right\} \tag{6.6}$$

$$\overline{f}_n^c(\theta) = f_n^o\left\{1 + a_n \cos 2(\theta - \theta_f)\right\} \tag{6.7}$$

$$\overline{f}_t^c(\theta) = -f_n^o\left\{a_t \sin 2(\theta - \theta_t)\right\} \tag{6.8}$$

Terms a, a_n and a_t are called *coefficients of anisotropy*. Terms θ_a, θ_b, θ_f and θ_t represent preferred directions for these distributions.

3) Substitution of expressions (6.6) through (6.8) into (6.5) together with simplifying assumptions led to manageable expressions between coefficients of anisotropy, principal directions of anisotropy, contact density, average contact length and the assembly stress tensor. Assuming coaxiality of the tensors describing assembly microfeatures, the following expressions were derived in a manner similar to that first reported by Rothenburg (1980):

$$\sigma_n = \frac{m_v \overline{l}_o f_n^o}{2} \tag{6.9}$$

$$\sigma_t = \frac{m_v \overline{l}_o f_n^o}{4}\left(a + a_n + a_t\right) \tag{6.10}$$

$$a_\sigma = \frac{\sigma_t}{\sigma_n} = \frac{1}{2}\left(a + a_n + a_t\right) \tag{6.11}$$

$$\frac{\sigma_{22}}{\sigma_{11}} = \frac{1 - \frac{1}{2}\left(a + a_n + a_t\right)\cos 2\theta_\sigma}{1 + \frac{1}{2}\left(a + a_n + a_t\right)\cos 2\theta_\sigma} \tag{6.12}$$

The results of numerical experiments showed that coaxiality of tensorial quantities was valid and invariant quantities σ_n, σ_t, σ_t/σ_n and the principal stress ratio σ_{22}/σ_{11} were predicted within 10% of directly measured values using the above relationships.

6.2.2 Tensorial Expressions for Fabric and Contact Forces

1) All essential information on the geometrical arrangement of two-dimensional granular media comprising discs can be described by a second-order *fabric* tensor $\mathbf{R}$ according to:

$$\mathbf{R}_{ij} = \frac{1}{V}\sum_{c\in V} n_i^c n_j^c \qquad i,j = 1,2 \tag{6.13}$$

The same expression (with $i,j = 1,2,3$) is valid for three-dimensional granular assemblies made up of spherical or near-spherical particles. Similarly, second-order tensorial quantities for average contact normal and tangential contact force components can be calculated from numerical experiments using:

$$\begin{aligned}\mathbf{F}_{N_{ij}} &= \frac{1}{N_g}\sum_{\theta_g} \overline{f}_n^c(\theta) n_i^c n_j^c \\ \mathbf{F}_{T_{ij}} &= \frac{1}{N_g}\sum_{\theta_g} \overline{f}_t^c(\theta) t_i^c n_j^c\end{aligned} \tag{6.14}$$

2) Coefficients of anisotropy a, a_n and a_t contained in the expressions (6.6), (6.7) and (6.8) were shown to be invariant quantities of *reduced* second-order *deviator* tensors $\overline{\mathbf{R}}'$, $\overline{\mathbf{F}}'_N$ and $\overline{\mathbf{F}}'_T$, respectively. Directions θ_a, θ_f and θ_t were seen to be major principal directions for these second-order tensors. Reduced deviator tensors are related to $\mathbf{R}$, $\mathbf{F}_N$ and $\mathbf{F}_T$ in the following manner:

$$\overline{\mathbf{R}}'_{ij} = \frac{\mathbf{R}'_{ij}}{\mathbf{R}_{kk}/2} = \frac{\mathbf{R}_{ij}}{\mathbf{R}_{kk}/2} - \delta_{ij} \tag{6.15}$$

$$\overline{\mathbf{F}}'_{N_{ij}} = \frac{\mathbf{F}'_{N_{ij}}}{\mathbf{F}_{N_{kk}}/2} = \frac{\mathbf{F}_{N_{ij}}}{\mathbf{F}_{N_{kk}}/2} - \delta_{ij} \tag{6.16}$$

$$\overline{\mathbf{F}}'_{T_{ij}} = \frac{\mathbf{F}'_{T_{ij}}}{\mathbf{F}_{N_{kk}}/2} = \frac{\mathbf{F}_{T_{ij}}}{\mathbf{F}_{N_{kk}}/2} - \delta_{ij} \tag{6.17}$$

Tensorial expressions for stress quantities can be formulated as follows:

$$\sigma_n = \frac{\bar{l}_c \mathbf{R}_{kk}\mathbf{F}_{N_{kk}}}{2} \tag{6.18}$$

$$\sigma_{ij} = \sigma_n\{\delta_{ij} + \overline{\mathbf{R}}'_{ij} + \overline{\mathbf{F}}'_{N_{ij}} + \overline{\mathbf{F}}'_{T_{ij}}\} \tag{6.19}$$

$$\sigma_t = \frac{\sigma_n}{\sqrt{2}}\{\sqrt{\overline{\mathbf{R}}'_{ij}\overline{\mathbf{R}}'_{ij}} + \sqrt{\overline{\mathbf{F}}'_{N_{ij}}\overline{\mathbf{F}}'_{N_{ij}}} + \sqrt{\overline{\mathbf{F}}'_{T_{ij}}\overline{\mathbf{F}}'_{T_{ij}}}\} \tag{6.20}$$

6.2.3 Essential Features of Two-Dimensional Numerical Experiments

1) Qualitative understanding of the micromechanical behaviour of two and three-dimensional granular assemblies during shearing deformations can be given by recognizing competing processes in these systems. The first process is associated with mechanisms of *disorder* manifest at the macroscale as sample dilation. A fundamental parameter which quantifies the average state of particle packing is contact density m_v. For idealized granular assemblies comprising a unimodal size-distribution for constituent discs or spheres, m_v can be shown to be a a function of γ, e and average particle radius $\bar{r}_o$. Superimposed on processes of disorder are micromechanical processes of *order* manifest as anisotropic microstructure. The development of anisotropic microstructure in response to shearing deformations, can be seen in two-dimensional numerical experiments as chains of contacts which carry higher than average interparticle forces in the direction of maximum loading. In two-dimensional assemblies, the intensity of anisotropic microstructure was measured by the coefficient of anisotropy term a. Physically, the superposition of processes of order and disorder lead to net loss of contacts oriented in the minor principal stress direction. All essential features of microstructure identified with the processes identified above can be measured by invariant quantities associated with the fabric tensor $\mathbf{R}$.

2) Careful examination of numerical assemblies while at, or about, their ultimate state (failure) leads to the concept of *steady state* of micromechanical behaviour for granular media at large strain. Steady state is characterized by limiting values of statistical quantities describing microstructure and contact force anisotropy while the assembly is subject to continuing shearing deformations. Functionally, the term steady state corresponds to the familiar concept of *critical state* in soil mechanics terminology; the former is preferred however, since it suggests a clearer notion of the internal processes which are occurring when a granular system achieves an ultimate condition under deviatoric load.

3) The results of numerical experiments show that the *direct* contribution of tangential (shear) contact forces (measured by coefficient of anisotropy a_t) to assembly shear capacity is small. Local cycles of interparticle *locking* and *unlocking* are though to be responsible for the inability of granular media to sustain significant interparticle tangential forces during shearing deformations. The numerical results support the conclusion that assembly microstructure evolves so that system shear capacity is due to contacts and *normal* interparticle forces which align themselves in the

direction of maximum loading. Chains of contacts carrying higher than average contact forces are characterized by contacts with little or no interparticle shear.

4) Analysis of mobilized friction between discs in numerical simulations showed that $|\overline{\mu}(\theta_g)|$ was always less than about 30% of the shearing capacity at assembly contacts. These numerical results are consistent with the results of physical tests on photo-elastic discs which have shown that frequency distributions for μ_{mob} are unimodal about $\mu_{mob} = 0$ (Oda and Konishi, 1974a).

5) Numerical tests on two-dimensional assemblies of discs under pure shear show that the macroscopic shearing angle ϕ_∞ for these systems at *steady state* (or *critical state*) is independent of the fully-mobilized friction angle available to disc contacts. The same phenomenon has been reported by Skinner (1969) from the results of shear box tests on glass ballotini.

6) The macroscopic stress-strain behaviour of numerical assemblies was observed to be sensitive to the magnitude of values assigned to disc properties. The tests show that, in general, tests with higher interparticle stiffness (defined by $k_n r$) and friction angle μ, are stiffer, exhibit greater shear capacity and are less likely to exhibit strain-softening at post-peak shear strength. The influence of the magnitude of disc properties on global response can be traced to increases in contributing anisotropies. In general, values for a, a_n and a_t were seen to increase with μ and $k_n r$.

7) At steady state, the quantity a_n/a describing the ratio of normal contact force anisotropy to contact normal anisotropy was observed to approach unity under monotonic shearing deformations. The steady state value $(a_n/a)_\infty \approx 1$ was observed only after limiting values for coordination number and void ratio were achieved through sample dilation. The steady state coordination number γ_∞, like other microstructure descriptors, was influenced by the magnitude of disc properties. The limiting value for coordination number, γ_∞ was observed to decrease with increasing assembly stiffness and interparticle shear capacity. For assemblies with *high* stiffness contacts considered typical of actual granular media, the steady state coordination number γ_∞ approaches the value of 3 predicted for static determinancy in these systems. Based on limited data, the ultimate value for coordination number from pure shear and biaxial compression tests appeared to be independent of normal stress levels applied to numerical assemblies.

8) Based on the observation that a_t is small and the ratio a_n/a tends to unity at steady state then, the anisotropic microstructure at (ultimate) failure in numerical assemblies can be related to a

macroscopic Coulomb friction angle ϕ_∞ according to:

$$\sin \phi_\infty = \left|\frac{\sigma_t}{\sigma_n}\right|_\infty \equiv a_\infty \tag{6.21}$$

9) The distribution of average contact vector lengths was found to be a constant at all strains according to $\overline{l}^c(\theta) = \overline{l}_o$ for assemblies of discs with a smooth size-distribution. However, the value of average contact vector length $\overline{l}_o$ was found to be biased in favour of the larger disc sizes when a bimodal size distribution was used.

10) The results of numerical simulations on two-dimensional assemblies of discs showed that fourth-order anisotropic microstructure measured by parameter b was pronounced at large deviatoric strain in samples close to steady state. However, the test results support the theoretically-based hypothesis that the direct contribution of fourth-order structure to assembly shear capacity is negligibly small.

6.3 Implications to Three-Dimensional Systems

6.3.1 General

The formulations presented for idealized two-dimensional granular systems have corresponding three-dimensional expressions. Micromechanical behaviour observed during numerical simulations offers some guidance in proposing fundamental relationships between stress quantities and quantities describing microstructure and the distribution and magnitude of contact forces in granular media comprising spherical or near-spherical particles.

6.3.2 Proposed Fundamental Relationships for Three-Dimensional Granular Assemblies

1) The inability of numerical assemblies to develop significant tangential (shear) contact forces during shearing deformations is considered a valid assumption for three-dimensional assemblies comprising cohesionless particles. Neglecting tangential contact forces leads to the following fundamental relationship between assembly stress and functions describing the distribution of normal contact forces and microstructure:

$$\sigma_{ij} = m_v \overline{l}_o \int_\Omega \overline{f}_n^c(\Omega) E(\Omega) n_i^c n_j^c \, d\Omega \qquad i,j = 1,2,3 \tag{6.22}$$

2) Tensorial expressions for stress quantities can be formulated as follows:

$$\sigma_n = \frac{\sigma_{kk}}{3} = \frac{\overline{l}_o \mathbf{R}_{kk} \mathbf{F}_{N_{kk}}}{3} \tag{6.23}$$

ight arising from

$$\sigma_{ij} = \sigma_n\{\delta_{ij} + \overline{\mathbf{R}}'_{ij} + \overline{\mathbf{F}}'_{N_{ij}}\} \tag{6.24}$$

$$\sigma_t = \sqrt{\frac{\overline{\sigma}'_{ij}\overline{\sigma}'_{ij}}{3}} = \sigma_n\left(\sqrt{\frac{\overline{\mathbf{R}}'_{ij}\overline{\mathbf{R}}'_{ij}}{3}} + \sqrt{\frac{\overline{\mathbf{F}}'_{N_{ij}}\overline{\mathbf{F}}'_{N_{ij}}}{3}}\right) \tag{6.25}$$

3) At *steady state* the ultimate invariant stress ratio may be usefully approximated using:

$$\left|\frac{\sigma_t}{\sigma_n}\right|_\infty \approx 2\left(\sqrt{\frac{\overline{\mathbf{R}}'_{ij}\overline{\mathbf{R}}'_{ij}}{3}}\right)_\infty \tag{6.26}$$

Based on experience from two-dimensional numerical studies, the limiting ratio for the invariant stress ratio may be expected to occur simultaneously with microstructure characterized by a steady state coordination number $\gamma_\infty \approx 4$.

6.4 Recommendations for Further Research

6.4.1 General

The results of the current investigation pose potentially rewarding avenues of research into the micromechanical behaviour of granular media. Minor modifications to program DISC will allow numerical experiments to be carried out on more complex cohesionless assemblies and *bonded* assemblies.

6.4.2 Two-Dimensional Cohesionless Assemblies

1) A major simplification in the theoretical developments leading to expression (6.6) for assemblies of *discs* is the (correct) assumption that contact vector lengths are independent of orientation (i.e. $\overline{l}^c(\theta) = \overline{l}_o$). However, this assumption is invalid for assemblies which comprise non-circular particles. The added degree of freedom afforded granular assemblies by more complex particle geometry must be accounted for in fundamental relations equivalent to (6.6). A review of the literature suggests that anisotropy in average contact vector lengths can be significant. As a first attempt, anisotropy in $\overline{l}^c(\theta)$ can be described by a truncated Fourier series expression such as:

$$\overline{l}^c(\theta) = \overline{l}_o\{1 + a_l \cos 2(\theta - \theta_l)\} \tag{6.27}$$

Coefficient of anisotropy a_l and direction of anisotropy θ_l can be equated to a symmetric second-order *contact length tensor* $\mathbf{L}$ defined by:

$$\mathbf{L}_{ij} = \frac{1}{N_g}\sum_{\theta_g} \overline{l}^c(\theta) n_i^c n_j^c \qquad i,j = 1,2 \tag{6.28}$$

Like the fabric tensor **R**, the tensor **L** retains its form in three-dimensions. If the same analytical approach reported in Chapters 2 and 3 is adopted then, stress quantities σ_{ij} for two-dimensional assemblies comprising (say) *oval*-shaped particles may be usefully approximated by:

$$\sigma_{ij} = \sigma_n\{\delta_{ij} + \overline{\mathbf{L}}'_{ij} + \overline{\mathbf{R}}'_{ij} + \overline{\mathbf{F}}'_{N_{ij}} + \overline{\mathbf{F}}'_{T_{ij}}\} \tag{6.29}$$

The relationship between the tensors comprising this expression would have to be carefully studied. It is likely that there is a significant correlation between quantities describing contact orientations and contact lengths in these systems.

2) The results of numerical simulations have shown that quantities describing microstructure are, in general, pressure sensitive, particularly systems with *soft* contacts. However, the results of the investigation hold out the enticing prospect that over a range of confining stress, steady state values for coordination number may be relatively pressure insensitive. The results of the current investigation suggest that a systematic study of the relationship between contact forces and parameters describing microstructure be undertaken for assemblies with a wider range of disc properties.

6.4.3 Bonded Assemblies of Discs

1) Fundamental equations of the form (6.5) are equally valid for *bonded* assemblies. These assemblies can be easily examined by using a slightly modified version of program DISC and assigning *infinite* cohesion to assembly contacts. Constitutive relationships for bonded systems with linear contact stiffnesses can be formulated using the following approach: Expression (5.13) can be rewritten as:

$$\begin{aligned} \overline{f}^c_n(\theta) &= \varsigma\frac{k_n r}{2}(\varepsilon_n + \varepsilon_t \cos 2(\theta - \theta_\varepsilon)) \\ \overline{f}^c_t(\theta) &= \varsigma\frac{k_s r}{2}(\varepsilon_\omega - \varepsilon_t \sin 2(\theta - \theta_\varepsilon)) \end{aligned} \tag{6.30}$$

Here, k_n and k_s are normal and tangential (shear) contact stiffnesses and ς is a parameter proposed by Rothenburg (1980) which is related to microstructure. Substitution of equations (6.30) into (6.5) leads to constitutive relationships of the form:

$$\sigma_{ij} = A_{ijkl}\,\varepsilon_{kl} \qquad i,j,k,l = 1,2 \tag{6.31}$$

Terms A_{ijkl} can be calculated from:

$$A_{ijkl} = m_v \bar{l}_o \varsigma k_n r \int_0^{2\pi} E(\theta)\{n^c_i n^c_j n^c_k n^c_l + \lambda t^c_i n^c_j t^c_k n^c_l\}\,d\theta \tag{6.32}$$

Here $\lambda = k_s/k_n$ and $E(\theta)$ is restricted to a second-order expression $E(\theta) = \frac{1}{2\pi}(1 + a_{mn}n^c_m n^c_n)$. Equivalent expressions to (6.32) can be recovered from relationships proposed by Rothenburg (1980). The above expressions directly equate macroscopic anisotropic elastic behaviour in these systems to parameters which describe anisotropic microstructure. Rothenburg (1980) points out that symmetry of the stress tensor σ_{ij} is not, in general, satisfied by (6.31). However, symmetry is unconditionally satisfied for isotropic microstructure (i.e. $E(\theta) = 1/2\pi$) or when $\lambda = 0$. Simple numerical experiments can be performed using a modified version of program DISC to verify the constitutive relations proposed above.

APPENDIX A

LISTINGS FOR PROGRAMS *DISC* AND *AUTODISC*

```
1.000 C
2.000       PROGRAM DISC
3.000 C
4.000 C*****2-D PROGRAM TO MODEL THE MECHANICS OF A GRANULAR
5.000 C     MEDIUM CONSISTING OF DISCS OF ARBITRARY RADII
6.000 C     PROGRAM IMPLEMENTS DISTINCT ELEMENT METHOD
7.000 C     (STRACK AND CUNDALL (1978))
8.000 C
9.000 C*****INITIALIZE PROGRAM
10.000 C
11.000      CALL INITP
12.000 C
13.000 C*****RUN PROGRAM
14.000 C
15.000      CALL CYCLE
16.000 C
17.000 C*****CLOSE FILES
18.000 C
19.000      CLOSE (1,STATUS='KEEP')
20.000      CLOSE (10,STATUS='KEEP')
21.000      CLOSE (13,STATUS='KEEP')
22.000      CLOSE (15,STATUS='KEEP')
23.000      CLOSE (UNIT=B,STATUS='DELETE')
24.000 C
25.000      STOP
26.000      END


1.000 C
2.000       SUBROUTINE INITP
3.000 C
4.000 C*****INITIALIZE DATA AND DISC ASSEMBLY
5.000 C
6.000      DIMENSION B(17000)
7.000      VIRTUAL B*(STATUS=UNKNOWN,BUF=200,IOSTAT=IT)
8.000 C
9.000      COMMON /ARAY/ A(108910)
10.000      COMMON /ERAY/ E(10000)
11.000      COMMON /BDAT/ R(50),DENS(50),AKN(50),AKS(50),AMU(50),COH(50),AMASS(50),AMOI(50)
12.000      COMMON /MOD/  EBVEL(2,2),SGAIN,BSTR(2,2)
13.000      COMMON /BSTR/ BSIG(2,2),BSIGO(2,2),BSIGD(2,2)
14.000      COMMON /BBAL/ BBALL(1000),NB,AREA
15.000      COMMON /CIRC/ IBCIRC(2000),NBT
16.000 C
17.000      GLOBAL ALPHA,BETA,PI,TDEL,FRAC,FIRST
18.000      GLOBAL CON1,CON2,BDT,ADDT,ADDX,TOL,M2,M3,NBALL,RMAX
19.000      GLOBAL NCBOX,M1,M4,NBOX,NX,NY,DEL,GRAVX,GRAVY,IAEND,BKEY
20.000      GLOBAL NCYC,NCYCS,NCYCF,NDUMP,NRCYC,NRLCYC,TITLE
21.000      GLOBAL XCR(10),YCR(10),RCR(10),NCIRC,NCHECK
22.000      GLOBAL SFLAG,FFLAG,RSFLAG,ZFLAG,MODE,EKEY
23.000 C
24.000      LOGICAL ZFLAG,RSFLAG,SFLAG,FFLAG
25.000      INTEGER BKEY,EKEY,FIRST
26.000      CHARACTER*60 STATUS,TYPE,ZERO,BINFILE,EFILE,TITLE
27.000 C
28.000      DATA RMAX/0.0/ TDEL/1.0E+20/ RMIN/1.0E+20/
29.000      DATA TOL/2.9/ ADDX/1.0/ AADT/0.0075/
30.000 C
31.000 C*****OPEN INSTRUCTION FILE
32.000 C
33.000      OPEN(1,FILE='INPT',STATUS='OLD',ACCESS='KEYED',FORM='FORMATTED')
34.000 C
35.000 C*****OPEN DATA FILES AND SET FLAGS
36.000 C
37.000      READ (1,'(A40)')      TITLE
38.000      READ (1,'(A10)')      STATUS
39.000      READ (1,'(A10)')      BINFILE
40.000      READ (1,'(G.0)')      BKEY
41.000      READ (1,'(A10)')      EFILE
42.000      READ (1,'(G.0)')      EKEY
43.000      READ (1,'(A10)')      ZERO
44.000      READ (1,'(A10)')      TYPE
45.000      READ (1,'(G.0)')      MODE
46.000      READ (1,'(G.0)')      FIRST
47.000 C
48.000      IF (STATUS.EQ.'START')   SFLAG=.TRUE.
49.000      IF (STATUS.EQ.'RESTART') RSFLAG=.TRUE.
50.000      IF (ZERO.EQ.'ZERO')      ZFLAG=.TRUE.
51.000      IF (FIRST.EQ.BKEY)       FFLAG=.TRUE.
52.000 C
```

```
53.000      OPEN (10,NAME=TYPE,STATUS='OLD',ACCESS='KEYED',FORM='FORMATTED')
54.000      OPEN (13,NAME=BINFILE,STATUS='OLD',USAGE='UPDATE',ACCESS='KEYED')
55.000      IF (SFLAG)GOTO 1000
56.000      OPEN (15,NAME=EFILE,STATUS='OLD',ACCESS='KEYED')
57.000      GOTO 1010
58.000 1000  OPEN (15,NAME=EFILE,STATUS='NEW',ACCESS='KEYED')
59.000 C
60.000 C*****READ CYCLE DATA
61.000 C
62.000 1010  READ (1,'(5G.0)') NCYCS,NCYCF,NDUMP,NRLCYC,NRCYC
63.000      NCYC=NCYCF-NCYCS
64.000 C
65.000 C*****INPUT DISC TYPE DATA
66.000 C     CALCULATE MASS AND MOMENT OF INERTIA OF DISC TYPES
67.000 C     CALCULATE TIME STEP
68.000 C
69.000      PI=4.0*ATAN(1.0)
70.000 C
71.000      DO 1020 I=1,50
72.000        NBTYP=I-1
73.000        READ (10,'(7G.0)',END=1030) R(I),DENS(I),AKN(I),AKS(I),AMU(I),COH(I)
74.000        RMIN=AMIN1(RMIN,R(I))
75.000        RMAX=AMAX1(RMAX,R(I))
76.000        AMASS(I)=PI*R(I)*R(I)*DENS(I)
77.000        AMOI(I)=AMASS(I)*R(I)*R(I)/2.0
78.000        TN=2.0*SQRT(AMASS(I)/AKN(I))
79.000        IF (AKS(I).EQ.0.0) TDEL=AMIN1(TN,TDEL);GOTO 1020
80.000        TS=2.0*SQRT(AMASS(I)/AKS(I))
81.000        TDEL=AMIN1(TN,TS,TDEL)
82.000 1020  CONTINUE
83.000 C
84.000 C*****READ CONTENTS OF BINARY FILE
85.000 C
86.000 1030  READ (13,KEY=BKEY) A(1)
87.000      IAEND=A(1)
88.000      READ (13,KEY=BKEY,ERR=1040) (A(I),I=1,IAEND)
89.000 1040  BKEY=BKEY+1000
90.000 C
91.000      W=A(2);H=A(3);NBOX=A(4);NBALL=A(6);NCBOX=A(7);NX=A(8)
92.000      NY=A(9);DEL=A(10);M1=A(11);M2=A(12);M3=A(13);M4=A(14)
93.000 C
94.000 C*****INPUT BOUNDARY STRAIN-RATE TENSOR VALUES;
95.000 C          SERVO GAIN;
96.000 C          BOUNDARY STRESS TENSOR VALUES;
97.000 C
98.000 1050  READ (1,'(7G.0)') EBVEL(1,1),EBVEL(1,2),EBVEL(2,2),SGAIN,BSTR(1,1),BSTR(1,2),BSTR(2,2)
99.000      EBVEL(2,1)=EBVEL(1,2)
100.000      BSTR(2,1)=BSTR(1,2)
101.000 C
102.000 C*****SETUP STRESS TENSOR ARRAYS FOR SERVO-CONTROL MODES 2-5
103.000 C     AND DETERMINE INITIAL ASSEMBLY BOUNDARY DISCS AND AREA
104.000 C
105.000      CALL BBOUND
106.000      CALL BVOLUME
107.000 1060  IF (MODE.EQ.1) NCHECK=10;GOTO 1080
108.000      CALL BSTRESS
109.000      DO 1070 I=1,2
110.000        DO 1070 J=1,2
111.000          BSIGO(I,J)=BSIG(I,J)
112.000 1070  BSIGD(I,J)=BSTR(I,J)-BSIGO(I,J)
113.000 C
114.000 C*****INPUT DAMPING PARAMETERS
115.000 C
116.000 1080  READ (1,'(2G.0)') ALPHA,BETA
117.000 C
118.000 C*****FRACTION OF CRITICAL TIME-STEP
119.000 C
120.000      READ (1,'(G.0)') FRAC
121.000      TDEL=FRAC*TDEL
122.000 C
123.000 C*****INPUT X AND Y GRAVITY ACCELERATIONS
124.000 C
125.000      READ (1,'(2G.0)') GRAVX,GRAVY
126.000 C
127.000 C*****SET UP DAMPING TERMS
128.000 C
129.000      CON1=1.0-ALPHA*TDEL/2.0
130.000      CON2=1.0/(1.0+ALPHA*TDEL/2.0)
131.000      BDT=BETA/TDEL
132.000 C
```

```
133.000 C*****INPUT SUB-ASSEMBLY CIRCLE DATA
134.000 C
135.000       READ (1,'(G.0)') NCIRC
136.000       IF (NCIRC) 1110,1110,1090
137.000 1090  DO 1100 I=1,NCIRC
138.000 1100  READ (1,'(3G.0)') XCR(I),YCR(I),RCR(I)
139.000 C
140.000 C*****ZERO DISC VELOCITIES
141.000 C
142.000 1110  IF (ZFLAG)GOTO 1120
143.000       GOTO 1140
144.000 C
145.000 1120  IAB=M2
146.000       DO 1130 I=1,NBALL
147.000         A(IAB+2)=0.0
148.000         A(IAB+3)=0.0
149.000         A(IAB+4)=0.0
150.000 1130  IAB=IAB+14
151.000 C
152.000 C*****INITIAL TEST CONDITIONS TO EXTRACT 'E' ARRAY
153.000 C
154.000 1140  IF (.NOT.FFLAG) READ (15,KEY=EKEY-1000,ERR=1160) (E(I),I=1,10000)
155.000       DO 1150 I=1,14
156.000 1150  E(I)=A(I)
157.000 1160  E(15)=NBTYP
158.000       E(16)=ALPHA
159.000       E(17)=BETA
160.000       E(18)=FRAC
161.000       E(19)=TDEL
162.000       E(20)=GRAVX
163.000       E(21)=GRAVY
164.000       E(22)=TOL
165.000       E(24)=ADDX
166.000       E(25)=AADT
167.000       E(26)=BDT
168.000       E(32)=NCIRC
169.000       E(33)=NRLCYC
170.000 C
171.000 C*****BOUNDARY-CONTROL DATA TO E ARRAY
172.000 C
173.000       E(64)=MODE
174.000       E(65)=SGAIN
175.000       E(66)=BSTR(1,1)
176.000       E(67)=BSTR(1,2)
177.000       E(68)=BSTR(2,2)
178.000       E(69)=EBVEL(1,1)
179.000       E(70)=EBVEL(1,2)
180.000       E(71)=EBVEL(2,2)
181.000 C
182.000 C*****IDENTIFY DISCS FORMING INITIAL BOUNDARY OF ENTIRE ASSEMBLY
183.000 C
184.000       IF (.NOT.FFLAG)GOTO 1180
185.000       IAB=400
186.000       E(IAB)=NB
187.000       E(IAB+1)=AREA
188.000       IAB=IAB+2
189.000       DO 1170 I=1,NB
190.000         E(IAB)=IAD=BBALL(I)
191.000         E(IAB+1)=A(IAD)+A(IAD+11)
192.000         E(IAB+2)=A(IAD+1)+A(IAD+12)
193.000 1170  IAB=IAB+3
194.000 C
195.000 C*****LOAD VIRTUAL FILE 'B' WITH INITIAL DISC DATA
196.000 C
197.000 1180  IF (.NOT.FFLAG) READ (13,KEY=FIRST,ERR=1190) (B(I),I=1,M3)
198.000 1190  IF (.NOT.FFLAG) RETURN
199.000       DO 1200 I=1,M3
200.000 1200  B(I)=A(I)
201.000 C
202.000 1210  RETURN
203.000       END
```

```
1.000 C
2.000      SUBROUTINE CYCLE
3.000 C
4.000 C*****THIS ROUTINE CONTROLS MAIN CALCULATION CYCLE FOR
5.000 C     NEAR-CIRCULAR ASSEMBLY OF DISCS
6.000 C
7.000      COMMON /ARAY/ A(108910)
8.000      GLOBAL NCYC,NBALL,M2,NDUMP,NN,IAEND,BKEY,BDFLAG,RFLAG
9.000      LOGICAL RFLAG,BDFLAG
10.000      INTEGER BKEY
11.000 C
12.000      NDUMPI=NDUMP
13.000      CALL BBOUND
14.000      CALL BVOLUME
15.000      CALL BSTRESS
16.000 C
17.000      DO 1040 NN=1,NCYC
18.000 C
19.000 C*****COMPILE X STATEMENT TO OUTPUT CYCLE COUNT TO TERMINAL DEVICE
20.000 C
21.000 X       OUTPUT,NN
22.000 C
23.000 C*****APPLY SERVO-CONTROLLED DISPLACEMENTS TO
24.000 C     ASSEMBLY BOUNDARY
25.000 C
26.000         CALL SRVMOT
27.000 C
28.000 C*****SCAN ALL DISCS
29.000 C
30.000         IAB=M2
31.000         DO 1010 I=1,NBALL
32.000           IF (A(IAB+8)) 1000,1000,1010
33.000 1000        CALL MOTION(IAB)
34.000           IF (RFLAG) CALL REBOX(IAB)
35.000 1010     IAB=IAB+14
36.000 C
37.000 C*****APPLY FORCE/DISPLACEMENT LAW TO ALL CONTACTS
38.000 C     COMPUTE BOUNDARY CONTACT CONTRIBUTIONS TO ASSEMBLY STRESS TENSOR
39.000 C
40.000         CALL FORD
41.000 C
42.000 C*****UPDATE BOUNDARY DISC LIST IF REQUIRED
43.000 C
44.000         IF (BDFLAG) CALL BBOUND2; CALL BVOLUME
45.000 C
46.000 C*****RELAX ASSEMBLY AND DUMP DATA TO EXTRACT FILE
47.000 C
48.000 1020     IF (NN-NDUMP) 1040,1030,1040
49.000 1030     CONTINUE
50.000         CALL RELAX
51.000         CALL EXTRACT
52.000         CALL BBOUND
53.000         CALL BVOLUME
54.000         NDUMP=NN+NDUMPI
55.000 C
56.000 1040  CONTINUE
57.000 C
58.000 C*****DUMP FINAL ASSEMBLY DATA TO BINARY CONFIGURATION FILE
59.000 C
60.000      WRITE (13,KEY=BKEY,ERR=1050) (A(I),I=1,IAEND)
61.000 1050  CONTINUE
62.000 C
63.000      RETURN
64.000      END


1.000 C
2.000      SUBROUTINE BBOUND
3.000 C
4.000 C*****PROGRAM IDENTIFIES DISCS FORMING CONVEX POLYGON BOUNDARY FOR
5.000 C     A NEAR-CIRCULAR ASSEMBLY OF DISCS
6.000 C     SEARCH BASED ON "ALL" ASSEMBLY DISCS
7.000 C
8.000      COMMON /ARAY/ A(108910)
9.000      COMMON /BBAL/ BBALL(1000),NB
10.000      GLOBAL M2,NBALL,PI
11.000      DATA SMALL/1.0E-20/ YO/10000./  BETO/0./
12.000 C
13.000 C*****ZERO BBALL ARRAY
14.000 C
```

```
15.000      DO 1000 I=1,NB
16.000 1000  BBALL(I)=0.
17.000 C
18.000 C*****FIND LOWEST DISC IN ASSEMBLY (address=IBFST)
19.000 C
20.000      IAB=M2
21.000      DO 1010 I=1,NBALL
22.000        A(IAB+8)=0.0
23.000        Y=A(IAB+1)+A(IAB+12)
24.000        IF (Y.LT.YO) IBLST=IAB;XO=A(IAB)+A(IAB+11);YO=A(IAB+1)+A(IAB+ 12)
25.000 1010  IAB=IAB+14
26.000      BBALL(1)=IBFST=IBLST
27.000      A(IBFST+8)=1.0
28.000 C
29.000 C*****FIND SEQUENCE OF BOUNDARY DISCS BY CONSIDERING
30.000 C     MINIMUM CHANGE IN ANGLE BETWEEN LINES CONNECTING
31.000 C     CENTRES OF DISCS
32.000 C
33.000      NB=1
34.000 1020  ALPMIN=2*PI
35.000      IAB=M2
36.000      DO 1040 I=1,NBALL
37.000        IF (IAB.EQ.IBLST)GOTO 1040
38.000        DX=A(IAB)+A(IAB+11)-XO
39.000        DY=A(IAB+1)+A(IAB+12)-YO
40.000        IF (ABS(DX).LT.SMALL) BET=SIGN(PI/2.,DY),GOTO 1030
41.000        BET=ATAN2(DY,DX)
42.000 1030    IF (BET.LE.SMALL) BET=2*PI+BET
43.000        ALP=BET-BETO
44.000        IF(ALP.EQ.0.0)GOTO 1031
45.000        IF (ALP.LT.-0.001)GOTO 1040
46.000        IF (ALP.GT.ALPMIN)GOTO 1040
47.000 1031    IBMIN=IAB
48.000        ALPMIN=ALP
49.000        BETMIN=BET
50.000 1040  IAB=IAB+14
51.000 C
52.000 C****FILTER TO CATCH CONDITION FOR ALP=ALPMIN
53.000 C
54.000      IF(ALP.EQ.ALPMIN) GOTO 1051
55.000      GOTO 1052
56.000 1051  XO=XO-A(IBLST+11)
57.000      YO=YO-A(IBLST+12)
58.000      GO TO 1020
59.000 1052  CONTINUE
60.000 C
61.000      DO 1050 I=1,10
62.000 1050  IF (IBMIN.EQ.BBALL(I)) RETURN
63.000 C
64.000      NB=NB+1
65.000      XO=A(IBMIN)+A(IBMIN+11)
66.000      YO=A(IBMIN+1)+A(IBMIN+12)
67.000      BBALL(NB)=IBLST=IBMIN
68.000      A(IBMIN+8)=1.0
69.000      BETO=BETMIN
70.000      GOTO 1020
71.000 C
72.000      END


1.000 C
2.000      SUBROUTINE BVOLUME
3.000 C
4.000 C*****PROGRAM CALCULATES AREA OF NEAR-CIRCULAR ASSEMBLY
5.000 C     OF DISCS (from TOTAL ASSEMBLY)
6.000 C       1) Volume described by convex polygon of straight-line
7.000 C          segments joining boundary discs
8.000 C
9.000      COMMON /ARAY/ A(108910)
10.000      COMMON /BBAL/ BBALL(1000),NB,AREA
11.000      REAL MIDY
12.000      DATA AREA/0./
13.000 C
14.000      DO 1030 I=1,NB
15.000        IF (I.EQ.NB)GOTO 1000
16.000        GOTO 1010
17.000 1000    IB2=BBALL(1)
18.000        GOTO 1020
19.000 1010    IB2=BBALL(I+1)
20.000 1020    IB1=BBALL(I)
```

```
21.000         MIDY=(A(IB2+1)+A(IB2+12)+A(IB1+1)+A(IB1+12))/2.0
22.000         DX=(A(IB2)+A(IB2+11)-A(IB1)-A(IB1+11))
23.000         PART=-MIDY*DX
24.000 1030  AREA=AREA+PART
25.000 C
26.000       RETURN
27.000       END

1.000 C
2.000      SUBROUTINE BSTRESS
3.000 C
4.000 C*****PROGRAM CALCULATES BOUNDARY STRESS TENSOR VALUES
5.000 C     FOR TOTAL ASSEMBLY OF DISCS USING SUM OF Fi x Lj TERMS
6.000 C
7.000       COMMON /ARAY/ A(108910)
8.000       COMMON /BBAL/ BBALL(1000),NB,AREA
9.000       COMMON /CIRC/ IBCIRC(2000),NBT,ICONT(4000),NCS
10.000      COMMON /BSTR/ BSIG(2,2)
11.000      COMMON /BDAT/ R(50)
12.000      GLOBAL M1,NBOX
13.000      DATA SUM11/0./ SUM12/0./ SUM21/0./ SUM22/0./
14.000 C
15.000      DO 1060 NBX=M1,M1+NBOX-1
16.000        IAD=A(NBX)
17.000 1000    IB1=A(IAD)
18.000        IF (IB1) 1060,1060,1010
19.000 1010    IB2=A(IAD+1)
20.000        ITAG1=A(IB1+8)
21.000        ITAG2=A(IB2+8)
22.000        L=ITAG1+ITAG2+1
23.000 C
24.000 C*****DO NOT INCLUDE CONTRIBUTION DUE TO CONTACT BETWEEN
25.000 C     TWO BOUNDARY DISCS
26.000 C
27.000         GO TO (1020,1020,1050)L
28.000 C
29.000 1020    XDIF=A(IB1)+A(IB1+11)-A(IB2)-A(IB2+11)
30.000         YDIF=A(IB1+1)+A(IB1+12)-A(IB2+1)-A(IB2+12)
31.000         D=SQRT(XDIF*XDIF+YDIF*YDIF)
32.000         CA=XDIF/D
33.000         SA=YDIF/D
34.000         FX=A(IAD+4)*CA+A(IAD+5)*SA
35.000         FY=A(IAD+4)*SA-A(IAD+5)*CA
36.000         GO TO (1040,1030,1050)L
37.000 C
38.000 1030    D=ITAG1*R(A(IB2+9))+ITAG2*R(A(IB1+9))
39.000 1040    SUM11=SUM11-FX*CA*D
40.000         SUM12=SUM12-FY*CA*D
41.000         SUM21=SUM21-FX*SA*D
42.000         SUM22=SUM22-FY*SA*D
43.000 C
44.000 1050    IAD=IAD+6
45.000         GOTO 1000
46.000 1060  CONTINUE
47.000 C
48.000       BSIG(1,1)=SUM11/AREA
49.000       BSIG(1,2)=SUM12/AREA
50.000       BSIG(2,1)=SUM21/AREA
51.000       BSIG(2,2)=SUM22/AREA
52.000 C
53.000       RETURN
54.000       END

1.000 C
2.000      SUBROUTINE SRVMOT
3.000 C
4.000 C*****PROGRAM APPLIES BOUNDARY VELOCITY INCREMENTS TO CENTRES
5.000 C     OF BOUNDARY DISCS OR NON-SERVO ACTIVATED DISC FORCES
6.000 C     ACCORDING TO A PRESCRIBED BOUNDARY STRESS TENSOR
7.000 C
8.000 C       1) APPLIED horizontal and vertical boundary velocities
9.000 C          are calculated from contribution of prescribed BOUNDARY
10.000 C           STRAIN-RATE TENSOR EBVEL(I,J) and servo BOUNDARY STRAIN-
11.000 C           RATE TENSOR ECVEL(I,J) required to keep boundary stresses
12.000 C           at desired levels.
13.000 C        2) SSRVX,SSRVY =x,y incremental velocities from
14.000 C                        prescribed boundary strain-rate tensor
15.000 C        3) BSRVX,BSRVY =x,y incremental velocities from
16.000 C                        servo boundary strain-rate tensor
```

```
C       4) SRVX= SSRVX+BSRVX applied boundary x velocity
C         SRVY= SSRVY+BSRVY applied boundary y velocity
C       5) SGAIN = gain on servo-control
C
C
      DIMENSION ECVEL(2,2)
      GLOBAL BDFLAG,MODE,RFLAG,NN,NRCYC
      GLOBAL CON1,CON2,GRAVX,GRAVY,TDEL,ADDX,ADDT
      COMMON /ARAY/ A(108910)
      COMMON /BDAT/ R(50),DENS(50),AKN(50),AKS(50),AMU(50),COH(50),AMASS(50),AMOI(50)
      COMMON /BBAL/ BBALL(1000),NBB
      COMMON /MOD/ EBVEL(2,2),SGAIN,BSTR(2,2)
      COMMON /BSTR/ BSIG(2,2),BSIGO(2,2),BSIGD(2,2)
      LOGICAL RFLAG,BDFLAG
      BDFLAG=.FALSE.
C
      IF (NN.GT.NRCYC) PROP=1.0;GOTO 1000
      PROP=FLOAT(NN)/NRCYC
1000  GO TO(1010,1020,1030,1040,1060,1070,1080) MODE
C
C*****MODE 1 (STRAIN-CONTROLLED BOUNDARY)
C
1010  ECVEL(1,1)=ECVEL(1,2)=ECVEL(2,1)=ECVEL(2,2)=0
      GOTO 1100
C
C*****MODE 2 (SIGMA11 CONSTANT)
C
1020  DIFF=BSIG(1,1)-BSIGO(1,1)-BSIGD(1,1)*PROP
      DENM=BSIGO(1,1)+BSIGD(1,1)*PROP
      ECVEL(1,1)=SGAIN*DIFF/DENM
      VEL=AMAX1(ABS(EBVEL(2,2)),ABS(ECVEL(1,1)))
      ECVEL(2,2)=SIGN(VEL,EBVEL(2,2))
      ECVEL(1,2)=ECVEL(2,1)=0.0
      GOTO 1100
C
C*****MODE 3 (HYDROSTATIC)
C
1030  HYDRO=(BSIG(1,1)+BSIG(2,2))/2.0
      HYDROC=(BSIGO(1,1)+BSIGO(2,2)+(BSIGD(1,1)+BSIGD(2,2))*PROP)/2.
      VEL=SGAIN*(HYDRO-HYDROC)/HYDROC
      IF (ABS(VEL).GT.SGAIN) VEL=SIGN(SGAIN,VEL)
      ECVEL(1,1)=ECVEL(2,2)=VEL
      ECVEL(1,2)=ECVEL(2,1)=0.0
      GOTO 1100
C
C*****MODE 4 (SERVO-CONTROLLED)
C
1040  DO 1050 I=1,2
        DIFF=BSIG(I,I)-BSIGO(I,I)-BSIGD(I,I)*PROP
        DENM=BSIGO(I,I)+BSIGD(I,I)*PROP
        VEL=SGAIN*DIFF/DENM
        IF (ABS(VEL).GT.SGAIN) VEL=SIGN(SGAIN,VEL)
1050  ECVEL(I,I)=VEL
      ECVEL(1,2)=ECVEL(2,1)=0.0
      GOTO 1100
C
C*****MODE 5 (BOUNDARY FORCE CONTROLLED)
C
1060  CALL BNDFORD
      ECVEL(1,1)=ECVEL(1,2)=ECVEL(2,1)=ECVEL(2,2)=0.
      GOTO 1100
C
C*****MODE 6 (SIGMA22 CONSTANT)
C
1070  DIFF=BSIG(1,1)-BSIGO(1,1)-BSIGD(1,1)*PROP
      DENM=BSIGO(1,1)+BSIGD(1,1)*PROP
      ECVEL(1,1)=SGAIN*DIFF/DENM
      ECVEL(2,2)=EBVEL(2,2)
      ECVEL(1,2)=ECVEL(2,1)=0.0
      GOTO 1100
C
C*****MODE 7 (USED FOR STRESS ROTATION)
C
1080  DO 1090 I=1,2
        DO 1090 J=1,2
          DIFF=BSIG(I,J)-BSIGO(I,J)-BSIGD(I,J)*PROP
          DENM=BSIGO(I,J)+BSIGD(I,J)*PROP
      VEL=SGAIN*DIFF/DENM
      IF(ABS(VEL).GT.SGAIN) VEL=SIGN(SGAIN,VEL)
1090  ECVEL(I,J)=VEL
```

```
97.000 C
98.000 C*****APPROXIMATE CENTRE OF ASSEMBLY
99.000 C
100.000 1100  XCA=A(2)/2.0
101.000       YCA=A(3)/2.0
102.000 C
103.000 C*****APPLY DISC VELOCITY INCREMENT CORRESPONDING TO PRESCRIBED
104.000 C     BOUNDARY CONDITION/CONTROL (see MOTION)
105.000 C
106.000       DO 1240 I=1,NBB
107.000         RFLAG=.FALSE.
108.000         IAB=BBALL(I)
109.000         ITYP=A(IAB+9)
110.000         AM=AMASS(ITYP)
111.000         AMI=AMOI(ITYP)
112.000         XX=A(IAB)-XCA
113.000         YY=A(IAB+1)-YCA
114.000 C
115.000 C*****COMPONENT OF DISC MOTION DUE TO SERVO-CONTROLLED BOUNDARY STRESS
116.000 C
117.000         BSRVX=ECVEL(1,1)*XX-ECVEL(1,2)*YY
118.000         BSRVY=ECVEL(2,2)*YY-ECVEL(2,1)*XX
119.000 C
120.000 C*****COMPONENT OF DISC MOTION DUE TO SERVO-CONTROLLED BOUNDARY
121.000 C     STRAIN-RATE TENSOR
122.000 C
123.000         SSRVX=EBVEL(1,1)*XX+EBVEL(1,2)*YY
124.000         SSRVY=EBVEL(2,2)*YY+EBVEL(2,1)*XX
125.000 C
126.000 C*****TOTAL SERVO
127.000 C
128.000         SRVX=BSRVX+SSRVX
129.000         SRVY=BSRVY+SSRVY
130.000 C
131.000         GO TO(1110,1120,1140,1140,1130,1120,1120)MODE
132.000 C
133.000 1110     A(IAB+2)=SRVX
134.000         A(IAB+3)=SRVY
135.000         GOTO 1200
136.000 1120     A(IAB+2)=BSRVX
137.000         A(IAB+3)=BSRVY
138.000         GOTO 1190
139.000 1130     A(IAB+2)=SRVX+A(IAB+2)
140.000         A(IAB+3)=SRVY+A(IAB+3)
141.000         GOTO 1190
142.000 C
143.000 C*****CHECK THAT SERVO-CONTROL OF BOUNDARY STRESS DOES NOT
144.000 C     SWAMP DESIRED BOUNDARY STRAIN-RATE (MODES 3,4)
145.000 C
146.000 1140     IF (BSRVX*SSRVX) 1150,1160,1160
147.000 1150     IF (ABS(BSRVX).GT.ABS(SSRVX)) SRVX=0.
148.000 1160     A(IAB+2)=SRVX
149.000         IF (BSRVY*SSRVY) 1170,1180,1180
150.000 1170     IF (ABS(BSRVY).GT.ABS(SSRVY)) SRVY=0.
151.000 1180     A(IAB+3)=SRVY
152.000 C
153.000 C*****CALCULATE REQUIRED BOUNDARY DISC MOTION
154.000 C
155.000 1190     A(IAB+2)=(A(IAB+2)*CON1+(A(IAB+5)/AM+GRAVX)*TDEL)*CON2
156.000         A(IAB+3)=(A(IAB+3)*CON1+(A(IAB+6)/AM+GRAVY)*TDEL)*CON2
157.000         A(IAB+4)=(A(IAB+4)*CON1+A(IAB+7)*TDEL/AMI)*CON2
158.000 1200     A(IAB+5)=0.0
159.000         A(IAB+6)=0.0
160.000         A(IAB+7)=0.0
161.000         A(IAB+11)=A(IAB+11)+A(IAB+2)*TDEL
162.000         A(IAB+12)=A(IAB+12)+A(IAB+3)*TDEL
163.000         A(IAB+13)=A(IAB+13)+A(IAB+4)*TDEL
164.000         IF (ABS(A(IAB+11)).LT.ADDX)GOTO 1210
165.000         A(IAB)=A(IAB)+A(IAB+11)
166.000         A(IAB+11)=0.0
167.000         RFLAG=.TRUE.
168.000 1210     IF (ABS(A(IAB+12)).LT.ADDX)GOTO 1220
169.000         A(IAB+1)=A(IAB+1)+A(IAB+12)
170.000         A(IAB+12)=0.0
171.000         RFLAG=.TRUE.
172.000 1220     IF (ABS(A(IAB+13)).LT.ADDT)GOTO 1230
173.000         A(IAB+10)=A(IAB+10)+A(IAB+13)
174.000         A(IAB+13)=0.0
175.000         RFLAG=.TRUE.
176.000 1230     IF (RFLAG) CALL REBOX(IAB); BDFLAG=.TRUE.
```

```
177.000 C
178.000 1240  CONTINUE
179.000 C
180.000       RETURN
181.000       END


1.000 C
2.000       SUBROUTINE MOTION(IAB)
3.000 C
4.000 C*****PROGRAM CALCULATES NEW VELOCITIES AND DISPLACEMENTS FOR EACH
5.000 C     DISC FROM CURRENT FORCES AND MOMENTS ACTING ON IT
6.000 C
7.000 C     NOTES:
8.000 C
9.000 C       a) Velocity damping operates on all degrees of freedom
10.000 C
11.000      COMMON /ARAY/ A(108910)
12.000      COMMON /BDAT/ R(50),DENS(50),AKN(50),AKS(50),AMU(50),COH(50),AMASS(50),AMOI(50)
13.000      GLOBAL CON1,CON2,GRAVX,GRAVY,TDEL,ADDX,ADDT,RFLAG
14.000      DATA SMALL/1.0E-20/
15.000 C
16.000      LOGICAL RFLAG
17.000      RFLAG=.FALSE.
18.000 C
19.000 C*****GET DISC TYPE NUMBER, MASS AND MOMENT OF INERTIA
20.000 C
21.000      ITYP=A(IAB+9)
22.000      AM=AMASS(ITYP)
23.000      AMI=AMOI(ITYP)
24.000 C
25.000 C*****INTEGRATE ACCELERATIONS TO GIVE NEW VELOCITIES
26.000 C     AT END OF TIME STEP (TDEL)
27.000 C
28.000      A(IAB+2)=(A(IAB+2)*CON1+(A(IAB+5)/AM+GRAVX)*TDEL)*CON2
29.000      A(IAB+3)=(A(IAB+3)*CON1+(A(IAB+6)/AM+GRAVY)*TDEL)*CON2
30.000      A(IAB+4)=(A(IAB+4)*CON1+A(IAB+7)*TDEL/AMI)*CON2
31.000      A(IAB+5)=0.0
32.000      A(IAB+6)=0.0
33.000      A(IAB+7)=0.0
34.000 C
35.000 C*****INTEGRATE VELOCITIES TO GIVE CHANGE IN COORDINATES AND
36.000 C     PARTICLE ROTATION
37.000 C
38.000      A(IAB+11)=A(IAB+11)+A(IAB+2)*TDEL
39.000      A(IAB+12)=A(IAB+12)+A(IAB+3)*TDEL
40.000      A(IAB+13)=A(IAB+13)+A(IAB+4)*TDEL
41.000      IF (ABS(A(IAB+11))-ADDX) 1010,1000,1000
42.000 1000  A(IAB)=A(IAB)+A(IAB+11)
43.000      A(IAB+11)=0.0
44.000      RFLAG=.TRUE.
45.000 1010  IF (ABS(A(IAB+12))-ADDX) 1030,1020,1020
46.000 1020  A(IAB+1)=A(IAB+1)+A(IAB+12)
47.000      A(IAB+12)=0.0
48.000      RFLAG=.TRUE.
49.000 1030  IF (ABS(A(IAB+13))-ADDT) 1050,1040,1040
50.000 1040  A(IAB+10)=A(IAB+10)+A(IAB+13)
51.000      A(IAB+13)=0.0
52.000 C
53.000 C*****PROTECT AGAINST UNDERFLOW ERROR
54.000 C
55.000 1050  CONTINUE
56.000 1060  IF (ABS(A(IAB+2)).LT.SMALL) A(IAB+2)=0.0
57.000      IF (ABS(A(IAB+3)).LT.SMALL) A(IAB+3)=0.0
58.000      IF (ABS(A(IAB+4)).LT.SMALL) A(IAB+4)=0.0
59.000 C
60.000      RETURN
61.000      END
```

```
1.000 C
2.000      SUBROUTINE REBOX(IAB)
3.000 C
4.000 C*****PROGRAM REBOXES DISC AND UPDATES CONTACT LISTS AS REQUIRED
5.000 C
6.000 C     IAB=ADDRESS OF DISC
7.000 C     NBL=ADDRESS OF POSSIBLE CONTACTING DISC
8.000 C
9.000       COMMON /ARAY/ A(108910)
10.000      COMMON /SRCH/ NBSAV(2000),NBMAP,IBSAV(2000),NBB
11.000      COMMON /BDAT/ R(50)
12.000      GLOBAL NX,NY,DEL,TOL,M1
13.000 C
14.000      X=A(IAB)+A(IAB+11)
15.000      Y=A(IAB+1)+A(IAB+12)
16.000 C
17.000 C*****CHECK FOR DISCS OUT OF ASSEMBLY AREA
18.000 C     COMPILE X STATEMENTS TO ACTIVATE DEBUGGER
19.000 C
20.000 X     IF (X.GT.A(2).OR.X.LT.0.0) CALL ERROR(2,IAB)
21.000 X     IF (Y.GT.A(3).OR.Y.LT.0.0) CALL ERROR(2,IAB)
22.000 C
23.000 C*****TO DETERMINE BOXES THAT DISC MAPS INTO (SEARCH RADIUS= RAD+TOL)
24.000 C
25.000      ITYP=A(IAB+9)
26.000      RT=TOL+R(ITYP)
27.000      NXL=IFIX((X-RT)/DEL)
28.000      NXU=IFIX((X+RT)/DEL)
29.000      NYL=IFIX((Y-RT)/DEL)
30.000      NYU=IFIX((Y+RT)/DEL)
31.000 C
32.000      NBMAP=0
33.000      DO 1000 NYY=NYL,NYU
34.000        DO 1000 NXX=NXL,NXU
35.000          NBMAP=NBMAP+1
36.000          NBSAV(NBMAP)=NYY*NX+NXX+M1
37.000 C
38.000 C*****CHECK THAT DISC IAB HAS AT LEAST ONE ENTRY IN BOXES NBSAV(NBMAP)
39.000 C
40.000 1000  CALL CHECK(IAB,NBSAV(NBMAP))
41.000 C
42.000 C*****IDENTIFY DISCS IN SCANNED BOXES
43.000 C
44.000      CALL SEARCH
45.000 C
46.000 C*****TEST FOR DISC-DISC CONTACT AND UPDATE CONTACT LIST AS REQUIRED
47.000 C
48.000      DO 1010 I=1,NBB
49.000        NBL=IBSAV(I)
50.000        IF (NBL.EQ.IAB)GOTO 1010
51.000        CALL BTEST(NBL,IAB)
52.000 1010  CONTINUE
53.000 C
54.000      RETURN
55.000      END


1.000 C
2.000      SUBROUTINE FORD
3.000 C
4.000 C*****SUBROUTINE COMPUTES FORCES AT ALL CONTACTS USING LINEAR
5.000 C     FORCE/DISPLACEMENT LAW AND----------------
6.000 C     CALCULATES ASSEMBLY STRESS TENSOR FROM CONTRIBUTION
7.000 C     OF ALL Fi X Lj TERMS
8.000 C
9.000 C     NOTES:
10.000 C
11.000 C     a) Damping is viscous and proportional to stiffnesses
12.000 C        and is switched off in the shear direction  during sliding
13.000 C     b) The stiffnesses of contacting discs are assumed to act
14.000 C        in series
15.000 C     c) If the 2 discs have different e or mu, the minimum
16.000 C        values are taken
17.000 C     d) Stiffness components are linear
18.000 C
19.000 C     IAD= INITIAL ADDRESS OF CONTACT LIST
20.000 C     IB1=  ADDRESS FOR DISC DATA ARRAY
21.000 C     IB2=  ADDRESS FOR CONTACTING DISC DATA ARRAY
22.000 C     NBX= BOX ADDRESS FOR CONTACT
23.000 C
```

```
24.000       COMMON /ARAY/ A(108910)
25.000       COMMON /BDAT/ R(50),DENS(50),AKN(50),AKS(50),AMU(50),COH(50),AMASS(50),AMOI(50)
26.000       COMMON /BBAL/ BBALL(1000),NB,AREA
27.000       COMMON /BSTR/ BSIG(2,2)
28.000       GLOBAL NCBOX,M3,TDEL,BDT,TOL,MODE,M1,NBOX
29.000       DATA SUM11/0./ SUM12/0./ SUM21/0./ SUM22/0./
30.000 C
31.000       DO 1320 NBX=M1,NBOX+M1-1
32.000         IAD=A(NBX)
33.000 1000     IB1=A(IAD)
34.000         IF (IB1) 1320,1320,1010
35.000 1010     IB2=A(IAD+1)
36.000 C
37.000         XDIF=A(IB1)+A(IB1+11)-A(IB2)-A(IB2+11)
38.000         YDIF=A(IB1+1)+A(IB1+12)-A(IB2+1)-A(IB2+12)
39.000         D=SQRT(XDIF*XDIF+YDIF*YDIF)
40.000 C
41.000 C*****GET DISC RADII
42.000 C
43.000         ITYP2=A(IB2+9)
44.000         ITYP1=A(IB1+9)
45.000         R1=R(ITYP1)
46.000         R2=R(ITYP2)
47.000 C
48.000 C*****TEST FOR CONTACT
49.000 C
50.000         RDIF=D-R1-R2
51.000         IF (RDIF) 1020,1140,1140
52.000 C
53.000 C*****SIN AND COS OF ANGLE BETWEEN 2 DISCS
54.000 C
55.000 1020     SA=YDIF/D
56.000         CA=XDIF/D
57.000 C
58.000 C*****NORMAL AND SHEAR DISPLACEMENT INCREMENTS
59.000 C
60.000         XDR=A(IB2+2)-A(IB1+2)
61.000         YDR=A(IB2+3)-A(IB1+3)
62.000         DN=(XDR*CA+YDR*SA)*TDEL
63.000         DS=(XDR*SA-YDR*CA-A(IB2+4)*R2-A(IB1+4)*R1)*TDEL
64.000 C
65.000 C*****NEW NORMAL DISPLACEMENT
66.000 C
67.000 1030     A(IAD+2)=A(IAD+2)+DN
68.000 C
69.000 C*****COMBINED NORMAL STIFFNESS
70.000 C
71.000         STIFN=AKN(ITYP1)*AKN(ITYP2)/(AKN(ITYP1)+AKN(ITYP2))
72.000 C
73.000 C*****NORMAL FORCE
74.000 C
75.000         DFN=DN*STIFN
76.000         FN=A(IAD+4)+DFN
77.000         A(IAD+4)=FN
78.000         IF (FN) 1140,1140,1040
79.000 C
80.000 C*****DAMPING CONTRIBUTION
81.000 C
82.000 1040     FNT=FN+DFN*BDT
83.000 C
84.000 C*****COMBINED SHEAR STIFFNESS
85.000 C
86.000         FST=0.
87.000         IF (AKS(ITYP1)+AKS(ITYP2)) 1110,1110,1050
88.000 1050     STIFS=AKS(ITYP1)*AKS(ITYP2)/(AKS(ITYP1)+AKS(ITYP2))
89.000 C
90.000 C*****SHEAR FORCE
91.000 C
92.000         DFS=DS*STIFS
93.000         FS=A(IAD+5)+DFS
94.000 C
95.000 C*****SLIDING TEST
96.000 C
97.000         FSMAX=AMIN1(COH(ITYP1),COH(ITYP2))+AMIN1(AMU(ITYP1),AMU(ITYP2))
98.000     1     *FN
99.000         IF (ABS(FS)-FSMAX) 1090,1090,1060
100.000 C
101.000 C*****MUST BE SLIDING
102.000 C
103.000 1060     IF (FS) 1070,1080,1070
```

```
104.000 1070     FS=SIGN(FSMAX,FS)
105.000 1080     FST=FS
106.000 C
107.000 C*****CUMULATIVE SLIDING DISPLACEMENT
108.000 C
109.000          A(IAD+3)=A(IAD+3)+ABS(DS)
110.000          GOTO 1100
111.000 C
112.000 C*****NOT SLIDING INCLUDE DAMPING
113.000 C
114.000 1090     FST=FS+DFS*BDT
115.000 1100     A(IAD+5)=FS
116.000 C
117.000 C*****RESOLVE FORCES BACK INTO X,Y,THETA COMPONENTS
118.000 C
119.000 1110     FX=FNT*CA+FST*SA
120.000          FY=FNT*SA-FST*CA
121.000          FT1=FST*R2
122.000          FT2=FST*R1
123.000 C
124.000 C*****ADD IN THIS CONTACTS CONTRIBUTION TO DISC FORCE SUMS
125.000 C
126.000          A(IB2+5)=A(IB2+5)+FX
127.000          A(IB2+6)=A(IB2+6)+FY
128.000          A(IB2+7)=A(IB2+7)+FT1
129.000          A(IB1+5)=A(IB1+5)+FX
130.000          A(IB1+6)=A(IB1+6)+FY
131.000          A(IB1+7)=A(IB1+7)+FT2
132.000 C
133.000 C*****CONTRIBUTION OF ALL CONTACTS TO BOUNDARY STRESS TENSOR
134.000 C     FOR ENTIRE ASSEMBLY
135.000 C     (DO NOT INCLUDE CONTACT BETWEEN TWO BOUNDARY DISCS)
136.000 C
137.000          IF (MODE.EQ.1)GOTO 1310
138.000 C
139.000          ITAG1=A(IB1+8)
140.000          ITAG2=A(IB2+8)
141.000          L=ITAG1+ITAG2+1
142.000          GO TO(1130,1120,1310)L
143.000 C
144.000 1120     D=ITAG1*R2+ITAG2*R1
145.000 1130     SUM11=SUM11-FX*CA*D
146.000          SUM12=SUM12-FY*CA*D
147.000          SUM21=SUM21-FX*SA*D
148.000          SUM22=SUM22-FY*SA*D
149.000          GOTO 1310
150.000 C
151.000 C*****TO DEAL WITH NON-TOUCHING DISCS
152.000 C     (DELETE CONTACT IF GAP.GT.TOL)
153.000 C
154.000 1140     DO 1150 I=3,6
155.000 1150     A(IAD+I-1)=0.0
156.000          IF (RDIF-TOL) 1310,1160,1160
157.000 1160     ICEND=A(NBX)+NCBOX*6-1
158.000          DO 1170 IAB=IAD,ICEND-6
159.000 1170     A(IAB)=A(IAB+6)
160.000          DO 1180 IAB=ICEND-5,ICEND
161.000 1180     A(IAB)=0.
162.000 C
163.000 C****CHECK THAT THERE IS AT LEAST ONE ENTRY FOR DISCS
164.000 C     IB1 AND IB2 IN BOX NBX
165.000 C
166.000          IRET=1
167.000          IAB=IB1
168.000          GOTO 1200
169.000 1190     IRET=2
170.000          IAB=IB2
171.000 1200     IAD=A(NBX)
172.000 1210     NB1=A(IAD)
173.000          IF (NB1) 1250,1290,1220
174.000 1220     IF (NB1-IAB) 1230,1300,1230
175.000 1230     NB2=A(IAD+1)
176.000          IF (NB2-IAB) 1240,1300,1240
177.000 1240     IAD=IAD+6
178.000          GOTO 1210
179.000 C
180.000 1250     NB1=-NB1
181.000 1260     IF (NB1-IAB) 1270,1300,1270
182.000 1270     IAD=IAD+1
183.000          NB1=A(IAD)
```

```
184.000         IF (NB1)  1260,1280,1260
185.000 C
186.000 1280     A(IAD)=IAB
187.000         GO TO(1190,1000) IRET
188.000 1290     A(IAD)=-IAB
189.000 1300     GO TO(1190,1000) IRET
190.000 C
191.000 1310     IAD=IAD+6
192.000         GOTO 1000
193.000 1320  CONTINUE
194.000 C
195.000       BSIG(1,1)=SUM11/AREA
196.000       BSIG(1,2)=SUM12/AREA
197.000       BSIG(2,1)=SUM21/AREA
198.000       BSIG(2,2)=SUM22/AREA
199.000 C
200.000       RETURN
201.000       END


1.000 C
2.000      SUBROUTINE BBOUND2
3.000 C
4.000 C*****Program identifies discs forming convex polygon of
5.000 C     near-circular assembly of discs
6.000 C     (Search based on previously identified boundary discs)
7.000 C
8.000       DIMENSION X(2),Y(2),NBM(4)
9.000       COMMON /ARAY/ A(108910)
10.000       COMMON /BBAL/ BBALL(1000),NB
11.000       COMMON /SRCH/ NBSAV(2000),NBMAP,IBSAV(2000),NBB
12.000       GLOBAL PI,DEL,TOL,NX,NY,M1
13.000       DATA SMALL/1.0E-20/ NBMAP/0/
14.000 C
15.000       DO 1040 N=1,NB
16.000         IF (N.EQ.NB) IB2=BBALL(1);GOTO 1000
17.000         IB2=BBALL(N+1)
18.000 1000     IB1=BBALL(N)
19.000 C
20.000 C*****FIND LARGEST AND SMALLEST ADDRESS OF BOX THAT POLYGON
21.000 C     SEGMENT (IB1 TO IB2) CAN BE MAPPED INTO (INCLUDING TOL)
22.000 C
23.000         X(1)=A(IB1)+A(IB1+11)
24.000         Y(1)=A(IB1+1)+A(IB1+12)
25.000         X(2)=A(IB2)+A(IB2+11)
26.000         Y(2)=A(IB2+1)+A(IB2+12)
27.000 C
28.000         T=TOL
29.000         K=1
30.000         DO 1020 J=1,2
31.000           DO 1020 I=1,2
32.000             IF (J.EQ.2) T=-TOL
33.000             XD=X(I)+T
34.000             YD=Y(I)+T
35.000             NXD=IFIX(XD/DEL)
36.000             NYD=IFIX(YD/DEL)
37.000             IF (J.EQ.2)GOTO 1010
38.000             IF (XD.GT.(NX*DEL)) NXD=NXD-1
39.000             IF (YD.GT.(NY*DEL)) NYD=NYD-1
40.000 1010          NBM(K)=NXD+NYD*NX+1
41.000 1020      K=K+1
42.000         NBMAX=AMAX0(NBM(1),NBM(2))
43.000         NBMIN=AMIN0(NBM(3),NBM(4))
44.000 C
45.000 C*****DETERMINE NUMBER OF COLUMNS OF BOXES THAT POLYGON SEGMENT
46.000 C     MAPS INTO
47.000 C
48.000         IRMAX=(NBMAX-1)/NX+1
49.000         ICMAX=NBMAX-NX*(IRMAX-1)
50.000         IRMIN=(NBMIN-1)/NX+1
51.000         ICMIN=NBMIN-NX*(IRMIN-1)
52.000         IC1=AMIN0(ICMAX,ICMIN)
53.000         IC2=AMAX0(ICMAX,ICMIN)
54.000         NC=IC2-IC1+1
55.000 C
56.000 C*****IDENTIFY RECTANGLE OF BOXES THAT POLYGON SEGMENT MAPS INTO
57.000 C     AND ADD TO TOTAL BOXES TO BE SEARCHED FOR POSSIBLE
58.000 C     BOUNDARY DISCS
59.000 C
60.000         DO 1030 I=NBMIN,NBMAX-NC+1,NX
```

```
61.000           DO 1030 J=1,NC
62.000             NBX=I+J-2+M1
63.000             NBMAP=NBMAP+1
64.000 1030     NBSAV(NBMAP)=NBX
65.000 1040   CONTINUE
66.000 C
67.000       CALL SEARCH
68.000 C
69.000 C*****FIND LOWEST DISC IN ASSEMBLY (address=IBFST)
70.000 C
71.000       YO=10000.
72.000       BBALL(2)=0.
73.000       DO 1050 I=1,NBB
74.000         IAB=IBSAV(I)
75.000         A(IAB+8)=0.0
76.000         YY=A(IAB+1)+A(IAB+12)
77.000         IF (YY.LT.YO) IBLST=IAB;XO=A(IAB)+A(IAB+11);YO=A(IAB+1)+A(IAB+12)
78.000 1050   CONTINUE
79.000       BBALL(1)=IBFST=IBLST
80.000       A(IBFST+8)=1.0
81.000 C
82.000 C*****FIND SEQUENCE OF BOUNDARY DISCS BY CONSIDERING
83.000 C     MINIMUM CHANGE IN ANGLE BETWEEN LINES CONNECTING
84.000 C     CENTRES OF DISCS
85.000 C
86.000       NB=1
87.000       BETO=0.0
88.000 1060   ALPMIN=2*PI
89.000       DO 1080 I=1,NBB
90.000         IAB=IBSAV(I)
91.000         IF (IAB.EQ.IBLST)GOTO 1080
92.000         DX=A(IAB)+A(IAB+11)-XO
93.000         DY=A(IAB+1)+A(IAB+12)-YO
94.000         IF (ABS(DX).LT.SMALL) BET=SIGN(PI/2.,DY);GOTO 1070
95.000         BET=ATAN2(DY,DX)
96.000 1070     IF (BET.LE.0.0) BET=2*PI+BET
97.000         ALP=BET-BETO
98.000         IF (ALP.LT.0.0)GOTO 1080
99.000         IF (ALP.GT.ALPMIN)GOTO 1080
100.000         IBMIN=IAB
101.000         ALPMIN=ALP
102.000         BETMIN=BET
103.000 1080   CONTINUE
104.000 C
105.000       IF (IBMIN.EQ.IBFST) RETURN
106.000       IF (IBMIN.EQ.BBALL(2)) RETURN
107.000       NB=NB+1
108.000       XO=A(IBMIN)+A(IBMIN+11)
109.000       YO=A(IBMIN+1)+A(IBMIN+12)
110.000       BBALL(NB)=IBLST=IBMIN
111.000       A(IBMIN+8)=1.0
112.000       BETO=BETMIN
113.000       GOTO 1060
114.000 C
115.000       END


1.000 C
2.000      SUBROUTINE RELAX
3.000 C
4.000 C*****PROGRAM FREEZES BOUNDARY DISCS FOR MAX #CYC=NRLCYC OR UNTIL
5.000 C     HORIZ. AND VERTICAL INERTIAL BOUNDARY STRESSES ARE
6.000 C     LESS THAN 5 PERCENT OF TOTAL BOUNDARY STRESSES
7.000 C
8.000       COMMON /ARAY/ A(108910)
9.000       COMMON /BBAL/ BBALL(1000),NB,AREA
10.000       COMMON /BSTR/ BSIG(2,2)
11.000       GLOBAL NR,PI,ALPHA
12.000       GLOBAL NRLCYC,M2,NBALL,RFLAG,CON1,CON2,TDEL
13.000       LOGICAL RFLAG
14.000 C
15.000       NCHECK=1
16.000 C
17.000 C*****INCREASE MASS DAMPING BY FACTOR OF 10 DURING RELAXATION
18.000 C
19.000       CON1I=CON1
20.000       CON2I=CON2
21.000       CON1=1.0-10*ALPHA*TDEL/2.
22.000       CON2=1.0/(1.0+10*ALPHA*TDEL/2.)
23.000 C
```

```
24.000       DO 1060 NR=1,NRLCYC
25.000         SUMFX=SUMFY=0.0
26.000 C
27.000 C*****CHECK BOUNDARY EVERY 10 CYCLES
28.000 C
29.000         IF (NR.EQ.NCHECK)GOTO 1000
30.000         GOTO 1010
31.000 1000     CALL BBOUND2
32.000         NCHECK=NCHECK+10
33.000 C
34.000 C*****ZERO BOUNDARY X-Y VELOCITIES AND FORCES
35.000 C
36.000 1010     DO 1020 I=1,NB
37.000           IAB=BBALL(I)
38.000           A(IAB+5)=0.0
39.000           A(IAB+6)=0.0
40.000           A(IAB+3)=0.0
41.000 1020     A(IAB+2)=0.0
42.000 C
43.000 C*****SCAN ALL DISCS
44.000 C
45.000         IAB=M2
46.000         DO 1030 I=1,NBALL
47.000           IF (A(IAB+8).EQ.1.0)GOTO 1030
48.000           RFLAG=.FALSE.
49.000 C
50.000 C*****DETERMINE OUT-OF-BALANCE DISC FORCE COMPONENTS
51.000 C
52.000           SUMFX=SUMFX+A(IAB+5)
53.000           SUMFY=SUMFY+A(IAB+6)
54.000 C
55.000           CALL MOTION(IAB)
56.000           IF (RFLAG) CALL REBOX(IAB)
57.000 1030     IAB=IAB+14
58.000 C
59.000 C*****SCAN ALL CONTACTS
60.000 C
61.000         CALL FORD
62.000 C
63.000 C*****CHECK INERTIAL STRESS CRITERION
64.000 C     (COARSE CHECK)
65.000 C
66.000         DIA=SQRT(4*AREA/PI)
67.000         SIGMAX=ABS(SUMFX/DIA)
68.000         SIGMAY=ABS(SUMFY/DIA)
69.000         IF ((20*SIGMAX).GT.ABS(BSIG(1,1)))GOTO 1060
70.000         IF ((20*SIGMAY).GT.ABS(BSIG(2,2)))GOTO 1060
71.000 C
72.000 C     (EXACT CHECK)
73.000 C
74.000         SUMFX=SUMFY=0.
75.000         IAB=M2
76.000         DO 1050 I=1,NBALL
77.000           ITAG=A(IAB+8)
78.000           IF (ITAG-1) 1040,1050,1040
79.000 1040       SUMFX=SUMFX+A(IAB+5)
80.000           SUMFY=SUMFY+A(IAB+6)
81.000 1050     CONTINUE
82.000 C
83.000         SIGMAX=ABS(SUMFX/DIA)
84.000         SIGMAY=ABS(SUMFY/DIA)
85.000         IF ((20*SIGMAX).GT.ABS(BSIG(1,1)))GOTO 1060
86.000         IF ((20*SIGMAY).GT.ABS(BSIG(2,2)))GOTO 1060
87.000         GOTO 1070
88.000 1060   CONTINUE
89.000 C
90.000 1070   CON1=CON1I
91.000       CON2=CON2I
92.000       RETURN
93.000       END
```

```
1.000 C
2.000       SUBROUTINE EXTRACT
3.000 C
4.000 C*****PROGRAM LOADS E ARRAY AND DUMPS E ARRAY TO BINARY FILE
5.000 C     E ARRAY CONTAINS MICROMECHANICAL DATA EXTRACTED FROM DISC
6.000 C     ASSEMBLY AND SUB-ASSEMBLIES
7.000 C
8.000       COMMON /ARAY/ A(108910)
9.000       COMMON /ERAY/ E(10000)
10.000      COMMON /CHCK/ NBMAX,KMAX,NCMAX
11.000      COMMON /BSTR/ BSIG(2,2)
12.000      COMMON /STRN/ EIJB(2,2),NBI,AREAI
13.000      COMMON /CIRC/ IBCIRC(2000),NBT,ICONT(4000),NCS,NBC,NPB
14.000      COMMON /BALF/ FX,FY,MO,FBMAX,MOMAX,VBMAX,FBAVG,MOAVG,VBAVG
15.000      COMMON /CONF/ FNMAX,FNMIN,FNAVG,FSMAX,FSMIN,FSAVG,FCMAX,FCAVG,DAVG
16.000      COMMON /FABR/ NCI(36),FNA(36),FSA(36),DCA(36),AA,BB,AA0,BB0,FNAA,F
17.000     *NBB,FNAA0,FNBB0,AW,AU,FSAA0,DAA,DBB,DAA0,DBB0
18.000      COMMON /BBAL/ BBALL(1000),NB,AREA
19.000      COMMON /HIST/ NFN(20),NFS(20)
20.000      GLOBAL M4,NBOX,NCBOX,ROR(1)
21.000      GLOBAL NN,NCYCS,PI,DNSTY,EKEY,NBALL,M2,NRLCYC,NR,NCIRC
22.000 C
23.000      INTEGER EKEY
24.000      REAL MO,MOAVG,MOMAX
25.000 C
26.000 C*****CYCLE DATA
27.000 C
28.000      E(27)=NN
29.000      E(28)=NN+NCYCS
30.000 C
31.000 C*****CHECK ON CONTACT PARTITION SPACE
32.000 C
33.000      CALL DISCCHECK
34.000      E(29)=NBMAX
35.000      E(30)=KMAX
36.000      E(31)=NCMAX
37.000 C
38.000 C*****ASSEMBLY BOUNDARY STRAINS
39.000 C
40.000 C     PDI = MAJOR PRINCIPAL STRAIN DIRECTION
41.000 C     PDII= MINOR PRINCIPAL STRAIN DIRECTION
42.000 C     EI  = MAJOR PRINCIPAL STRAIN
43.000 C     EII = MINOR PRINCIPAL STRAIN
44.000 C
45.000      CALL STRAIN(400)
46.000 C
47.000 C*****CURRENT TOTAL STRAIN VALUES
48.000 C
49.000      EN=EIJB(1,1)+EIJB(2,2)
50.000      ET=SQRT((EIJB(1,1)-EIJB(2,2))**2+(EIJB(1,2)+EIJB(2,1))**2)
51.000      EW=EIJB(2,1)-EIJB(1,2)
52.000      EV=(AREA-AREAI)/AREAI
53.000      PDI=0.5*ATAN2(EIJB(1,2)+EIJB(2,1),EIJB(1,1)-EIJB(2,2))
54.000      IF (PDI.LT.0.) PDI=PI+PDI
55.000      IF (PDI.GT.PI) PDI=PDI-PI
56.000      PDII=PDI+PI/2.
57.000      IF (PDII.GT.PI) PDII=PDII-PI
58.000      EI=0.5*(ET+EN)
59.000      EII=0.5*(EN-ET)
60.000 C
61.000 C*****ASSEMBLY INCREMENTAL STRAINS
62.000 C
63.000      E(350)=EIJB(1,1)-E(50)
64.000      E(351)=EIJB(1,2)-E(51)
65.000      E(352)=EIJB(2,1)-E(52)
66.000      E(353)=EIJB(2,2)-E(53)
67.000      E(354)=EN-E(54)
68.000      E(355)=ET-E(55)
69.000      E(356)=EW-E(56)
70.000      E(358)=EV-E(58)
71.000      E(359)=PDI-E(59)
72.000      E(360)=PDII-E(60)
73.000      E(375)=EI-E(75)
74.000      E(376)=EII-E(76)
75.000      IF (E(376)) 1000,1010,1000
76.000 1000  E(357)=E(375)/E(376)
77.000 1010  IF (E(355)) 1020,1030,1020
78.000 1020  E(377)=ABS(E(354)/E(355))
79.000 1030  CONTINUE
80.000 C
```

```
81.000 C*****CURRENT TOTAL STRAIN DATA
82.000 C
83.000       E(50)=EIJB(1,1)
84.000       E(51)=EIJB(1,2)
85.000       E(52)=EIJB(2,1)
86.000       E(53)=EIJB(2,2)
87.000       E(54)=EN
88.000       E(55)=ET
89.000       E(56)=EW
90.000       IF (EII) 1040,1050,1040
91.000 1040  E(57)=EI/EII
92.000 1050  E(58)=EV
93.000       E(59)=PDI
94.000       E(60)=PDII
95.000       E(75)=EI
96.000       E(76)=EII
97.000       IF (ET) 1060,1070,1060
98.000 1060  E(77)=ABS(EN/ET)
99.000 1070  CONTINUE
100.000 C
101.000 C*****ASSEMBLY BOUNDARY STRESS DATA
102.000 C
103.000      CALL BBOUND
104.000      CALL BVOLUME
105.000      CALL BSTRESSA
106.000 C
107.000 C*****CURRENT TOTAL STRESS VALUES
108.000 C
109.000      SN=(BSIG(1,1)+BSIG(2,2))*0.5
110.000      ST=SQRT(.25*((BSIG(1,1)-BSIG(2,2))**2)+0.25*((BSIG(1,2)+BSIG(2,1))**2))
111.000      PDI=.5*ATAN2((BSIG(1,2)+BSIG(2,1))/2.(BSIG(1,1)-BSIG(2,2))/2)
112.000      IF (PDI.LT.0.) PDI=PI+PDI
113.000      IF (PDI.GT.PI) PDI=PDI-PI
114.000      PDII=PDI+PI/2
115.000      IF (PDII.GT.PI) PDII=PDII-PI
116.000      SI=SN+ST
117.000      SII=SN-ST
118.000 C
119.000 C*****INCREMENTAL STRESS VALUES
120.000 C
121.000      E(340)=BSIG(1,1)-E(40)
122.000      E(341)=BSIG(1,2)-E(41)
123.000      E(342)=BSIG(2,1)-E(42)
124.000      E(343)=BSIG(2,2)-E(43)
125.000      E(347)=PDI-E(47)
126.000      E(348)=PDII-E(48)
127.000      E(373)=SI-E(73)
128.000      E(374)=SII-E(74)
129.000      IF (E(373)) 1080,1090,1080
130.000 1080  E(344)=E(374)/E(373)
131.000 1090  E(345)=SN-E(45)
132.000      E(346)=ST-E(46)
133.000      IF (E(345)) 1100,1110,1100
134.000 1100  E(349)=E(346)/E(345)
135.000 1110  CONTINUE
136.000 C
137.000 C*****CURRENT BOUNDARY STRESSES
138.000 C
139.000      E(40)=BSIG(1,1)
140.000      E(41)=BSIG(1,2)
141.000      E(42)=BSIG(2,1)
142.000      E(43)=BSIG(2,2)
143.000      IF (SI) 1120,1130,1120
144.000 1120  E(44)=SII/SI
145.000 1130  E(45)=SN
146.000      E(46)=ST
147.000      E(47)=PDI
148.000      E(48)=PDII
149.000      IF (SN) 1140,1150,1140
150.000 1140  E(49)=ABS(ST/SN)
151.000 1150  E(73)=SI
152.000      E(74)=SII
153.000 C
154.000 C*****FABRIC AND FORCE DATA FOR ENTIRE ASSEMBLY
155.000 C     NOTE: Disc force/velocity data does not include boundary discs
156.000 C
157.000 C*****LOAD ADDRESSES OF ASSEMBLY DISCS INTO ARRAY IBCIRC(NBT)
158.000 C     (Do not include boundary discs)
159.000 C
160.000 1160  NBT=0
```

```
161.000      IAB=M2
162.000      DO 1170 I=1,NBALL
163.000        NBT=NBT+1
164.000        IBCIRC(NBT)=IAB
165.000 1170  IAB=IAB+14
166.000 C
167.000 C*****LOAD ADDRESSES OF ASSEMBLY CONTACTS INTO ARRAY ICONT(NCS)
168.000 C     (Do not include contacts between boundary discs)
169.000 C     (Consider only stressed contacts)
170.000 C     NBC= total number of contacts
171.000 C     NCS= total number of PHYSICAL contacts
172.000 C
173.000      NCS=NBC=0
174.000      IAD=M4
175.000      DO 1250 I=1,NBOX
176.000        IAB=IAD
177.000 1180    IB1=A(IAB)
178.000        IF (IB1) 1250,1250,1190
179.000 1190    FN=A(IAB+4)
180.000        IF (FN) 1240,1240,1200
181.000 1200    IB2=A(IAB+1)
182.000        ITAG1=A(IB1+8)
183.000        ITAG2=A(IB2+8)
184.000        L=ITAG1+ITAG2+1
185.000        GO TO (1220,1210,1240)L
186.000 1210    NBC=NBC+1
187.000        GOTO 1230
188.000 1220    NBC=NBC+2
189.000 1230    NCS=NCS+1
190.000        ICONT(NCS)=IAB
191.000 1240    IAB=IAB+6
192.000        GOTO 1180
193.000 1250  IAD=IAD+NCBOX*6
194.000 C
195.000      CALL DISCNCS
196.000      CALL NPDISC
197.000 C
198.000      E(61)=NBT
199.000      E(80)=NBC
200.000      E(81)=NB
201.000      E(82)=FLOAT(NBC)/(NBALL-NB-NFB)
202.000      E(83)=AREA
203.000      E(84)=DNSTY
204.000      E(85)=NCS*2/AREA
205.000 C
206.000      CALL FORCE
207.000      CALL MICROFEATURES
208.000 C
209.000      E(86)=FX
210.000      E(87)=FY
211.000      E(88)=MO
212.000      E(89)=FBMAX
213.000      E(90)=MOMAX
214.000      E(91)=VBMAX
215.000      E(92)=FBAVG
216.000      E(93)=MOAVG
217.000      E(94)=VBAVG
218.000      E(95)=FNMAX
219.000      E(96)=FNAVG
220.000      E(97)=FSMAX
221.000      E(98)=FSAVG
222.000      E(99)=FCMAX
223.000      E(100)=FCAVG
224.000      E(101)=FNMIN
225.000      E(102)=FSMIN
226.000      E(103)=NR
227.000      E(104)=DAVG
228.000 C
229.000 C*****CONTACT ORIENTATION DISTRIBUTION FUNCTION PARAMETERS
230.000 C
231.000      E(105)=AA
232.000      E(106)=BB
233.000      E(107)=AA0
234.000      E(108)=BB0
235.000 C
236.000 C*****AVERAGE NORMAL FORCE DISTRIBUTON FUNCTION PARAMETERS
237.000 C
238.000      E(109)=FNAA
239.000      E(110)=FNBB
240.000      E(111)=FNAA0
```

```
241.000      E(112)=FNBB0
242.000 C
243.000 C*****AVERAGE SHEAR FORCE DISTRIBUTION FUNCTION PARAMETERS
244.000 C
245.000      E(113)=AU
246.000      E(114)=AW
247.000      E(116)=FSAA0
248.000 C
249.000 C*****AVERAGE CONTACT LENGTH DISTRIBUTION FUNCTION PARAMETERS
250.000 C
251.000      E(118)=DAA
252.000      E(119)=DBB
253.000      E(120)=DAAO
254.000      E(121)=DBBO
255.000 C
256.000 C*****HISTOGRAM OF CONTACT ORIENTATIONS
257.000 C
258.000      IAB=130
259.000      DO 1260 I=1,36
260.000        E(IAB)=NCI(I)
261.000 1260  IAB=IAB+1
262.000 C
263.000 C*****HISTOGRAM OF AVERAGE NORMAL FORCES WRT ORIENTATION
264.000 C
265.000      DO 1270 I=1,36
266.000        E(IAB)=FNA(I)
267.000 1270  IAB=IAB+1
268.000 C
269.000 C*****HISTOGRAM OF AVERAGE SHEAR FORCES WRT ORIENTATION
270.000 C
271.000      DO 1280 I=1,36
272.000        E(IAB)=FSA(I)
273.000 1280  IAB=IAB+1
274.000 C
275.000 C*****HISTOGRAM OF AVERAGE CONTACT LENGTH WRT ORIENTATION
276.000 C
277.000      DO 1290 I=1,36
278.000        E(IAB)=DCA(I)
279.000 1290  IAB=IAB+1
280.000 C
281.000 C*****HISTOGRAM OF NORMAL FORCES
282.000 C
283.000      DO 1300 I=1,20
284.000        E(IAB)=NFN(I)
285.000 1300  IAB=IAB+1
286.000 C
287.000 C*****HISTOGRAM OF SHEAR FORCES
288.000 C
289.000      DO 1310 I=1,20
290.000        E(IAB)=NFS(I)
291.000 1310  IAB=IAB+1
292.000 C
293.000 C*****SUB-ASSEMBLY DATA
294.000 C
295.000      IPOINT=1003
296.000      DO 1570 IC=1,NCIRC
297.000        IAB=4600+IC*400
298.000 C
299.000        CALL CIRCLE(IC)
300.000        CALL BVOLUME2
301.000        CALL DISCDENS
302.000        CALL NPDISC
303.000 C
304.000 C*****SUB-ASSEMBLY BOUNDARY STRESS DATA
305.000 C
306.000        CALL STRESS
307.000 C
308.000 C*****CURRENT STRESSES
309.000 C
310.000        SN=(BSIG(1,1)+BSIG(2,2))*0.5
311.000        ST=SQRT(.25*((BSIG(1,1)-BSIG(2,2))**2)+0.25*((BSIG(1,2)+BSIG(2,1))**2))
312.000        PDI=0.5*ATAN2((BSIG(1,2)+BSIG(2,1))/2.,ABS(BSIG(1,1)-BSIG(2,2))/2.)
313.000        IF (PDI.LT.0.0) PDI=PDI+PI
314.000        IF (PDI.GT.PI) PDI=PDI-PI
315.000        PDII=PDI+PI/2
316.000        IF (PDII.GT.PI) PDII=PDII-PI
317.000        SI=SN+ST
318.000        SII=SN-ST
319.000 C
320.000 C*****INCREMENTAL STRESSES
```

```
321.000 C
322.000         E(IAB+300)=BSIG(1,1)-E(IAB)
323.000         E(IAB+301)=BSIG(1,2)-E(IAB+1)
324.000         E(IAB+302)=BSIG(2,1)-E(IAB+2)
325.000         E(IAB+303)=BSIG(2,2)-E(IAB+3)
326.000         E(IAB+305)=SN-E(IAB+5)
327.000         E(IAB+306)=ST-E(IAB+6)
328.000         IF (E(IAB+305)) 1320,1330,1320
329.000 1320     E(IAB+309)=E(IAB+306)/E(IAB+305)
330.000 1330     E(IAB+333)=SI-E(IAB+33)
331.000         E(IAB+334)=SII-E(IAB+34)
332.000         IF (E(IAB+333)) 1340,1350,1340
333.000 1340     E(IAB+304)=E(IAB+334)/E(IAB+333)
334.000 1350     E(IAB+307)=PDI-E(IAB+7)
335.000         E(IAB+308)=PDII-E(IAB+8)
336.000 C
337.000 C*****CURRENT STRESS DATA
338.000 C
339.000         E(IAB)=BSIG(1,1)
340.000         E(IAB+1)=BSIG(1,2)
341.000         E(IAB+2)=BSIG(2,1)
342.000         E(IAB+3)=BSIG(2,2)
343.000         E(IAB+5)=SN
344.000         E(IAB+6)=ST
345.000         E(IAB+7)=PDI
346.000         E(IAB+8)=PDII
347.000 1360     IF (SN) 1370,1380,1370
348.000 1370     E(IAB+9)=ST/SN
349.000 1380     IF (SI) 1390,1400,1390
350.000 1390     E(IAB+4)=SII/SI
351.000 1400     CONTINUE
352.000         E(IAB+33)=SI
353.000         E(IAB+34)=SII
354.000 C
355.000 C*****SUB-ASSEMBLY BOUNDARY STRAINS
356.000 C
357.000 1410     CONTINUE
358.000         CALL STRAIN2
359.000 C
360.000 C*****CURRENT STRAINS
361.000 C
362.000         EN=EIJB(1,1)+EIJB(2,2)
363.000         ET=SQRT((EIJB(1,1)-EIJB(2,2))**2+(EIJB(1,2)+EIJB(2,1))**2)
364.000         EI=0.5*(EN+ET)
365.000         EII=0.5*(EN-ET)
366.000         EW=EIJB(2,1)-EIJB(1,2)
367.000         EV=(AREA-AREAI)/AREAI
368.000         PDI=0.5*ATAN2(EIJB(1,2)+EIJB(2,1),EIJB(1,1)-EIJB(2,2))
369.000         IF (PDI.LT.0.) PDI=PI+PDI
370.000         IF (PDI.GT.PI) PDI=PDI-PI
371.000         PDII=PDI+PI/2.
372.000         IF (PDII.GT.PI) PDII=PDII-PI
373.000 C
374.000 C*****INCREMENTAL STRAINS
375.000 C
376.000         E(IAB+310)=EIJB(1,1)-E(IAB+10)
377.000         E(IAB+311)=EIJB(1,2)-E(IAB+11)
378.000         E(IAB+312)=EIJB(2,1)-E(IAB+12)
379.000         E(IAB+313)=EIJB(2,2)-E(IAB+13)
380.000         E(IAB+314)=EN-E(IAB+14)
381.000         E(IAB+315)=ET-E(IAB+15)
382.000         E(IAB+316)=EW-E(IAB+16)
383.000         E(IAB+335)=EI-E(IAB+35)
384.000         E(IAB+336)=EII-E(IAB+36)
385.000         IF (E(IAB+315)) 1420,1430,1420
386.000 1420     E(IAB+337)=ABS(E(IAB+314)/E(IAB+315))
387.000 1430     E(IAB+319)=PDI-E(IAB+19)
388.000         E(IAB+320)=PDII-E(IAB+20)
389.000         IF (E(IAB+336)) 1440,1450,1440
390.000 1440     E(IAB+317)=E(IAB+335)/E(IAB+336)
391.000 1450     E(IAB+318)=EV-E(IAB+18)
392.000 C
393.000 C*****LOAD CURRENT STRAINS
394.000 C
395.000         E(IAB+10)=EIJB(1,1)
396.000         E(IAB+11)=EIJB(1,2)
397.000         E(IAB+12)=EIJB(2,1)
398.000         E(IAB+13)=EIJB(2,2)
399.000         E(IAB+14)=EN
400.000         E(IAB+15)=ET
```

```
401.000         E(IAB+16)=EW
402.000         E(IAB+18)=EV
403.000         IF (EII) 1460,1470,1460
404.000 1460     E(IAB+17)=EI/EII
405.000 1470     E(IAB+19)=PDI
406.000         E(IAB+20)=PDII
407.000         IF (ET) 1480,1490,1480
408.000 1480     E(IAB+37)=ABS(EN/ET)
409.000 1490     E(IAB+35)=EI
410.000         E(IAB+36)=EII
411.000         IPOINT=IPOINT+5+NBI*3
412.000 C
413.000 C*****FABRIC AND FORCE DATA FOR SUBASSEMBLY AREAS
414.000 C
415.000         E(IAB+21)=NBT
416.000         E(IAB+40)=NBC
417.000         E(IAB+41)=NB
418.000         IF ((NBT-NB-NFB).EQ.0.)GOTO 1500
419.000         E(IAB+42)=FLOAT(NBC)/(NBT-NB-NFB)
420.000 1500     E(IAB+43)=PI*RCR(IC)*RCR(IC)
421.000         E(IAB+44)=DNSTY
422.000         E(IAB+45)=NCS*2/AREA
423.000 C
424.000         CALL FORCE
425.000         CALL MICROFEATURES
426.000 C
427.000         E(IAB+46)=FX
428.000         E(IAB+47)=FY
429.000         E(IAB+48)=MO
430.000         E(IAB+49)=FBMAX
431.000         E(IAB+50)=MOMAX
432.000         E(IAB+51)=VBMAX
433.000         E(IAB+52)=FBAVG
434.000         E(IAB+53)=MOAVG
435.000         E(IAB+54)=VBAVG
436.000         E(IAB+55)=FNMAX
437.000         E(IAB+56)=FNAVG
438.000         E(IAB+57)=FSMAX
439.000         E(IAB+58)=FSAVG
440.000         E(IAB+59)=FCMAX
441.000         E(IAB+60)=FCAVG
442.000         E(IAB+61)=FNMIN
443.000         E(IAB+62)=FSMIN
444.000         E(IAB+63)=NR
445.000         E(IAB+64)=DAVG
446.000 C
447.000 C*****CONTACT ORIENTATION DISTRIBUTION FUNCTION PARAMETERS
448.000 C
449.000         E(IAB+65)=AA
450.000         E(IAB+66)=BB
451.000         E(IAB+67)=AA0
452.000         E(IAB+68)=BB0
453.000 C
454.000 C*****AVERAGE NORMAL FORCE DISTRIBUTON FUNCTION PARAMETERS
455.000 C
456.000         E(IAB+69)=FNAA
457.000         E(IAB+70)=FNBB
458.000         E(IAB+71)=FNAA0
459.000         E(IAB+72)=FNBB0
460.000 C
461.000 C*****AVERAGE SHEAR FORCE DISTRIBUTION FUNCTION PARAMETERS
462.000 C
463.000         E(IAB+73)=AU
464.000         E(IAB+74)=AW
465.000         E(IAB+76)=FSAA0
466.000 C
467.000 C*****AVERAGE CONTACT LENGTH DISTRIBUTION FUNCTION PARAMETERS
468.000 C
469.000         E(IAB+78)=DAA
470.000         E(IAB+79)=DBB
471.000         E(IAB+80)=DAAO
472.000         E(IAB+81)=DBBO
473.000 C
474.000 C*****HISTOGRAM OF CONTACT ORIENTATIONS
475.000 C
476.000         IAB=IAB+90
477.000         DO 1510 I=1,36
478.000           E(IAB)=NCI(I)
479.000 1510     IAB=IAB+1
480.000 C
```

```
481.000 C*****HISTOGRAM OF AVERAGE NORMAL FORCES WRT ORIENTATION
482.000 C
483.000       DO 1520 I=1,36
484.000         E(IAB)=FNA(I)
485.000 1520   IAB=IAB+1
486.000 C
487.000 C*****HISTOGRAM OF AVERAGE SHEAR FORCES WRT ORIENTATION
488.000 C
489.000       DO 1530 I=1,36
490.000         E(IAB)=FSA(I)
491.000 1530   IAB=IAB+1
492.000 C
493.000 C*****HISTOGRAM OF AVERAGE CONTACT LENGTH WRT ORIENTATION
494.000 C
495.000       DO 1540 I=1,36
496.000         E(IAB)=DCA(I)
497.000 1540   IAB=IAB+1
498.000 C
499.000 C*****HISTOGRAM OF NORMAL FORCES
500.000 C
501.000       DO 1550 I=1,20
502.000         E(IAB)=NFN(I)
503.000 1550   IAB=IAB+1
504.000 C
505.000 C*****HISTOGRAM OF SHEAR FORCES
506.000 C
507.000       DO 1560 I=1,20
508.000         E(IAB)=NFS(I)
509.000 1560   IAB=IAB+1
510.000 C
511.000 1570  CONTINUE
512.000 C
513.000 C*****DUMP E ARRAY TO BINARY FILE
514.000 C
515.000      WRITE (15,KEY=EKEY,ERR=1580) (E(I),I=1,10000)
516.000      EKEY=EKEY+1000
517.000 C
518.000 1580  DO 1590 I=1,121
519.000 1590  A(I)=E(I)
520.000 C
521.000      RETURN
522.000      END
```

```
1.000 C
2.000      SUBROUTINE BNDFORD
3.000 C
4.000 C*****PROGRAM APPLIES FORCES TO BOUNDARY DISCS TO GIVE
5.000 C    PRESCRIBED BOUNDARY STRESS TENSOR "BSIG(2,2)"
6.000 C    IAB= CURRENT ADDRESS OF BOUNDARY DISC
7.000 C    IABL=ADDRESS OF BOUNDARY DISC AT CLOCKWISE LOCATION TO
8.000 C        CURRENT BOUNDARY DISC
9.000 C
10.000      COMMON /ARAY/ A(108910)
11.000      COMMON /BDAT/ R(50)
12.000      COMMON /BBAL/ BBALL(1000),NBB
13.000      COMMON /MOD/ EBVEL(2,2),SGAIN,BSTR(2,2)
14.000      LOGICAL BPASS,LGAP
15.000 C
16.000      BPASS=.FALSE.
17.000 C
18.000 C*****APPLY BALANCED FORCES AND MOMENTS TO BOUNDARY DISCS
19.000 C
20.000      BBALL(NBB+1)=BBALL(1)
21.000      DO 1050 I=1,NBB+1
22.000        LGAP=.FALSE.
23.000        IF (I.EQ.1) IABL=BBALL(NBB);GOTO 1000
24.000        IABL=BBALL(I-1)
25.000 1000    IAB=BBALL(I)
26.000 C
27.000        XDIF=A(IAB)-A(IABL)
28.000        YDIF=A(IAB+1)-A(IABL+1)
29.000        Z=SQRT(XDIF*XDIF+YDIF*YDIF)
30.000        ST=YDIF/Z
31.000        CT=XDIF/Z
32.000        ITYP=A(IAB+9)
33.000        ITYPL=A(IABL+9)
34.000        GAP=Z-R(ITYP)-R(ITYPL)
35.000        GAP2=.5*GAP
36.000        IF (GAP.LE.0.) LGAP=.TRUE.;GOTO 1010
```

```
37.000          XP=A(IABL)+R(ITYPL)*CT
38.000          YP=A(IABL+1)+R(ITYPL)*ST
39.000          XQ=A(IAB)-R(ITYP)*CT
40.000          YQ=A(IAB+1)-R(ITYP)*ST
41.000          GOTO 1020
42.000 1010      RG2=R(ITYPL)+GAP2
43.000          XP=A(IABL)+RG2*CT
44.000          YP=A(IABL+1)+RG2*ST
45.000          XQ=XP
46.000          YQ=YP
47.000 C
48.000 1020      IF (BPASS)GOTO 1030
49.000          BPASS=.TRUE.
50.000          GOTO 1040
51.000 C
52.000 C*****INTERIOR BOUNDARY SEGMENT
53.000 C
54.000 1030      XDIF=XP-XPO
55.000          YDIF=YP-YPO
56.000          F1=BSTR(1,1)*YDIF-BSTR(1,2)*XDIF
57.000          F2=BSTR(2,1)*YDIF-BSTR(2,2)*XDIF
58.000          A(IABL+5)=A(IABL+5)+F1
59.000          A(IABL+6)=A(IABL+6)+F2
60.000          XAV=0.5*(XP+XPO)
61.000          YAV=0.5*(YP+YPO)
62.000          A(IABL+7)=A(IABL+7)-F1*(YAV-A(IABL+1))+F2*(XAV-A(IABL))
63.000          IF (LGAP)GOTO 1040
64.000 C
65.000 C*****BOUNDARY SEGMENT SPANNING DISCS
66.000 C
67.000          XDIF=XQ-XP
68.000          YDIF=YQ-YP
69.000          F1=BSTR(1,1)*YDIF-BSTR(1,2)*XDIF
70.000          F2=BSTR(2,1)*YDIF-BSTR(2,2)*XDIF
71.000          RATL=(R(ITYP)+GAP2)/Z
72.000          RAT=(R(ITYPL)+GAP2)/Z
73.000          A(IABL+5)=A(IABL+5)+F1*RATL
74.000          A(IABL+6)=A(IABL+6)+F2*RATL
75.000          A(IAB+5)=A(IAB+5)+F1*RAT
76.000          A(IAB+6)=A(IAB+6)+F2*RAT
77.000 1040      XPO=XQ
78.000          YPO=YQ
79.000 1050  CONTINUE
80.000 C
81.000       RETURN
82.000       END


1.000 C
2.000       SUBROUTINE ERROR(NO,IAB)
3.000 C
4.000 C*****PROGRAM IDENTIFIES ERROR ASSOCIATED WITH PROGRAM CRASH
5.000 C
6.000 C     NO= ERROR NUMBER
7.000 C     IAB=BALL ADDRESS
8.000 C
9.000       COMMON /ARAY/ A(108910)
10.000       GLOBAL NN,NR
11.000 C
12.000 C*****OPEN ERROR FILE
13.000 C
14.000       OPEN (20,NAME="ERR",STATUS='NEW',FORM='FORMATTED')
15.000       GO TO (1000,1010)NO
16.000 C
17.000 C*****CONTACT MEMORY PARTITION EXCEEDED
18.000 C
19.000 1000  WRITE (20,9000)
20.000       GOTO 1020
21.000 C
22.000 C*****BALL OUT OF ASSEMBLY AREA
23.000 C
24.000 1010  WRITE (20,9010)
25.000       X=A(IAB)+A(IAB+11)
26.000       Y=A(IAB+1)+A(IAB+12)
27.000       VX=A(IAB+4)
28.000       VY=A(IAB+5)
29.000       V=SQRT(VX*VX+VY*VY)
30.000       WRITE (20,9020) IAB
31.000       WRITE (20,9030) X
32.000       WRITE (20,9040) Y
```

```
33.000       WRITE (20,9050) V
34.000 C
35.000 1020  WRITE (20,9060) NN
36.000       WRITE (20,9070) NR
37.000 C
38.000       CLOSE (20,STATUS='KEEP')
39.000       STOP
40.000 9000  FORMAT(/,1X,'MEMORY PARTITION EXCEEDED')
41.000 9010  FORMAT(/,1X,'BALL OUT OF ASSEMBLY AREA')
42.000 9020  FORMAT(1X,'BALL ADDRESS= ',I6)
43.000 9030  FORMAT(1X,'X COORDINATE OF BALL= ',E12.6)
44.000 9040  FORMAT(1X,'Y COORDINATE OF BALL= ',E12.6)
45.000 9050  FORMAT(1X,'BALL VELOCITY      = ',E12.6)
46.000 9060  FORMAT(  1X,'NUMBER OF ACTIVE CYCLES= ',I6)
47.000 9070  FORMAT(  1X,'NUMBER OF RELAXATION CYCLES= ',I6)
48.000       END

1.000 C
2.000      SUBROUTINE CHECK(IAB,NB)
3.000 C
4.000 C*****PROGRAM CHECKS THAT THERE IS AT LEAST ONE ENTRY FOR DISC IAB
5.000 C     IN CONTACT LIST FOR BOX NB
6.000 C     IF NOT- ENTRY IS ADDED
7.000 C
8.000       COMMON /ARAY/ A(108910)
9.000 C
10.000 C*****CHECK FOR SINGLE DISC ENTRIES IN BOX NB
11.000 C
12.000      IAD=A(NB)
13.000 1000  IB1=A(IAD)
14.000      IF (IB1) 1020,1050,1010
15.000 1010  IB2=A(IAD+1)
16.000      IF (IB1.EQ.IAB.OR.IB2.EQ.IAB) RETURN
17.000      IAD=IAD+6
18.000      GOTO 1000
19.000 C
20.000 C*****CONTINUE SEARCH IN LIST OF SINGLE DISC ENTRIES
21.000 C
22.000 1020  IB1=-IB1
23.000 1030  IF (IB1.EQ.IAB) RETURN
24.000      IAD=IAD+1
25.000      IB1=A(IAD)
26.000      IF (IB1.EQ.0)GOTO 1040
27.000      GOTO 1030
28.000 C
29.000 C*****ADD NON-CONTACTING DISC ENTRY TO LIST
30.000 C
31.000 1040  A(IAD)=IAB
32.000      RETURN
33.000 1050  A(IAD)=-IAB
34.000      RETURN
35.000      END

1.000 C
2.000      SUBROUTINE SEARCH
3.000 C
4.000 C*****SUBROUTINE IDENTIFIES ADDRESSES OF DISCS
5.000 C*****MAPPING INTO BOXES STORED IN ARRAY NBSAV
6.000 C
7.000 C       NBSAV=BOX ADDRESSES
8.000 C       NBMAP=NUMBER OF BOXES
9.000 C       IBSAV=ARRAY OF DISC ADDRESSES MAPPING INTO BOXES
10.000 C       NBB=  NUMBER OF DISCS IN SCANNED BOXES
11.000 C       ITAG¿1 (TEMPORARILY IDENTIFIES DISC AS INCLUDED IN ARRAY
12.000 C            IBSAV)
13.000 C       COMPILE X STATEMENTS TO ACTIVATE DEBUGGER
14.000 C
15.000      COMMON /ARAY/ A(108910)
16.000      COMMON /SRCH/ NBSAV(2000),NBMAP,IBSAV(2000),NBB
17.000      GLOBAL NCBOX
18.000 C
19.000      NBB=0
20.000      DO 1110 I=1,NBMAP
21.000        IAD=A(NBSAV(I))
22.000 X       ICEND=IAD+NCBOX*6-1
23.000 C
24.000 1000    CONTINUE
25.000 X       IF (IAD.GT.ICEND) CALL ERROR(1,0)
26.000         IB1=A(IAD)
```

```
27.000          IB2=A(IAD+1)
28.000          IF (IB1) 1060,1110,1010
29.000 1010      ITAG=A(IB1+8)
30.000          IF (ITAG-1) 1020,1020,1030
31.000 1020      NBB=NBB+1
32.000          IBSAV(NBB)=IB1
33.000          A(IB1+8)=A(IB1+8)+2
34.000 1030      ITAG=A(IB2+8)
35.000          IF (ITAG-1) 1040,1040,1050
36.000 1040      NBB=NBB+1
37.000          IBSAV(NBB)=IB2
38.000          A(IB2+8)=A(IB2+8)+2
39.000 1050      IAD=IAD+6
40.000          GOTO 1000
41.000 C
42.000 1060      IF (IB1) 1070,1110,1080
43.000 1070      IB1=-IB1
44.000 1080      ITAG=A(IB1+8)
45.000          IF (ITAG-1) 1090,1090,1100
46.000 1090      NBB=NBB+1
47.000          IBSAV(NBB)=IB1
48.000          A(IB1+8)=A(IB1+8)+2
49.000 1100      IAD=IAD+1
50.000 X         IF (IAD.GE.ICEND) CALL ERROR(1,0)
51.000          IB1=A(IAD)
52.000          GOTO 1060
53.000 1110  CONTINUE
54.000 C
55.000 C*****RESET TAGS
56.000 C
57.000       DO 1120 I=1,NBB
58.000 1120  A(IBSAV(I)+8)=A(IBSAV(I)+8)-2
59.000 C
60.000       RETURN
61.000       END


1.000 C
2.000       SUBROUTINE BTEST(IB1,IB2)
3.000 C
4.000 C*****PROGRAM TESTS FOR DISC-DISC CONTACT
5.000 C     IF CONTACT EXISTS, BOX CONTACT MAPS INTO IS DETERMINED
6.000 C     AND BOX CONTACT LIST IS UPDATED AS REQUIRED
7.000 C
8.000       COMMON /ARAY/ A(108910)
9.000       COMMON /BDAT/ R(50)
10.000       GLOBAL TOL,M1,DEL,NX
11.000 C
12.000       ITYP1=A(IB1+9)
13.000       ITYP2=A(IB2+9)
14.000       R1=R(ITYP1)
15.000       R2=R(ITYP2)
16.000       X=A(IB2)+A(IB2+11)
17.000       Y=A(IB2+1)+A(IB2+12)
18.000       XDIF=A(IB1)+A(IB1+11)-X
19.000       YDIF=A(IB1+1)+A(IB1+12)-Y
20.000       D=SQRT(XDIF*XDIF+YDIF*YDIF)
21.000       GAP=D-R1-R2
22.000       TOUCH=GAP-TOL
23.000       IF (TOUCH.GT.0.0) RETURN
24.000 C
25.000 C*****BOX CONTACT MAPS INTO
26.000 C
27.000       RAT=(R2+GAP/2.0)/D
28.000       XC=X+XDIF*RAT
29.000       YC=Y+YDIF*RAT
30.000       NB=IFIX(XC/DEL)+IFIX(YC/DEL)*NX+M1
31.000 C
32.000 C*****UPDATE CONTACT LIST FOR BOX NB IF REQUIRED
33.000 C
34.000       CALL UPDATE(IB1,IB2,NB)
35.000 C
36.000       RETURN
37.000       END
```

```
1.000 C
2.000       SUBROUTINE DISCCHECK
3.000 C
4.000 C*****PROGRAM FINDS BOX CONTACT LIST WITH MAXIMUM USED STORAGE
5.000 C     AND MAXIMUM NUMBER OF CONTACTS/BOX
6.000 C
7.000       COMMON /ARAY/ A(108910)
8.000       COMMON /CHCK/ NBMAX,KMAX,NCMAX
9.000       GLOBAL NBOX,M1,NCBOX
10.000 C
11.000       KMAX=NCMAX=0
12.000       DO 1060 NB=M1,NBOX+M1-1
13.000         KOUNT=0
14.000         IAB=A(NB)
15.000         ICEND=IAB+NCBOX*6-1
16.000 1000     CONTINUE
17.000         NCMAX=AMAX0(NCMAX,KOUNT)
18.000         IF (A(IAB)) 1020,1050,1010
19.000 1010     KOUNT=KOUNT+1
20.000         IF (IAB.GT.ICEND) CALL ERROR(1,0)
21.000         IAB=IAB+6
22.000         GOTO 1000
23.000 1020     KOUNT=KOUNT*6
24.000 1030     KOUNT=KOUNT+1
25.000         IAB=IAB+1
26.000         IF (A(IAB)) 1050,1050,1040
27.000 1040     IF (IAB.GT.ICEND) CALL ERROR(1,0)
28.000         GOTO 1030
29.000 1050     CONTINUE
30.000         IF (KOUNT.GT.KMAX) NBMAX=NB-M1+1
31.000         KMAX=AMAX0(KOUNT,KMAX)
32.000 1060   CONTINUE
33.000 C
34.000       RETURN
35.000       END


1.000 C
2.000       SUBROUTINE STRAIN(IPOINT)
3.000 C
4.000 C*****PROGRAM CALCULATES INCREMENTAL STRAIN TENSOR VALUES
5.000 C     (For total and sub-assemblies)
6.000 C
7.000       COMMON /ARAY/ A(108910)
8.000       COMMON /ERAY/ E(10000)
9.000       COMMON /STRN/ EIJB(2,2),NBI,AREAI
10.000       COMMON /BBAL/ BBALL(1000),NB,AREA
11.000       REAL MIDX,MIDY,MIDY2
12.000       DATA SUM11/0./ SUM12/0./ SUM21/0./ SUM22/0./ AREA/0./
13.000 C
14.000 C*****NOTES:
15.000 C
16.000 C       1) AREAI=    initial area formed by boundary discs
17.000 C       2) AREA =    current area formed by SAME initial
18.000 C                  boundary discs
19.000 C       3) NBI  =    initial number of boundary discs
20.000 C
21.000       IAD=IPOINT
22.000       NBI=E(IAD)
23.000       AREAI=E(IAD+1)
24.000       IAD=IAD+2
25.000 C
26.000       DO 1020 I=1,NBI
27.000         IB1=E(IAD)
28.000         XS1=E(IAD+1)
29.000         YS1=E(IAD+2)
30.000         XF1=A(IB1)+A(IB1+11)
31.000         YF1=A(IB1+1)+A(IB1+12)
32.000         IF (I.EQ.NBI)GOTO 1000
33.000         XS2=E(IAD+4)
34.000         YS2=E(IAD+5)
35.000         IB2=E(IAD+3)
36.000         XF2=A(IB2)+A(IB2+11)
37.000         YF2=A(IB2+1)+A(IB2+12)
38.000         GOTO 1010
39.000 1000     IAD=IPOINT+2
40.000         XS2=E(IAD+1)
41.000         YS2=E(IAD+2)
42.000         IB2=E(IAD)
43.000         XF2=A(IB2)+A(IB2+11)
```

```
44.000         YF2=A(IB2+1)+A(IB2+12)
45.000 1010     CONTINUE
46.000 C
47.000         DX=(XS1-XF1+XF2-XS2)
48.000         DY=(YS1-YF1+YF2-YS2)
49.000         MIDX=(XS1+XF1+XF2+XS2)/4.
50.000         MIDY=(YS1+YF1+YS2+YF2)/4.
51.000         SUM11=SUM11-DX*MIDY
52.000         SUM12=SUM12+DX*MIDX
53.000         SUM21=SUM21-DY*MIDY
54.000         SUM22=SUM22+DY*MIDX
55.000 C
56.000         DX2=XF2-XF1
57.000         MIDY2=(YF2+YF1)/2.
58.000         PART=-MIDY2*DX2
59.000         AREA=PART+AREA
60.000 C
61.000 1020  IAD=IAD+3
62.000       VOL=(AREA+AREAI)/2.
63.000       EIJB(1,1)=SUM11/VOL
64.000       EIJB(1,2)=SUM12/VOL
65.000       EIJB(2,1)=SUM21/VOL
66.000       EIJB(2,2)=SUM22/VOL
67.000 C
68.000       RETURN
69.000       END
```

```
1.000 C
2.000       SUBROUTINE DISCDENS
3.000 C
4.000 C*****PROGRAM CALCULATES DENSITY OF ASSEMBLY OR SUB-ASSEMBLY
5.000 C
6.000       COMMON /ARAY/ A(108910)
7.000       COMMON /BDAT/ R(50)
8.000       COMMON /BBAL/ BBALL(1000),NB,AREA
9.000       COMMON /CIRC/ IBCIRC(2000),NBT
10.000       GLOBAL DNSTY,PI
11.000       DATA SUM/0./
12.000 C
13.000       DO 1020 I=1,NBT
14.000         IAB=IBCIRC(I)
15.000         ITYP=A(IAB+9)
16.000         RAD=R(ITYP)
17.000         IF (A(IAB+8).EQ.1)GOTO 1000
18.000         GOTO 1010
19.000 1000     SUM=SUM+0.5*PI*RAD*RAD
20.000         GOTO 1020
21.000 1010     SUM=SUM+PI*RAD*RAD
22.000 1020  CONTINUE
23.000 C
24.000       IF (AREA.EQ.0.0) DNSTY=0.0; RETURN
25.000       DNSTY=SUM/AREA
26.000 C
27.000       RETURN
28.000       END
```

```
1.000 C
2.000       SUBROUTINE DISCNCTS
3.000 C
4.000 C*****PROGRAM DETERMINES:
5.000 C
6.000 C        1) No. of PHYSICAL stressed contacts over entire assembly
7.000 C           =NCS
8.000 C           (Does not include contacts between two(2) boundary discs)
9.000 C        2) Determines contact addresses of stressed contacts
10.000 C             ICONT(NCS)
11.000 C        3) NBC= Contact number
12.000 C        4) NCS= Number of PHYSICAL contacts
13.000 C
14.000       COMMON /ARAY/ A(108910)
15.000       COMMON /CIRC/ IBCIRC(2000),NBT,ICONT(4000),NCS,NBC
16.000       DATA  NBC/0/
17.000 C
18.000       N=NCS
19.000       NCS=0
20.000       DO 1020 I=1,N
21.000         IAB=ICONT(I)
22.000         IB1=A(IAB)
23.000         IB2=A(IAB+1)
```

```
24.000         FN=ABS(A(IAB+4))
25.000         FS=ABS(A(IAB+5))
26.000         IF (FN+FS) 1020,1020,1000
27.000 1000     IF ((A(IB1+8)+A(IB2+8)).EQ.2.0)GOTO 1020
28.000         IF (A(IB1+8).EQ.1.OR.A(IB2+8).EQ.1) NBC=NBC+1;GOTO 1010
29.000         NBC=NBC+2
30.000 1010     NCS=NCS+1
31.000         ICONT(NCS)=IAB
32.000 1020   CONTINUE
33.000 C
34.000       RETURN
35.000       END


1.000 C
2.000       SUBROUTINE NPDISC
3.000 C
4.000 C*****PROGRAM DETERMINES NUMBER OF DISCS WHICH ARE UNLOADED
5.000 C     (Does not include boundary discs)
6.000 C
7.000       DIMENSION NBSAV(10)
8.000       COMMON /ARAY/ A(108910)
9.000       COMMON /BDAT/ R(50)
10.000       COMMON /CIRC/ IBCIRC(2000),NBT,ICONT(4000),NCS,NBC,NPB
11.000       GLOBAL DEL,NX,NY,TOL,M1
12.000       DATA NPB/0/
13.000 C
14.000       DO 1090 I=1,NBT
15.000         IAB=IBCIRC(I)
16.000         ITAG=A(IAB+8)
17.000         IF (ITAG-1) 1000,1090,1090
18.000 1000     IBTYP=A(IAB+9)
19.000         RT=R(IBTYP)+TOL
20.000         X=A(IAB)+A(IAB+11)
21.000         Y=A(IAB+1)+A(IAB+12)
22.000 C
23.000 C*****TO DETERMINE BOXES THAT DISC MAPS INTO (SEARCH RADIUS= RAD+TOL)
24.000 C
25.000         NXL=IFIX((X-RT)/DEL)
26.000         NXU=IFIX((X+RT)/DEL)
27.000         IF ((X+RT).GT.(NX*DEL)) NXU=NXU-1
28.000         NYL=IFIX((Y-RT)/DEL)
29.000         NYU=IFIX((Y+RT)/DEL)
30.000         IF ((Y+RT).GT.(NY*DEL)) NYU=NYU-1
31.000 C
32.000         NBMAP=0
33.000         DO 1030 NYY=NYL,NYU
34.000           NA=NYY*NX
35.000           DO 1030 NXX=NXL,NXU
36.000             NB=NA+NXX+M1
37.000             IF (NBMAP.EQ.0)GOTO 1020
38.000             DO 1010 N=1,NBMAP
39.000               IF (NBSAV(N).EQ.NB)GOTO 1030
40.000 1010          CONTINUE
41.000 1020          NBMAP=NBMAP+1
42.000             NBSAV(NBMAP)=NB
43.000 1030     CONTINUE
44.000 C
45.000         DO 1080 J=1,NBMAP
46.000           IAD=A(NBSAV(J))
47.000 1040        IB1=A(IAD)
48.000           IF (IB1) 1080,1080,1050
49.000 1050        FN=A(IAD+4)
50.000           IF (FN) 1070,1070,1060
51.000 1060        IF (IB1.EQ.IAB)GOTO 1090
52.000           IB2=A(IAD+1)
53.000           IF (IB2.EQ.IAB)GOTO 1090
54.000 1070        IAD=IAD+6
55.000           GOTO 1040
56.000 1080     CONTINUE
57.000 C
58.000         NPB=NPB+1
59.000 1090   CONTINUE
60.000 C
61.000       RETURN
62.000       END
```

```
1.000 C
2.000       SUBROUTINE FORCE
3.000 C
4.000 C*****PROGRAM CALCULATES FOR ENTIRE ASSEMBLY AND SUB-ASSEMBLIES:
5.000 C
6.000 C         1) OUT-OF-BALANCE forces and moments
7.000 C            (FX,FY,MO)
8.000 C         2) Maximum and average disc forces,moments and velocities
9.000 C            (FBMAX,FBAVG,MOMAX,MOAVG,VBMAX,VBAVG)
10.000 C         3) MAX,MIN and AVERAGE normal and shear contact forces
11.000 C            (FNMAX,FNMIN,FSMAX,FSMIN,FNAVG,FSAVG)
12.000 C         4) MAX and AVERAGE resultant contact forces (FCMAX,FCAVG)
13.000 C         5) NORMAL and SHEAR force FREQUENCY DISTRIBUTIONS
14.000 C            (NFN(20),NFS(20))
15.000 C         6) Average contact length (ie average disc centre to contact
16.000 C            distance DAVG)
17.000 C
18.000       COMMON /ARAY/ A(108910)
19.000       COMMON /BALF/ FX,FY,MO,FBMAX,MOMAX,VBMAX,FBAVG,MOAVG,VBAVG
20.000       COMMON /CIRC/ IBCIRC(2000),NBT,ICONT(4000),NCS,NBC
21.000       COMMON /CONF/ FNMAX,FNMIN,FNAVG,FSMAX,FSMIN,FSAVG,FCMAX,FCAVG,DAVG
22.000       COMMON /HIST/ NFN(20),NFS(20)
23.000       COMMON /BDAT/ R(50)
24.000       REAL MO,MOAVG,MOMAX,MOSUM,MBO
25.000 C
26.000 C*****INITIALIZATION
27.000 C
28.000       FX=FY=MO=FBMAX=MOMAX=VBMAX=FNMAX=FSMAX=FNSUM=FSSUM=MOSUM=0.0
29.000       VBSUM=FBSUM=FCSUM=FCMAX=DAVG=DSUM=0.0
30.000       FNMIN=FSMIN=1.0E+20
31.000 C
32.000       DO 1000 I=1,20
33.000 1000  NFN(I)=NFS(I)=0
34.000 C
35.000 C*****OUT-OF-BALANCE DISC FORCES, MOMENT AND VELOCITIES
36.000 C     (Do not include boundary discs)
37.000 C
38.000       DO 1010 I=1,NBT
39.000         IAB=IBCIRC(I)
40.000         IF (A(IAB+8).EQ.1)GOTO 1010
41.000         VX=A(IAB+2)
42.000         VY=A(IAB+3)
43.000         FBX=A(IAB+5)
44.000         FBY=A(IAB+6)
45.000         MBO=A(IAB+7)
46.000         FX=FX+FBX
47.000         FY=FY+FBY
48.000         MO=MO+MBO
49.000         VB=SQRT(VX*VX+VY*VY)
50.000         FB=SQRT(FBX*FBX+FBY*FBY)
51.000         VBMAX=AMAX1(VB,VBMAX)
52.000         FBMAX=AMAX1(FB,FBMAX)
53.000         MOMAX=AMAX1(ABS(MBO),MOMAX)
54.000         MOSUM=MOSUM+ABS(MBO)
55.000         VBSUM=VBSUM+VB
56.000 1010  FBSUM=FBSUM+FB
57.000       FBAVG=FBSUM/NBT
58.000       VBAVG=VBSUM/NBT
59.000       MOAVG=MOSUM/NBT
60.000 C
61.000 C*****MAX,MIN AND AVERAGE NORMAL,SHEAR AND RESULTANT CONTACT FORCES
62.000 C     AVERAGE CONTACT LENGTH
63.000 C     (STRESSED CONTACTS ONLY)
64.000 C
65.000       IF (NCS.EQ.0) RETURN
66.000       DO 1040 I=1,NCS
67.000         IAB=ICONT(I)
68.000         KOUNT=2
69.000         FN=A(IAB+4)
70.000         FS=ABS(A(IAB+5))
71.000         FC=SQRT(FN*FN+FS*FS)
72.000         FNMAX=AMAX1(FNMAX,FN)
73.000         FNMIN=AMIN1(FNMIN,FN)
74.000         FSMAX=AMAX1(FSMAX,FS)
75.000         FSMIN=AMIN1(FSMIN,FS)
76.000         FCMAX=AMAX1(FCMAX,FC)
77.000         IB1=A(IAB)
78.000         IB2=A(IAB+1)
79.000         ITAG1=A(IB1+8)
80.000         ITAG2=A(IB2+8)
```

```
81.000          KOUNT=KOUNT-ITAG1-ITAG2
82.000          XDIF=A(IB1)+A(IB1+11)-A(IB2)-A(IB2+11)
83.000          YDIF=A(IB1+1)+A(IB1+12)-A(IB2+1)-A(IB2+12)
84.000          D=SQRT(XDIF*XDIF+YDIF*YDIF)
85.000          FNSUM=FNSUM+FN*KOUNT
86.000          FSSUM=FSSUM+FS*KOUNT
87.000          FCSUM=FCSUM+FC*KOUNT
88.000          L=ITAG1+ITAG2+1
89.000          GO TO (1030,1020,1040)L
90.000 1020       D=ITAG1*R(A(IB2+9))+ITAG2*R(A(IB1+9))
91.000 1030       DSUM=DSUM+D
92.000 1040   CONTINUE
93.000        FNAVG=FNSUM/NBC
94.000        FSAVG=FSSUM/NBC
95.000        FCAVG=FCSUM/NBC
96.000        DAVG=DSUM/NBC
97.000 C
98.000 C*****NORMAL AND SHEAR CONTACT FORCE FREQUENCY DISTRIBUTIONS(stressed
99.000 C     contacts only and 20 intervals)
100.000 C
101.000 C*****NORMAL FORCE
102.000 C
103.000       RANGE=FNMAX-FNMIN
104.000       STEP=RANGE/20
105.000       DO 1070 I=1,NCS
106.000         IAB=ICONT(I)
107.000         FN=A(IAB+4)
108.000         KOUNT=2
109.000         IB1=A(IAB)
110.000         IB2=A(IAB+1)
111.000         ITAG1=A(IB1+8)
112.000         ITAG2=A(IB2+8)
113.000         KOUNT=KOUNT-ITAG1-ITAG2
114.000 1050      START=FNMIN
115.000         DO 1060 J=1,20
116.000           END=START+STEP
117.000           IF (FN.GE.START.AND.FN.LT.END) NFN(J)=NFN(J)+KOUNT;GOTO 1070
118.000           IF (J.EQ.20.AND.FN.EQ.FNMAX) NFN(J)=NFN(J)+KOUNT;GOTO 1070
119.000 1060      START=END
120.000 1070  CONTINUE
121.000 C
122.000 C*****SHEAR FORCE
123.000 C
124.000       RANGE=FSMAX-FSMIN
125.000       STEP=RANGE/20
126.000       DO 1100 I=1,NCS
127.000         IAB=ICONT(I)
128.000         FS=ABS(A(IAB+5))
129.000         KOUNT=2
130.000         IB1=A(IAB)
131.000         IB2=A(IAB+1)
132.000         ITAG1=A(IB1+8)
133.000         ITAG2=A(IB2+8)
134.000         KOUNT=KOUNT-ITAG1-ITAG2
135.000 1080      START=FSMIN
136.000         DO 1090 J=1,20
137.000           END=START+STEP
138.000           IF (FS.GE.START.AND.FS.LT.END) NFS(J)=NFS(J)+KOUNT;GOTO 1100
139.000           IF (J.EQ.20.AND.FS.EQ.FSMAX) NFS(J)=NFS(J)+KOUNT;GOTO 1100
140.000 1090      START=END
141.000 1100  CONTINUE
142.000 C
143.000       RETURN
144.000       END


1.000 C
2.000       SUBROUTINE MICROFEATURES
3.000 C
4.000 C*****PROGRAM DETERMINES:
5.000 C
6.000 C     a) Contact normal orientation distribution over 36 increments
7.000 C        between 0 and PI for a given circle NCI(36)
8.000 C     b) Average normal contact force, average shear force values
9.000 C        and average contact vector length distributions over the
10.000 C         the orientation interval 0 to PI.
11.000 C         ie FNA(36),FSA(36),DCA(36)
12.000 C     c) Coefficient of anisotropy terms for 4'th-order distribution
13.000 C         functions ie AA,BB,FNAA,FNBB,FSAA,FSBB,AW,DAA,DBB
14.000 C     d) Principal directions ie THETA2,THETA4,FNTHETA2,
```

```
15.000 C       FNTHETA4,FSTHETA2,DTHETA2,DTHETA4
16.000 C     e) NOTE: Only stressed contacts considered
17.000 C
18.000       COMMON /ARAY/ A(108910)
19.000       COMMON /BDAT/ R(50)
20.000       COMMON /CIRC/ IBCIRC(2000),NBT,ICONT(4000),NCS,NBC
21.000       COMMON /CONF/ FNMAX,FNMIN,FNAVG,FSMAX,FSMIN,FSAVG,FCMAX,FCAVG,DAVG
22.000       COMMON /FABR/ NCI(36),FNA(36),FSA(36),DCA(36),AA,BB,THETA2,THETA4,
23.000      *FNAA,FNBB,FNTHETA2,FNTHETA4,AW,AU,FSTHETA2,DAA,DBB,DTHETA2,DTH
24.000      *ETA4
25.000       GLOBAL PI
26.000 C
27.000 C*****INITIALIZATION
28.000 C
29.000       DO 1000 I=1,36
30.000 1000  NCI(I)=FNA(I)=FSA(I)=DCA(I)=0.0
31.000 C
32.000       AA=BB=THETA2=THETA4=0.0
33.000       FNAA=FNBB=FNTHETA2=FNTHETA4=0.0
34.000       FSAA=FSBB=FSTHETA2=AU=AW=0.0
35.000       DAA=DBB=DTHETA2=DTHETA4=0.0
36.000       SUMAS=SUMAC=SUMBS=SUMBC=0.
37.000       SUMFNAS=SUMFNAC=SUMFNBS=SUMFNBC=0.
38.000       SUMFSAS=SUMFSAC=0.
39.000       SUMDAS=SUMDAC=SUMDBS=SUMDBC=0.
40.000       IF (NCS.EQ.0) RETURN
41.000 C
42.000 C*****CONTACT SEARCH
43.000 C
44.000       DO 1060 I=1,NCS
45.000         IAB=ICONT(I)
46.000         IB1=A(IAB)
47.000         IB2=A(IAB+1)
48.000         FN=A(IAB+4)
49.000         FS=A(IAB+5)
50.000         XDIF=A(IB2)+A(IB2+11)-A(IB1)-A(IB1+11)
51.000         YDIF=A(IB2+1)+A(IB2+12)-A(IB1+1)-A(IB1+12)
52.000         D=SQRT(XDIF*XDIF+YDIF*YDIF)
53.000         IF (XDIF*YDIF) 1020,1020,1010
54.000 1010      THETA=ACOS(ABS(XDIF)/D)
55.000         GOTO 1030
56.000 1020      THETA=PI-ACOS(ABS(XDIF)/D)
57.000 1030      ITAG1=A(IB1+8)
58.000         ITAG2=A(IB2+8)
59.000         KOUNT=2-ITAG1-ITAG2
60.000         ITYP1=A(IB1+9)
61.000         ITYP2=A(IB2+9)
62.000         D=R(ITYP1)+R(ITYP2)-ITAG1*R(ITYP1)-ITAG2*R(ITYP2)
63.000         SUMAS=SUMAS+SIN(2*THETA)*KOUNT
64.000         SUMAC=SUMAC+COS(2*THETA)*KOUNT
65.000         SUMBS=SUMBS+SIN(4*THETA)*KOUNT
66.000         SUMBC=SUMBC+COS(4*THETA)*KOUNT
67.000 C
68.000 C*****CONTRIBUTION OF CONTACT SHEAR FORCE TO AW TERM IN
69.000 C     CONTACT SHEAR FORCE DISTRIBUTION
70.000 C
71.000         AW=AW-KOUNT*FS
72.000 C
73.000 C*****CONTRIBUTION OF CONTACT TO CONTACT DISTRIBUTION HISTOGRAM
74.000 C
75.000         STEP=END=PI/36
76.000         START=0.0
77.000         DO 1040 J=1,36
78.000           END=START+STEP
79.000           IF (THETA.GE.START.AND.THETA.LT.END)GOTO 1050
80.000           IF (J.EQ.36.AND.THETA.EQ.PI)GOTO 1050
81.000 1040      START=END
82.000         GOTO 1060
83.000 1050      NCI(J)=NCI(J)+KOUNT
84.000         DCA(J)=DCA(J)+D
85.000         FNA(J)=FNA(J)+FN*KOUNT
86.000         FSA(J)=FSA(J)+FS*KOUNT
87.000 1060  CONTINUE
88.000 C
89.000 C*****CONTRIBUTION OF CONTACT TO NORMAL/SHEAR FORCE DISTRIBUTION
90.000 C     AND CONTACT LENGTH HISTOGRAM
91.000 C
92.000       DO 1080 J=1,36
93.000         IF (NCI(J)) 1080,1080,1070
94.000 1070      FNA(J)=FNA(J)/NCI(J)
```

```
95.000         FSA(J)=FSA(J)/NCI(J)
96.000         DCA(J)=DCA(J)/NCI(J)
97.000 1080  CONTINUE
98.000       AS=2*SUMAS/NBC
99.000       AC=2*SUMAC/NBC
100.000       BS=2*SUMBS/NBC
101.000       BC=2*SUMBC/NBC
102.000 C
103.000 C*****COEFFICIENT TERMS FOR FABRIC DISTRIBUTION FUNCTION
104.000 C
105.000 1090  CALL FS4(AS,AC,BS,BC,AA,BB,THETA2,THETA4)
106.000 C
107.000 C*****COEFFICIENT TERMS AND PRINCIPAL DIRECTIONS FOR AVERAGE NORMAL/
108.000 C     SHEAR FORCE DISTRIBUTION FUNCTIONS AND AVERAGE CONTACT LENGTH
109.000 C     DISTRIBUTION FUNCTION BASED ON 18 INTERVAL HISTOGRAM (0-2PI)
110.000 C
111.000       THETA1=0
112.000       FNSUM=0
113.000       DSUM=0
114.000       DO 1180 N=1,18
115.000 C
116.000         THETA22=THETA1+PI/18.
117.000         ANG=(THETA1+THETA22)/2
118.000         FNS=0
119.000         FSS=0
120.000         DSS=0
121.000         KT=0
122.000         DO 1150 I=1,NCS
123.000 C
124.000           IAB=ICONT(I)
125.000           IF (IAB) 1150,1150,1100
126.000 1100        FN=A(IAB+4)
127.000           FS=A(IAB+5)
128.000           IB1=A(IAB)
129.000           IB2=A(IAB-1)
130.000           XDIF=A(IB2)+A(IB2+11)-A(IB1)-A(IB1+11)
131.000           YDIF=A(IB2+1)+A(IB2+12)-A(IB1+1)-A(IB1+12)
132.000           D=SQRT(XDIF*XDIF+YDIF*YDIF)
133.000           IF (XDIF*YDIF) 1120,1120,1110
134.000 1110        THETA=ACOS(ABS(XDIF/D))
135.000           GOTO 1130
136.000 1120        THETA=PI-ACOS(ABS(XDIF/D))
137.000 1130        IF (THETA.GE.THETA1.AND.THETA.LT.THETA22)GOTO 1140
138.000           IF (N.EQ.18.AND.THETA.EQ.THETA22)GOTO 1140
139.000           GOTO 1150
140.000 C
141.000 1140        ITAG1=A(IB1+8)
142.000           ITAG2=A(IB2+8)
143.000           KOUNT=2-ITAG1-ITAG2
144.000           FNS=FN*KOUNT+FNS
145.000           FSS=FS*KOUNT+FSS
146.000           ITYP1=A(IB1+9)
147.000           ITYP2=A(IB2+9)
148.000           D=R(ITYP1)+R(ITYP2)-ITAG1*R(ITYP1)-ITAG2*R(ITYP2)
149.000           DSS=D+DSS
150.000           KT=KT+KOUNT
151.000           ICONT(I)=-ICONT(I)
152.000 C
153.000 1150     CONTINUE
154.000         IF (KT) 1170,1170,1160
155.000 1160     FNS=FNS/KT
156.000         FSS=FSS/KT
157.000         DSS=DSS/KT
158.000         FNSUM=FNSUM+FNS
159.000         DSUM=DSUM+DSS
160.000         SUMFNAS=SUMFNAS+FNS*SIN(2*ANG)
161.000         SUMFNAC=SUMFNAC+FNS*COS(2*ANG)
162.000         SUMFNBS=SUMFNBS+FNS*SIN(4*ANG)
163.000         SUMFNBC=SUMFNBC+FNS*COS(4*ANG)
164.000         SUMDAS=SUMDAS+DSS*SIN(2*ANG)
165.000         SUMDAC=SUMDAC+DSS*COS(2*ANG)
166.000         SUMDBS=SUMDBS+DSS*SIN(4*ANG)
167.000         SUMDBC=SUMDBC+DSS*COS(4*ANG)
168.000         SUMFSAS=SUMFSAS+FSS*COS(2*ANG)
169.000         SUMFSAC=SUMFSAC-FSS*SIN(2*ANG)
170.000 1170     THETA1=THETA22
171.000 1180  CONTINUE
172.000 C
173.000       FNAS=2*SUMFNAS/FNSUM
174.000       FNAC=2*SUMFNAC/FNSUM
```

```
      FNBS=2*SUMFNBS/FNSUM
      FNBC=2*SUMFNBC/FNSUM
      DAS=2*SUMDAS/DSUM
      DAC=2*SUMDAC/DSUM
      DBS=2*SUMDBS/DSUM
      DBC=2*SUMDBC/DSUM
      FSAS=-2*SUMFSAS/FNSUM
      FSAC=-2*SUMFSAC/FNSUM
C
      CALL FS4(FNAS,FNAC,FNBS,FNBC,FNAA,FNBB,FNTHETA2,FNTHETA4)
      CALL FS4(DAS,DAC,DBS,DBC,DAA,DBB,DTHETA2,DTHETA4)
      IF (FSAVG) 1190,1200,1190
1190  CALL FS2(FSAS,FSAC,AU,FSTHETA2)
      AW=AW/FNSUM
C
1200  RETURN
      END
C
      SUBROUTINE FS4(AS,AC,BS,BC,AA,BB,THETA2,THETA4)
C
C*****Subroutine calculates coefficients and principal directions
C      for FOURTH-ORDER FOURIER SERIES EXPRESSIONS
C      EXPRESSION
C
      GLOBAL PI
C
      AA=SQRT(AS*AS+AC*AC)
      BB=SQRT(BS*BS+BC*BC)
      IF (AS.EQ.0.0) THETA2=PI/4.;GOTO 1000
      THETA2=0.5*ATAN2(AS,AC)
1000  IF (BS.EQ.0.0) THETA4=PI/4.; RETURN
      THETA4=0.25*ATAN2(BS,BC)
      IF (THETA2.LT.0.0) THETA2=PI+THETA2
      IF (THETA4.LT.0.0) THETA4=PI+THETA4
C
      RETURN
      END
C
      SUBROUTINE FS2(AS,AC,AA,THETA2)
C
C*****Subroutine calculates coefficients and principal direction
C      for a SECOND-ORDER FOURIER SERIES EXPRESSION
C      of the form: aaxsin2(0-02)
C
      GLOBAL PI
C
      AA=SQRT(AS*AS+AC*AC)
      IF (AS.EQ.0.0) THETA2=PI/4.; RETURN
      THETA2=0.5*ATAN2(AS,AC)
      IF (THETA2.LT.0.0) THETA2=PI+THETA2
C
      RETURN
      END
```

```
C
      SUBROUTINE CIRCLE(IC)
C
C*****PROGRAM DETERMINES FOR CIRCLE LOCATED AT XC,YC AND RADIUS RC:
C
C        1) BOUNDARY DISCS (ie discs intersecting circle cicumference)
C        2) DISCS FALLING ON AND WITHIN CIRCLE
C        3) CONTACTS FALLING WITHIN AND ON CIRCLE
C           (stressed contacts only)
C         4) Addresses of discs falling WITHIN and ON circle
C            boundary identified in array IBCIRC(NBT)
C         5) Addresses of discs falling ON circle boundary
C            identified in array BBALL(NB)
C         6) A(IAB+8)=1 identifies boundary disc
C         7) Addresses of contacts falling WITHIN and ON circle
C            identified in array ICONT(NCS)
C         8) NCS  = TOTAL NUMBER OF PHYSICAL CONTACTS
C                   WITHIN AND ON CIRCLE PERIMETER
C         9) NBC  = TOTAL NUMBER OF CONTACTS
C                   NBC=NBC+2 FOR TWO CONTACTING DISCS WITHIN CIRCLE
C                   NBC=NBC+1 FOR ONE BOUNDARY DISC AND ONE INTERNAL
C                            DISC FORMING CONTACT
C                   NBC=NBC+0 FOR TWO CONTACTING BOUNDARY DISCS
C
      DIMENSION XX(2),YY(2),NBM(4)
```

```
      COMMON /ARAY/ A(108910)
      COMMON /BDAT/ R(50)
      COMMON /SRCH/ NCSAV(2000),NBMAP,IBSAV(2000),NBB
      COMMON /BBAL/ BBALL(1000),NB,AREA
      COMMON /CIRC/ IBCIRC(1000),NBT,ICONT(4000),NCS,NBC
      GLOBAL DEL,NX,NY,TOL,M1,PI,XCR(1),YCR(1),RCR(1)
C
C*****DETERMINE BOXES THAT CIRCLE MAPS INTO
C
C*********FIND LARGEST AND SMALLEST ADDRESS OF BOX THAT CIRCLE
C       AND ENCLOSED AREA MAPS INTO
C
      XC=XCR(IC);YC=YCR(IC);RC=RCR(IC)
      XX(1)=XC-RC
      YY(1)=YC-RC
      XX(2)=XC+RC
      YY(2)=YC+RC
      AREA=PI*RCR(IC)*RCR(IC)
C
      T=TOL
      K=1
      DO 1010 J=1,2
        DO 1010 I=1,2
          IF (J.EQ.2) T=-TOL
          XD=XX(I)+T
          YD=YY(I)+T
          NXD=IFIX(XD/DEL)
          NYD=IFIX(YD/DEL)
          IF (J.EQ.2)GOTO 1000
          IF (XD.GT.(NX*DEL)) NXD=NXD-1
          IF (YD.GT.(NY*DEL)) NYD=NYD-1
1000        NBM(K)=NXD+NYD*NX+1
1010  K=K+1
      NBMAX=AMAX0(NBM(1),NBM(2))
      NBMIN=AMIN0(NBM(3),NBM(4))
C
C*********DETERMINE NUMBER OF COLUMNS OF BOXES THAT CIRCLE MAPS INTO
C
      IRMAX=(NBMAX-1)/NX+1
      ICMAX=NBMAX-NX*(IRMAX-1)
      IRMIN=(NBMIN-1)/NX+1
      ICMIN=NBMIN-NX*(IRMIN-1)
      IC1=AMIN0(ICMAX,ICMIN)
      IC2=AMAX0(ICMAX,ICMIN)
      NC=IC2-IC1+1
C
C*********IDENTIFY BOXES THAT CIRCLE MAPS INTO
C
      NBMAP=0
      DO 1020 I=NBMIN,NBMAX-NC+1,NX
        DO 1020 J=1,NC
          NBX=I+J-2+M1
          NBMAP=NBMAP+1
1020  NCSAV(NBMAP)=NBX
C
C*****DETERMINE DISCS WHICH MAP INTO VICINITY OF CIRCLE
C
      CALL SEARCH
C
C*****IDENTIFY DISCS FALLING WITHIN AND ON CIRCLE BOUNDARIES
C
      NB=NBT=0
      DO 1050 I=1,NBB
        IAB=IBSAV(I)
        A(IAB+8)=0
        XB=A(IAB)+A(IAB+11)
        YB=A(IAB+1)+A(IAB+12)
        ITYP=A(IAB+9)
        RB=R(ITYP)
        XDIF=XC-XB
        YDIF=YC-YB
        D=SQRT(XDIF*XDIF+YDIF*YDIF)
        IF (D-RB-RC) 1030,1030,1050
1030    NBT=NBT+1
        IBCIRC(NBT)=IAB
        IF (D+RB-RC) 1050,1040,1040
1040    NB=NB+1
        A(IAB+8)=1
1050  CONTINUE
C
```

```
106.000 C*****GENERATE LIST OF CONTACTS WHICH FALL WITHIN CIRCLE PERIMETER
107.000 C
108.000      NCS=NBC=0
109.000      DO 1140 I=1,NBMAP
110.000        IAB=A(NCSAV(I))
111.000 1060    IB1=A(IAB)
112.000        IF (IB1) 1140,1140,1070
113.000 C
114.000 C*****NON-STRESSED CONTACTS NOT CONSIDERED
115.000 C
116.000 1070    FN=A(IAB+4)
117.000        IF (FN) 1130,1130,1080
118.000 1080    IB2=A(IAB+1)
119.000 C
120.000 C*****CONTACT FORMED BY TWO BOUNDARY DISCS          L=1
121.000 C    CONTACT BETWEEN BOUNDARY DISC AND INTERNAL DISC L=2
122.000 C    CONTACT BETWEEN TWO BOUNDARY DISCS             L=3
123.000 C
124.000        ITAG1=A(IB1+8)
125.000        ITAG2=A(IB2+8)
126.000        L=ITAG1+ITAG2+1
127.000 C
128.000 1090    X=A(IB2)+A(IB2+11)
129.000        Y=A(IB2+1)+A(IB2+12)
130.000        XDIF=A(IB1)+A(IB1+11)-X
131.000        YDIF=A(IB1+1)+A(IB1+12)-Y
132.000        D=SQRT(XDIF*XDIF+YDIF*YDIF)
133.000        ITYP1=A(IB1+9)
134.000        ITYP2=A(IB2+9)
135.000        R1=R(ITYP1)
136.000        R2=R(ITYP2)
137.000        GAP=D-R1-R2
138.000        RAT=(R2+GAP/2.0)/D
139.000 C
140.000 C**********CONTACT COORDINATES
141.000 C
142.000        XCT=X+XDIF*RAT
143.000        YCT=Y+YDIF*RAT
144.000 C
145.000 C**********CONTACT WITHIN CIRCLE?
146.000 C
147.000        XDIF=XCT-XC
148.000        YDIF=YCT-YC
149.000        D=SQRT(XDIF*XDIF+YDIF*YDIF)
150.000        IF (D-RC) 1100,1100,1130
151.000 1100    NCS=NCS+1
152.000        ICONT(NCS)=IAB
153.000        GO TO (1120,1110,1130)L
154.000 1110    NBC=NBC+1
155.000        GOTO 1130
156.000 1120    NBC=NBC+2
157.000 1130    IAB=IAB+6
158.000        GOTO 1060
159.000 C
160.000 1140  CONTINUE
161.000 C
162.000      RETURN
163.000      END


1.000 C
2.000      SUBROUTINE BVOLUME2
3.000 C
4.000 C*****PROGRAM DETERMINES BOUNDARY DISCS FORMING CONVEX POLYGON
5.000 C    BOUNDARY FOR NEAR-CIRCULAR "SUB-ASSEMBLY" OF DISCS AND
6.000 C    CALCULATES ENCLOSED AREA
7.000 C
8.000 C       1) Boundary disc addresses loaded into array BBALL(NB)
9.000 C
10.000      COMMON /ARAY/ A(108910)
11.000      COMMON /CIRC/ IBCIRC(2000),NBT
12.000      COMMON /BBAL/ BBALL(1000),NB,AREA,N
13.000      GLOBAL PI
14.000      DATA SMALL/1.0E-20/ YO/10000./
15.000      REAL MIDY
16.000 C
17.000 C*****FIND LOWEST DISC ALONG SUB-ASSEMBLY BOUNDARY(address=IBFST)
18.000 C
19.000      DO 1010 I=1,NBT
20.000        IAB=IBCIRC(I)
```

```
21.000        ITAG=A(IAB+8)
22.000        IF (ITAG) 1010,1010,1000
23.000 1000     Y=A(IAB+1)+A(IAB+12)
24.000        IF (Y.LT.YO) IBLST=IAB;XO=A(IAB)+A(IAB+11);YO=A(IAB+1)+A(IAB+12)
25.000 1010   CONTINUE
26.000      BBALL(1)=IBFST=IBLST
27.000 C
28.000 C*****FIND SEQUENCE OF BOUNDARY DISCS BY CONSIDERING
29.000 C     MINIMUM CHANGE IN ANGLE BETWEEN LINES CONNECTING
30.000 C     CENTRES OF DISCS
31.000 C
32.000      N=1
33.000      BETO=0.0
34.000 1020   ALPMIN=2*PI
35.000      DO 1050 I=1,NBT
36.000        IAB=IBCIRC(I)
37.000        ITAG=A(IAB+8)
38.000        IF (ITAG) 1050,1050,1030
39.000 1030     IF (IAB.EQ.IBLST)GOTO 1050
40.000        DX=A(IAB)+A(IAB+11)-XO
41.000        DY=A(IAB+1)+A(IAB+12)-YO
42.000        IF (ABS(DX).LT.SMALL) BET=SIGN(PI/2.,DY);GOTO 1040
43.000        BET=ATAN2(DY,DX)
44.000 1040     IF (BET.LE.0.0) BET=2*PI+BET
45.000        ALP=BET-BETO
46.000        IF (ALP.LT.-.5)GOTO 1050
47.000        IF (ALP.GT.ALPMIN)GOTO 1050
48.000        IBMIN=IAB
49.000        ALPMIN=ALP
50.000        BETMIN=BET
51.000 1050   CONTINUE
52.000 C
53.000      DO 1060 I=1,N
54.000 1060   IF (IBMIN.EQ.BBALL(I))GOTO 1070
55.000      N=N+1
56.000      XO=A(IBMIN)+A(IBMIN+11)
57.000      YO=A(IBMIN+1)+A(IBMIN+12)
58.000      BBALL(N)=IBLST=IBMIN
59.000      BETO=BETMIN
60.000      GOTO 1020
61.000 C
62.000 C*****CALCULATE SUB-ASSEMBLY AREA
63.000 C
64.000 1070   AREA=0.0
65.000      DO 1110 I=1,N
66.000        IF (I.EQ.N)GOTO 1080
67.000        GOTO 1090
68.000 1080     IB2=BBALL(1)
69.000        GOTO 1100
70.000 1090     IB2=BBALL(I+1)
71.000 1100     IB1=BBALL(I)
72.000        MIDY=(A(IB2+1)+A(IB2+12)+A(IB1+1)+A(IB1+12))/2.0
73.000        DX=(A(IB2)+A(IB2+11)-A(IB1)-A(IB1+11))
74.000        PART=-MIDY*DX
75.000 1110   AREA=AREA+PART
76.000 C
77.000      RETURN
78.000      END

1.000 C
2.000       SUBROUTINE STRESS
3.000 C
4.000 C*****PROGRAM CALCULATES BOUNDARY STRESS TENSOR VALUES
5.000 C     FOR INTERIOR ASSEMBLY OF DISCS
6.000 C     (BOUNDARY CORRESPONDS TO CIRCLE "IC" WITH RADIUS "RC"
7.000 C     AND CENTRED AT "XC" AND "YC")
8.000 C
9.000       COMMON /ARAY/ A(108910)
10.000      COMMON /BBAL/ BBALL(1000),NB,AREA
11.000      COMMON /CIRC/ IBCIRC(2000),NBT,ICONT(4000),NCS
12.000      COMMON /BSTR/ BSIG(2,2)
13.000      COMMON /BDAT/ R(50)
14.000      DATA SUM11/0./ SUM12/0./ SUM21/0./ SUM22/0./
15.000 C
16.000      DO 1020 I=1,NCS
17.000        IAD=ICONT(I)
18.000        IB1=A(IAD)
19.000        IB2=A(IAD+1)
20.000        XDIF=A(IB1)+A(IB1+11)-A(IB2)-A(IB2+11)
```

```
21.000        YDIF=A(IB1+1)+A(IB1+12)-A(IB2+1)-A(IB2+12)
22.000        D=SQRT(XDIF*XDIF+YDIF*YDIF)
23.000        CA=XDIF/D
24.000        SA=YDIF/D
25.000        FX=A(IAD+4)*CA+A(IAD+5)*SA
26.000        FY=A(IAD+4)*SA-A(IAD+5)*CA
27.000 C
28.000        ITAG1=A(IB1+8)
29.000        ITAG2=A(IB2+8)
30.000        L=ITAG1+ITAG2+1
31.000        GO TO (1010,1000,1020)L
32.000 C
33.000 1000    D=ITAG1*R(A(IB2+9))+ITAG2*R(A(IB1+9))
34.000 1010    SUM11=SUM11-FX*CA*D
35.000        SUM12=SUM12-FY*CA*D
36.000        SUM21=SUM21-FX*SA*D
37.000        SUM22=SUM22-FY*SA*D
38.000 C
39.000 1020  CONTINUE
40.000 C
41.000      BSIG(1,1)=SUM11/AREA
42.000      BSIG(1,2)=SUM12/AREA
43.000      BSIG(2,1)=SUM21/AREA
44.000      BSIG(2,2)=SUM22/AREA
45.000 C
46.000      RETURN
47.000      END


1.000 C
2.000      SUBROUTINE STRAIN2
3.000 C
4.000 C*****PROGRAM CALCULATES INTERNAL STRAIN TENSAR VALUES FOR
5.000 C     NEAR CIRCULAR INTERIOR SUB-ASSEMBLIES
6.000 C
7.000      GLOBAL M2
8.000      DIMENSION B(17000)
9.000      VIRTUAL B*(STATUS=UNKNOWN,BUF=200,IOSTAT=IT)
9.100      COMMON /ARAY/ A(108910)
10.000      COMMON /ERAY/ E(10000)
11.000      COMMON /STRN/ EIJB(2,2)
12.000      COMMON /BBAL/ BBALL(1000),NB,AREA,NAREA
13.000 C
14.000 C*****NOTES:
15.000 C       1) B(15000) =BALL DATA FROM REFERENCE DUMP FILE
16.000 C       2) BBALL(NB)=CURRENT BOUNDARY BALL ADDRESSES FOR
17.000 C                INTERIOR SUB-ASSEMBLY
18.000 C       3)      NB= NUMBER OF BOUNDARY BALLS
19.000 C       4)    AREA= SUB-ASSEMBLY AREA
20.000 C
21.000      SUM11=SUM12=SUM21=SUM22=0.
22.000      DO 10 I=1,NAREA
23.000      IB1=BBALL(I)
24.000      XS1=B(IB1)+B(IB1+11)
25.000      YS1=B(IB1+1)+B(IB1+12)
26.000      XF1=A(IB1)+A(IB1+11)
27.000      YF1=A(IB1+1)+A(IB1+12)
28.000      IF(I.EQ.NB) GO TO 30
29.000      IB2=BBALL(I+1)
30.000    50 XS2=B(IB2)+B(IB2+11)
31.000      YS2=B(IB2+1)+B(IB2+12)
32.000      XF2=A(IB2)+A(IB2+11)
33.000      YF2=A(IB2+1)+A(IB2+12)
34.000      GO TO 40
35.000    30 IB2=BBALL(1)
36.000      GO TO 50
37.000    40 CONTINUE
38.000 C
39.000      DX=(XS1-XS2-XF1+XF2)/2.
40.000      DY=(YS1-YS2-YF1+YF2)/2.
41.000      SX=XF2-XF1
42.000      SY=YF2-YF1
43.000      SUM11=SUM11-DX*SX/AREA
44.000      SUM12=SUM12+DX*SY/AREA
45.000      SUM21=SUM21-DY*SX/AREA
46.000      SUM22=SUM22+DY*SY/AREA
47.000    10 CONTINUE
48.000 C
49.000      EIJB(1,1)=SUM11
50.000      EIJB(1,2)=SUM12
```

```
51.000      EIJB(2,1)=SUM21
52.000      EIJB(2,2)=SUM22
53.000 C
54.000      RETURN
55.000      END


1.000 C
2.000      SUBROUTINE UPDATE(NB1,NB2,NB)
3.000 C
4.000 C******PROGRAM UPDATES CONTACT LIST FOR BOX NB
5.000 C     CONTACTS FOR BOX NB WHICH WERE PREVIOUSLY IN ADJACENT BOXES
6.000 C     ARE MOVED TO THEIR CURRENT BOX LOCATION
7.000 C
8.000 C     IB1= HIGHER DISC ADDRESS
9.000 C     IB2= LOWER DISC ADDRESS (ZERO IF LIST IS BEING SCANNED
10.000 C         ONLY TO CHECK FOR IB1 ENTRY)
11.000 C     NB= BOX ADDRESS CONTAINING ENTRY
12.000 C     NBSAV(NBMAP)=ADJACENT BOXES
13.000 C
14.000      DIMENSION OLD(6)
15.000      COMMON /ARAY/ A(108810)
16.000      COMMON /SRCH/ NBSAV(2000),NBMAP
17.000      GLOBAL NCBOX
18.000 C
19.000 C*****SCAN CONTACT LIST FOR BOX NB AND CHECK FOR EXISTING
20.000 C     CONTACT FOR NB1/NB2
21.000 C
22.000      IAD=A(NB)
23.000 1000  IB1=A(IAD)
24.000      IF (IB1) 1020,1020,1010
25.000 1010  IB2=A(IAD+1)
26.000      IF ((IB1*IB2).EQ.(NB1*NB2)) RETURN
27.000      IAD=IAD+6
28.000      GOTO 1000
29.000 C
30.000 C*****CHECK SINGLE ENTRY LIST OF BOX NB FOR NB1 AND NB2
31.000 C     ISLIST= START ADDRESS OF SINGLE ENTRY LIST OF BOX NB
32.000 C     IFLIST= LAST  ADDRESS OF SINGLE ENTRY LIST OF BOX NB
33.000 C
34.000 1020  ISLIST=IFLIST=IAD
35.000 1030  IB1=ABS(A(IAD))
36.000      IF (IB1) 1080,1080,1040
37.000 1040  IF (IB1.EQ.NB1.OR.IB1.EQ.NB2)GOTO 1060
38.000      IFLIST=IFLIST+1
39.000 1050  IAD=IAD+1
40.000      GOTO 1030
41.000 C
42.000 C****REMOVE SINGLE ENTRY FROM CONTACT LIST FOR BOX NB
43.000 C
44.000 1060  ICEND=A(NB)+NCBOX*6-1
45.000      DO 1070 IAB=IAD,ICEND-1
46.000 1070  A(IAB)=A(IAB+1)
47.000      IF (IAD.EQ.ISLIST) A(IAD)=-A(IAD)
48.000      A(ICEND)=0.
49.000      GOTO 1030
50.000 C
51.000 C*****SCAN ADJACENT BOXES FOR CONTACT NB1/NB2
52.000 C
53.000 1080  DO 1110 I=1,NBMAP
54.000        IF (NB.EQ.NBSAV(I))GOTO 1110
55.000        IAD=A(NBSAV(I))
56.000 1090    IB1=A(IAD)
57.000        IF (IB1) 1110,1110,1100
58.000 1100    IB2=A(IAD+1)
59.000        IF ((IB1*IB2).EQ.(NB1*NB2))GOTO 1130
60.000        IAD=IAD+6
61.000        GOTO 1090
62.000 1110  CONTINUE
63.000 C
64.000 C*****NEW CONTACT CREATED FOR BOX NB
65.000 C     INITIALIZE TEMPORARY CONTACT STORAGE ARRAY
66.000 C
67.000      DO 1120 K=1,6
68.000 1120  OLD(K)=0.
69.000      GOTO 1170
70.000 C
71.000 C*****STORE DATA FOR CONTACT NB1/NB2 FROM ADJACENT BOX NBSAV(I)
72.000 C     TEMPORARILY IN ARRAY OLD(J)
73.000 C
```

```
74.000 1130  DO 1140 J=1,6
75.000 1140  OLD(J)=A(IAD+J-1)
76.000 C
77.000 C*****DELETE CONTACT NB1/NB2 FROM CONTACT LIST FOR ADJACENT BOX
78.000 C     NBSAV(I)
79.000 C
80.000       ICEND=A(NBSAV(I))+NCBOX*6-1
81.000       DO 1150 IAB=IAD,ICEND-6
82.000 1150  A(IAB)=A(IAB+6)
83.000       DO 1160 IAB=ICEND-5,ICEND
84.000 1160  A(IAB)=0.
85.000 C
86.000 C*****CHECK THAT THERE IS AT LEAST ONE ENTRY LEFT FOR EACH DISC
87.000 C     IN BOX NBSAV(I)
88.000 C
89.000       CALL CHECK(NB1,NBSAV(I))
90.000       CALL CHECK(NB2,NBSAV(I))
91.000 C
92.000 C*****UPDATE CONTACT LIST FOR BOX NB TO INCLUDE CONTACT DATA NB1/NB2
93.000 C     TRANSFERED FROM ADJACENT BOX NBSAV(I)
94.000 C
95.000 1170  IAD=IFLIST+6
96.000       DO 1180 J=1,IFLIST-ISLIST+1
97.000         A(IAD)=A(IAD-6)
98.000 1180  IAD=IAD-1
99.000       A(ISLIST+6)=SIGN(A(ISLIST+6),-1.0)
100.000 C
101.000       A(ISLIST)=NB1
102.000       A(ISLIST+1)=NB2
103.000       A(ISLIST+2)=OLD(3)
104.000       A(ISLIST+3)=OLD(4)
105.000       A(ISLIST+4)=OLD(5)
106.000       A(ISLIST+5)=OLD(6)
107.000       RETURN
108.000       END
```

```
1.000 C
2.000       PROGRAM AUTODISC
3.000 C
4.000 C*****PROGRAM GENERATES RANDOMLY LOCATED DISCS WITHIN A CIRCULAR
5.000 C     AREA AND INITIALIZES "A" ARRAY
6.000 C
7.000       DIMENSION PERC(50),ITYPE(50),NBT(50)
8.000       COMMON /ARAY/ A(110000)
9.000       COMMON /BDAT/ R(50)
10.000       COMMON /BBAL/ BBALL(1500),NBB,AREA
11.000       GLOBAL TRY,DEL,NBOX,NX,NY,M1,M2,M3,M4,TOL,NCBOX
12.000       GLOBAL TDEL,XC,YC,RC,PI,NBALL,DSTEP,NCYC,DNSTY
13.000 C
14.000       INTEGER W,H,RC,TRY,ARANGE,IR(1),ITHETA(1)
15.000       CHARACTER*40 BINFILE,AUTOLOG
16.000       DOUBLE PRECISION DSEED,THETA
17.000 C
18.000       DATA RMIN/1.0E+20/ RMAX/0.0/ TOL/1.0/ TDEL/0.0/ DSEED/123456.D0/
19.000 C
20.000 C*****OPEN INSTRUCTION FILE="FILE"
21.000 C
22.000       OPEN (5,FILE='FILE',STATUS='OLD',ACCESS='KEYED',FORM='FORMATTED')
23.000 C
24.000 C*****READ INSTRUCTIONS TO CREATE ASSEMBLY
25.000 C
26.000       READ (5,'(2G.0)') W,H
27.000       READ (5,'(G.0)') RC
28.000       READ (5,'(2G.0)') NBALLMAX,NCBOX
29.000       READ (5,'(A40)') BINFILE
30.000       READ (5,'(A40)') AUTOLOG
31.000       READ (5,'(2G.0)') DSTEP,NCYC
32.000 C
33.000 C*****OPEN ADDITIONAL FILES
34.000 C
35.000       OPEN (1,NAME=BINFILE,STATUS='NEW',ACCESS='KEYED')
36.000       OPEN (2,NAME='TYPE',STATUS='OLD',ACCESS='SEQUENTIAL',FORM='FORMATTED')
37.000       OPEN (3,NAME='DISTRB',STATUS='OLD',ACCESS='SEQUENTIAL',FORM='FORMATTED')
38.000       OPEN (4,NAME=AUTOLOG,STATUS='NEW',ACCESS='SEQUENTIAL',FORM='FORMATTED')
39.000 C
40.000 C*****INPUT DISC RADII DATA
41.000 C
42.000       DO 1000 I=1,50
43.000         NBTYP=I-1
44.000         READ (2,'(G.0)',END=1010) R(I)
45.000         IF (R(I).LT.RMIN) RMIN=R(I)
46.000         IF (R(I).GT.RMAX) RMAX=R(I)
47.000 1000  CONTINUE
48.000 C
49.000 C*****SETUP BOXES
50.000 C
51.000 1010  NBOX=W*H/((2*RMAX)**2)+0.5
52.000       NX=SQRT(FLOAT(NBOX)*W/H)+0.5
53.000       NY=SQRT(FLOAT(NBOX)*H/W)+0.5
54.000       DEL=AMAX1(W/FLOAT(NX),H/FLOAT(NY))
55.000       NBOX=NX*NY
56.000 C
57.000 C*****SETUP MEMORY PARTITIONS
58.000 C
59.000       M1=300
60.000       M2=NBOX+M1
61.000       M4=(NBALLMAX)*14+M2
62.000 C
63.000 C*****INPUT DISC RADII DISTRIBUTION DATA
64.000 C
65.000       DO 1020 I=1,NBTYP
66.000 1020  READ (3,'(2G.0)',END=1030) ITYPE(I),PERC(I)
67.000 C
68.000 C*****CALCULATE MAXIMUM ADDRESS OF A ARRAY
69.000 C
70.000 1030  IAEND=NCBOX*6*NBOX+M4-1
71.000 C
72.000 C*****INITIALIZE A ARRAY TO ZERO
73.000 C
74.000       DO 1040 I=1,IAEND
75.000 1040  A(I)=0.0
76.000 C
77.000 C*****INITIAL DATA FOR A ARRAY
78.000 C
79.000       A(1)=IAEND
80.000       A(2)=W
```

```
81.000       A(3)=H
82.000       A(4)=NBOX
83.000       A(7)=NCBOX
84.000       A(8)=NX
85.000       A(9)=NY
86.000       A(10)=DEL
87.000       A(11)=M1
88.000       A(12)=M2
89.000       A(13)=A(14)=M3=M4
90.000       A(20)=NBTYP
91.000 C
92.000 C*****SETUP A ARRAY ADDRESSES TO CONTACT LISTS FOR BOXES
93.000 C
94.000       IAB=M4
95.000       DO 1050 I=M1,NBOX+M1-1
96.000         A(I)=IAB
97.000 1050  IAB=NCBOX*6+IAB
98.000 C
99.000 C*****LOCATE DISCS USING ISMLD LIBRARY RANDOM NUMBER GENERATORS
100.000 C
101.000      IAB=M2
102.000      PI=4.0*ATAN(1.0)
103.000 Z    ARANGE=2*PI*1E+08
104.000      XC=W/2.0
105.000      YC=H/2.0
106.000      KT=0
107.000      DO 1090 K=1,NBTYP
108.000        KOUNT=0
109.000        IF (PERC(K).EQ.0.0)GOTO 1080
110.000        NB=(PERC(K)*NBALLMAX/100.0)
111.000        I=1
112.000        IF (KOUNT.GE.NB)GOTO 1080
113.000        REPEAT 1070,WHILE I.LT.5000
114.000 1060       CONTINUE
115.000 C
116.000 C*****LOCATE TRIAL DISCS USING (RADIAL DISTANCE, ANGLE)
117.000 C    RANDOM GENERATOR (COMPILE Z STATEMENTS)
118.000 C
119.000 Z          CALL GGUD(DSEED,RC,1,IR)
120.000 Z          CALL GGUD(DSEED,ARANGE,1,ITHETA)
121.000 Z          THETA=ITHETA(1)/1.E+08
122.000 Z          X=XC+IR(1)*DCOS(THETA)
123.000 Z          Y=YC+IR(1)*DSIN(THETA)
124.000 C
125.000 C*****LOCATE TRIAL DISCS USING (X,Y) RANDOM GENERATOR
126.000 C    (COMPILE Y STATEMENTS)
127.000 C
128.000 Y          CALL GGUD(DSEED,W,1,IR)
129.000 Y          X=IR(1)
130.000 Y          CALL GGUD(DSEED,H,1,IR)
131.000 Y          Y=IR(1)
132.000 Y          DIST=(X-W/2)**2+(Y-H/2)**2-RC**2
133.000 Y          IF (DIST.GT.0.)GOTO 1060
134.000 C
135.000            CALL AUTOREBOX(IAB,X,Y,ITYPE(K))
136.000            IF (TRY.GT.10)GOTO 1070
137.000            IXX=X
138.000            IYY=Y
139.000            A(IAB)=IXX
140.000            A(IAB+11)=X-IXX
141.000            A(IAB+1)=IYY
142.000            A(IAB+12)=Y-IYY
143.000            A(IAB+9)=ITYPE(K)
144.000            IAB=IAB+14
145.000            KOUNT=KOUNT+1
146.000            IF (KOUNT.GE.NB)GOTO 1080
147.000 1070     I=I+1
148.000 1080     CONTINUE
149.000          KT=KOUNT+KT
150.000 C
151.000 C****COMPILE X STATEMENTS TO OUTPUT DISC COUNT TO TERMINAL DEVICE
152.000 C
153.000 X        OUTPUT,KT
154.000 C
155.000          NBT(K)=KOUNT
156.000 1090  CONTINUE
157.000 1100  NBT(K)=KOUNT
158.000       A(6)=NBALL=KT
159.000 C
160.000 C*****COMPACT ASSEMBLY ISOTROPICALLY
```

```
161.000 C
162.000       IF (NCYC.NE.0) CALL ISOPAC
163.000 C
164.000 C*****SETUP CONTACT LIST
165.000 C
166.000       IAB=M2
167.000       DO 1110 I=1,NBALL
168.000         CALL REBOX(IAB)
169.000 1110  IAB=IAB+14
170.000 C
171.000 C*****WRITE RANDOM DISC GENERATION RESULTS TO AUTOLOG FILE
172.000 C
173.000 1120  WRITE (4,9000)
174.000       WRITE (4,9010) BINFILE
175.000       WRITE (4,9020)
176.000       WRITE (4,9030) W
177.000       WRITE (4,9040) H
178.000       WRITE (4,9050) NBOX
179.000       WRITE (4,9060)
180.000       WRITE (4,9070)
181.000 C
182.000       DO 1130 I=1,NBTYP
183.000         NB=(NBALL*PERC(I)/100.0)+0.5
184.000 1130  WRITE (4,9080) ITYPE(I),NB,PERC(I),R(I)
185.000 C
186.000       WRITE (4,9090) NBALLMAX
187.000       WRITE (4,9100)
188.000       WRITE (4,9070)
189.000 C
190.000       DO 1140 I=1,NBTYP
191.000         PC=100.0*NBT(I)/KT
192.000 1140  WRITE (4,9080) ITYPE(I),NBT(I),PC,R(I)
193.000 C
194.000       WRITE (4,9110) NBALL
195.000       CALL BBOUND
196.000       CALL BVOLUME
197.000       CALL BALLDENS
198.000       WRITE (4,9120) AREA
199.000       WRITE (4,9130) DNSTY
200.000 C
201.000 C*****WRITE A ARRAY TO BINARY CONFIGURATION FILE
202.000 C
203.000       WRITE (1,KEY=1000) (A(I),I=1,IAEND)
204.000 C
205.000       CLOSE (1,STATUS='KEEP')
206.000       CLOSE (2,STATUS='KEEP')
207.000       CLOSE (3,STATUS='KEEP')
208.000       CLOSE (4,STATUS='KEEP')
209.000 C
210.000       STOP
211.000 9000  FORMAT(/,1X,'RANDOM PARTICLE GENERATION',/)
212.000 9010  FORMAT(  1X,'FID FOR BINARY FILE OUTPUT          = ',A40)
213.000 9020  FORMAT(  1X,'       RECORD KEY                  = 1',/)
214.000 9030  FORMAT(  1X,'WIDTH OF RECTANGULAR AREA          W = ',I5)
215.000 9040  FORMAT(  1X,'HEIGHT OF RECTANGULAR AREA        H = ',I5)
216.000 9050  FORMAT(  1X,'NO. OF BOXES                  NBOX = ',I5)
217.000 9060  FORMAT(/,1X,'INITIAL BALL DATA')
218.000 9070  FORMAT(  1X,'BALL TYPE NUMBER   PERCENT   RADIUS',/)
219.000 9080  FORMAT(  1X,I2,8X,I4,6X,F5.1,5X,I3,7X)
220.000 9090  FORMAT(/,1X,'TOTAL NUMBER OF BALLS ATTEMPTED TO PLACE = ',I4)
221.000 9100  FORMAT(/,1X,'FINAL BALL DATA')
222.000 9110  FORMAT(/,1X,'TOTAL NUMBER OF BALLS PLACED          = ',I4)
223.000 9120  FORMAT(  1X,'VOLUME OF ASSEMBLY                = ',E12.6)
224.000 9130  FORMAT(  1X,'DENSITY OF ASSEMBLY               = ',E12.6)
225.000       END
```

```
1.000 C
2.000       SUBROUTINE AUTOREBOX(IAB,X,Y,ITYPF)
3.000 C
4.000 C*****PROGRAM LOADS NON-OVERLAPPING DISCS INTO CONTACT LIST
5.000 C     FOR ASSEMBLY AREA
6.000 C
7.000       COMMON /ARAY/ A(110000)
8.000       COMMON /BDAT/ R(50)
9.000       COMMON /SRCH/NBSAV(2000),NBMAP,IBSAV(2000),NBB
10.000      GLOBAL DEL,NX,M1,NY,TOL,M3
11.000      GLOBAL MFLAG,TRY,XC,YC,RC
12.000 C
13.000      LOGICAL MFLAG
14.000      INTEGER TRY,RC
15.000 C
16.000      TRY=0
17.000 1000  IF (TRY.GT.10) RETURN
18.000 C
19.000 C*****TO DETERMINE ADDRESSES OF BOXES THAT DISC MAPS INTO
20.000 C     (SEARCH RADIUS = RAD+TOL)
21.000 C
22.000      NBMAP=0
23.000      RAD=R(ITYPF)
24.000      RT=RAD+TOL
25.000      NXL=IFIX((X-RT)/DEL)
26.000      NXU=IFIX((X+RT)/DEL)
27.000      IF ((X+RT).GE.(NX*DEL)) NXU=NXU-1
28.000      NYL=IFIX((Y-RT)/DEL)
29.000      NYU=IFIX((Y+RT)/DEL)
30.000      IF ((Y+RT).GE.(NY*DEL)) NYU=NYU-1
31.000 C
32.000      DO 1030 NYY=NYL,NYU
33.000        NA=NYY*NX
34.000        DO 1030 NXX=NXL,NXU
35.000          NB=NA+NXX+M1
36.000          IF (NBMAP.EQ.0)GOTO 1020
37.000          DO 1010 N=1,NBMAP
38.000            IF (NBSAV(N).EQ.NB)GOTO 1030
39.000 1010       CONTINUE
40.000 1020       NBMAP=NBMAP+1
41.000          NBSAV(NBMAP)=NB
42.000 1030  CONTINUE
43.000 C
44.000 C*****IDENTIFY DISCS IN SCANNED BOXES
45.000 C
46.000      CALL SEARCH
47.000 C
48.000 C*****TEST FOR DISC-DISC CONTACT
49.000 C
50.000      DO 1040 I=1,NBB
51.000        NBL=IBSAV(I)
52.000        IF (NBL.EQ.IAB)GOTO 1040
53.000        CALL AUTOBTEST(NBL,X,Y,ITYPF)
54.000        XDIF=X-XC;YDIF=Y-YC;D=SQRT(XDIF*XDIF+YDIF*YDIF)
55.000        IF (D.GT.FLOAT(RC)) TRY=11;RETURN
56.000        IF (MFLAG) TRY=TRY+1;GOTO 1000
57.000 1040  CONTINUE
58.000 C
59.000 C*****INCLUDE DISC IN CONTACT LIST
60.000 C
61.000      DO 1050 I=1,NBMAP
62.000 1050  CALL CHECK(IAB,NBSAV(I))
63.000 C
64.000      RETURN
65.000      END
```

```
1.000 C
2.000       SUBROUTINE ISOPAC
3.000 C
4.000 C*****PROGRAM ISOTROPICALLY COMPACTS INITIAL NEAR-CIRCULAR ASSEMBLY
5.000 C
6.000       COMMON /ARAY/ A(110000)
7.000       GLOBAL NBALL,M2,NCYC,DSTEP,BBALL(1500),XCA,YCA,TRY
8.000       INTEGER TRY
9.000 C
10.000       XCA=A(2)/2.0
11.000       YCA=A(3)/2.0
12.000       CALL ORDER
13.000       DO 1000 NN=1,NCYC
14.000         DO 1000 NB=1,NBALL
15.000           IAB=BBALL(NB)
16.000           XO=A(IAB)+A(IAB+11)
17.000           YO=A(IAB+1)+A(IAB+12)
18.000           XDIF=XCA-XO
19.000           YDIF=YCA-YO
20.000           DO=SQRT(XDIF*XDIF+YDIF*YDIF)
21.000           DX=DSTEP*XDIF/DO
22.000           DY=DSTEP*YDIF/DO
23.000           X=XO+DX
24.000           Y=YO+DY
25.000           ITYP=A(IAB+9)
26.000           CALL AUTOREBOX(IAB,X,Y,ITYP)
27.000           IF (TRY.GT.10)GOTO 1000
28.000           XDIF=XCA-X
29.000           YDIF=YCA-Y
30.000           D=SQRT(XDIF*XDIF+YDIF*YDIF)
31.000           IF (D.GT.DO)GOTO 1000
32.000           A(IAB)=IXX=X
33.000           A(IAB+1)=IYY=Y
34.000           A(IAB+11)=X-IXX
35.000           A(IAB+12)=Y-IYY
36.000 1000  IAB=IAB+14
37.000 C
38.000       RETURN
39.000       END

1.000 C
2.000       SUBROUTINE ORDER
3.000 C
4.000 C*****Program orders discs with respect to increasing
5.000 C     distance from centre of assembly
6.000 C
7.000       COMMON /ARAY/ A(110000)
8.000       GLOBAL NBALL,M2,BBALL(1500),XCA,YCA
9.000       DATA DMIN/1.0E+20/
10.000 C
11.000       NB=1
12.000 1000  IAB=M2
13.000       DO 1030 I=1,NBALL
14.000         IF (A(IAB+9)) 1030,1030,1010
15.000 1010      X=A(IAB)+A(IAB+11)
16.000         Y=A(IAB+1)+A(IAB+12)
17.000         XDIF=X-XCA
18.000         YDIF=Y-YCA
19.000         D=SQRT(XDIF*XDIF+YDIF*YDIF)
20.000         IF (D.LE.DMIN)GOTO 1020
21.000         GOTO 1030
22.000 1020      BBALL(NB)=IAB
23.000         DMIN=D
24.000 1030  IAB=IAB+14
25.000       IAB=BBALL(NB)
26.000       A(IAB+9)=-A(IAB+9)
27.000       NB=NB+1
28.000       IF (NB.EQ.(NBALL+1))GOTO 1040
29.000       GOTO 1000
30.000 C
31.000 1040  IAB=M2
32.000       DO 1050 I=1,NBALL
33.000         A(IAB+9)=ABS(A(IAB+9))
34.000 1050  IAB=IAB+14
35.000 C
36.000       RETURN
37.000       END
```

APPENDIX B

Normal Contact Compliances for Systematic Packings of Equi-Diameter Elastic Spheres and Two-Dimensional Random Assemblies of Discs

The majority of tests in the current study were carried out with interparticle stiffnesses defined by the constant product term $k_n r = 3.75 \times 10^{10}$. This value is typical of values reported by Strack and Cundall (1978) during numerical experiments simulating actual assemblies of photo-elastic discs. Contact stiffnesses k_n and k_s have been chosen such that $k_n/k_s = 1$. According to Mindlin (1949), this ratio may be considered a lower limit on the ratio of tangential to normal compliances for equi-diameter *elastic* spheres in contact. Elastic solutions for spheres in contact can also be invoked to give guidance in determining the magnitude of interparticle stiffnesses for discs made up of less compressible materials.

Consider a systematic packing of *bonded* equi-diameter elastic spheres of radius r. Imagine that within an assembly volume V, there are a very large number of these spheres arranged in a dense regular array. The number of spheres N in the assembly volume can be calculated as:

$$N = \frac{3(1-n)V}{4\pi r^3} \tag{B.1}$$

where n is the assembly porosity. The contact density m_v for the assembly is:

$$m_v = \frac{3\gamma(1-n)}{4\pi r^3} \tag{B.2}$$

Here γ is the (average) coordination number for the assembly. Imagine that the assembly is subject to a uniform hydrostatic stress condition σ_n where:

$$\sigma_n = \frac{\sigma_{kk}}{3} \qquad k = 1,2,3 \tag{B.3}$$

It is reasonable to assume that under the given stress condition the systematic arrangement of particles will result in a constant uniform normal contact force f_n^o. From (B.2), (B.3) and (2.17) the normal stress acting on the system is:

$$\sigma_n = \frac{m_v r f_n^o}{3} \tag{B.4}$$

The Hertz solution (Deresiewicz, 1958) for a pair of contacting elastic spheres of radius r subject only to normal contact forces is:

$$\frac{\Delta r}{f_n^o} = \frac{2}{3}\left[\frac{1}{r f_n^o}\right]^{1/3}\left[\frac{3(1-\nu^2)}{4E}\right]^{2/3} \tag{B.5}$$

Term Δr refers to the change in particle radius and ν and E are the Poisson's ratio and Young's Modulus for the sphere material. Substitution of (B.2) and (B.4) into (B.5) and rearrangement leads to:

$$\frac{\Delta r}{r} = \frac{2}{3}\left[\frac{3\pi(1-\nu^2)}{\gamma E(1-n)}\right]^{2/3} {\sigma_n}^{2/3} \tag{B.6}$$

The quantity $\Delta r/r$ represents the normalized radial deformation for each contacting sphere. Expression (B.6) can be modified by assuming that the normal stress quantity σ_n is due only to assembly self-weight. Letting ρ represent the sphere material density and H a certain depth of assembly then, the normalized radial deformations acting at H can be approximated by:

$$\frac{\Delta r}{r} = \frac{2}{3}\left[\frac{3\pi(1-\nu^2)\rho G H}{\gamma E}\right]^{2/3} \tag{B.7}$$

Term G is the gravitational constant.

Now let us consider assemblies of spheres in a rhombohedral packing and comprising a variety of materials. For a rhombohedral array $\gamma = 12$. Figure B-1 shows the results of calculations using equation (B.7) and several materials. The plot shows that the deformation in elastic spheres is dependent on load level and that spheres comprising quartz or steel material may be expected to exhibit deformations which are up to 7 times that anticipated for similar discs constructed from photo-elastic materials. Superimposed on the plot is the average value for $\Delta r/r$ extracted from the initial dense isotropic assembly which was used for the majority of the numerical experiments carried out in the current investigation ($k_n r = 3.75 \times 10^{10}$). For this numerical two-dimensional assembly of discs, $\Delta r/r$ was calculated according to:

$$\frac{\Delta r}{r} = \left|\frac{f_n^o}{k_n r}\right| \tag{B.8}$$

If we assume that the magnitude of the difference in curves for *soft* and *hard* spheres is comparable to that anticipated for discs comprising photo-elastic and quartz or steel materials then, the lower straight line with $k_n r = 3.75 \times 10^{11}$ may be representative of physical discs with stiffer contacts.

As a result of the foregoing arguments, a limited number of tests were performed with values $k_n r = 3.75 \times 10^{11}$ to examine the micromechanical and global response of numerical experiments simulating assemblies of discs with stiffer contacts.

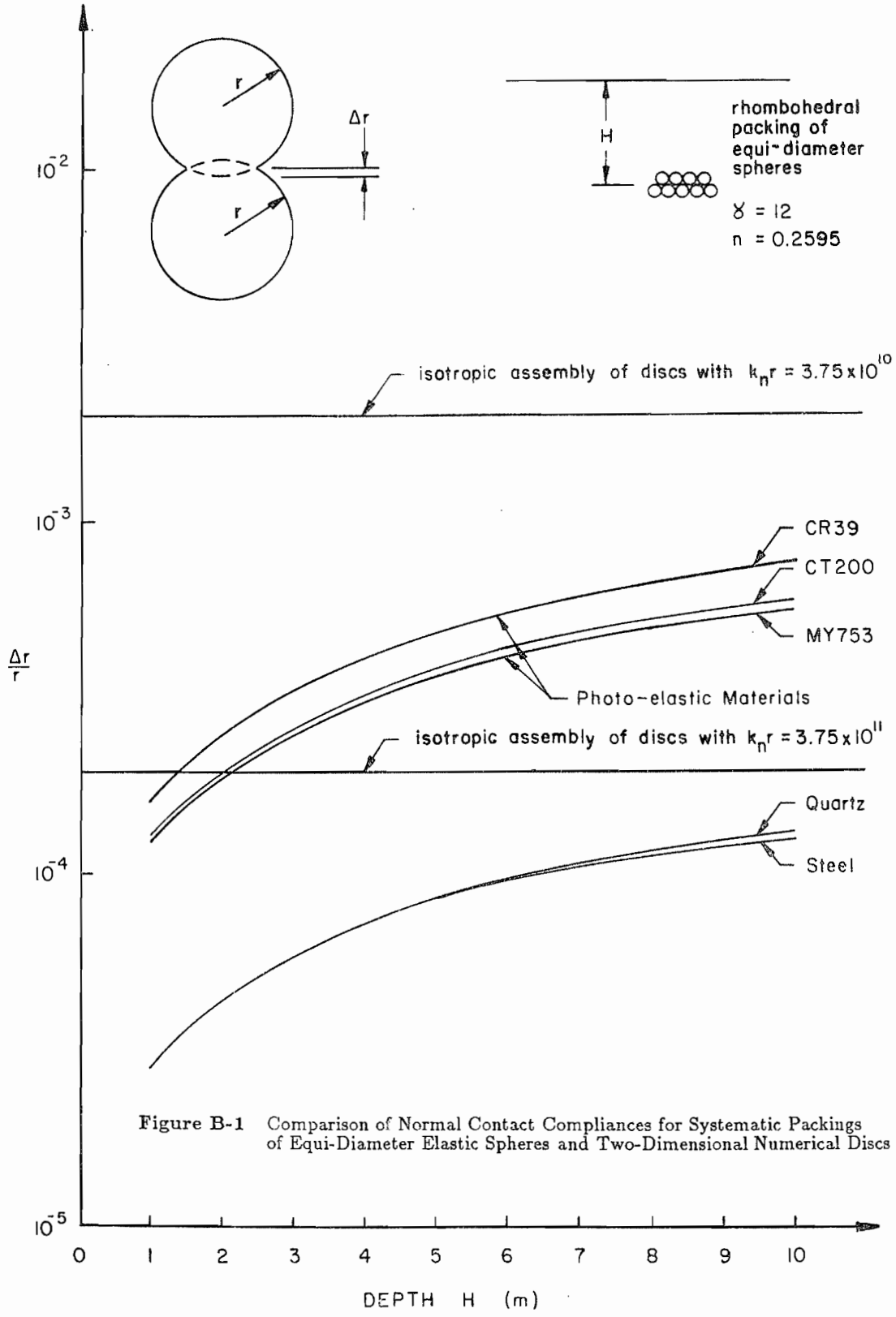

Figure B-1 Comparison of Normal Contact Compliances for Systematic Packings of Equi-Diameter Elastic Spheres and Two-Dimensional Numerical Discs

BIBLIOGRAPHY

ATHANASIOU-GRIVAS, D., & HARR, M.E. (1980)
Particle Contacts in Discrete Materials
Jour. Geotechnical Engr. ASCE, Vol. 106, No. GT5, pp. 559-564

BERNAL, J.D. (1964)
Proc. Royal Soc. Vol. 280. p. 299

BIAREZ, J., & WIENDIECK, K. (1963)
La Comparaison Qualitative entre L'anisotropie Mécanique et L'anisotropie de Structure des Milieux Pulvérulents
Academie de Sciences Comptes Rendus, Vol. 256, pp. 1217-1220

CHRISTOFFERSEN, J., MEHRABADI, M.M, & NEMAT-NASSER, S. (1981)
A Micromechanical Description of Granular Material Behaviour
Jour. Applied Mech. Trans. ASME, Vol. 48, pp. 339-344

CUNDALL, P.A. (1971)
A Computer Model for Simulating Progressive, Large-Scale Movements in Blocky Rock Systems
Proc. Symp. Int. Soc. Rock Mech., Nancy, France
Vol. 2, No. 8

CUNDALL, P.A., & STRACK, O.D.L. (1979a)
A Discrete Numerical Model for Granular Assemblies
Géotechnique, Vol. 29, No. 1, pp. 47-65

CUNDALL, P.A., & STRACK, O.D.L. (1979b)
The Development of Constitutive Laws for Soil using the Distinct Element Method
Third Int. Conf. Numerical Methods in Geomechanics, Aachen, pp. 289-298

CUNDALL, P.A., & STRACK, O.D.L. (1979c)
The Distinct Element Method as a Tool for Research in Granular Media
NSF Report ENG 76-20711, PART II, Dept. Civil & Mining Engineering
Univ. of Minnesota

CUNDALL, P.A., DRESCHER, A., & STRACK, O.D.L. (1982)
Numerical Experiments on Granular Assemblies; Measurements and Observations
IUTAM Conference on Deformation and Failure of Granular Materials
Delft, pp. 355-370

CURRAY, J.R., (1956)
The Analysis of Two-Dimensional Orientation Data
Jour. Geol., Vol. 64, pp. 117-131

DANTU, P., (1957)
Contribution à L'Étude Mécanique et Géométrique des Milieux Pulvérulents
Proc. 4'th ICSMFE, Vol. 1, pp. 144-148

DANTU, P., (1968)
Étude Statistique des Forces Intergranulaires Dans un Milieu Pulvérulent
Géotechnique, Vol. 18, pp. 50-55

DE JOSSELIN DE JONG, G. & VERRUIJT, A. (1969)
Étude Photo-Élastique D'un Empilement de Disques
Can. Grpe. fr. Etude. Rheol., No. 2, pp. 73-86

DERESIEWICZ, H. (1958)
Advances in Applied Mechanics, (Drydon, H.L., & von Karman, Th. editors)
Academic Press Inc., New York

DRESCHER, A., & DE JOSSELIN DE JONG, G. (1972)
Photoelastic Verification of a Mechanical Model for the
Flow of a Granular Material
Jour. Mech. Phys. Solids, Vol. 20, pp. 337-351

FIELD, W.G. (1963)
Towards the Statistical Definition of a Granular Mass
Proc. 4'th Aust. and N.Z. Conf. on Soil Mech.
and Foundation Engineering, pp. 143-148

HILL, R. (1963)
Elastic Properties of Reinforced Solids: Some Theoretical Principles
Jour. Mech. Phys. Solids, Vol. 11, pp. 357-372

HORNE, M.R. (1965)
The Behaviour of an Assembly of Rotund, Rigid, Cohesionless Particles I & II
Proc. Royal Soc. of London, Vol. 286, pp. 62-97

KONISHI, J. (1974)
Discussion: A Microscopic Study on Shear Mechanism of Granular Materials
Jap. Soc. Soil Mech. Found. Eng., Vol. 14, No. 4, pp. 98-102

KONISHI, J., (1978)
Microscopic Model Studies on the Mechanical Behaviour of Granular Materials
Proc. U.S-Jap. Seminar on Continuum-Mechanical and Statistical Approaches
in the Mechanics of Granular Materials, Tokyo, pp. 27-45

LANDAU, L.D., & LIFSHITZ, E.M. (1959)
Statistical Physics: Course of Theoretical Physics Vol. 5
Pergamon Press Ltd. Oxford, U.K., pp. 1-2

MEHRABADI, M.M., NEMAT-NASSER, S., & ODA, M. (1982)
On Statistical Description of Stress and Fabric in Granular Materials
Int. Jour. Num. Anal. Methods in Geomechanics
Vol. 6, pp. 95-108

MINDLIN, R.D., (1949)
Compliance of Elastic Bodies in Contact
Jour. Applied Mechanics, Vol. 16, No. 3, pp. 259-268

ODA, M., (1972a)
Initial Fabrics and their Relations to Mechanical Properties of Granular Material
Jap. Soc. Soil Mech. Found. Eng., Vol. 12, No. 1, pp. 17-36

ODA, M., (1972b)
The Mechanism of Fabric Changes During Compressional Deformation of Sand
Jap. Soc. Soil Mech. Found. Eng., Vol. 12, No. 2, pp. 1-18

ODA, M., (1972c)
Deformation Mechanism of Sand in Triaxial Compression Tests
Jap. Soc. Soil Mech. Found. Eng., Vol. 12, No. 4, pp. 45-63

ODA, M., (1977)
Co-Ordination Number and its Relation to Shear Strength of Granular Material
Jap. Soc. Soil Mech. Found. Eng., Vol. 17, No. 2, pp. 29-42

ODA, M., (1978)
Significance of Fabric in Granular Mechanics
Proc. U.S-Jap. Seminar on Continuum-Mechanical and Statistical Approaches in the Mechanics of Granular Materials
Tokyo, pp. 7-26

ODA, M., (1982)
Fabric Tensor for Discontinuous Geological Materials
Jap. Soc. Soil Mech. Found. Eng., Vol. 22, No. 4, pp. 96-108

ODA, M., & KONISHI, J. (1974a)
Microscopic Deformation Mechanism of Granular Material in Simple Shear
Jap. Soc. Soil Mech. Found. Eng., Vol. 14, No. 4, pp. 25-38

ODA, M., & KONISHI, J. (1974b)
Rotation of Principal Stresses in Granular Material During Simple Shear
Jap. Soc. Soil Mech. Found. Eng., Vol. 14, No. 4, pp.39-53

ODA, M., KONISHI, J., & NEMAT-NASSER, S. (1980)
Some Experimentally Based Fundamental Results on the Mechanical Behaviour of Granular Materials
Géotechnique, Vol. 30, No. 4, pp. 479-495

ODA, M., NEMAT-NASSER, S., & MEHRABADI, M.M. (1982)
A Statistical Study of Fabric in a Random Assembly of Spherical Granules
Int. Jour. Num. Anal. Methods in Geomechanics, Vol. 6, pp.77-94

ODA, M., KONISHI, J. & NEMAT-NASSER, S. (1983)
Experimental Micromechanical Evaluation of the Strength of Granular Materials: Effects of Particle Rolling
Mechanics of Granular Materials: New Models and Constitutive Relations, (Jenkins, J.T. & Satake, M. editors), pp. 21-30

ROTHENBURG, L. (1980)
Micromechanics of Idealized Granular Systems, *Ph.D Thesis*
Civil Engineering Dept., Carleton University, Ottawa

ROTHENBURG, L. (1985)
State Parameter for Beaufort Sea Sands
Report to Gulf Canada Resources (unpublished)

ROTHENBURG, L., & SELVADURAI, A.P.S. (1981a)
Anisotropic Fabric of Plane Granular Assemblies and Elements of their Mechanical Response, *Colloque Int. du CNRS*, No. 319

ROTHENBURG, L., & SELVADURAI, A.P.S. (1981b)
A Micromechanical Definition of the Cauchy Stress Tensor for Particulate Media
Proc. Int. Symposium on the Mech. Behaviour of Structured Media (Selvadurai, A.P.S., editor), Ottawa

ROTHENBURG, L., & SELVADURAI, A.P.S. (1981c)
Micromechanical Aspects of Plane Random Anisotropic Assemblies of Material Discs
Eighth Canadian Congress of Applied Mechanics
University of Moncton, Moncton, pp. 215-218

SATAKE, M., (1978)
Constitution of Mechanics of Granular Materials Through the Graph Theory
Proc. U.S-Jap. Seminar on Continuum-Mechanical and Statistical Approaches in the Mechanics of Granular Materials
Tokyo, pp. 47-62

SCHNEEBELI, G. (1956)
C.R. Hebd. Seanc. Acad. Sci., Vol. 243, p. 125

SKINNER, A.E. (1969)
A Note on the Influence of Interparticle Friction on the Shearing Strength of a Random Assembly of Spherical Particles
Géotechnique, Vol. 19, No. 1, pp. 150-157

SMITH, W.O., FOOTE, P.D. & BUDANG, P.F. (1929)
Packing of Homogeneous Spheres
Physics Review, Vol. 34, pp. 1271-1274

STRACK, O.D.L., & CUNDALL, P.A. (1978)
The Distinct Element Method as a Tool for Research in Granular Media
NSF Report ENG 76-20711, PART I
Dept. Civil & Mining Engineering, Univ. of Minnesota

WEBER, J. (1966)
Recherches Concernant les Contraintes Intergranulaires dans les Milieux Pulvérulents
Bull. de Liais. Ponts et Chaussées, No. 20

ZIMAN, J.M. (1979)
Models of Disorder, *Cambridge University Press*
Cambridge, U.K.

VITA

Name:	Richard John Bathurst
Place and Year of Birth:	Edmonton, Alberta, 1952
Education:	Senior Matriculation (Grade 13)- First Class Honours Merivale H.S., Ottawa, Ontario- completed May, 1971
	B.Sc. (Civil Engineering)- First Class Honours Queen's University, Kingston, Ontario- completed May, 1976
	M.Sc. (Geotechnical Engineering) Queen's University, Kingston, Ontario- completed Jan., 1978
Awards:	Ontario Scholarship, 1971
	Inco Participating Scholarship (Mining Engineering), 1972-1973
	Inco Participating Scholarship (Civil Engineering), 1973-1974
	Martin Wolf Memorial Scholarship, 1974-1975
	Dean's Scholarship, 1974-1975
	Ontario Graduate Scholarship, 1976-1977
	National Research Council Scholarship, 1977
Professional Experience:	Geotechnical Engineer, Golder Associates 1978-1980
	Lecturer, Dept. of Civil Engineering Royal Military College of Canada, Kingston, Ontario 1980-1982
	Assistant Professor, Dept. of Civil Engineering Royal Military College of Canada, Kingston, Ontario 1982 to present
Publications:	A New Method for Effective Reinforcement of Asphalt Pavements *with* O.A. Abdlehalim *Transportation Forum*, Vol. 2-1, June, 1985
	Frictional Development at a Gravel-Geosynthetic-Peat Interface *with* P.M. Jarrett Second Canadian Symposium on Geotextiles and Geomembranes Edmonton, Alberta, Sept., 1985